Establishing the earthworm as a model to study natural processes of neuronal regeneration
new insights from histological, transcriptomic and biophysical studies

Katsiamides, Andreas

Awarding institution:
King's College London

Establishing the earthworm as a model to study natural processes of neuronal regeneration: new insights from histological, transcriptomic and biophysical studies

A thesis submitted in partial fulfilment of the requirement for the degree

of

Doctor of Philosophy

to the

Department of Analytical, Environmental and Forensic Sciences

at

King's College London

by

Andreas Katsiamides

2019

Declaration

I certify this work contains no material which has been submitted for the award of any other degree or diploma in my name, in any university or other institution of higher learning and, to the best of my knowledge and belief, contains no material previously published or written by another person, except where due reference has been made in the text. I also certify that the thesis has been written by me and that, to the best of my knowledge and belief, any help I received in preparing the thesis, and all sources used, have been acknowledged in this thesis

25-09-2019 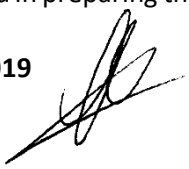

Acknowledgments

Firstly, I would like to express my sincere gratitude to Professor Stephen Stürzenbaum for giving me the opportunity to work in such an exciting project and for his overall support and guidance in the past four years. Through this time, I developed utmost respect and appreciation, not only for his scientific work and work-ethic but also for his consistency and open-hearted character, on which I knew I could rely on at any point.

To Professor László Molnar, for his valuable input in experimental design, his guidance throughout and the discussion of scientific ideas. His expertise in earthworm biology really taught me a lot. Special thanks to Mr Carl Hobbs, for all his support with histological work and for his welcoming personality which made our collaboration an enjoyable one. To Dr Tina Geraki and Dr Fred Mosselmans for their support at the Diamond Light Source in Oxford; your help is greatly appreciated.

To all the present and past members of the laboratory who helped me along the way and made this a rewarding and engaging experience; I have learnt a lot from you. Special mention must go to Mustafa Abbass, a PowerPoint powerhouse, organisational wizard, philosopher and an unexpected friendship; it has been a pleasure sharing this journey with you.

To my family (especially Rona and Rooney), I could not have reached this point if it wasn't for you. Your support and advice gave me direction and kept me focused on my goals.

Lastly, I dedicate this to my lovely partner Maria Papachristodoulou, for all her patience and care throughout this period. I could not have done this without you.

Table of Contents

Table of Figures

Table of Tables

1. Abstract

The hallmark of neurodegenerative disease in humans, including Alzheimer's, Amyotrophic Lateral Sclerosis and Parkinson's, lies in our inability to efficiently restore damaged neurons. Contrary to widespread belief, humans can regenerate neurons within the Peripheral Nervous System (PNS) and some areas of the Central Nervous System (CNS), however the underlying mechanisms which drive or repress complete functional and structural neuronal regeneration remain elusive. To develop our understanding of this natural phenomenon one should focus on species which are capable of efficient neuronal regeneration following neurotrauma. The earthworm species *Eisenia fetida* can regenerate their Cerebral Ganglion (CG) - loosely defined as the brain, within a few weeks following surgical removal. The characterization of fundamental aspects of neuronal regeneration in the earthworm promises to provide an insight as to why humans have largely lost that capability. Here we present a detailed micro-dissection protocol that has been developed to excise the CG and study the progression of its regeneration. The Ventral Nerve Cord (VNC) of the worm is a tissue which connects the CG to the rest of the nervous system via the Circumpharyngeal Connectives (CC). Exploration of molecular dynamics through changes in the transcriptome were determined in the VNC and CC at 1 week and 5-week post-decerebration using an RNAseq approach (90 million reads/condition, 100bp Paired End). RNAseq established that specific groups of genes are up- or downregulated in the regenerating VNC. More than 500 significantly enriched biological processes were identified throughout the regeneration process, including vascular development, neurogenesis and extracellular matrix organization, as well as more than 100 significantly enriched molecular functions, including calcium ion binding, metal ion binding and metalloendopeptidase activity. Differential expression of transcripts was confirmed via qPCR. Examples of transcripts which have been validated at 1w post-decerebration, include catalase (~34-fold), superoxide dismutase 1 (*sod-1*) (~12-fold) and transcription factor jun-B (*junb)* (~3-fold). On the other hand, examples of transcripts which have been validated at 5w post-decerebration, include Glial Fibrillary Acidic Protein (GFAP) (~101-fold), *adam19* (~17-fold) and Bone Morphogenetic Protein 1 (BMP1) (~3-fold). Moreover, the large number of differentially expressed metalloproteins (ADAMs, BMPs, MMPs, metallothionein) identified in the transcriptome, led to the hypothesis that metal trafficking could play a role in the course of regeneration. This was confirmed using a synchrotron-based approach, namely X-Ray Fluorescence (XRF) spectroscopy, where Zinc (Zn) and Iron (Fe) show a differential distribution pattern across different stages (at 1 week to 10-weeks post-decerebration) of regeneration. Lastly, various histological techniques were implemented to characterize/describe neuronal structures during the regenerating process, including immunohistochemistry and Terminal deoxynucleotidyl transferase dUTP Nick End Labeling (TUNEL). Furthermore, numerous novel markers and biological processes have been identified which, to date, have not been linked to neuronal regeneration. In summary, the results suggest that the increase of axon growth promoting factors as well the decrease of growth inhibitory factors act in conjunction to ensure efficient neuronal regeneration in the earthworm.

2. Introduction

2.1. Preface

The capacity of the Central Nervous System (CNS) to regenerate following injury or degeneration, is limited in adult mammals. This leads to several permanent debilitating conditions in cases of neurotrauma, stroke, as well as in Parkinson's, Alzheimer's and Huntington's diseases. As opposed to the CNS, Peripheral Nervous System (PNS) damaged axons readily regenerate to restore normal function. The underlying mechanisms which drive or repress complete functional and structural neuronal regeneration have been elusive. Ongoing research over the last few decades has revealed growth-inhibitory, as well as growth-promoting factors, which, either collectively or individually, have been the subject of pharmacological targeting, with limited success. To this day, the treatment of neuronal trauma or degeneration has been primarily restricted to treating the symptoms of the patient, rather than the underlying cause of the problem (Silva *et al.*, 2014). This is especially true in cases of Spinal Cord Injuries (SCI) where the patients often suffer from loss of motor and sensory functions, which can have severe implications that manifest, not only physically and physiologically, but perhaps most importantly in a psychological manner as well. In an ageing population, where the incidence of neurological-based diseases is prevalent, it is imperative, therefore, to transition into more effective therapeutic strategies, in order to provide patients with hope for an improved standard of living.

2.2. CNS neuronal regeneration in a PNS environment

It has been suggested that the ability of a neuron to fully regenerate can be attributed to its intrinsic and extrinsic properties. Intrinsic properties in this context refer to the ability of the neuron to promote its self-repair via the induction or repression of molecular cues. On the other hand, the extrinsic properties of a neuron refer to the environment in which it resides (Tedeschi and Bradke, 2017). Despite what we are faced with today in terms of the diminished ability of mammalian CNS neuronal repair, CNS neurons *can* regenerate. One of the first attempts to show whether CNS neurons can regenerate was made by Tello in 1911 where cortical neurons of young rabbits were recorded to enter transplanted pieces of peripheral nerves grafts (Tello, 1911). However, the experimental design and results came under severe scrutiny and were largely neglected until the work of Aguayo and colleagues who performed, in a systematic way, one of the most significant and revolutionary series of experiments to challenge the belief at the time about neuronal regeneration in the CNS (Richardson *et al.*, 1980; David and Aguayo, 1981). They described a procedure where rat

sciatic nerve graft substrates were transplanted, as 'bridges', into damaged sites of the spinal cord. Remarkably, they showed, through retrograde neuronal tracing, that CNS axons could elongate and grow into the transplanted PNS environment. The transplanted sciatic nerve graft was considered; therefore, a permissive substrate for CNS axonal growth. This simple experiment revolutionised developmental neurobiology as it challenged the prevailing dogma at the time, namely that neurons of the CNS just lack the intrinsic capabilities of regeneration and growth. Thus, different from the infamous statement by Ramon y Cajal's that *'…in adult centres, the nerve paths are something fixed, ended, immutable. Everything may die, nothing may be regenerated…*' (Ramon y Cajal, 1928). It was shown that the CNS retained the intrinsic capacity for axon growth. It follows then that the inability of the CNS to spontaneously repair itself under normal conditions lies in the inhibitory environment in which it operates.

Glial cells, originating from the Greek word *γλία* meaning 'glue', are non-neuronal cells and constitute between 33% and 66% of mammalian brain mass, thus form a large portion of the CNS environment (Azevedo *et al.*, 2009; Herculano-Houzel, 2014). They maintain homeostasis, form myelin, act as neuroinflammatory molecules provide support and protection for neurons as well as regulating synaptic development (Stevens *et al.*, 2007; Stephan *et al.*, 2012). There are 6 different types of glial cells; ependymal cells, oligodendrocytes, astrocytes and microglia in the CNS – their progenitors called NG2-glia, also known as Oligodendrocyte Progenitor Cells (OPCs), are often considered as a glial subtype in the CNS. On the other hand, the PNS glia consist of satellite cells and Schwann cells. The differences in glial cell population may very well be one of the confounding factors as to why the CNS has a poor regenerative profile. There is a large body of evidence focussing on the positive effects of Schwann cells in facilitating regeneration in the PNS. Moreover, the permissive environment of the PNS to neuronal regeneration is further supported by studies of Schwann cells transplantation, which were used as substrates for CNS neuronal growth (Schwann cells are the glial cells that form the myelin sheath around PNS neurons), either as a cell suspension (Li and Raisman, 1994) or supported with collagen (Paíno *et al.*, 1994). Similarly, to the PNS graft experiments, CNS axons were able to migrate into the Schwann cell substrates.

Conversely, the normal myelin environment and presence of oligodendrocytes (responsible for myelination) in the CNS has long been suspected of having an inhibitory effect (Kiernan, 1979). Since then there have been several studies which have identified several inhibitory factors in the CNS microenvironment at the site of neuronal injury, including myelin-

associated components and debris (Mukhopadhyay *et al.*, 1994; GrandPré *et al.*, 2000; Wang *et al.*, 2002; Silver *et al.,* 2015), Chondroitin Sulphate Proteoglycans (CSPGs) and the glial scar at the lesion site (Dou and Levine, 1994; Davies *et al.*, 1997; Sivasankaran *et al.*, 2004; Case and Tessier-Lavigne, 2005; Lang *et al.*, 2015) and axon guidance molecules (Chilton, 2006) amongst others. Moreover, it has been shown that following a spinal cord injury, the use of a modified collagen scaffold enabled the removal of inhibitory components in the microenvironment and promoted neuronal growth via the incorporation of neural stem cells (Fan et al., 2017).

Even though the studies above highlighted the role and importance of these CNS inhibitory molecules in regeneration, in most cases, despite the neutralization of these inhibitory components, only a small number of injured CNS axons can regenerate, suggesting, therefore, that ultimately neuronal capacity for complete regeneration lies in their intrinsic profile (He and Jin, 2016). Despite the plethora of experimental evidence and the difference in opinion, as to what plays a central role in regeneration, intrinsic or extrinsic factors, efficient structural and functional neuronal regeneration in the CNS can only be achieved when all these elements interact within a cooperative network. It is therefore first of all, of crucial importance to appreciate the key events that take place following CNS injury in mammals.

2.3. Tissue-specific response to mammalian CNS injury

It is now widely accepted that the limited capacity of the CNS to initiate and sustain neuronal regeneration can be classified into three major categories. (1) there is a low level of neurotrophic and growth-promoting influences in the lesion site, (2) there are inhibitory signals which prevent neurite outgrowth and (3) there is a cascade of events that take place which eventually leads to multi-layered scar formation, that acts as physical and chemical barrier through which growing axons cannot pass through (Carbonetto, 1991; Schwab and Bartholdi, 1996). This section will focus on the latter.

The ability to respond to injury and repair damaged tissue has been fundamental to survival. Each tissue responds to injury in a tissue-specific way, and the CNS is no exception. The cellular response elicited by the CNS involves a multi-faceted complex of interactions. These interactions take place between intrinsic neural cells – which include neurons, oligodendrocytes, astrocytes and NG2-OPCs amongst others and non-neuronal cells – which include microglia the ‘macrophage-like cells of the CNS and fibroblasts amongst others. In addition to intrinsic components, extrinsic CNS cells, which originate from the blood

circulation and eventually cross the blood-brain barrier (Burda and Sofroniew, 2014) also play a role in CNS tissue repair.

Similarly to other tissue repair paradigms, the CNS response to injury can be divided into three overlapping phases; (1) cell death and inflammation, (2) tissue replacement and (3) tissue remodelling. In the CNS, these stages take place within seconds, days and can last for years from the moment of injury (Burda and Sofroniew, 2014). A brief description of the main events that apply in this context will be outlined below.

In the seconds after the neuronal damage, the site is characterised by intense apoptosis and the rapid infiltration of platelets, which form aggregates and signal to neighbouring cells to form a fibrillin/collagen scaffold. The scaffolding serves as a docking site for further leukocyte and macrophage infiltration, to remove debris and provide molecular cues which will assist in tissue repair (Popovich and Longbrake, 2008; Perry, 2010). In fact, the density of inflammatory cells at the lesion site has been shown to increase dramatically (Ertürk *et al.*, 2012). Following injury within the CNS, two types of 'scars' are formed; the fibrotic and the glial scar. The non-glial scar is formed, through the interaction of migrating fibroblasts with the infiltrating inflammatory cells, which results in the secretion of ExtraCellular Matrix (ECM) proteins, namely, fibronectin, collagen and laminin. Deposition of these proteins onto the lesion site forms a dense fibrotic scar which seals off the lesion (Fitch and Silver, 2008; Schreiber *et al.*, 2013; Fernández-Klett and Priller, 2014). In addition to fibroblasts, pericytes (which wrap around the endothelial cells that line the capillaries around the body) have also been speculated to be another source for these scar-forming proteins and contribute to the formation a fibrotic scar. Genetic fate mapping revealed that type-A pericytes could give rise to stromal cells, which in turn play a significant role in the ECM and scar formation — blocking the generation of these pericytes through genetic manipulation results in a lesion devoid of a fibronectin scar (Göritz *et al.*, 2011; Dias and Göritz, 2018).

Moreover, astrocytes become hypertrophic where they increase in size and proliferate. They are characterised by a high expression of intermediate filament proteins, namely GFAP, vimentin and nestin (Bignami and Dahl, 1976; Barrett *et al.*, 1981; Yang *et al.*, 1994) . This process is collectively known as reactive astrocytosis - the increased activity of astrocytes is a hallmark of the early response to CNS injury. The recruited astrocytes flush the site of injury and take part in an inflammatory cascade, which leads to the formation of a dense filamentous glial scar around the fibrotic scar that ultimately protects intact neurons from further damage by incoming inflammatory cells (Faulkner, 2004; Cregg *et al.*, 2014). The

phenomenon of reactive astrocytosis is prevalent throughout vertebrate evolution and thus pertains to a survival advantage (Larner *et al.*, 1995). The glial and fibrotic scars persist indefinitely and have been associated with the weak regenerative profile of the CNS.

2.4. The glial scar: A strong candidate of inhibition in the CNS

Astrocytes are the critical regulators of the innate and adaptive immunity of the CNS and provide neuronal structural support. In healthy CNS, astrocytes exhibit a form a physiological excitation through an influx of Ca^{2+} into the intracellular space (Verkhratsky *et al.*, 1998) and subsequent neurotransmitter secretion (Parpura *et al.*, 1994; Bezzi *et al.*, 1998; Schousboe *et al.*, 2014). There is strong evidence to suggest that astrocytes are linked to blood flow regulation (Attwell *et al.*, 2010) as well as synaptic development and function in a tripartite configuration, consisting of the presynaptic and postsynaptic nerve terminals, and the astrocyte (Pfrieger and Barres, 1996, 1997; Araque *et al.*, 1999; Chung *et al.,* 2015). The presence of a glial scar, in the lesion site of the CNS has long been suspected to be the main impediment to regeneration (Cajal, 1928; Luizzi and Lasek, 1987; Rudge and Silver, 1990; Davies *et al.*, 1997) by serving as a physical barrier to axon growth. The astrocytes begin to secrete CSPGs, which are deposited in the ECM at the lesion site and constitute the primary component of the scar (McKeon *et al.,* 1999; Jones *et al.,* 2003a; Tang *et al.,* 2003).

One of the first studies to demonstrate the importance of the glial scar in neuronal regeneration in the CNS was by Davies and colleagues (Davies *et al.*, 1997). They used a microtransplantation technique to inject small dissociated neurons from PNS Dorsal Root Ganglia (DRG), from adult rats, into the white matter of the corpus callosum or the fimbria in adult rats. This procedure, in theory, was atraumatic and minimised glial scarring. The authors used DRG neurons, as they have been previously shown not to regenerate their axons in a CNS environment in rat pups beyond the second postnatal day (Gibson *et al.*, 1984; Carlstedt *et al.*, 1987), and also because their growth has been shown to be inhibited by oligodendrocytes or CNS myelin components (Bandtlow *et al.*, 1990; Kobayashi *et al.*, 1995). Remarkably, they showed that there was considerable long-distance axon growth into the white matter of the corpus callosum. Interestingly, the axons aborted their growth in areas of high proteoglycan content within the ECM. Their reforming work demonstrated, unlike previously thought, that the myelinated white matter of the CNS can be highly permissive to axon growth, given that the axons can bypass and avoid the immediate glial scar inhibitory effect. There is an ongoing need to further understand and manipulate the CNS environment into a creating permissive matrix for axon growth.

A more recent attempt to demonstrate the inhibitory effect of a glial scar produced somewhat conflicting results (Canty *et al.*, 2013). The authors used an exact approach of *in vivo* single-neuron laser-mediated axotomy, which resulted in minimal inflammation, glial scarring and deposition of CSPGs. Surprisingly, the severed axons exhibited minimal growth, and no *de novo* axonal branches could be seen. Interestingly, they revealed that there are some intrinsic differences of different subclasses of neurons in their ability to regenerate. The authors concluded that their data were consistent with the fact that CNS neurons have a limited capacity for growth following injury, even in areas in the CNS with limited myelin effect, such as in the grey matter. They also went on to state that the glial scar might not be the primary reason why regeneration fails in the CNS. Also, for those subsets of neurons that exhibited a small regrowth, synaptic boutons could be seen mirroring the density of pre-axotomized axons. According to the authors, the formation of synaptic boutons implied the existence of an 'intrinsic homeostatic programme' that can regulate synaptic formation in regenerating axons.

In the light of all the available evidence which points towards the central role that the environment holds, it is important to understand how the ECM microenvironment, and all its components, interact during neuronal regeneration, as this might be the key to explain why CNS neuronal regeneration is limited in mammals.

2.5. ECM and its role in CNS injury

It is imperative to start this section off by stating that the ECM is dynamic and exhibits remarkable plasticity in response to development and pathophysiological alterations within the CNS. It follows then that its manipulation holds great promise in how we approach the treatment of neurological disease. The workings of the ECM in the CNS is undoubtedly one of the most fascinating and at the same time enigmatic aspects of modern neurobiology. The ECM is naturally produced and maintained by the cells within it, both neuronal and non-neuronal, and is made up of fibrous proteins (collagen, laminin, fibronectin, and elastin) and a large number of Glycosaminoglycans (GAGs) subdivided into 4 components in ascending order of complexity: (1) hyaluronan, a non-protein bound GAG, (2) CSPGs, (3) link protein which is able to bind hyaluronan and aggrecan and (4) tenascin, an adhesive molecule which associates with fibronectin and laminin (Novak and Kaye, 2000; Galtrey and Fawcett, 2007; Chiquet-Ehrismann and Tucker, 2011; Song and Dityatev, 2018). The integrity and ultimately, the function of the ECM depends on the interaction of these components. Once thought to play a structural role solely, it is now known that the ECM interacts with the diverse cell

population within it and largely determines their function. A brief overview of three of its main components (collagen, laminin and CSPGs) will follow in an attempt to highlight why the composition of the ECM has such a strong influence on the workings of the CNS. The sections describing the ECM components below are by no means exhaustive; a detailed description is beyond the scope of this project. The reader is advised to refer to the references provided for more information.

2.5.1. Collagen

Collagen is one of the most abundant proteins in nature. They are primarily extracellular matrix molecules which form a dense structural network, even though some types of collagens can also be embedded within the cell membrane. Some 49 collagen α-chain gene products have been described thus far, which combine to form at least 29 collagen types. The α-chains form trimeric molecules which fold into a triple helical tertiary structure and are classified into fibrillar and non-fibrillar collagen. In the PNS, collagens have been shown to promote neuronal growth after injury by forming a scaffold-like mesh, that acts as a docking and guiding site for the growth of axons. At the same time, Schwann cells can proliferate and migrate along that scaffold to form structures called the 'bands of Büngner', which help to guide growth cones (the actin-rich axonal extensions of the regenerating neuron), as well as express several growth-promoting factors, including laminins, integrins, NGF, BDNF and GDNF (Lindholm *et al.*, 1987; Chernousov *et al.*, 2008; Goto *et al.*, 2010; Gao *et al.*, 2013). The majority of the collagen expressed by neurons is collagen type I, which has been extensively used in nerve tissue engineering (Prockop and Kivirikko, 1995; Masand *et al.*, 2012; Gao *et al.*, 2013). One of the collagens which has been more extensively studied in its role in regeneration is collagen type IV, which predominantly resides in the Basal Membrane (BM). The BM is a dense network, rich in collagen IV, laminin, nidogen and Heparan Sulfate ProteoGlycans (HSPGs) molecules. In healthy CNS, it is normally found at the interface of the blood-brain barrier and forms a supporting frame for associated proteins and cells to adhere to (Timpl and Dziadek, 1986; Hermanns *et al.*, 2001; Thomsen *et al.*, 2017; Yurchenco and Schittny, 2018). During CNS injury, early studies have demonstrated that a BM ECM is deposited at the lesion core as a part of the scar-forming process (Berry *et al.*, 1983) and it was hypothesised that the depletion of the BM via collagen IV inhibition would improve the regenerative capacity in the CNS. This was confirmed through experiments which involved locally injecting anti-collagen IV antibodies, directing into the lesion site *in vivo* (Stichel *et al.*, 1999). Remarkably, they observed that there was a reduction in BM deposition, followed by a significant increase in axon growth and recovery of function,

measured through the degree of conduciveness, myelination by oligodendrocytes and synapse formation. Similar results were obtained when the biosynthesis of collagen IV was pharmacologically inhibited, with the iron chelator α, α′ dipyridyl (DPY) (Stichel *et al.*, 1999). Conversely, *in vitro* studies have demonstrated that the co-culture of PNS neurons with collagen IV enhances axon growth through an integrin/collagen interaction (Lein *et al.*, 1991). It is important, however, to remember that when it comes to studying the effects of an ECM molecule, *in vitro* work can have substantial limitations since the ECM is a complex interaction of multiple components. Therefore, studying one in isolation might not be a good proxy for neuropathological conditions. Nevertheless, the work mentioned above helped to solidify the ECM, and collagen in particular, as another important 'player', besides the glial scar, in the inhibition of neuronal regeneration.

2.5.2. Laminin

One of the most prominent components of the ECM is laminin, a trimeric protein composed of α, β and γ subunits. Laminin exerts its physiological effects, primarily via the signalling downstream of transmembrane receptors, which are classified as either integrin or non-integrin receptors (discussed further in section 1.5.3). It is involved in a range of biological processes including cell adhesion, cell migration, axon guidance, cell differentiation and neurite outgrowth (Cohen and Johnson, 1991; Garcia *et al.*, 1996; Huang *et al.*, 2003; Miner *et al.*, 2004; Schéele *et al.*, 2007; Barros *et al.,* 2011; Kerstein *et al.*,2015). Evidence shows that is has a strong positive effect in regenerating neurons *in vitro* (Manthorpe *et al.*, 1983; Rogers *et al.*, 1983; Edgar *et al.*, 1984; Calof and Reichardt, 1985; Bates and Meyer, 1997). *In* vivo, laminin correlates with neuronal migration in embryonic and postnatal brains, and similarly to collagen IV, it is also present within the basal membrane (Liesi, 1985). Following neuronal trauma, it is transiently upregulated by astrocytes, but interestingly, under healthy conditions, laminin is continuously expressed by astrocytes in areas of the CNS that can support neuronal regeneration (i.e. olfactory bulb), but not in those which cannot (Liesi, 1985).

2.5.3. Integrins

Integrins are the main cellular receptors for ECM proteins in the CNS, which connect the ECM with the intracellular actin cytoskeleton and regulate several intracellular signalling pathways (Hynes, 2002). They are composed of two subunits; at the time of writing 18 α- and 8 β- subunits have been identified, which assemble into 24 integrin heterodimers (Takada *et al.,* 2007). Different combinations of types of subunits exhibit differential affinity

towards different ECM ligands, namely collagens, laminin and fibronectin (Roca-Cusachs *et al.*, 2012). The integrins have a remarkable capacity to convey bidirectional messages through the cell membrane, either via inside-out or outside-in signalling (Giancotti and Ruoslahti, 1999; Hynes, 2002). Inside-out signalling refers to the fact that ECM ligand binding onto the integrin receptor is largely regulated by the intracellular activity which induces a differential conformation of the receptor. In other words, the cell itself can 'decide' how receptive the integrin receptor can be to external stimuli. In the case of outside-in signalling, ECM ligand binding also induces a conformational change to the receptor, which in turn relays a signal intracellularly. Integrins are highly expressed in developing neurons and in some regions of the brain which have been linked to neuronal plasticity, synaptic stability and axonal growth cone motility (Jones, 1996; Park and Goda, 2016).

2.5.4. CSPGs: Friend or foe?

The CSPG family is a group of molecules, within the ECM of the CNS, which consist of Chondroitin Sulphate-GlycosAminoGlycan chains (CS-GAG) covalently linked to their protein core. It is primarily made up of six proteins: aggrecan, versican, neurocan, and brevican are classified as lecticans, due to the characteristics of their N-terminal and C-terminal domains. Phosphacan is a splice variant of the Receptor-Type Protein Tyrosine Phosphatase (RPTP) which represents its extracellular domain (Maurel *et al.*, 1994). On the other hand, the Neuron-Glial antigen 2 (NG2) is a transmembrane protein even though it can also be secreted into the ECM and does not exhibit any homology to other CSPGs (Nishiyama *et al.*, 1991; Jones *et al.*, 2003a; Galtrey and Fawcett, 2007; Siebert *et al.,* 2014). CSPGs are abundant in both the developing and adult CNS and have been reported to have a wide range of functions (Bandtlow and Zimmermann, 2000; Oohira *et al.*, 2000; Rhodes and Fawcett, 2004; Laabs *et al.*, 2005). They are produced by both neuronal and non-neuronal cells within the CNS.

Deciphering their role in ECM formation and maintenance has long been the 'holy grail' of neurobiology due to their perceived central role as the main inhibitory component of the glial scar. Following CNS injury, CSPGs are upregulated within the glial scar which forms a protective microenvironment that prevents further neuronal damage, while at the same time inhibits regeneration (Jones *et al.*, 2003b; Faulkner, 2004; Myer *et al.*, 2006; Sofroniew, 2009). CSPGs form part of the PeriNeuronal Net (PNN) which encircles neuronal bodies and dendrites (Rhodes and Fawcett, 2004) and has been linked to the protection of neurons from damage as well as inhibition of neural plasticity (Qing-Long *et al.*, 2014; Wen *et al.*, 2018). Dysregulation of the PNN is associated with several CNS-related pathologies (Lorenzl *et al.*,

2003; Yamamori *et al.*, 2013; Rankin-Gee *et al.*, 2015; Lepeta *et al.*, 2017). For example, CSPGs inhibit axon growth, limit neuronal plasticity and disrupt axon guidance (Matsui and Oohira, 2004; Rhodes and Fawcett, 2004; Gilbert *et al.*, 2005; Wang *et al.*, 2008) during CNS injury. More recently, CSPGs have also been shown to suppress the migration of Neural Stem/Progenitor Cells (NSPCs) in a concentration-dependent manner, *in vitro*, which is thought to contribute to the inhibitory effect induced by the CSPGs (Zhong *et al.*, 2019).

Several studies have demonstrated, *in* vitro, how increasing concentrations of immobilised and soluble CSPGs, can have a strong negative effect on neurite outgrowth and axonal growth cone development (Snow *et al.*, 1996; Sherman and Back, 2008; Jin *et al.*, 2018). On the contrary, in studies where the GAG chain was degraded using Chondroitinase ABC (ChABC), an enhanced regenerative potential was observed both *in vitro* (McKeon *et al.,* 1995) and *in vivo* (Bradbury *et al.*, 2002; Pizzorusso *et al.*, 2002; Corvetti, L., Rossi, 2005). A similar effect was also seen when inhibitors of proteoglycan synthesis, namely β-D- xylosides and sodium chlorate, were applied to astrocytic cell lines, DRG neurons were able to extend axonal processes twice the length compared to their control counterparts (Smith-Thomas *et al.*, 1995).

The inhibitory effect of CSPGs on neuronal growth has been suggested to be mediated through the interaction of the CS-GAG chains with the transmembrane receptors Protein Tyrosine Phosphatase, (PTPσ), Leukocyte common Antigen-Related (LAR) and the Nogo Receptors (NgR) 1 and 3 (Shen *et al.*, 2009; Fisher *et al.*, 2011; Dickendesher *et al.*, 2012). Regenerating axons have been shown to become immobilised within CSPG-rich regions of a lesion site, through the interaction with PTPσ, which leads to growth cone collapse and development of axonal dystrophy (Cajal, 1928; Lang *et al.*, 2015; Rauvala *et al.*, 2017). The interaction of CSPGs with either PTPσ or LAR has been demonstrated to initiate an inhibitory intracellular cascade that is mediated via the RhoA, Akt/mTOR, Erk and ACTN4 signalling pathways (Monnier *et al.*, 2003; Ohtake *et al.*, 2016; Zhong *et al.*, 2019).

The notion that the interaction of CSPGs with their receptors can initiate an inhibitory cascade has led to the hypothesis that when this interaction is blocked, then the inhibitory effect could be reversed. To this end, several studies have been conducted where PTPσ was specifically targeted. Pharmacological modulation of the receptor using a PTPσ antagonist termed Intracellular Sigma Peptide (ISP), restored serotonergic innervation to the injured spinal cord in mice, which lead to an improvement in functional outputs in locomotor and urinary systems (Lang *et al.*, 2015). Also, sympathetic neuronal regeneration was observed

in mice following cardiac infarction after the administration of ISP (Gardner *et al.*, 2015). More recently, the use of ISP as a potential therapeutic was explored further, which, similarly to earlier studies, showed that systemic administration of the PTPσ antagonist resulted in an enhanced innervation of serotonergic fibres (Rink *et al.*, 2018) and an increase in sensory axon regeneration accompanied with functional recovery (Yao *et al.*, 2019), in a rat damaged spinal cord injury model. The authors argued that the ISP administration could potentially hold promise in the clinic as well. Genetic abrogation of the PTPσ receptor yielded similar results, where enhanced neuronal regeneration was observed both *in vitro* and *in vivo,* even in CSPG-rich areas of the CNS (Shen *et al.*, 2009).

Moreover, despite the production of synthetic molecules, like ISP, which can block the CSPG/PTPσ binding, an endogenous molecule called HB-GAM/pleiotrophin was discovered and has also been shown to interfere with the interaction above (Paveliev *et al.*, 2016; Rauvala *et al.*, 2017). HB-GAM/pleiotrophin is a heparin-binding protein that is secreted by neurons and glial cells and has been shown to bind to CSPGs. It was initially identified in the rat perinatal brain and was shown to be associated with axon and dendrite sprouting (Rauvala, 1989; Merenmies and Rauvala, 1990a). It was subsequently demonstrated to promote cell proliferation and neuronal growth (Li *et al.*, 1990). Furthermore, cultured CNS neurons were able to overcome the inhibitory effect of both aggrecan and neurocan, but only when HB-GAM was added into the culture medium or when it was pre-coated with the CPSGs (Paveliev *et al.*, 2016). The authors used ChABC to demonstrate that HB-GAM binds to and effectively hides the CS chains of CSPGs. They also noted that when the CS chains are digested, the neuronal growth-promoting effect of HB-GAM, is effectively abolished; questioning whether CSPGs can truly be perceived as inhibitory. It is therefore important to acknowledge that, given the right conditions, the CSPGs effect can be reversed from being inhibitory to being growth-promoting. Lastly, HB-GAM was shown to interact with the neuronal cell surface receptor glypican-2, which ultimately prevents the interaction of CSPGs with PTPσ and promotes neuronal growth (Figure 2.1). The neuroregeneration-promoting effect of HB-GAM has also been confirmed *in vivo*, where the protein was injected locally into injured regions of the cerebral cortex (Paveliev *et al.*, 2016; Rauvala *et al.*, 2017). In recent studies, a peptide which specifically binds to Chondroitin-4-Sulphate (C4S) was identified. Similarly, the binding of CSPGs to HB-GAM was shown to reverse the inhibitory effects of C4S and promoted neurite outgrowth *in vitro* (Loers *et al.*, 2019).

The inhibitory effect of CSPGs is relative and cannot be quantified in absolute terms. *In vitro* studies have shown a molecular 'tug-of-war' between growth-permissive substrates

expressed by astrocytes, and CSPGs (Tom *et al.*, 2004). Tom et al., developed an *in vitro* model of a glial scar, through which they were able to show that the balance between concentration gradients of laminin and aggrecan are crucial for neuronal growth. This is consistent with observations that during CNS injury, inhibitory components of the ECM are

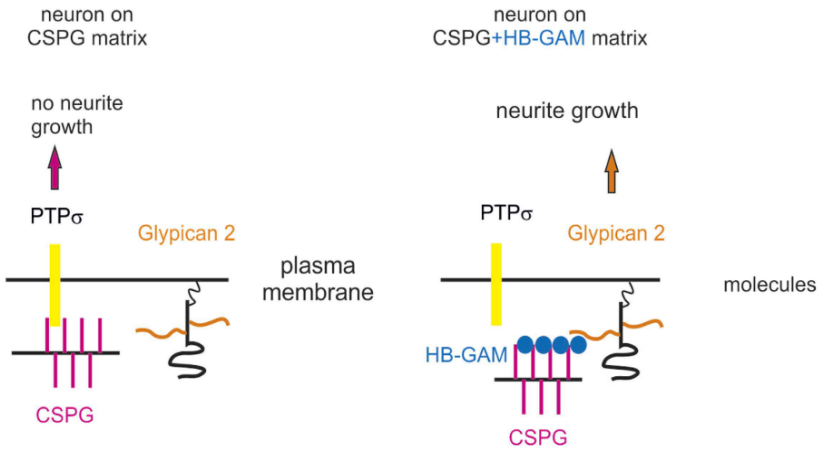

Figure 2.1 Proposed mechanism by which HB-GAM promotes neurite outgrowth. HB-GAM can bind to CSPGs and block its interaction with PTPσ, leading to a disinhibition effect for neuronal growth. At the same time HB-GAM can bind to glypican-2 on the neuronal surface, through which it can actively promote neuronal growth. *CSPGs; Chondroitin Sulphate Proteoglycans, HB-GAM; pleiotrophin. Adapted from Paveliev et al. 2016*

upregulated to such an extent that they are able to mask the effect of growth permissive laminin, which is expressed by astrocytes (McKeon *et al.*, 1991; Sun *et al.*, 2017). Consistent with their findings, studies have shown that during CNS injury damaged axons become dystrophic and dieback away from the inflammatory cell-filled space, and have been postulated to be entrapped in the lesion site by NG2, a member of the CSPG family (Filous *et al.*, 2014; Ruschel *et al.*, 2015). Interestingly, the damaged axons dieback further in NG2 knockout mice, which suggests that CSPGs can also be growth-promoting (Filous *et al.*, 2014). The interaction between PTPσ and CSPG is believed to be the key in creating an adhesive environment from which growing axons cannot escape (Lang *et al.*, 2015).

There is strong evidence that CSPGs and the glial scar are inhibitory to regeneration in the mammalian CNS. Even though this statement has been widely accepted as valid, recently it has been the subject of controversy. Within this context, there is evidence which challenges this predominant conception amongst the scientific community. Increased synthesis of CSPGs has been linked to neurogenesis in the hippocampus, whereas depletion of CSPGs caused cognitive memory impairment in adult mice (Yamada *et al.*, 2018). Additionally, Anderson et al. used transgenic mice, in which the capacity to form a glial scar was

eliminated, either by the targeted killing of astrocytes or by inhibiting the STAT3 proliferative signalling of astrocytes. They showed that in the absence of a glial scar not only was there no significant growth of sensory, corticospinal or serotonergic neurons following spinal cord injury, but also there was an increase in axon dieback from the lesion centre (Anderson *et al.*, 2016), which agrees with previous findings as described above (Filous *et al.*, 2014). The authors also discovered that the glial scar itself is required to promote axon growth when axon-specific growth factors are introduced, via a hydrogel, into the lesion site. Lastly, they showed that in the transgenic mice, scar-forming astrocytes are not the primary source of CSPGs within the glial scar, since there was no change in CSPG expression. Their experimental design, assumptions and conclusions, however, have been strongly challenged (Silver, 2016). Nevertheless, what Anderson et al. have demonstrated is that abolishing the astrocytic glial scar alone is not sufficient to create a permissive environment for neuronal growth in the CNS. In summary, there is conflicting evidence regarding the importance of the glial scar, and consequently CSPGs, in the inhibition of CNS regeneration, even though the consensus leans heavily towards the strong inhibitory effect of these components.

2.5.5. ECM remodelling and metalloproteases

The main focus thus far, has revolved around the importance of the extrinsic environment of neuronal cells in regeneration, through the active role of the extracellular matrix and its diverse array of components. All ECM components, including laminins, fibronectin, collagens and CSPGs, can be subjected to proteolytic degradation (Wee Yong *et al.*, 2002; Mott and Werb, 2004). This section will focus on the way the ECM can be remodelled or reorganised by proteases to enhance neuronal regeneration. The capacity of proteases to digest large insoluble proteins within the ECM, as well as ECM-linked proteins, is the cornerstone of transforming the ECM into a dynamic and biologically active environment. The main focus will be on two of the best-researched metalloproteases in particular, namely Matrix Metalloproteases (MMPs) and A Disintegrin and Metalloproteases (ADAMs). These proteins belong to the metzincin family of metalloproteases, which bind a zinc ion in their active site and have been shown to digest a wide range of ECM molecules (Yong, 2005). Metalloproteases were once thought to regulate and enhance neuronal regeneration by opening up a passage for the growing axons within the ECM and the developing scar. It is known, through recent studies, that these proteases do not simply serve as ubiquitous molecular scissors, but rather interact with specific ligands in the ECM, as well as receptors on neurons and growth cones, to orchestrate neuronal migration and axon growth (Löffek *et al.*, 2011; Myers *et al.*, 2011).

2.5.5.1. MMPs

There are, to date, 24 known mammalian MMPs which are mainly secreted from neuronal and non-neuronal cells but can also be found embedded within the cell membrane. They have been extensively studied for their role in revealing the hidden biological regulatory potential of the ECM. For example, the Vascular Endothelial Growth Factor (VEGF), a potent neuroregeneration-promoting molecule (Hobson *et al.*, 2000; Theis and Theiss, 2018) interacts with Heparan Sulphate Proteoglycans (HSPGs), which are highly expressed in the ECM, and limits its bioavailability. MMP9 is the metalloprotease which can free VEGF from that interaction in the ECM and induce its biological activity (Bergers *et al.*, 2000). Moreover, the Transforming Growth Factor β (TGFβ) is a pleiotropic cytokine which plays a significant role in a range of biological processes, including cell differentiation and proliferation, embryonic development, ECM remodelling and neuronal regeneration (Massagué, 2012; Li *et al.*, 2017). When secreted in the ECM, TGFβ is trapped in a dormant state through the interaction with the Latency-Associated Peptide (LAP) the Latent TGFβ Binding Protein (LTBP). Again, the MMPs can cleave that binding and detach LAP and LTBP from TGFβ, and in effect activate it (Yu and Stamenkovic, 2000; D'Angelo *et al.*, 2001; Dallas *et al.*, 2002; Maeda *et al.*, 2002; Mu *et al.*, 2002). Dysregulation of TGFβ signalling is thought to contribute to Marfan syndrome (Neptune *et al.*, 2003) and bipolar disorder (Balcioglu *et al.*, 2017). Interestingly, another protease which is involved in ECM remodelling is Bone Morphogenetic Protein 1 (BMP1). It too has been demonstrated to aid in the activation of TGFβ by cleaving the interaction between LTBP and TGFβ (Mott and Werb, 2004; Ge and Greenspan, 2006; Vadon-Le Goff *et al.*, 2015; Muir *et al.*, 2016).

Several studies have demonstrated that the presence of MMPs *in vitro* can induce neuronal growth. First, in PC12 neuronal cell cultures, MMP9 has been shown to increase the expression of phosphorylated NeuroFilament M (NFM-p), a marker for neuronal regeneration and axon growth (Shubayev and Myers, 2004). Early studies with Dorsal Root Ganglion (DRG) neurons which were cultured in a 3-D gel matrix of ECM components, containing laminin and collagen type IV, were shown to overcome its growth retarding effects through the secretion of MMPs. Also, selective inhibition of the MMP release resulted in the abrogation of that effect (Muir, 1994). In a similar experiment where laminin and CSPGs were used as constituents of the matrix, the use of recombinant MMP-2, similarly to the use of chondroitinase, enhanced DRG neuronal growth, by degrading the inhibitory CSPGs (Zuo *et al.*, 1998), a process referred to as disinhibition. Along the same lines, Cua and colleagues cultured primary mouse cortical neurons on an astrocyte-derived ECM and also

on purified CSPG substrate mixture consisting of aggrecan, neurocan, phosphacan and versican. Neurite outgrowth was observed only when co-cultured with selected MMPs and ADAMs (Cua *et al.*, 2013). These findings provide additional layers of evidence that firstly, confirm the inhibitory role of CSPGs and secondly, that MMPs have the capacity to remodel the ECM through selective digestion of its inhibitory components.

Subsequent studies have confirmed the role of MMP-2, as well as MMP-9, in enhancing neonatal and adult DRG neuronal growth (Ferguson and Muir, 2000). Additionally, in experiments where DRG neurons were cultured in 3D synthetic hydrogels, made of a PEGylated fibrinogen matrix, the neurons failed to grow in the presence of MMP-2 or MMP-9 inhibitors (Sarig-Nadir and Seliktar, 2010). Interestingly, the positive effects of MMPs have been suggested not to be universal across the entire family, since MMP-3 was not demonstrated to exhibit a similar growth-promoting effect (Ferguson and Muir, 2000), even though there is conflicting evidence which suggests that MMP-3 can also have, to a lesser extent, a role in axon growth (Nordstrom *et al.*, 1995; Sarig-Nadir and Seliktar, 2010).

As mentioned above, these studies helped to shape the misconception that MMPs are solely effective by carving their way through a matrix, a path through which axons can grow into, similar to how a train moves through a tunnel. There is a large body of evidence which suggests that the above statement does not do justice to the importance of MMPs and metalloproteases in general in a neuroregenerative context. In addition to the ECM, there are several other types of substrates which MMPs can interact with, including growth factors, adhesion molecules and receptors, through which they regulate a range of biological processes (McCawley and Matrisian, 2001; Sternlicht and Werb, 2001; Yong, 2005). MMPs have been shown to act as axon-guiding molecules *in vivo*. This was demonstrated through the pharmacological inhibition of MMPs in *Xenopus laevis* embryos, which caused axonal guidance defects on retinal ganglion cells, at the optic chiasm (Webber *et al.*, 2002; Hehr *et al.*, 2005). Also, MMPs have been shown to bind to integrin receptors and have been discovered to cleave the interaction between integrins and ECM proteins, thereby detaching them from the substratum leading to apoptosis, a process called anoikis ('homelessness') (Dumin *et al.*, 2001; Yong, 2005). It follows that overexpression of specific subsets of MMPs in the ECM can have detrimental effects on cell survival and neuronal regeneration. Consistent with this notion is the fact that MMP-9 deficiency in mice has been linked, following injury, to a reduced level of apoptosis in retinal ganglion neurons (Chintala *et al.*, 2002).

The process of efficient remyelination is a prerequisite for successful neuronal regeneration following neuronal injury. Because myelination by oligodendrocytes in the CNS demands for several branches to be formed and forge connections with regenerating axons, it has long been speculated that ECM remodelling has to take place to facilitate this. *In vitro* studies have shown that the ability of oligodendrocytes to form these extending branches is severely impaired in MMP-9 deficient mice (Oh *et al.*, 1999). Further *in vivo* studies focussing on MMP-9 employed a spinal cord model in adult mice, in which the myelin was disrupted using lysolecithin (Larsen *et al.*, 2003). Interestingly, using this model, the authors observed a decrease in remyelination efficiency in mice which were MMP-9 deficient. Additionally, it is not surprising that the authors suggested that MMP-9 serves as a protease for the digestion and processing of NG2 (CSPG4), a potent inhibitor of regeneration and oligodendrocyte differentiation.

Due to the similarity of the different types of MMPs and other proteases, it is often difficult to differentiate between specific members of the family using standard pharmacological inhibitors. For this reason, a more reliable way to look at the effects of the individual proteins would be to study specific knockouts; the review by Yong provides a comprehensive overview of knockout studies, which have revealed both beneficial as well as unfavourable outcomes when specific MMPs were eliminated (Yong, 2005, see Table 1).

Despite the positive effects of MMPs, there is evidence to suggest that they can also be the source of considerable damage to developing and adult neurons. They have been negatively associated with BBB dysfunction, stroke, neurotoxicity, multiple sclerosis and in some cases, neurogenesis (Yong, 2005). Due to the detrimental effects that MMPs can induce, their activity is very tightly regulated. First, MMPs are initially translated as zymogens, the inactive form of the enzyme, which requires cleavage to expose their catalytic domain. Second, their levels are controlled through stringent transcription processes (only expressed when needed and notably baseline levels of expression are low) and post-translational modifications. Lastly, physiological inhibitors ensure that the activity of MMPs does not exceed the required amount to induce a physiological benefit. Nevertheless, an interesting question is how can the same group of proteins, even the same type of MMPs, have such a strong effect on the opposite side of the spectrum? It is extremely likely that MMPs effect on regeneration is largely dependent not only on the type of protease but also on the concentration at which it operates. Also, the type of neuronal injury can also have an effect, due to the range of inflammatory cells that flood the site of injury. (Yong, 2005; Löffek *et al.*, 2011). This could be one of the reasons why the CNS is less equipped to repair neuronal damage. Even though

MMPs have been proven to be beneficial, the potential overexpression of these proteins can do more harm than good.

2.5.5.2. ADAMs

The ADAM family belongs to another class of metalloproteases called adamalysins, a family comprised of more than 30 members, of which only half are proteolytically active. ADAMs are transmembrane proteins, and compared to the MMPs, have additional features in their protein core structure, including a disintegrin domain, a cysteine-rich domain, an Epidermal Growth Factor (EGF)-like domain and a cytoplasmic tail (Yong, 2005). Each of these domains has developed specialised functions, through which ADAMs can regulate cell-cell interactions, cell-ECM interactions as well as induce ECM remodelling through selective digestion of ECM components. The disintegrin domain of ADAMs serves to mediate cell-cell interaction through the binding to integrin receptors (Blobel *et al.*, 1992; White, 2003). The cysteine-rich domain, also called the adhesive domain, has been shown to bind syndecan proteoglycans and complement the binding of the disintegrin domain. This was demonstrated in studies using recombinant ADAM12 and transfected syndecan substrates on cancerous and non-cancerous cell lines (Iba *et al.*, 1999, 2000). Recombinantly expressed disintegrin and cysteine-rich domains of ADAM13 have been shown to bind to a specific domain on fibronectin, which under normal conditions interacts with syndecans (Gaultier *et al.*, 2002). All ADAMs exert a proteolytic effect on their substrates through their metalloprotease domain, which has positioned these proteins as a key component of ECM remodelling. It is well established that syndecans and integrins work in unison to firmly adhere to the ECM and form strong cell-matrix interactions (Rapraeger, 2001). Since ADAMs can interact with both integrins and syndecans via their disintegrin and cysteine-rich domains respectively, it has been postulated that this would uncouple the binding and thus enable the cleavage of ECM proteins (White, 2003). Furthermore, ADAM10, ADAM12 and ADAM13 all have the capacity to degrade the ECM components collagen IV and fibronectin (Alfandari *et al.*, 2001; Roy *et al.*, 2004); a feature which has been linked to the *Xenopus* Cranial Neural Crest (CNC) cell migration along predefined paths, as shown in studies with ADAM13 (Alfandari *et al.*, 2001; Alfandari and Taneyhill, 2018).

Moreover, the best-known function of ADAM proteins, which has gathered significant research interest in the last 15 years, is the proteolytic cleavage of the ectodomains on precursor proteins which are anchored onto the cell membrane, via a process called ‘ectodomain shedding'. The cleavage of these domains can then activate said proteins, which are released into the ECM and in turn regulate the signalling in a diverse range of pathways

(Seals and Courtneidge, 2003; Scharfenberg *et al.*, 2019). Due to their role in shedding the ectodomain of other proteins, they are often referred to as 'sheddases'. Cell migration and proliferation are limited mainly by the interactions with extracellular structural components, as well as by the interactions with neighbouring cells. One of the glycoproteins which mediate this interaction is E-cadherin, a transmembrane Cell Adhesion Molecule (CAM) that binds with other cadherins on adjacent cells to form calcium-dependent adherens junctions. ADAM-10 has been shown to promote cell migration and regulate cell-cell adhesion both *in vitro* and *in vivo* through β-catenin intracellular signalling, by cleaving the E-cadherin ectodomain (Maretzky *et al.*, 2005).

ECM remodelling by proteases has long been speculated to be a deciding factor in the repair of damaged neurons. ADAMs have consistently demonstrated to play a significant part in establishing a permissive environment for growing axons and that they are at the forefront of multifaceted cell signalling cascades that ultimately promote neuronal regeneration. ADAM17/TACE (the tumour necrosis factor-α-converting enzyme) has been recently shown to cleave the Neurotrophic Factor Neuregulin 1 (NRG1), a protein which regulates neuronal development via the activation of the Protein Kinase C (PKC) signalling pathway (Iwakura *et al.*, 2017). The role of G-Protein Coupled Receptors (GPCR), and PKC signalling has previously been linked to the activation of the Epidermal Growth Factor Receptor (EGFR) via ADAM10 and ADAM17-mediated shedding of EGFR ligands (Prenzel *et al.*, 1999; Yan *et al.,* 2002). *In vivo* work on postnatal transgenic mouse models of cuprizone-induced demyelination, revealed that ADAM17 loss of function could delay oligodendrocyte regeneration and subsequent CNS remyelination (Palazuelos *et al.*, 2015). Consistent with previous observations that EGFR and ADAMs could be inherently linked, the authors bypassed ADAM-mediated activation of EGFR in ADAM17 deficient mice, through overexpression of the receptor by genetic manipulation, and demonstrated that they could restore normal oligodendrogenesis and CNS remyelination. There are several lines of evidence which have convincingly revealed that the shedding of EGFR ligands (Transforming Growth Factor (TGF), heparin-binding EGF; HB-EGF and amphiregulin) via ADAM-mediated processing, actively regulates EGFR signalling (see reviews by White, 2003; Blobel, 2005 and original references therein).

Furthermore, studies on *Drosophila melanogaster* have demonstrated that ADAM10/Kuzbanian defects can have detrimental effects on axon pathfinding and neuronal development (Fambrough *et al.*, 1996; Rooke *et al.*, 1996). This coincides with the fact that ADAM10 can also cleave ephrin; an axon guidance molecule, resulting in termination of

ephrin-mediated signalling on the growth cone (Hattori *et al.,* 2000). Moreover, the Notch pathway, which is an established pathway of neurogenesis, is also a target for ADAM-mediated shedding, where both the Notch receptor and its ligand Delta can act as substrates (Rooke *et al.*, 1996; Ma *et al.*, 2013). In Alzheimer's Disease (AD), ADAM10 has been proposed as a potential therapeutic against this neurodegenerative condition, as it can cleave Amyloid Precursor Protein (APP) aggregates; the root cause of pathogenesis in AD (Lichtenthaler, 2012; Peron *et al.*, 2018).

Additionally, besides the shedding of the substrates discussed above, collectively referred to as the sheddome, there is sufficient evidence to suggest that ADAMs themselves can be the subject of proteolytic cleavage by ADAM sheddases. Both ADAM10 and ADAM17 can be cleaved and secreted into the ECM by ADAM9 (Parkin and Harris, 2009) and ADAM8 (Scharfenberg *et al.*, 2019), respectively. This can have a plethora of implications, such as long-distance signalling and a more extensive range of substrates that can be targeted by the shedded ADAM ectodomains. Indeed, the latter has been demonstrated by Scharfenberg and colleagues, where they recorded 134 incidents of proteolytic cleavage by the soluble ectodomains of ADAM10 and ADAM17, of which 45 substrates appear to be a target for both (Scharfenberg *et al.*, 2019).

As previously discussed, the ECM is a dynamic milieu of molecules whose composition varies according to the stage of CNS development or injury, which is especially true in terms of CSPG levels (Milev *et al.*, 1998). There is not sufficient information to decipher the exact mechanisms by which the turnover of these molecules is regulated in the ECM. Nevertheless, the ADAM family of proteases has been hypothesised to play a role. There is a sub-category within the ADAM family, which has an additional domain with thrombospondin-like motifs as a core structural component. They are highly active collagen and CSPG proteases (Porter *et al.*, 2005) and thereby are able to reorganise the structure of the Perineuronal Net (PNN) and the ECM. However, unlike ADAMs, they lack a transmembrane domain (Tang and Hong, 1999; Rivera *et al.*, 2010). ADAMTSs are expressed throughout the mammalian CNS, of which ADAMTS4 exhibits the highest expression. ADAMTS1, 4, 5 and 9 are upregulated following SCI in mice (Demircan *et al.*, 2013; Gottschall and Howell, 2015), leading to enhanced digestion of CSPGs which is thought to contribute to the inhibitory deposition of CSPG fragments in the glial scar. However, it seems that ADAMTS4 can also have a beneficial role in functional recovery following SCI *in vivo*, as well as *in vitro*. Local administration of exogenous ADAMTS4 promoted axonal growth and functional recovery through the degradation CSPGs, analogous to the effects exerted by ChABC (Tauchi *et al.*, 2012). The

discrepancy between the fact that ADAMTS4 is upregulated following SCI and that it induces a neuroregenerative outcome can be attributed to the relative amounts of ADAMTS4 present at the site of neurotrauma and also to additional components, which might accompany its expression that can potentially mask its beneficial effect. In other words, the concentration of ADAMTS4 following CNS injury might not be sufficient to overcome the inhibitory barriers imposed by other ECM components.

It is therefore necessary, to revisit the idea that ECM components can likely both exert physiological benefits as well as impose physiological hindrances. To this end, in a neuroregenerative context, one can argue that similarly to the mantra that has been used in toxicological studies which states that the 'concentration makes the poison', the concentration at which proteases act upon the ECM and on neighbouring cells can also be the key in establishing a permissive environment to neuronal regeneration.

2.6. Metals and neuronal regeneration

Based on the above, the importance of metalloproteases in regulating ECM components and how they can have an impact on neuronal regeneration is apparent, namely the function of these proteins is highly dependent on the binding with metal ions. The role of metals, however, in healthy and damaged neuronal tissues remains poorly understood. Here, some of the research conducted on the roles of metals in normal neuronal function, regeneration and in neurodegenerative disorders is briefly summarised. The following section will focus on iron (Fe), zinc (Zn) and calcium (Ca).

2.6.1. Iron

A common theme within this introduction has been the notion that some players during neuronal regeneration appear to exert positive and negative effects in regulating this process, and iron is no exception.

Iron is a key element for healthy cell function, as it can serve as either an electron donor or electron acceptor, which makes it highly reactive as a cofactor in oxygen metabolism and subsequent ATP production. In the CNS, iron is an integral part of the enzymes that synthesise neurotransmitters, namely dopamine, noradrenaline, GABA and serotonin. Iron deficiency impairs the synthesis of these neurotransmitters (Lehmann and Heinrich, 1986; Shukla *et al.*, 1989; Hidalgo and Núñez, 2007; Unger *et al.*, 2007; Hare *et al.*, 2013). Oligodendrocytes are also rich in iron, whose myelinating function is tightly regulated by normal levels of the metal. Iron deficiency in both animal models and humans, leads to a

severe hypomyelination phenotype (Ortiz *et al.*, 2004; Lozoff *et al.*, 2006; Badaracco *et al.*, 2008; Todorich *et al.*, 2009) which is indicative of the high energy demand in oligodendrocytes activity, in order to maintain normal levels of myelination in the CNS (Bartzokis, 2002). Additionally, iron accumulation and myelin breakdown have both been suggested as possible causal factors in the early onset of Huntington's Disease (HD) (Bartzokis *et al.*, 2007). Interestingly, loss of the transferrin receptor in transgenic mice leads to a decrease in intracellular iron uptake, which ultimately results in iron deficiency. Research conducted on dopaminergic neurons with these iron-deficient models demonstrated severe neuronal degeneration and impaired motor function (Matak *et al.*, 2016).

Iron has also been extensively studied for its role in cognitive functions. In humans, anaemia-related iron deficiency appears to negatively impact the ability of infants to perform well in mental tests (Lazoff *et al.*, 1996). Indeed, it is now universally accepted that Brain Iron Deficiency (BID) is associated with cognitive impairment and poor mental state in infants (Palti *et al.*, 1985; Lozoff *et al.*, 1991; Hurtado *et al.*, 1999). The same is true about animal models of iron deficiency. BID in rats has been shown to cause a reduction in the ability of these animals to learn, as indicated by water maze experiments (Yehuda *et al.,* 1986) and by studies done on hippocampus neuronal activity (Jorgenson *et al.,* 2003; Jorgenson *et al.*, 2005; McEchron *et al.*, 2005). Even though there is an established link between iron deficiency and neuronal function, the biological mechanisms by which iron exerts its regulatory effect has largely been elusive. There are some studies, however, on synaptic plasticity, which have hinted on a co-operative role of iron and calcium in the activation of the ERK pathway (Serrano and Klann, 2004; Hidalgo *et al.*, 2006; Muñoz *et al.*, 2006; Kemmerling *et al.*, 2007).

Conversely, because of its strong reactivity, in cases when the intracellular iron load becomes too high, it can be extremely damaging to cells. Free iron takes part in the Fenton/Haber-Weiss reaction, through which Fe^{2+} interacts with hydrogen peroxide to produce free oxygen radicals, thus increasing Reactive Oxygen Species (ROS), which eventually leads to oxidative stress and cell damage (Kruszewski, 2003). Indeed, elevated levels of intracellular iron have been shown to be extremely toxic to both neuronal cells and oligodendrocytes *in vitro* (Kress *et al.*, 2002). In the CNS following injury, astrocytes are the primary defence against iron toxicity, as they employ free radical scavengers, such as catalase, superoxide dismutase, and glutathione peroxidase (Liddell *et al.*, 2004; Kudin *et al.*, 2012). The brain is particularly vulnerable to damage by oxidative stress, as it exhibits an extremely high metabolic activity, and thus requires high amounts of ATP, a process that increases the probability of free radical

generation (Bélanger *et al.*, 2011). For this reason, it is imperative that iron levels always remain under normal physiological levels. Iron homeostasis controls the bioavailability of iron, which is vital for the normal function of neuronal systems. It is regulated via the joint action of (1) the iron chaperone protein transferrin and its receptor which transports iron into the cell, (2) divalent metal transporters that assist iron uptake (e.g. DMT1), (3) transmembrane iron-exporter proteins which carry excess iron outside of the cell, namely ferroportin and (4) the intracellular iron storage protein ferritin (Ashraf *et al.*, 2018; Lumsden *et al.*, 2018). Excessive iron levels have been linked to the biochemical process of ageing and apoptosis, as well as in neurodegenerative disorders. Excessive accumulation of iron is a hallmark of ageing as indicated by elevated levels of ferritin (Connor *et al.*, 1992; Zecca *et al.*, 2004). Recently, it has been shown to accelerate the ageing process, by inducing DNA damage (Mollet *et al.*, 2016) and there is also evidence suggesting that excessive iron can interfere with p53-mediated DNA repair mechanisms (Shen *et al.*, 2014). Interestingly, post-mortem analysis of ageing brains in humans demonstrated a compromised iron homeostatic regulation and an elevation of iron in specific areas of the brain and subsets of CNS components (Hallgren and Sourander, 1958; Connor *et al.*, 1990, 1992, 1995; Hebbrecht *et al.*, 1999; Ramos *et al.*, 2014; Ward *et al.*, 2014). Also, early studies carried out on *Drosophila* demonstrated that iron accumulation was directly proportional to the degree of ageing (Massie, Aiello and Williams, 1985) and inversely proportional to their life span (Massie *et al.*, 1993). On the contrary, *in* vitro studies have demonstrated that iron homeostasis is thought to be disrupted as a result of the ageing process, rather than cause it (Killilea *et al.*, 2004). Nevertheless, the failure of the neuronal system to control iron influx in the cell has been deemed as one of the contributors to neuronal pathologies (Ward *et al.*, 2014). Elevated levels of iron and oxidative stress have been identified in neurodegenerative diseases such as PD, AD and Multiple Sclerosis (MS) and are now deemed as reliable neurodegenerative markers (Bartzokis *et al.*, 2000; Wagner *et al.*, 2003; Zecca *et al.*, 2006; Ropele *et al.*, 2011; Sian-Hülsmann *et al.*, 2011; Sfera *et al.*, 2018).

One of the ways that excessive iron is thought to exert its toxic effects is through regulated cell-death. Recently, a novel type of iron-dependent cell death has been identified in neuronal systems, called ferroptosis (Dixon *et al.*, 2012). Classical apoptotic mechanisms primarily involve the expression of caspases and mitochondrial cytochrome c release. Ferroptosis appears to be biochemically distinct and is taking place independently of classical apoptotic mediators. Instead, it is characterised by the peroxidation of PolyUnsaturated long-chain Fatty Acids (PUFAs), which is caused by iron-dependent generation of ROS

through the Fenton reaction (Figure 2.2). Neuronal systems are characterised by high amount of PUFAs and as such the dysregulation of these lipids can have detrimental effects on healthy neurophysiology (Bazinet and Laye, 2014). Even though, there is still limited information on how this non-apoptotic cell death is regulated, it has been suggested it involves the dysregulation of the cysteine/glutamate antiporter (system x_c^-), which leads to the depletion of glutathione (GSH) within the cell, a peptide that serves as a co-substrate for Glutathione Peroxidase 4 (GPX4); an antioxidant enzyme that can repair oxidised

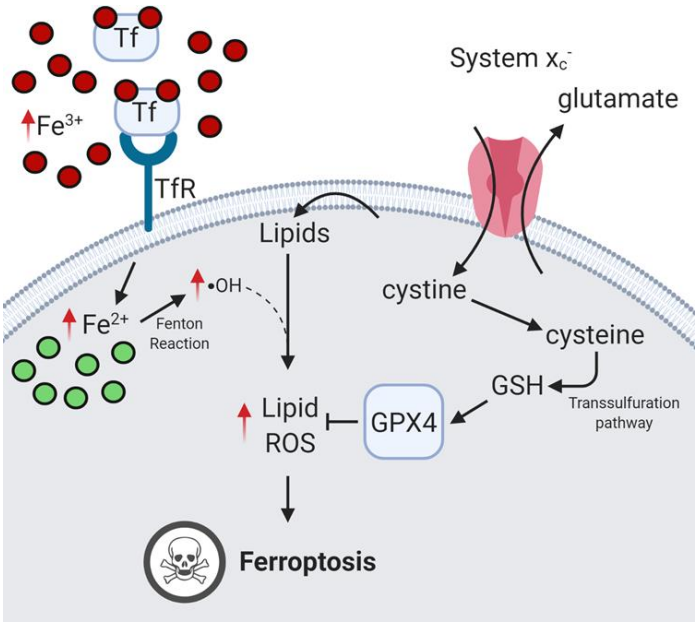

Figure 2.2 Ferroptosis as a non-classical mode of cell death. Excessive circulating ferric iron (Fe^{3+}) bound to transferrin (Tf) is transported into cells via Tf receptors (TfR). When inside the cell, Fe^{3+} is reduced to ferrous iron (Fe^{2+}) and as such the potential of generating free radicals via the Fenton reaction is increased. In turn, the free radicals generated, can oxidise lipids situated on the plasma membrane creating lipid Reactive Oxygen Species (ROS). Conversely, System x_c^- is involved in transporting intracellular glutamate into the extracellular space and cystine from the extracellular space into the cell. Cystine is broken down to cysteine and in turn converted to glutathione (GSH), via the Transsulfuration pathway, a tripeptide that serves as a co-substrate for glutathione peroxidase 4 (GPX4). GPX4 has the capacity to lessen the effects of lipids ROS. Dysregulation of System x_c^- in conjunction with high levels of iron, can lead to ferroptosis and cell death.

phospholipids. Therefore, the diminished activity of GPX4, results in the accumulation of the oxidised phospholipids which renders the cell vulnerable to oxidising damage and eventually, death. Even though it has been confirmed that the process is iron-dependent, the specific contribution of iron in this process is yet to be deciphered (Dixon *et al.*, 2012; Yang and Stockwell, 2016; Angeli *et al.*, 2017; Cardoso *et al.*, 2017). Since the discovery of this novel non-apoptotic cell death phenomenon, ferroptosis has been linked to neurodegeneration

(Chen *et al.*, 2015) and neurodegenerative diseases including, PD (Do Van *et al.*, 2016) and Periventricular Leukomalacia (PVL) (Inder *et al.*, 2002).

Moreover, searching for studies that specifically investigated iron levels in damaged axons, it was surprising to see that there is limited information in the literature regarding the uptake of iron in neurons following axon damage and a potential inhibitory role this might have in regenerative potential. Nevertheless, two studies provide some evidence to suggest that iron levels can play a role in the response of CNS and peripheral neurons to injury, namely where both iron and ferritin receptors were shown to be elevated in the cell body of motor neurons and the sciatic nerve in rats, following injury (Graeber *et al.*, 1989; Raivich *et al.*, 1991). The exact role of the uptake of iron in these experiments, during neurite regeneration, has yet to be adequately explained.

It is now evident that neurons and the workings of the CNS are intricate pieces of machinery that depend on homeostatic regulation, for a wide range of components, in order to ensure healthy function. Iron appears to be one of those substances which can lead to alterations in the normal activity of neuronal systems, equally when deficient or in excess.

2.6.2. Zinc

Zinc is another example of bimodal action, a classical *tug-of-war* in terms of concentration and effect. It is an essential heavy metal micronutrient and is an indispensable component of metalloproteins involved in DNA transcription, catalytic reactions and several signalling cascades (Berg, 1990; McCall *et al.*, 2000; Lee, 2018). Zinc can exist either as protein-bound, in an exchangeable reactive pool, or as free Zn^{2+}. For simplicity purposes, the word zinc will be used to encompass all forms of zinc. It has been more than 60 years since the discovery of specialised neurons in the brain, which release both zinc and glutamate into the synaptic cleft (Maske, 1955). A general description of zinc transport between neurons goes as follows: zinc is located in vesicles (often co-localised with glutamate) which express the zinc transporter, ZnT3. The vesicles are transported along the axon towards the pre-synaptic terminal, where they are exocytosed via a Ca-dependent mechanism (Smart *et al.*, 1994). It is then transported into the post-synaptic terminal via zinc transporters positioned on the post-synaptic membrane. Once in the post-synaptic terminal, they can be transported by zinc-binding chaperones, called MetalloThioneins (MT). MTs are small proteins, rich in cysteine residues that make them excellent at binding zinc and other metals (Vallee, 1995; Frederickson *et al.*, 2005; Kochańczyk *et al.*, 2015). We now know a lot more about the role of zinc in neuronal communication. It has been demonstrated to be highly active at excitatory

synapses and can interact with numerous components in the pre- and post-synaptic membranes (Vogt *et al.*, 2000; Pan *et al.*, 2011; Vergnano *et al.*, 2014; Kalappa *et al.*, 2015). Zinc appears to have a significant role in neurotransmitter regulation, as it can affect the expression of several neurotransmitter receptors (see review by Frederickson *et al*., 2005; Table 1).

The hydrophilic nature of free zinc does not allow it to pass through cell membranes unassisted. Zinc homeostasis in neurons, therefore, is mediated by secondary components such as zinc-binding proteins (e.g. MTs), specialised transmembrane zinc transporters which (1) transport zinc into the cell cytoplasm (ZIP family; designated SLC39) from intracellular organelles or the extracellular space or (2) transport zinc from the cytoplasm into the organelles or into the extracellular space (CDF/ZnT family; designated SLC30) and lastly through Divalent Cation Transporters (DCT1) (Colvin *et al.*, 2000; Eide, 2004, 2006; Liuzzi and Cousins, 2004; Palmiter and Huang, 2004).

As in the case of iron, zinc is also contributing to oxidative stress regulation, through which its bimodal activity is made apparent, as both an antioxidant and a prooxidant. Zinc exerts strong antioxidant properties through a plethora of pathways. Zinc supplementation is indeed beneficial in mounting an inflammatory response and in preventing some age-related phenotypes (Mocchegiani *et al.*, 2011; Swindell, 2011). Moreover, in a mouse model of Alzheimer's disease, zinc supplementation has been shown to decrease some of the memory-deficits and Amyloid beta (Aβ) associated with the neuropathology of the condition (Corona *et al.*, 2010).

It is important to note that free zinc is not redox active and thus is not able to combat oxidative stress induced by ROS directly. It needs to be either bound to ROS scavengers (e.g. MTs, Superoxide Dismutase (SOD), induce transcriptional responses of genes involved in antioxidant pathways either indirectly through stabilisation of zinc finger transcription factors (AP-1, NfKB, p53), or directly (e.g. MTs) (Bousleiman *et al.*, 2017). Moreover, zinc can also reduce oxidative stress as it is an active competitor of other metals such as iron and copper that regulate ROS production through the Fenton reaction. Indeed, zinc deficiency in neuronal systems *in vitro* has shown to be associated with enhanced production of ROS and changes in microtubule polymerisation and assembly (Oteiza *et al.*, 1990; Verstraeten *et al.*, 2004; Mackenzie *et al.*, 2006). Interestingly, there is evidence to suggest that zinc deficiency can create an environment where increased ROS production and caspase-mediated apoptotic signalling pathways are more prevalent and thus contribute to cell death (Truong-

Tran *et al.*, 2001; Clegg *et al.*, 2005). Lastly, zinc can also protect the sulfhydryl groups of proteins from oxidative stress (Cousins, 1985; Gibbs *et al.*, 1985; Bray and Bettger, 1990; Powell, 2000; Jarosz *et al.*, 2017; Lee, 2018). The are several lines of evidence to suggest that MTs play a protective role in the CNS in mammals. Astrocytes primarily express MTs in the CNS, which upregulate their expression following traumatic neuronal injury (Chung *et al.*, 2004, 2008; Anderson *et al.*, 2016) and remarkably they can also promote neuronal regeneration (Chung *et al.*, 2003a; Køhler *et al.*, 2003a; Fitzgerald *et al.*, 2007). In addition, MTs have been shown in several studies to play a significant role as one of the most effective neuroprotective components of the CNS (M Penkowa *et al.*, 1999; Milena Penkowa *et al.*, 1999; Giralt *et al.*, 2002; Trendelenburg *et al.*, 2002; Santos *et al.*, 2012). MTs can also act as an additional reservoir of zinc in times of zinc deficiency, and conversely, in times of zinc overload in the cellular environment, they can serve as molecular zinc scavengers (Kelly *et al.*, 1996).

As mentioned previously, zinc is of paramount importance for the folding and activity of metalloproteases. Zinc supplementation in the diet of mice models of AD has been shown to increase the activity of MMP2 and MMP9 in zymography assays (Corona *et al.*, 2010). Also, in the same study, the authors demonstrated that zinc supplementation increased the levels of the Brain-Derived Neurotrophic Factor (BDNF) and improved the pathological symptoms of AD. BDNF interacts with the Tropomyosin-related kinase B (TrkB) receptor and is highly active in both the CNS and PNS, and it is involved in neuronal regeneration and functional recovery (Kamei *et al.*, 2007; Han *et al.*, 2009; Sasaki *et al.*, 2009). TrkB and neurotrophin signalling serve an essential role in neuronal differentiation and synaptic development and have been linked to several neuropathological conditions (McAllister *et al.*, 1999; Poo, 2001; Chao *et al.*, 2006; McNamara *et al.*, 2006). Interestingly, it has been postulated that zinc-dependent MMPs convert pro-BDNF, the inactive form of the protein, to its mature pro-BDNF form, which can then activate the TrkB receptor *in vitro* (Jung *et al.*, 2005). Extracellular administration of zinc was shown to play a critical role in this process. Therefore, they concluded that zinc induces the activation of TrkB through the activation of BDNF via MMPs. However, a study by Huang and colleagues challenged the conclusions drawn by Jung and colleagues (Huang *et al.*, 2008). The premise of their hypothesis was based on the fact that if zinc indirectly induces the activation of Trk, via BDNF, then removing BDNF from the equation would limit zinc-induced Trk signalling. However, this was not what they observed. They firstly pre-treated cultured cortical neurons with the natural binding domain of BDNF, TrkB-Ig (Naylor *et al.*, 2002) in order to 'mop-up' and effectively inactivate any BDNF

molecules present. Subsequent exposure with BDNF, as expected, did not activate TrkB, as indicated by the lack of TrkB receptor phosphorylation, and by the absence of downstream TrkB signalling molecules. If zinc-induced activation of TrkB were mediated by BDNF, then treatment with zinc, instead of BDNF, would also lead to a lack of receptor activation. Surprisingly, zinc treatment in the same experimental set-up resulted in the activation of the TrkB receptor and its signalling molecules. The same results were seen in BDNF knockout mice as well. This suggests that zinc activates TrkB, not through BDNF, but through a neurotrophin-independent pathway. Additionally, in the same study, the authors demonstrated that addition of exogenous zinc to hippocampal slices significantly enhanced synaptic activity. It was suggested that this takes place through Long Term Potentiation (LTP) mechanisms, involving the activation of TrkB, regulated by synaptically released zinc (Li *et al.*, 2001; Huang *et al.*, 2008).

On the other hand, excessive zinc has been shown to induce severe cellular damage, induce apoptosis and in some cases prevent neuronal regeneration. High levels of intracellular zinc can be brought about through dysregulation of the zinc homeostasis components, namely the zinc transporters and MTs, which can lead to toxic levels of zinc accumulating inside the cell. Following optic nerve injury in mice, a large influx of free Zn^{2+} was seen in retinal neurons, which was mediated via the ZnT3 (SLC30A3) transporter. Interestingly, when the same injury was induced on *slc30a3*$^{-/-}$ knockout mice, and thus decreasing the amounts of vesicular zinc present in retinal neurons, there was a pronounced Retinal Ganglion Cell (RGC) survival and axon regeneration. Also, a similar effect was seen on wild type mice when high-affinity zinc chelators were used (TPEN and ZX1) (Li *et al.*, 2017). This study demonstrates that increased concentrations of zinc following a neuronal injury can impede the progress of regeneration. There is more evidence, by a study conducted recently by the same group which corroborated their earlier findings. They showed that, following optic nerve injury, knocking down Kruppel Like Factor 9 (*klf9)* – an axon growth inhibitor - in conjunction with the treatment with TPEN can enhance axon regeneration more so than any of these components could by themselves (Trakhtenberg *et al.*, 2018). This effect of high concentrations of zinc can be attributed to the fact that it can induce neuronal and glial cell toxicity and death (Yokoyama *et al.*, 1986; Frederickson *et al.*, 2005). Interestingly, studies have shown that following depolarization of neuronal cell membranes, zinc is released from vesicles (Assaf and Chung, 1984; Howell *et al.*, 1984). CNS injury is often accompanied by high degrees of depolarization (Siesjö, 1993), and thus could explain why CNS injury shows a poor regenerative capacity. In addition, contrary to what some studies have shown in

regards to the beneficial role that zinc can exert in the pathology of AD (Corona *et al.*, 2010), there is evidence to the contrary, namely that free Zn^{2+} can, in fact, contribute to amyloid plaque formation in AD.

2.6.3. Calcium-dependent signalling

Calcium's role in neuronal regeneration is one of a mediator in signalling cascades that can affect synaptic formation and plasticity, axon growth and cell-to-cell communication (Zündorf and Reiser, 2011). Calcium ions (Ca^{2+}) can serve as second messenger molecules, either by triggering neurotransmitter release or through the binding and activation of calcium-dependent signalling molecules, which induces a conformational change to the target protein. For simplicity purposes, Ca^{2+} will be referred to as calcium hereafter. As in the case of other metals, we have already discussed in this section, intracellular levels of calcium concentration have to be tightly regulated. Before we discuss the role of calcium in how a neuron responds to injury, it is important to briefly mention some of the avenues by which calcium can enter the cell.

Calcium can enter the cytosol either through the extracellular space or via intracellular calcium stores, namely the Endoplasmic Reticulum (ER) (Koch, 1990). Several types of channels and transporters mediate the entry of calcium ions into the cytosol from the extracellular space. First, calcium influx can take place via Voltage-Gated Calcium Channels (VGCC) that are opened or closed according to local action potentials that are generated at a synapse and propagated along the axon through a series of depolarising waves (i.e. inducing a positive charge onto the cell membrane) (Gerard *et al.*, 1998). Depolarisation of the cell membrane can also occur through ionotropic channels/receptors that are opened following selective agonist binding. These include the kainate, AMPA and NMDA receptors which bind glutamate (note that glycine and serine can serve as co-agonists for the NMDA receptor). Moreover, while the opening of the glutamate receptors results in a direct influx of calcium ions into the cytosol, other inotropic receptors can be targeted and indirectly contribute to this effect. $GABA_A$ and glycine receptors are chloride ion (Cl^-) channels and are generally perceived as inhibitory receptors, in the sense that they allow Cl^- to enter the cytoplasm hence preventing depolarisation of the membrane. However, there are examples of the contrary, as in the case of developing neurons which are characterised by a high intracellular concentration of Cl^-. When $GABA_A$ and glycine receptors are opened in these cells, they promote membrane depolarisation by inducing outflow of Cl^- (Ben-Ari *et al.*, 1989, 1997; Cherubini *et al.*, 1991). Therefore, through their activation, $GABA_A$ and glycine

receptors, can contribute to the opening of VGCC and a subsequent increase in intracellular levels of calcium.

Intracellular calcium stores are mainly found within the ER. Calcium can be released into the cytoplasm by the action of secondary messengers. Inositol Triphosphate (IP_3) can be produced through the digestion of PhosphatIdylinositol 4,5-bisPhosphate (PIP_2) by PhosphoLipase C (PLC). A type of receptor through which PLC can be activated is called the G-Protein Coupled Receptors (GPCR). GPCR can be activated by a wide range of ligands and has a prominent place in signalling within neuronal systems. The generation of IP_3 has a profound effect on intracellular levels of calcium as it can bind to its receptor on the ER and stimulate the secretion of calcium into the cytoplasm (Putney and Tomita, 2012). Calcium signalling has been linked to neuronal migration and development; Adenosine Triphosphate (ATP) and Wnt5a can activate the GPCRs $P2Y_1$ and Frizzled respectively, (Scemes *et al.,* 2003; Liu *et al.*, 2008; Horigane *et al.*, 2016), and Neurotrophin-3 (NT-3) can activate TrkC, a tyrosine kinase receptor (Nakamuta *et al.*, 2011). The activation of these receptors brings about an IP_3-mediated influx of calcium into the cytoplasm. Elevated levels of calcium can regulate the activity of several calcium-sensitive kinases and phosphatases.

Thus far, we have discussed some of the extrinsic or the environmental inhibitory components of the CNS that limit neuronal regeneration. There is evidence, however, which point towards intrinsic differences between the PNS and the CNS that can explain the disparity in the regenerative capacity between the two systems. The neuronal response to axonal injury can be classified into the rapid response characterised by calcium flux and high cyclic AMP (cAMP) activity, and a later response which is regulated by the action of microtubules, molecular motors and intense transcriptional activity (Ziv and Spira, 1993, 1995; Ambron and Walters, 1996; Ghosh-Roy *et al.*, 2010). From what we have mentioned thus far, it is not at all shocking that both calcium overload as well as calcium deficiency can be unfavourable towards neuronal growth. Following axon damage, high or low levels of calcium can equally prevent growth cone formation that eventually leads to cell death (Rehder *et al.*, 1992; Stirling and Stys, 2010). Also, calcium has been demonstrated to assist in neuronal regeneration by promoting cytoskeletal/microtubule changes and the formation of a new growth cone (Chierzi *et al.*, 2005; Bradke *et al.,* 2012; Chen, 2018).

There is evidence to suggest that calcium signalling is paramount in axon guidance through the interaction of slit2 with its receptor robo2, which initiates a cascade that ultimately results in the release of calcium from the ER, not via the IP_3 receptor, but via the ryanodine

receptor (Guan *et al.*, 2007). Slit2 induces a repulsive signalling mechanism by which the growth cone collapses, resulting in the reversal of the direction of migration. This is mediated by a so-called 'calcium wave' that is propagated from the growth cone to the neuronal soma in a retrograde fashion. Calcium influx at the growth cone can cause the redistribution of a RhoA, a GTPase that regulates cytoskeletal arrangements, and thus determine the direction to which the neuron will migrate (Guan *et al.*, 2007; Horigane *et al.*, 2019). In this way, calcium signalling has the potential to regulate when the growth cone stops, turns or extends. Other examples of calcium signalling transducers, which regulate various aspects of neuronal migration, can be found in a review by Horigane and colleagues (Horigane *et al.*, 2019, figure 3). (Komuro and Rakic, 1992; Schneggenburger *et al.,* 1993; Brini *et al.*, 2014; Horigane *et al.*, 2019)

One of the initial responses to axonal injury is the rapid accumulation of calcium inside the cytoplasm of the axon (axoplasm), which generates an action potential (called injury discharge) at the site of injury and is then propagated to the soma by the calcium wave (Ziv and Spira, 1995; Ambron and Walters, 1996; Rishal and Fainzilber, 2014). This effect has been observed across several species ranging from nematodes to mammals (Rishal and Fainzilber, 2014). Interestingly, in the CNS, sodium ions (Na^+) also enter the axoplasm following axon injury, which leads to the reversal of the Na^+/Ca^+ exchanger activity, an attempt by the axon to excrete excess Na^+, however, by doing so, it allows more calcium in (Mandolesi *et al.*, 2004). Moreover, the activity of the calcium-dependent protease calpain increases, which can mediate the proteolytic digestion of the voltage-gated Na^+ channels (NaChs), which further increases the concentration of intracellular calcium (Wolf *et al.*, 2001; von Reyn *et al.*, 2009). There is also evidence to suggest that calpain is vital in restoring neuronal membrane integrity following injury (Howard *et al.*, 1999). The calcium wave is also maintained and propagated by VGCC and intracellular ER stores, which ultimately has a robust transcriptional and epigenetic impact. Recent studies on Dorsal Root Ganglion (DRG) neurons have demonstrated that the retrograde calcium-signalling can drive the nuclear export of Histone Deacetylase 5 (HDAC5) via a Protein Kinase C (PKC)-mediated pathway; an event that promoted histone acetylation on the H3 histone subunit (Cho *et al.*, 2013). In the same study, the authors demonstrated that this pathway promoted axon regeneration *in vitro* and *in vivo*, through the transcription of Regeneration-Associated Genes (RAGs), such as *vegf* and *jun* (Cho *et al.*, 2013). Histone acetylation can alter chromatin interaction with the DNA, activate pro-regenerative gene transcription, and has been associated with promoting axon regeneration of CNS neurons (Gaub *et al.*, 2010, 2011; Lv *et al.*, 2012).

HDAC5 has been previously shown to accumulate at the site of injury and promote axon regeneration via the deacetylation of tubulin (Cho and Cavalli, 2012). Also, *in vitro* work by Cho and colleagues on DRG neurons, where they mutated HDAC5 so that it's not allowed to be exported from the nucleus, has demonstrated a substantial inhibition of axon growth (Cho *et al.*, 2013). Remarkably, however, PKC activation and HDAC5 export are absent following injury in CNS neurons (Cho *et al.*, 2013), highlighting some of the potential differences that underlie the regenerative capacity of CNS and PNS neurons. Indeed, calcium signalling has been postulated as one of the factors that can hinder neuronal regeneration in the CNS. In CNS neurons, both sodium and calcium channels are required for the propagation of the calcium wave (Mandolesi *et al.*, 2004), whereas in the PNS, no such reliance on sodium influx was observed (Sattler *et al.*, 1996). Mandolesi and colleagues have showed that blocking the sodium channels *in vitro* with Tetrodoxin (TTX) on CNS neurons, and thus preventing the influx of sodium ions, significantly reduced the damage induced by injury. This finding implicates excessive calcium load in the damaged axon as a potential inhibitor to regeneration.

One of the most critical aspects of successful regeneration is the efficient relay of a 'message' from the damaged axon to the cell soma. There is strong evidence which suggests that calcium influx can initiate 'positive injury signalling' through a complex pro-regenerative biochemical cascade that results in the phosphorylation and subsequent activation of the transcription factors Jun and Signal Transducer and Activator of Transcription 3 (STAT3). Briefly, high levels of calcium can cause disinhibition of the axonal dual leucine zipper kinase (DLK), which can then be engaged with a functional signalling complex made of JNK-Interacting Protein 3 (JIP3) and JUN amino-terminal Kinase 3 (JNK3). These three components assemble onto the motor proteins kinesin and dynactin, which migrate across microtubules in a regressive fashion. DLK can then be phosphorylated by JNK3, which in turn phosphorylates STAT3, that is retrogradely transported into the nucleus and regulates gene transcription. The DLK-JIP3-JNK signalling complex also phosphorylates Jun, which is also translocated to the nucleus and regulate gene transcription (Xiong *et al.*, 2010; Rishal and Fainzilber, 2014; Doron-Mandel *et al.* , 2015). Even though DLK is a prerequisite for efficient axon outgrowth (Itoh *et al.*, 2009; Shin *et al.*, 2012) there are several lines of evidence to suggest that DLK-mediated mechanisms are heavily inducive to neurotoxicity and cell death (Xu *et al.*, 2001; Itoh *et al.*, 2011; Pinan-Lucarre *et al.*, 2012; Watkins *et al.*, 2013; Welsbie *et al.*, 2013). Interestingly, however, there are studies which have shown that caspase-mediated neuronal cell death brought about by DLK, is essential for axonal regeneration

(Pinan-Lucarre *et al.*, 2012). Additionally, indirectly, calcium has also been shown to be an intrinsic inhibitor to neuronal regeneration both *in vitro* and *in vivo*. The inhibition of the mechanosensitive calcium channel DmPiezo in *Drosophila*, either via genetic knockout or pharmacological inhibition enhanced axon regeneration for both PNS and CNS neurons (Song *et al.*, 2019).

The association of metals and their role in neuronal regeneration is remarkably complex. At this stage it cannot be claimed with any certainty that either iron, zinc or calcium are beneficial or detrimental to neuronal regeneration; it is possible that both opinions are true. The ancient Greeks believed in the concept of *'μέτρον ἄριστον'*, which loosely translates to 'everything in moderation'. This phrase is perfectly suited in molecular pathways that regulate neuronal regeneration, where an ideal balance should be achieved amongst all the components that form the regenerative orchestra. Therefore, in order to understand more about where that balance lies, one should divert the focus on organisms which have naturally mastered the 'art' of regenerating complex neuronal systems.

2.7. Earthworm: An invertebrate model to study neuronal regeneration

2.7.1. Earthworm neuronal regeneration

Annelida is a large phylum of over 17,000 species, which are grouped into three classes; Polychaeta, Oligochaeta and Hirudinea, which can be either marine or terrestrial animals. They have been extensively studied due to their remarkable regenerative capabilities. Annelid species, as a group, generally share similar morphological characteristics. They are bilaterally symmetrical worms, which are divided into several segments. They are further characterised by a gut, a Ventral Nerve Cord (VNC), blood vessels which run longitudinally along the length of the body, a brain-like tissue located at the anterior and hair-like structures (bristles or setae) on the body wall which assist in movement and sensory input (Özpolat and Bely, 2016).

Most of the Annelids possess the ability to regenerate to some extent according to individual species (Bely, 2006). Tissue regeneration; has been defined as the restoration of lost body parts, and has been observed across several different phyla; however, the degree of regeneration depends on the species and the source of injury (Bely and Nyberg, 2010; Zheng *et al.*, 2016). There are two types of regenerative paradigms which have been characterised; the epimorphic and morphallactic regeneration. In epimorphic regeneration,

dedifferentiated stem cell-like components proliferate into a mass of undifferentiated progenitor cells, called the blastema, which will be the source of the cells that will eventually form the new tissue (Seifert and Muneoka, 2018). These progenitor cells have been demonstrated to have restricted fates according to what tissue they originated from (Kragl *et al.*, 2009). On the other hand, in cases of morphallactic regeneration new cells do not form, and tissue restoration solely depends on existing cells being reorganised through an intricate tissue remodelling process (Planques *et al.*, 2019). Annelids can exhibit both epimorphic and morphallactic regenerative capabilities (Agata *et al.*, 2007; Zattara and Bely, 2011; Weidhase *et al.*, 2015). Time-lapse imaging studies in the annelid, *Pristina leidyi*, have shown that regeneration is characterised by the migration of neoblasts, towards their target destination (Zattara *et al.*, 2016). However, the origin of these cells is still a matter of debate; whether there is a population of resident neoblasts in the regenerating tissues, whether differentiated cells assume a state of pluripotency following a traumatic event or if there is a migration of cells from distant tissues. Interestingly, a recent study on posteriorly amputated *Platynereis dumerilii* suggested that there is indeed a pre-existing population of resident cells that exhibit a proliferative capability, indicative of a stem cell population (Planques *et al.*, 2019). Also, they showed that there was no migration of neoblasts from distant tissues, but rather any source of neoblasts was limited to the tissue adjacent to the amputation site. However, their approach of amputating entire segments, might not be indicative of what happens when a specific tissue type is being targeted.

In this work, the earthworm (Annelida, Oligochaeta) has been employed, an organism which has been extensively used in the standard Organization for Economic Co-operation and Development (OECD) toxicological testing, to deepen our understanding of neuronal regeneration at the molecular level. The earthworm possesses a relatively simple, yet extremely sensitive and well-coordinated nervous system, which enables it to respond to various environmental stimuli such as heat, light, vibrations and moisture. Briefly, the CNS is comprised of a dorsal Cerebral Ganglion (CG) located at the 3rd anterior segment, which is connected to the VNC via Circumpharyngeal Connectives (CC) (Figure 2.3). Also, two nerves called the Prostomial Nerves (PN) emanate from the CG and attach to the prostomium of the worm. The VNC is made up of segmentally repeated ganglia which runs down the length of the earthworm's body. The cell number the ganglion of the VNC varies across different ganglia and between species; in *Lumbricus terrestris* it is projected to host 2000 cell bodies, of which 800 is thought to be neurons, whereas in *E. fetida* the cell number drops to about 1200 cells per VNC ganglion (Solt and Molnar, 2001; Herbert *et al.*, 2009). Note that the first

two ganglia of the VNC are fused and are defined as the SubOesophageal/pharyngeal Ganglion (SOG) (Bullock and Horridge 1965, Herbert et al., 2009). Even though the brain is considered to be vital for social behaviour (Gopi Daisy *et al.*, 2016) and an essential sensory centre for the earthworm a vital, its removal does not significantly affect the muscle contractions required for movement, as this is regulated by the VNC (Mill, 1982). Additionally, three pairs of nerve connectives project from each segmental ganglion and innervate the body wall, which constitutes part of the peripheral nervous system.

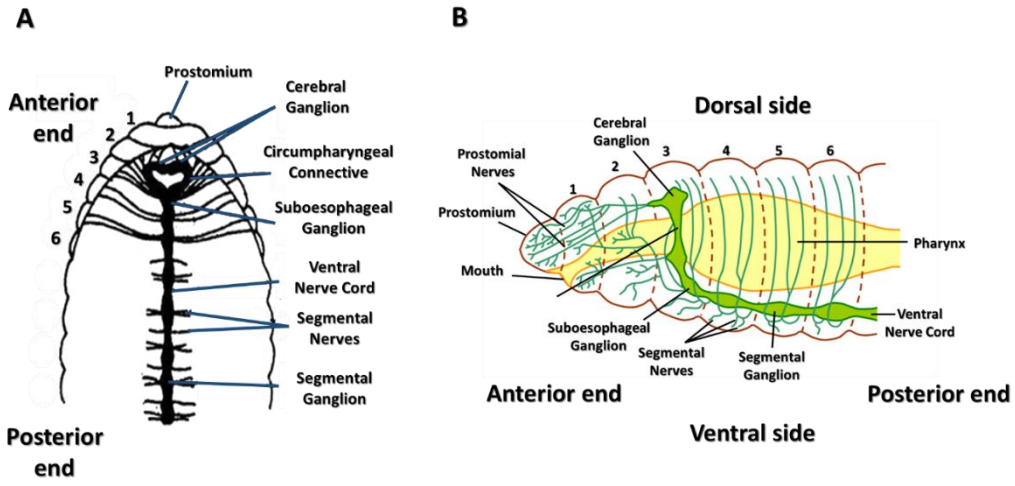

Figure 2.3 Diagrammatic representation of the earthworm's central nervous system. Dorsal **(A)** and lateral **(B)** views of the CNS are presented. The CG can be observed at segment 3 where it is connected to the SOG via the CCs, forming a ring around the pharynx. Segmental nerves are also shown stemming from each VNC ganglion. *CG; Cerebral Ganglion, CC; Circumpharyngeal Connectives, SOG; Suboesophageal Ganglion, VNC; Ventral Nerve Cord*
A: Adapted from **http://www.biologydiscussion.com**
B: Adapted from **https://cronodon.com/BioTech/Earthworm_NS.html**

The earthworm, for reasons yet unknown, exhibits the capacity for complete restoration of lost parts of its nervous system, including the complete loss of its CG, loosely defined as the 'brain' (Aros and Vigh, 1962). It has been proposed that this takes place via a process involving cell dedifferentiation through the expression of pluripotency factors and migration towards the regenerating area via the Ventral Nerve Cord (VNC) and the SOG, which connect the CG to the rest of the nervous system (Lubics *et al.*, 2002; Zheng *et al.*, 2016). More specifically, the earthworm species, *Eisenia fetida,* can fully regenerate its CG within 8-11 weeks following its precise surgical removal. Studies of CG regeneration in *E. fetida* demonstrated that there is a steady increase in total cell number in the regenerated CG until the 80th day post-surgery (Csoknya *et al.*, 2003a). Also, Csoknya and colleagues showed that all dopaminergic and serotonergic neuronal elements are restored in the regenerated brain

at roughly 11 weeks post-extirpation. It has been suggested that undifferentiated cells migrate towards the connectives from the SOG, and drive the rebuilding of the neuronal network of the brain (Lubics *et al.*, 2002). Furthermore, in accordance to studies in other annelids, neuroblasts located within the VNC and adjacent intact ganglia appear to be the source of serotonin- and dopamine positive neurons, in the regenerating brain (Csoknya *et al.*, 2003a). Interestingly, there is evidence to suggest that despite the input from the VNC and SOG in regeneration, the pharyngeal nerve plexus also contributes to the formation of the new CG. Neurons within the pharynx proliferate and extend towards the dorsal and central parts of the regenerating tissue to form a neuropil (Csoknya *et al.*, 2003a). It is important to highlight, however, that the temperature in which the worms are stored and allowed to regenerate, can have a profound effect on the speed of regeneration, and thus one has to be careful when comparing the time course of regeneration and the first appearance of neuronal tissue structures and functional restoration (Okrzesik *et al.*, 2013).

Moreover, it has also been speculated that immune cell accumulation to the damaged site and capillary growth into the regeneration blastema, from which the new brain develops, are processes that are likely to dictate the efficiency of regeneration (Aros and Vigh, 1962, Lubics *et al*., 2002, Zheng *et al*., 2016). Interestingly, studies in recent years have identified an interplay between the immune and nervous systems during regeneration (Nguyen *et al.*, 2002; Jung *et al.*, 2012; Russo and McGavern, 2015). Several lines of evidence support this claim in annelids. Depletion of coelomocytes via electrostimulation, the immunocompetent cells of earthworms, delays the efficiency of brain regeneration in *Dendrobaena veneta* (Okrzesik *et al.*, 2013; Molnar *et al.*, 2015). Indeed, the importance of coelomocytes in regeneration was highlighted more than 75 years ago, where their depletion resulted in an inhibition in the capacity of *E. fetida* to regenerate tail segments, following amputation (Liebmann, 1942, 1943). Coelomocytes, and in particular the chloragocyte-derived eleocytes, have an intrinsic autofluorescence capacity in several earthworm species (Cholewa *et al.*, 2006), that is mainly attributed to the presence of riboflavin (Vitamin B2) stores (Koziol *et al.*, 2006). Remarkably, when the earthworms, *Eudrilus eugeniae*, were supplemented with riboflavin, there was an induction of blastema formation and a marked increase in the rate of tail regeneration (Samuel *et al.*, 2012). Furthermore, coelomocytes have been shown positivity for the Thyroid-Stimulating Hormone (TSH), Thyroglobulin (TGB) and for their receptors, all of which have been implicated in regulating neuronal cell metabolic functions (Wilhelm *et al.*, 2006). Coelomocytes have also been suggested to have a protective function against oxidative stress and neuronal apoptosis, through the expression of Pituitary

Adenylate Cyclase-Activating Polypeptide (PACAP)-like proteins, an established neuroprotective protein whose action appears to be conserved in several species (Vaudry *et al.*, 2002; Somogyi *et al.*, 2009; Hajji *et al.*, 2019; Ye *et al.*, 2019).

In addition, xenobiotic challenge can elicit positive effects within a neuroregenerative context. Remarkably, even in the presence of highly noxious compounds, such as the heavy metal cadmium, earthworms show high resilience and can not only overcome its toxic effect, but studies show it can enhance its ability to regenerate severed tail segments (Takacs *et al.*, 2016; Rorat *et al.*, 2017). The authors claimed that the positive effect of cadmium is mediated through the upregulation of metallothionein; however, this is based on circumstantial evidence and can only be inferred at this point. Moreover, further evidence on the beneficial role of the immune system on regeneration can be found in a different annelid species, namely the medicinal leech *Hirudo medicinalis*, in which a bacterial infection can greatly enhance neuronal regeneration via the induction of antimicrobial peptides in neuronal and non-neuronal components of the CNS (Schikorski *et al.*, 2008; Tasiemski and Salzet, 2017).

Humans indeed have 'sacrificed' the ability to repair neuronal damage, possibly, in return for more efficient neuronal protection from further harm. There is overwhelming evidence that this is not a permanent state and there is the potential to overturn the *status quo*. Our knowledge surrounding the topic of neuronal regeneration is extremely limited, at least in comparison to most biological processes. The characterization of fundamental aspects of neuronal regeneration in the earthworm promises to provide an insight as to why mammals have largely lost that capability.

2.8. Aims and Objectives

The main goal of this project was to establish the earthworm as an organism that can be universally accepted as a reliable model to study neuronal regeneration across various scientific disciplines. Due to the limitations in genomic and transcriptomic knowledge, it has been challenging to conduct robust molecular studies on the earthworm. I wanted to understand what the underlying differences are between mammals and earthworms, namely *Eisenia fetida,* in their ability to regenerate neuronal tissue, through a series of molecular, histochemical and biophysical experiments. To the best of my knowledge this is the first study to conduct high-throughput transcriptomic studies on cerebral ganglion regeneration in *E. fetida*; an attempt to uncover new gene targets and biological processes that enable the worm to perform a task so complex and tightly regulated, which in humans was once thought to be impossible to achieve. Moreover, here, for the first time, the spatial and temporal distribution of elements, with a focus on metals, throughout the time course of cerebral ganglion regeneration, is described. My work aims to shed some light into how neuronal regeneration can be enhanced and be the starting point from which we can build comprehensive methodologies to unlock the untapped potential of the earthworm as a research tool.

3. Materials and Methods

For all experimental work conducted in this project, appropriate personal protective equipment was always worn. Bench surfaces and dissection tools were cleaned regularly using 70% Industrial Methylated Spirit (IMS). Hazardous or toxic materials used throughout were disposed of in a way which adhered to safety regulations.

3.1. Earthworm acquisition and maintenance

For all the experiments conducted, the earthworm species *Eisenia fetida* was used. Unless otherwise stated, the earthworms used in all experiments were kindly donated by Professor Molnar (University of Pécs, Hungary). Sexually mature adult worms, with a developed clitellum, were used throughout this project. The worms were kept in moist soil (40% peat moss, 40% compost, 20% top soil), stored in well-ventilated plastic boxes in the dark at 15°C (± 0.2 °C) in a constant temperature incubator (SANYO MIR 154) and were fed vegetable and fruit scraps *ad libitum*. The worms used in the experiments were transferred to small plastic boxes and were stored under the same conditions as above, until further processing.

3.2. Microsurgery

3.2.1. Anaesthetisation

The earthworms were anaesthetised via submersion in cold (4-7 °C) carbonated water for 3-5 minutes but no longer than 10 minutes to minimise stress and avoid the risk of drowning. Carbonated water was prepared using a Soda Siphon (Olympic) and two 8g CO_2 canisters (ISI). The siphon was stored at 4 °C.

3.2.2. Cerebral ganglion extirpation

The worm was immobilised onto a silicone dissection mat, using sharp steel pins, by adding one pin onto each side at the 5th anterior segment (Figure 3.1A) followed by a small dorsal incision between the second and fourth anterior segments using stainless steel scissors (Figure 3.1B). Next, the incision was kept open by adding a pin onto each side of the cut. The cerebral ganglion (CG) was identified and gently pulled to expose the two circumpharyngeal connectives (CC). The CG was then removed by cutting the two CC and the prostomial nerves connecting the CG and the 1st anterior segment. Note that for illustration purposes alone, in Figure 3.1C, the pharynx was also removed to show severing points (black dotted lines) (Figure 3.1C) – this was not carried out under normal circumstances. Once the CG was extirpated successfully, the pins were removed, and the worm was subsequently placed in a

separate plastic container and stored under the same conditions as 3.1. The process was carried out under a stereomicroscope (Nikon SMZ800).

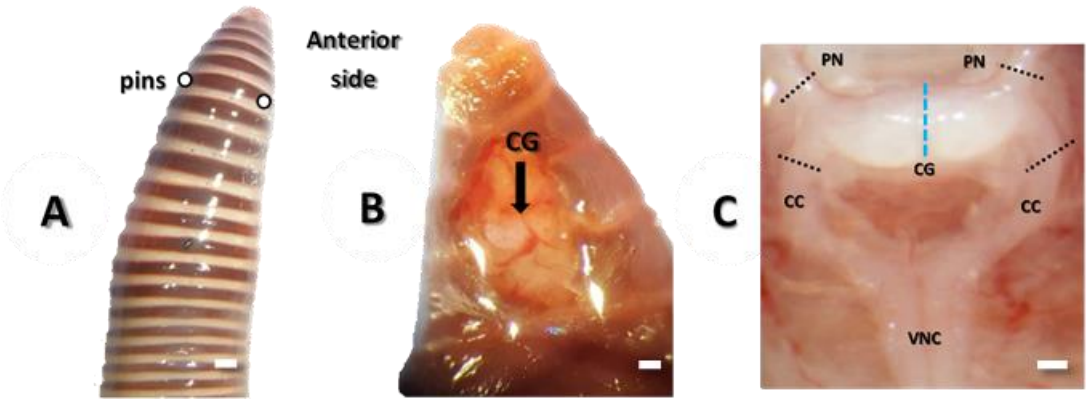

3.2.3. Sham microsurgery

Figure 3.1 Microdissection for the removal of the Cerebral Ganglion (CG) in the earthworm, *Eisenia fetida*. A. An adult worm is anesthetised via immersion in ice-cold carbonated water for 3-5 minutes and pinned on a dissection mat on its ventral side at the fifth anterior segment (white circles). **B**. A dorsal incision is performed to expose the CG, the Circumpharyngeal Connectives (CC) and Prostomial Nerves (PN). **C**. Pharyngeal tissue was carefully removed to expose the underlying Ventral Nerve Cord (VNC). The appropriate cutting level for CG extirpation is indicated by the black dotted lines. The hemiganglioctomy CG mid-sagittal severing point is indicated by the light blue dotted line. Images captured with a Nikon DS-2Mv camera. Scale bars: 200µm

The worms were anaesthetised, and a small dorsal incision was performed as in 3.2.1. and 3.2.2. However, in this case, the cerebral ganglion and circumpharyngeal connectives remained intact. The animals were placed in separate plastic containers and stored under the same conditions as 3.1.

3.2.4. Hemiganglioctomy surgical procedure

In order to study the capacity of neuronal tissue to form connections with existing and regenerating neuronal tissue, a surgical technique was implemented, termed hemiganglioctomy (Figure 3.1C). With this approach, one ganglion of the brain was removed by cutting the mid-sagittal plane (light blue dotted line), one circumpharyngeal connective and one prostomial nerve. The preparation (i.e. anaesthetisation, pinning) and subsequent storage of the worms was the same as described above.

3.3. Time course of neuronal regeneration

To study the progression of cerebral ganglion regeneration following its surgical removal, in *E. fetida*, a series of pictures were taken across 5 weeks following decerebration. Images were captured with a Nikon DS-2Mv camera.

3.4. Sample collection

Two types of samples were used to extract RNA from – neuronal and pharyngeal tissue. The former was used to study transcriptomic changes at different time points during cerebral ganglion regeneration in the earthworm. The latter was used to carry out phylogenetic analysis on individual worms, either to confirm species identity or to group worms based on evolutionary divergence.

3.4.1. Central Nervous System (CNS)

The earthworms (decerebrated or shams) were anaesthetised as in 3.2.1. The only difference was the time of immersion in the carbonated water. In order to minimise the extrusion of coelomic fluid, which could contaminate the RNA sample, the animals were placed in the carbonated water for 6-7 minutes. The anaesthetised worms were pinned down on a silicon mat, by adding a steel pin in the middle of the dorsal side of the eighth segment, followed by pinning the first segment and slightly stretching the worm. The first ten segments were then cut using stainless steel scissors. To 'open' the worm up and expose the underlying organs, an incision was then made along its dorsal side from the tenth segment to the prostomium, splitting the dorsal side in two. Two additional pins were used on the posterior end and two additional pins on the anterior end, on either side to firmly fix the edges onto the silicon mat. Next, the pharynx and the alimentary canal was cut away to expose the underlying Central Nervous System (CNS). The segmental nerves connecting each VNC ganglion to the rest of the body were cut, allowing for the VNC and the circumpharyngeal connectives to be extracted. Extra care was taken to minimise contamination with other types of tissue surrounding the neuronal structures. In cases where a regenerated cerebral ganglion had been formed, this was discarded by performing two incisions on the connectives, similarly to the decerebration protocol (see Figure 3.1C). The extracted neuronal tissue was placed in 200µl of RNA Lysis Buffer (Zymo Research, Irvine, USA) for further processing. Unless otherwise stated, the neuronal tissues of 5-6 worms were pooled for every biological replicate.

3.4.2. Pharyngeal tissue extirpation for genotypic analysis

For genotyping, the pharyngeal tissue of an individual worm was removed, and the RNA extracted (see 3.5). The worms were anaesthetised and cut open as described in 3.4.1. The pharynx was then extracted and placed in 200µl of RNA Lysis Buffer (Zymo Research, Irvine, USA) for further processing.

3.5. Total RNA extraction

Total RNA was extracted, from either the CNS or pharyngeal tissue, using the Quick-RNA™ MiniPrep kit (Zymo Research, Irvine, USA). Unless stated otherwise, all centrifugation steps were carried out at 16,000g (Eppendorf Centrifuge 5418) for 30 seconds at room temperature, and all the reagents used were obtained from Zymo Research. The excised tissues were placed in 200µl of RNA Lysis Buffer in a 1.5ml tube (ABGene) and then centrifuged in order to pellet the contents. Next, the tissues were mechanically homogenised directly in the RNA lysis buffer using Kontes™ Pellet Pestle™ and Kontes™ Pellet Pestle™ cordless motor. The pestle was stored in 0.1% SDS at room temperature. Firstly, the pestle was thoroughly cleaned under running distilled H_2O and 70% IMS (Merck). The pestle was then attached firmly onto the motor and gently positioned at the bottom of the tube to homogenise the tissue for 1-2 minutes, while periodically checking for suspended tissue. The process was then repeated: centrifugation, pestle cleaning and homogenisation for 1 minute. Next, 200µl of 100% Ethanol (Merck) was added to the lysis buffer and mixed thoroughly for 10 seconds using a vortex mixer. The contents of the tube (~400µl) were transferred to a nuclease-free Zymo-Spin™ IC Column, which was positioned inside a collection tube provided by Zymo Research, and then centrifuged. The flow-through was discarded. The column was washed with 400µl of RNA wash buffer and centrifuged. To ensure the highest degree of RNA purity, a DNase step was implemented, where 5µl of DNase I solution (5U/µl, Zymo Research) was mixed with 35µl of DNA Digestion Buffer and added directly onto the column. The sample was then incubated for 15 minutes at room temperature, before centrifugation. The flow-through was discarded and 400µl of RNA prep buffer was added to the column, and then centrifuged. The flow-through was discarded and the column washed with 700µl of RNA wash buffer and centrifuged. The flow-through was discarded and the column washed further with 400µl of RNA wash buffer and centrifuged for 2.5 minutes to ensure complete removal of the wash buffer and the associated ethanol. The column was then transferred to a nuclease-free 1.5ml tube (ABGene). Nuclease-free water was added directly onto the column and allowed to incubate for 2 minutes at room temperature, followed by 30-second centrifugation to elute the RNA. Finally, to minimise any possibility of contamination the eluted RNA sample was transferred to a new nuclease-free 1.5ml tube. The sample was stored at -75^{o}C for further processing. It is important to highlight that the CNS tissue used for extraction was VNC, the SOG and the CC. This ensured that gene expression differences were not due the lack of a regenerated brain in the early time point samples.

3.6. RNA quantification and purity

The purity and quantity of the extracted total RNA were evaluated using a spectrophotometer (Nanodrop ND-1000, ThermoFisher). For the RNA sample to pass the quality control and be used in subsequent experiments, it had to exhibit the following absorbance measurements: for 260nm/280nm between 2.0 - 2.2 and 230/260 between 2.0 - 2.3. To further confirm the purity of the RNA, 5µl of the sample was mixed with 1µl of Loading Dye (Promega) and separated on a 1.5% agarose gel (see 3.11 for further information on agarose gel electrophoresis).

3.7. Reverse transcription

The extracted mRNA was reverse transcribed to cDNA, in 0.2ml tube using the following reaction mix: 4µl M-MLV RT 5x Buffer (Promega), 2µl dNTPs (10 mM, Promega), 1µl oligo dT (5'- TTT TTT TTT TTT TTT TTT TTV N -3', 10 µM, Merck), 1µl M-MLV RT enzyme (200units/µl, Promega) and 1000ng of extracted total RNA were used per reaction. The mixture was made up to 20µl with nuclease-free H_2O accordingly and centrifuged to ensure all contents were collected at the bottom of the tube and placed in a thermal cycler at 42°C for 60min followed by 72°C for 10min. The resulting cDNA was diluted 10-fold before used in subsequent experiments. The cDNA samples were stored at -20°C.

3.8. Quantitative Polymerase Chain Reaction (qPCR)

The expression levels of genes of interest at different experimental conditions (sham or after decerebration) were assessed via quantitative polymerase chain reaction (qPCR) (Applied Biosystems 7500 Fast Real-Time PCR System). All reactions were carried out in MicroAmp Fast Optical 96-well plates (Applied Biosystems). The reaction mix in each well consisted of 5 µl SYBR select master mix (Applied Biosystems), 0.5µl sense primer (10µM), 0.5µl antisense primer (10µM), 2µl H_2O and 2µl of cDNA (diluted), for a total of 10µl reaction mix / well. Each sample was run in triplicates, and for each condition, a minimum of three biological replicates was used. For all qPCR experiments conducted, glyceraldehyde 3-phosphate dehydrogenase (*gapdh*) was the reference gene and was used for normalisation across different samples. Moreover, due to the non-specificity of the SYBR stain, it was imperative to ensure that the signal output was due to a single amplicon product. For this reason, a melting curve analysis step was added in the run method parameters. Based on the melting curve output, any well/reaction which revealed two or more melting temperatures (i.e. two amplicons formed) were omitted from any subsequent analysis. Lastly, the $2^{-\Delta\Delta Ct}$ Livak method (Livak and Schmittgen, 2001) was applied for relative gene expression data

investigation. Statistical significance in changes of gene expression between control and decerebrated samples was carried out via a two-tailed t-test in Microsoft Excel, using the ΔCt for each sample. Note that qPCR performed on catalase (*cat*) and superoxide dismutase 1 (*sod-1)* was carried out by Mr Thomas Kaminski (King's College London, UK) on *E. fetida* worms kindly provided by Dr Spurgeon (Centre for Ecology & Hydrology (CEH), UK) and purchased by Mr Stephan Kloppert (South Africa). Furthermore, the qPCR performed on ADAMs on the 1wD time point was also carried out on worms provided by Dr Spurgeon and Mr Stephan Kloppert.

3.9. Polymerase Chain Reaction (PCR)

Diluted cDNA, obtained in 3.7., was used in a Polymerase Chain Reaction (PCR) reaction to amplify a specific region of a transcript using gene-specific primers. All reactions were prepared in 0.2ml tubes (ABGene). For each reaction, the following was used: 2µl 5X Green GoTaq Flexi Buffer (Promega), 1.5µl $MgCl_2$ (25mM, Promega),0.5µl sense primer, 0.5µl antisense primer, 0.25µl PCR nucleotide mix (10mM, Promega), 0.25µl Taq Polymerase (5U/µl, Promega) and 1µl of cDNA. The reaction mix was made up to 10µl, followed by 5-second centrifugation to get the contents at the bottom. The PCR reaction took place in a thermal cycler (Applied Biosystems 2720) under the following conditions: Heat activation of Taq polymerase – 94^{o}C for 5 minutes. 28-32 cycles of DNA double-strand denaturation - 94^{o}C for 30 seconds, primer annealing - 60^{o}C for 30 seconds, Extension – 72^{o}C for 30 seconds to 1 minute depending on the expected amplicon size.

3.10. Primer design

All oligonucleotides used in either PCR or qPCR experiments were designed using the Primer3Plus platform and obtained from Merck. For additional details on primer design parameters, as well as primer sequences, please refer to the Appendix Table 7.1.

3.11. Agarose gel electrophoresis

For visualising PCR amplicons, 1% agarose gel was prepared by dissolving 0.5g of agarose in 60ml 1X TAE buffer. The mixture was heated in a microwave to dissolve the agarose (in the process bringing the total volume of the solution to 50ml) and then allowed to cool down at room temperature for 1 minute, before adding 5µl of ethidium bromide (10mg/mL; Fisher Chemical). Subsequently, the solution was poured in a gel tray, a gel comb added and then allowed to solidify at room temperature. Once the gel solidified, the comb was gently removed so as not to break the underlying wells that had been formed and placed in a gel tank. The gel was then covered with 1X TAE until fully immersed in the solution. A 100bp or

1kb DNA ladder (Promega) was used as a reference. The PCR reactions were then added into the wells, ensuring no leakage into neighbouring wells. The gel was subjected to a constant voltage of 111V for 25 minutes and visualised using the GeneGenius Bio Imaging System (Syngene) and the GeneSys software (Syngene). To test for RNA quality via agarose gel electrophoresis, a 1.5% gel was used instead. The integrity of the signal pertaining to the 18S and 28S ribosomal subunits were used to determine RNA quality.

3.12. Plasmid subcloning by PCR

3.12.1. PCR product purification

The PCR amplicons to be sequenced were firstly separated in a 1% agarose gel as described in 3.11. The amplicon section was then excised from the gel, using sterile scalpels under a UV box and transferred to 1.5ml tubes (ABGene). Extra care was taken to minimise UV exposure and thus minimise any damage to the DNA, which could decrease cloning efficiency. The DNA was cleared of any impurities using the Wizard® SV Gel and PCR Clean-Up System (Promega). Unless otherwise stated, all reagents in this experimental process were provided with the clean-up kit. All centrifugation steps were performed at 16,000g at room temperature (Eppendorf Centrifuge 5418). Briefly, 10µl of Membrane Binding Solution for every 10mg of gel slice was added into the tube, vortexed and then incubated at 60^{o}C for 5-6 minutes. The mixture was vortexed for 5 seconds every 2 minutes, to ensure complete dissolution of the gel. The dissolved mixture was then transferred into the SV Minicolumn and incubated for 1 minute for maximum adherence of the DNA onto the column, before being centrifuged for 1 minute. The flow was discarded, followed by the addition of 700µl Membrane Wash Solution (ethanol was added according to the manufacturer's instructions). The sample was centrifuged for 1 minute and the flow through discarded. An additional 500µl of Membrane Wash Solution was added and centrifuged for 6 minutes. To elute the DNA, the column was transferred to a nuclease-free 1.5ml microcentrifuge tube. Nuclease-free water (30µl) was added directly onto the column and allowed to incubate for 1 minute at room temperature, before being centrifuged for 1 minute. The eluent was collected in the 1.5ml tube. Finally, to minimise any possibility of contamination, the eluted DNA sample was transferred to a new nuclease-free 1.5ml tube. The purified amplicon samples were stored at -20^{o}C until further processing.

3.12.2. T - cloning

The purified PCR product was cloned into the p-GEMT Easy Vector system (Promega), following a T-overhang cloning approach. Briefly, T-cloning takes advantage of the fact that *Taq* Polymerase incorporates an adenine nucleotide at the 3' end of every amplicon, which complementary binds to Thymine overhangs at the 3' end of the vector (Figure 3.2). The

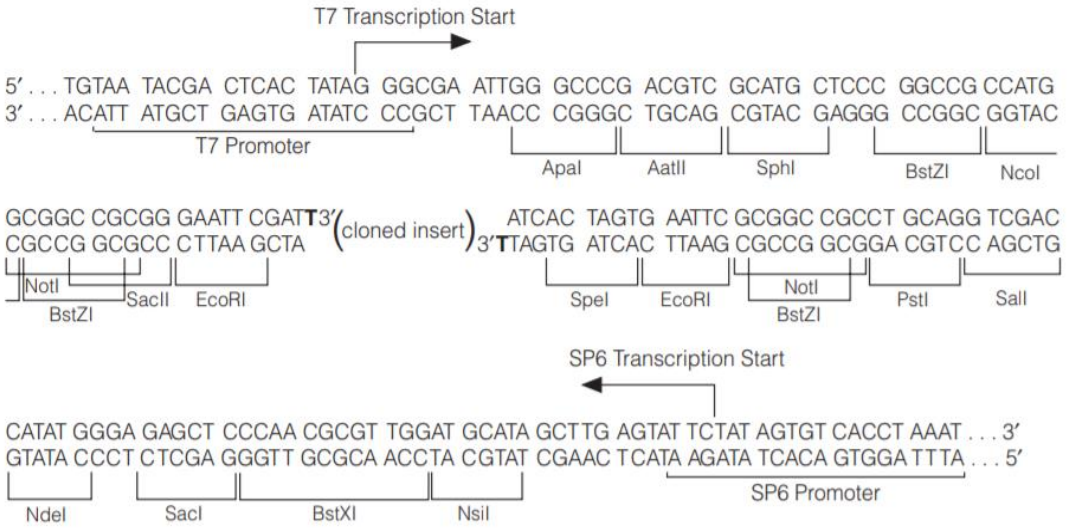

Figure 3.2 The p-GEMT Easy vector system, by Promega, allows for DNA sequences with an adenine at the 3' end to be cloned into the plasmid. The points of interest of the vector sequence are shown, including the T7 and SP6 promoter sequences sites. In brackets, the location where the DNA sequence would be inserted, is indicated.

cloning, therefore, of the DNA insert allows the plasmid to adopt a circular conformation which enables it to be transformed into bacterial cells. For maximum cloning efficiency of the target amplicons, 1µl T4 DNA ligase (3 Weiss units/µl), 1µl p-GEMT easy vector (50ng/µl), 1µl of Rapid Ligation Buffer, T4 DNA Ligase (10X) and 7µl of the purified PCR product were added in a 0.2ml microfuge tube. The mixture was mixed through pipetting and centrifuged to ensure all contents were at the bottom of the tube. The sample was then allowed to incubate overnight (O/N) at 4°C.

3.12.3. Preparation of chemically induced competent *E.coli* (DH5α) cells

Competent bacterial cells were prepared in house. Firstly, 100µl of a previously prepared *E. coli* (DH5α) stock (stored in 10% glycerol at -75°C) was inoculated on LB agar plates O/N at 37°C. A single colony was then picked with a sterile pipette tip and dropped into 20ml of LB Broth. The culture was incubated at 37°C O/N, while agitated at 150rpm. At the end of the incubation, 5ml of the liquid culture was transferred to 195ml of LB broth in a 500ml flask and placed on a shaker at 150rpm at 37°C and incubated for 2.5 hours. The flask was then

placed on ice for 15 minutes. At this point in the protocol, it was imperative to maintain the culture cold and thus, all the following centrifugation steps were carried out at 4°C. The 200ml culture was equally distributed in 4 x 50ml tubes and centrifuged at 3000g for 10 minutes to pellet the bacterial cells. Next, the supernatant was discarded without disrupting the pellet. The pellets were then resuspended in 20ml of 100mM CaCl2 (Merck) and left on ice for 20 minutes, before being centrifuged at 3000g for 10 minutes and the supernatant discarded. The use of the divalent Ca^{2+} induces pore formation on bacterial cell walls and consequently facilitates the uptake of foreign DNA molecules into the cell. The pellets were then resuspended in 14.4ml of 100mM $CaCl_2$ and kept on ice at 4°C O/N. Following the O/N incubation, 1.6ml of ice-cold 100% sterile glycerol was added to the suspension (for a 10% glycerol stock). The stock was then aliquoted into sterile microfuge 1.5ml tubes (200µl / tube) and stored at -75°C.

3.12.4. Transformation

Competent DH5α which were prepared in house were used in bacterial transformations. Following the O/N ligation reaction, 5µl of the sample was mixed with 50µl of competent bacteria and were incubated for 20 minutes on ice. The mixture was then heat-shocked for 50 seconds at 42°C before immediately returned to the ice for a further 10 minutes. 200µl of LB broth was then added to the mixture and incubated at 37°C for 2 hours, while agitated at 150rpm. At the end of the incubation, 100µl of the liquid culture was inoculated onto LB agar plates, containing 100µg/ml of Ampicillin (Amp^+). Ampicillin was used in order to select for those cells which have successfully been transformed with the pGEM-T vector and thus been made resistant to the antibiotic, due to the Ampicillin resistance gene carried by the plasmid. Once the plates were dried, they were then incubated at 37°C O/N.

3.12.5. Liquid culture

Single medium-sized colonies were selected using a sterile pipette tip and dropped into 5ml of LB Broth (Amp^+). The cultures were then incubated at 37°C, under agitation at 150rpm for no more than 16 hours, to avoid bacterial overgrowth.

3.12.6. Plasmid extraction

For plasmid extraction from bacterial cells, the PureYield™ Plasmid Miniprep System (Promega) was used according to the manufacturer's protocol. Liquid bacterial cultures were centrifuged at 3000g for 5 minutes to pellet the cells. The supernatant was discarded, and the pellet resuspended in 500µl of sterile water. The suspension was then transferred to sterile 1.5ml tubes, followed by the addition of 100µl of Cell Lysis Buffer. The tubes were

inverted ten times until a clear blue solution was obtained. Immediately after (no more than 1 minute) 350µl of cold Neutralisation Buffer (stored at 4°C) was added to stop the lysis reaction. The tubes were inverted ten times to form a yellow precipitate. The samples were then centrifuged at 16,000g at room temperature for 3 minutes. The supernatant was then transferred to a PureYield™ Minicolumn without disrupting the pellet. The minicolumn was positioned into a PureYield™ Collection Tube and centrifuged at 16,000g for 15 seconds at room temperature. The flow-through was discarded, 200µl of Endotoxin Removal Wash was then added to the column and centrifuged at 16,000g for 15 seconds at room temperature. The flow-through was discarded and 400µl of Column Wash Solution was added onto the column and centrifuged at 16,000g for 30 seconds at room temperature. The minicolumn was transferred to a sterile nuclease-free 1.5ml tube. The plasmid was eluted by adding 20µl of Elution Buffer directly onto the column matrix. The column was allowed to stand for 2 minutes at room temperature before being centrifuged for 30 seconds. Finally, to minimise any possibility of contamination, the eluted plasmid was transferred to a new nuclease-free 1.5ml tube and stored at -20°C.

3.12.7. Confirming successful ligation via PCR

In order to confirm that the plasmids had ligated with the DNA insert as intended, a PCR was carried using the T7 and SP6 promoter primers (shown in Figure 2). The location of the primers flanks the region of the DNA ligation point. In cases where the DNA insertion had failed, but the plasmid managed to ligate to itself, the resulting amplicon from the PCR would be shorter (177bp) compared to the amplicon produced when the DNA insert had successfully been incorporated into the vector. The PCR conditions were similar as in 3.9. However, the annealing temperature of the primers was set to 45°C, and the extension step was set to 1 minute. The amplicon produced was run on a 1% agarose gel and visualised as described in 3.11.

3.12.8. Sanger sequencing

The identity plasmids were determined via Sanger sequencing (using the T7 and SP6 promoter primers) by Genewiz. The concentration of the plasmids that were sent for sequencing had to be more than 100ng/µl, which was determined via a spectrophotometer in a volume of 15µl.

3.13. Obtaining the full-length sequence of transcripts utilising a Switching Mechanism at the 5' end of RNA Template - Rapid Amplification of cDNA Ends (SMARTer RACE)

Because the earthworm genome has yet to be fully sequenced, the availability of full-length gene sequences is low. One approach one can follow in order to obtain full-length transcript sequences would be to utilise a known partial sequence, via a RACE reaction. The end point of this reaction results in a cDNA library where specific adaptor sequences are added to the 5' and 3' ends of each cDNA sequence. These adaptors, in turn, act as priming sites for specialised primers which in conjunction with gene-specific primers (designed using the known part of the sequence) can amplify the 5' and the 3' end of the transcript. For a visual description of the methodology and scientific rationale of the approach, please refer to Figure 3 by (Zhu *et al.*, 2001).

3.13.1. Generating RACE-Ready cDNA – First Strand cDNA synthesis

For the following protocol, the SMARTer® RACE 5'/3' Kit was used (Takara Bio, USA). Firstly, two reactions, the 5'-RACE-Ready cDNA and 3'-RACE-Ready cDNA, were prepared in 0.2ml microfuge tubes (ABGene). For the 5' RACE reaction 10µl of total RNA and 1µl of 5'-CDS Primer A were used. On the other hand, for the 3' RACE reaction 10µl of total RNA, 1µl of 3'-CDS Primer A and 1µl of nuclease-free H_2O were used. Note that the 5' and 3' CDS Primers used are modified oligo dT primers, which anneal to the poly-A tail of the mRNA, through which the adaptor sequences are being incorporated in the resulting cDNA. The total RNA template used in both reactions were extracted from different time points following decerebration (2µl from 3 days, 1 week, 3 weeks and 5 weeks post-decerebration as well as 2µl from 1week post-sham). The inclusion of RNA from a multitude of conditions was performed in order to include as many transcripts as possible within the RACE libraries produced. The contents of the tubes were mixed thoroughly and spun briefly in a microcentrifuge. Next, using a thermal cycler the tubes were incubated at 72°C for 3 minutes, then cooled to 42°C for 2 minutes. While the tubes were being incubated, the buffer mix for each of the reactions above was prepared by adding 4µl of First-Strand Buffer (5X), 0.5µl DTT (100mM) and 1µl dNTPs (20mM) in a fresh 0.2ml microfuge tube. The reagents were mixed via pipetting and centrifuged briefly to collect the contents at the bottom of the tubes. After the incubation of the 5' and 3' reactions, 1 µl of the SMARTer II A Oligonucleotide was added only to the 5' RACE reaction, for a total volume of 12µl. Finally, for the reverse transcription

reaction, the following was added to the denatured RNA (i.e. to the reactions incubated in the thermal cycler): 5.5µl of the buffer mix prepared previously, 0.5µl of RNase inhibitor (40U/µl) and 2µl of the 2.0 µl SMARTScribe™ Reverse Transcriptase (50U / µl), for a total volume of 20µl for both the 5' and 3' RACE cDNA reactions. The contents in the tubes were mixed thoroughly via gentle pipetting and centrifuged briefly. The tubes were then incubated at 42°C for 90 minutes, followed by 70°C for 10 minutes, in a thermal cycler. Each of the cDNA libraries was then diluted by adding 90µl of Tricine-EDTA Buffer and stored at -20°C.

3.13.2. Rapid Amplification of cDNA Ends (RACE)

To generate the 5' and 3' RACE, which in unison represent the full-length sequence of the target transcript, a standard PCR reaction was carried out as follows: for the 5' RACE library 2µl 5X Green GoTaq Flexi Buffer (Promega), 1.5µl $MgCl_2$ (25mM, Promega), 0.5µl of the antisense gene-specific primer, 1µl of the Universal Primer Mix (Takara), 0.25µl PCR nucleotide mix (10mM, Promega), 0.25µl Taq Polymerase (5U/µl, Promega) and 1µl of the 5' RACE cDNA library were mixed together in a 0.2ml tube. On the other hand, for the 3' RACE reaction, the antisense gene-specific primer was used instead of the sense. The reaction mix was made up to 10µl, followed by 5-second centrifugation to collect the contents at the bottom. The PCR reaction took place in a thermal cycler (Applied Biosystems 2720) under the following conditions: heat activation of Taq polymerase – 94°C for 5 minutes. 28-32 cycles of DNA double-strand denaturation - 94°C for 30 seconds, primer annealing - 60°C for 30 seconds and **Extension** – 72°C for 2.5 minutes. The longer extension time was because the expected amplicon size was unknown.

3.13.3. Characterisation of RACE Products

From this point onwards, the protocol was identical as described in 3.11 and 3.12. Briefly, the PCR reactions were separated on a 1% agarose gel, followed by the excision and purification of the resulting amplicons. The amplicon was then cloned into pGEM-T Easy vectors and transformed into DH5α competent bacteria as previously described. The plasmids were then isolated from the bacteria, checked for the presence of the insert, and send for Sanger sequencing.

3.14. Confirming species identity

Due to the similar phenotypic profile of *E. fetida* with other earthworm species, it was imperative to confirm species identity. This was achieved in two ways. Firstly, through the characterisation of the setae, the hair-like structures on their body wall and, through the

genotypic characterisation of the cytochrome c oxidase subunit 2 (COII) via Sanger sequencing. Briefly, RNA was extracted from individual animals and reverse transcribed, followed by a PCR to amplify a region of the COII transcript. Next, the amplicon was purified, cloned, sequenced and analysed as described in 3.11 and 3.12.

3.15. Cadmium exposure

In experiments where the effects of cadmium (Cd) were to be examined, 200mg $CdCl_2$ was added per kilogram of soil, and was mixed thoroughly to ensure uniform distribution, and allowed to equilibrate for 48 hours. *E. fetida* worms were then exposed to cadmium for 20 days. The worms were then washed in distilled water before being transferred to filter paper (Whatman), soaked in distilled water, for 24 hours in order to void the gut content, from any residual soil. The worms were then processed accordingly, as described below.

3.16. Histology

3.16.1. Fixation

For histological evaluation, either the first six anterior segments or the first six post-clitellar segments were cut, accordingly. The worms were anaesthetised as described previously. They were then placed on the dissection mat under a light microscope. Either the first six anterior segments or the post-clitellar segments were identified and cut with a pair of stainless-steel scissors. Immediately they were placed in 1ml of formaldehyde solution (Merck, 4% buffered formaldehyde, buffered, pH 6.9). The fixative was then replaced with fresh formaldehyde solution after 5 minutes. The samples were fixed for 48 hours at room temperature under gentle agitation.

3.16.2. Sample Processing

Following fixation, the samples were washed in distilled water to remove excess fixative and then placed in 70% ethanol (Merck) for 1 hour to start the dehydration process. The dehydration process is carried out to remove the water found either within the tissue itself, which would prevent paraffin wax infiltration. From this point, onwards all processing steps were carried out in an automated tissue processor (TP1020, Leica). The tissues were then placed into a plastic cassette, followed by submersion in 90% Industrial Methylated Spirit (IMS, Fisher Chemicals) for two hours and in 100% IMS for a further two hours. The gradual increase in alcohol concentration is to ensure that there is a minimal distortion of the tissue. The ethanol then had to be removed, since ethanol and paraffin wax are immiscible. To clear the sample for ethanol, therefore, xylene was used, which is miscible with both ethanol and

paraffin wax. Firstly, the samples were transferred into IMS: xylene (1:1 ratio, Merck) for two hours, followed by a further two-hour wash in 100% xylene. Lastly, in the final step of 'infiltration', the Xylene was removed from the tissue and was replaced with paraffin wax, by immersing the samples in molten wax for twelve hours (the samples were immersed in two different wax chambers in order to ensure complete removal of the clearing agent). All steps in the processing run were carried out under gentle vertical agitation.

3.16.3. Embedding

After sample processing, the cassettes were transferred to an embedding station (Leica EG 1150H). The infiltrated tissue was removed from the cassette and placed in a metal mould filled with paraffin wax. The tissue was orientated at a 90^{o} angle and in such a way that the prostomium was the first to be sectioned. Next, prior to the wax setting a plastic cassette was positioned on top of the mould and pressed down firmly. Additional wax was added on top, and the mould was then allowed to solidify at room temperature for ten minutes and on a cold plate for a further thirty minutes. The wax block was taken out of the metal mould, and the edges of the plastic cassette were scraped with a steel knife to remove excess wax. The block was then trimmed and cut into a trapezium-like shape.

3.16.4. Sectioning

The wax block was positioned on a microtome (Reichert-Jung, Mod. 1140 / Autocut) and 6µm sections were cut and placed in a paraffin section mounting bath (~42^{o}C, Barnstead Electrothermal) to smoothen and flatten out. Unless stated otherwise all sections prepared were mounted on Super Frost Plus slides (Thermo Scientific) and allowed to dry at room temperature for 1 hour before being transferred to a 60^{o}C oven for 2 hours. The slides were then stored at room temperature for downstream experimental procedures.

3.16.5. Cryosectioning

The samples were fixed as before in 3.16.1 and then placed in 15% sucrose in 1X PBS until the tissue sunk to the bottom of the tube (~1 hour). The samples were transferred to 30% sucrose in 1X PBS until the tissue sunk to the bottom of the tube (~2 hours) and stored at 4^{o}C until further processing. The tissues were embedded in a cryomatrix gel (ThermoFisher Scientific) in the correct orientation, similarly to 3.16.3. The matrix was then allowed to solidify in a cryostat chamber (Leica, CM1950). 10µm sections were then cut and mounted on Super Frost Plus slides (ThermoFisher Scientific) and allowed to dry at room temperature for 24 hours, before being stored at 4^{o}C

3.17. Immunohistochemistry

3.17.1. Avidin-Biotin Complex (ABC) staining

Paraffin sections were cut as described in 3.16 and mounted on Superfrost Plus slides (Thermo Scientific) and allowed to dry O/N followed by 1 hour in a 60^{o}C oven. Unless stated otherwise, all steps in this procedure were performed at room temperature, with the slides positioned in a slide rack. The sections were dewaxed in xylene, for two washes of 5 minutes each, followed by rehydration of the sections by sequential immersion through graded ethanol washes (100%, 90, 80%, 70%, 50%) for 3 minutes each at room temperature. The activity of endogenous peroxidases was blocked by immersing the slides in 3% hydrogen peroxide (H_2O_2) for 10 minutes. Following the H_2O_2 incubation, the slides were thoroughly washed with tap water and rinsed in deionised water. Next, for antigen retrieval, the citric acid method was used, in order to expose the underlying epitopes, or antigenic determinant, which were cross-linked and hidden following fixation. A stock (1M) of the citric acid solution was prepared by dissolving 105g of citric acid (VWR) in 500ml of deionized water. The stock was then diluted, in a pressure cooker base, to 1mM using deionised water and mixed well with a magnetic stirrer for a final volume of 800ml. The solution was adjusted to pH6 using 5M NaOH (VWR). The pressure cooker was then placed in a microwave and was heated up for 9 minutes at 900-1000w until the solution just started to boil. The slides were then placed into the citric acid solution using long forceps. The base of the pressure cooker was then covered with the lid and placed back into the microwave and reheated at full power for a further 6 minutes. On completion, the pressure cooker was allowed to stand at room temperature for 15 minutes, until the pressure valve was fully depressed. The pressure cooker lid was removed, and all the traces of the citric acid buffer eliminated by placing the base of the pressure cooker (with the slide rack still inside) under cold running tap water for 10 minutes. The slides were then gently dried off on absorbent tissue paper. A ring was then drawn around the sections using a PAP pen. The slides were then taken out of the slide rack and covered with blocking solution (2% BSA) for 6-7 minutes. The blocking solution was prepared as follows: firstly, a stock TBS solution was prepared (0.5M) by adding 30g TRIS (VWR) and 44g NaCl (VWR) to 350ml of deionised water. The solution was adjusted to ph7.6 using 25% HCl (VWR) and then made up to 500ml with deionised water. 20ml of the stock TBS solution (0.5M) was added to 4g of Bovine Serum Albumin (BSA, Merck) and 0.2g of sodium azide (VWR) and made up to 200ml with deionised water and allowed to dissolve using a magnetic stirrer. The solution was stored at 4^{o}C. The blocking solution was then flicked off and the primary antibody, at its specific dilution factor (using blocking solution as

the diluent) was added onto the sections and allowed to incubate for 2 hours at room temperature. The following primary antibodies were used: an earthworm specific rabbit anti-MT2 (Stürzenbaum, 2001), a rabbit anti-NG2/CSPG4 (1:300, Chemicon International, AB5320) and a rabbit anti-mouseADAM10 (kindly provided by Professor Jörg-Walter Bartsch). The slides were rinsed in 0.05M TBS and then washed for 10 minutes in 0.05 TBS with periodic stirring of the slides, in order to ensure complete removal of the primary antibody. The excess TBS was then flicked off and the slides were incubated in biotinylated secondary antibody for 1 hour at room temperature. The secondary antibodies used were either goat anti-rabbit (1:300, Vectolab BA-1000) or goat anti-mouse (1:300, Vectorlab BA-9200). Both of the secondary antibodies were diluted using blocking solution. The StreptABComplex/HRP (VectorLabs PK6100 Vectastain Elite ABC HRP kit) was then prepared by mixing 10µl of Reagent A (Streptavidin) with 10µl of Reagent B (Biotinylated HRP) in 1ml of 0.05 TBS. The mixture was allowed to complex and bind together for 30 minutes before using in the next step. The volume that was made up was adjusted based on the number of slides at the time of the experiment, intended for immediate use. The secondary antibody was rinsed off the slides with 0.05 TBS and washed once with 0.05 TBS, with periodic stirring. The StreptABC-HRP complex was then added to the sections and allowed to incubate for 30 minutes at room temperature. Following the incubation, the slides were rinsed off with 0.05 TBS and washed in 0.05 TBS for 5 minutes with periodic stirring, to ensure complete removal of the complex. The DAB solution (Merck) was prepared using a 0.1 TRIS buffer as a diluent for a final concentration of 0.03% DAB. The TRIS buffer stock (1M) was prepared as follows: 60g of TRIS was dissolved in 350ml of deionised water and adjusted to pH 7.6 using 25% HCl. The stock solution was then made up to 500ml. The slides were then immersed in DAB solution and allowed to develop (towards a brown precipitate) for 10 minutes, with periodic agitation. The slides were then washed under running tap water for 5 minutes and counterstained with haematoxylin for 2 minutes. The slides were then rewashed under running tap water. Finally, the sections were dehydrated in 100% IMS in four 2-minute washes, followed by clearing in xylene for two 5-minute washes and then mounted with a coverslip under DPX and allowed to set. Images were taken under a Nikon Eclipse 2000-S microscope with the Nikon DS-2Mv camera and the NIS elements software.

3.17.2. Immunofluorescence staining

The dewaxing, dehydrating and antigen retrieval procedures were carried out as described in 3.17.1. Following the antigen retrieval, however, the sections were dried off on absorbent paper and covered with 3% ammonium chloride for 30 minutes in order to minimise

formalin-induced fluorescence. The excess was then flicked off and the blocking solution added onto the sections for 5 minutes. The blocking solution was prepared as before; however, in IF staining, 200µl of TRITON X was also added into the blocking solution. The blocking solution was then flicked off and the primary antibody, either rabbit anti-earthworm MT2 or anti-tubulin, were applied for 2 hours at room temperature (the antibody preparation is described above). The slides were then rinsed in 0.05M TBS and washed in 0.05M TBS for 10 mins, with periodic stirring. The excess TBS was washed off and the sections were then incubated for 2 hours at room temperature in fluorochrome-secondary antibodies. For the anti-MT2 and anti-tubulin secondary antibodies, the Alexa 594 and the Alexa 488 fluorochromes were used, respectively. Counterstaining of cell nuclei was achieved using by adding Hoechst stain directly into the secondary antibody diluent buffer (i.e. blocking solution) in both secondary antibodies used, for a final concentration of 0.5µg/ml. The slides were then rinsed in 0.05M TBS and washed in 0.05M TBS for 10 mins, with periodic stirring. Finally, the Mowiol mountant (see more details below on the in-house preparation) was added, and the sections were covered with a coverslip and allowed to set. The Mowiol mountant was prepared as follows: 40ml of TRIS buffer 0.2M (12.12g TRIS dissolved in 400ml distilled water; adjusted to pH8.5 with HCl and made up to 500ml), was added to 25ml of distilled water in a glass beaker. Next, on a heated magnetic stirrer, 9.5g of Mowiol (Merck) was added into the beaker gradually, to avoid clumping. The mixture was allowed to stir for 2 hours and then transferred to a 60^{o}C oven for 24 hours. While stirring, 25g of glycerol and 1ml of 10% sodium azide was added to the solution. When all reagents were dissolved, DABCO (Merck) was added and stirred until dissolved. The solution was then aliquoted into 50ml tubes and centrifuged at 5000g for 10 minutes. The supernatant was collected, without disturbing the pellet, and poured into dispensing bottles. The mountant was stored at room temperature, in the dark. Images were taken under a Nikon Eclipse 2000-S microscope with the Nikon DS-2Mv camera and the NIS elements software.

3.18. Haematoxylin and Eosin staining

Following the rehydration of the samples, as described in 3.17.1, the slides were washed in 1X PBS for 5 minutes. Excess PBS was flicked off and the slides immersed in haematoxylin solution (basic dye which binds to the negatively charged DNA) for 5 minutes at room temperature. The slides were then rinsed in running tap water and washed in 1X PBS for 5 minutes. Excess PBS was flicked off, and the slides were immersed in eosin solution (cytoplasmic staining) for 30 seconds at room temperature. The slides were once again rinsed in running tap water and washed in 1X PBS for 5 minutes. Finally, the sections were

dehydrated in 100% IMS in four 2-minute washes, followed by clearing in xylene for two 5-minute washes and then mounted with a coverslip under DPX and allowed to set. Images were taken under a Nikon Eclipse 2000-S microscope with the Nikon DS-2Mv camera and the NIS elements software.

3.19. Transcriptomic analysis of cerebral ganglion regeneration via RNAseq

3.19.1. Experimental design

Three experimental conditions were used, in order to build an understanding of the transcriptomic landscape which governs neuronal regeneration in the earthworm *Eisenia fetida*; 1-week post-sham surgery (1wS), 1-week post-decerebrated (1wD) and 5 weeks post-decerebrated (5wD). The time points selected covered early, as well later time points in neuronal regenerative processes. The preparation of experimental animals was carried out as described in 3.2. The Cytochrome c Oxidase subunit 2 (*coII*) transcripts were sequenced, via Sanger sequencing (see 3.12) of seven worms from each of the three conditions. A phylogenetic tree was then built based on the *coII* sequences in order to select the worms which exhibited the least evolutionary divergence. Three individual worms were then selected for every condition. Differential Gene Expression (DGE) analysis was conducted between the sham vs 1wD, sham vs 5wD and 1wD vs 5wD. The RNAseq experimental procedure, including the *de novo* transcriptome assembly, sequencing, mapping and differential expression analysis, was carried out by Genewiz (South Plainfield, NJ, USA). Sample preparation and selection annotation and further bioinformatics analysis were done by me.

3.19.2. RNA extraction

The experimental animals were prepared as described in 3.2 for 1wS, 1wD and 5wD. RNA was extracted from seven individual worms from each experimental condition as described in 3.5 from the first 10 anterior segments. As mentioned above, the tissue used for extraction was the Ventral Nerve Cord (VNC), the Suboesophageal Ganglion (SOG) and the Circumpharyngeal Connectives (CC). The control cerebral ganglion in the sham-operated worms, as well as the regenerated cerebral ganglion in the 5-week decerebrated worms, were discarded. In addition to the CNS, the pharyngeal tissue was also extracted which was used to genotype and phylogenetically analyse each individual worm based on their co*II* transcript sequence.

3.19.3. Assessing the RNA quality

The extracted total RNA was tested for its concentration, purity and quality using RNA pico chip (Agilent Technologies) according to the manufacturer's instructions. Each RNA chip is comprised of an interconnected set of microchannels which were used to separate the RNA fragments electrophoretically through a gel medium, according to their size. For a more detailed explanation please refer to https://www.arboretum.harvard.edu/wp-content/uploads/RNA-Agilent-Pico-Quick-Protocol.pdf. The chip was analysed in the Agilent 2100 Bioanalyser System. The quality of the samples was assessed based on the integrity of the 18S on the pico chip gel. Genewiz conducted additional quality control assessments of the nine samples provided to them, including spectrophotometric analysis (Nanodrop 2000), fluorometric analysis (Qubit) and a run using an RNA ScreenTape (Agilent Technologies) which was analysed using TapeStation software (Agilent Technologies). It is important to note that an RNA Integrity Number (RIN) was only possible to be obtained using the 5S ribosomal subunit peak, due to the almost negligible peak produced at the 28S.

3.19.4. Phylogenetic Analysis

Total RNA was extracted from the pharynx of 21 worms (7 worms / experimental condition). The mRNA was reverse transcribed, and the COII transcript was amplified in a PCR using gene-specific primers. The annealing step temperature was set at 54^{o}C, and the extension step at 45 seconds. The amplicon was run on a 1% agarose gel, excised from the gel, purified, cloned and sequenced as described in 3.12. The sequences obtained from the Sanger sequencing were input into MEGAX, and a phylogenetic tree was constructed. The CLUSTALW algorithm was used for building the multiple sequence alignment. The evolutionary history was inferred using the Maximum Likelihood Method, and the evolutionary distances were computed using the Maximum Composite Likelihood (MCL) method. The evolutionary divergence between samples, quality and quantity of RNA were considered before selecting three RNA samples for each condition to be used in the experiment.

3.19.5. RNAseq workflow

The experiment was conducted on the Illumina HiSeq2500 platform. The RNA library was prepared via poly-A selection, in a 2x100bp paired-end (PE) configuration in High Output mode (V4 chemistry). Due to the lack of a fully sequenced genome, a *de novo* transcriptome scaffold had to be built onto which the resulting sequences could be mapped.

3.19.5.1. RNA sample preparation for RNAseq

mRNAs were purified via Poly(A) selection from a total RNA sample provided to the company, followed by fragmentation. The first strand of cDNA was synthesized using random priming, followed by the synthesis of the second strand of cDNA. The resulting double-strand cDNA was end repaired, phosphorylated and A-tailed which allowed for specific adapter sequences to be ligated. Next, the cDNA was amplified via PCR. This process adds additional motifs on either end of the tagged sequence, such as the sequencing primer binding sites, indices (specific to each sample) and complementary regions to the two types of oligonucleotides attached to the flow cell.

3.19.5.2. Clustering

The clustering procedure took place in a flow cell, which is a glass slide with lanes in which a lawn of two types of oligonucleotide sequences were attached. The modified cDNA sequence hybridised to the oligonucleotide through one of the two complementary adaptor regions previously incorporated. Once hybridised, DNA polymerase created a complement of the hybridised fragment. The double-stranded molecule was then denatured, and the single strand was then clonally amplified through bridge amplification, using the second complementary adaptor region. Another DNA polymerase reaction formed a double-stranded bridge, followed by denaturation through which two single-stranded copies of the original molecule were attached to the flow cell, one for each of the two oligonucleotides. This process was repeated for a cluster generation of one single fragment and occurred simultaneously for all the fragments in the sample. The antisense strands were then cleaved and washed off.

3.19.5.3. Sequencing by Synthesis

The first sequencing primer attached to the adaptor sequence on the sense strand which initiated the sequencing reaction. In each sequencing cycle, four uniquely fluorescently tagged nucleotides bound based on sequence complementarity. The nucleotides were excited by a light source, through which a fluorescent signal was emitted, unique to each nucleotide. 100 cycles were performed to obtain 100bp reads for each fragment. Once the desired read length was reached, the read product was washed away. Next, to identify the sample, the first index primer hybridised to the template adaptor sequence on the sense strand, and a sequencing read was generated as before. The read product was then washed off. For better accuracy and reliability of the resulting sequences, a paired-end sequencing approach was followed. The sense template then folded and attached to the second oligonucleotide on the flow cell following by a second index read in the same way as the first

index. Next, the double-stranded bridge was formed through a polymerase reaction. The bridge was denatured and the sense strand cleaved and washed off. A second sequencing reaction then took place as described above using the second sequencing primer. Finally, based on the indices signal, overlapping sequences were clustered based on local sequence clustering.

3.19.5.4. De novo Transcriptome assembly

Low-quality bases at the ends of the raw sequences were trimmed and removed. The *de nono* transcriptome was assembled using the CLC Genomics Workbench v. 9.0.1, using all the resulting sequencing data across all nine samples.

3.19.5.5. Trimmed sequence mapping

Trimmed sequences were then mapped onto the newly assembled *de novo* transcriptome, and total hit counts of those sequences within each of the 9 samples were determined, as well as the Reads Per Kilobase of transcript per Million mapped reads (RPKM) expression values.

3.19.5.6. Differential Gene Expression analysis

The total counts of the contig/transcript sequences were used in the DESeq2 package to determine differential gene expression within the three experimental groups (i.e. 1wS vs 1wD, 1wS vs 5wD and 1wD vs 5wD). Through the DESeq2 package an internal normalization was performed where the geometric mean was calculated for each gene/contig across all samples. The counts for a gene in each sample was then divided by this mean. To address the transcript composition bias in the three different experimental groups, shrinkage estimation for dispersions and fold changes was then employed. To correct for multiple testing and, p-values for each contig, obtained via the Wald test, were then adjusted to minimise false-positives using the Benjamini and Hochberg method Differentially expressed genes were designated those which exhibited an adjusted (adj) p-value of <0.05 and a Log2Fold change >1. (Benjamini and Hochberg, 1995; Love *et al.*, 2014).

3.19.6. Local nucleotide database BLAST analysis

One of the limitations of conducting an RNAseq experiment, especially in the case where a *de novo* transcriptome will be built, the transcripts which do not exhibit differential expression between the experimental conditions will not be identified and are indeed often overlooked. In order to identify genes of interest (GOI), the LBlastPycli software (https://gitlab.com/klel/LBlastPycli) was used which was built for this purpose by Katariina Latvala (Tampere University of Technology, Finland) in association with Tom Kaminski (King's

College London, UK). The software was built using Python and NCBI's BLAST command-line tools. Effectively, this tool enables us to run BLAST of either a selected protein (tblastn) or nucleotide (blastn) sequence, against the *de novo* transcriptome that has been produced and obtain a list of contigs, of close homology with the query sequence. We then proceeded to characterise the baseline levels of expression of the GOIs through their raw counts obtained from the RNAseq and evaluate their contribution towards neuronal regeneration.

3.20. Gene Ontology

3.20.1. BLASTx

The differentially expressed contigs/transcripts (a cut-off was set at 4-fold up- (+) or downregulation for all comparisons, with the exception of 1wD vs 5wD (-) in which a 9-fold cutoff was set) were annotated using the BLASTx tool on NCBI, where a translated contig sequence was queried against the database, for any potential homology. Due to the limited availability of published *E. fetida* sequences on the database, the contig was annotated based on the top hit within *Homo sapiens* sequences, only if that identity was sensibly consistent with the identity obtained in BLASTx across all species. The use of the *H. sapiens* identities eliminated the problem where the naming of the top hit overall varied across several species, or when that identity was not prevalent in the scientific literature. All identities recorded had to meet the Expect value (E) threshold, which was set at 10^{-4}. This is a parameter that describes the number of hits that can be obtained by chance alone. The E value dramatically decreases as the reliability of the reported identity increases. Also, the conserved protein domains of the query sequences were identified in BLASTx.

3.20.2. STRING

An over-representation analysis was performed using the web-based tool, STRING, in which a pre-defined list of gene IDs, build from the differentially expressed contigs identified in 3.20.1, was used to uncover enriched biological processes, molecular functions and cellular components. The whole genome of *Homo sapiens* was used a statistical background. Enriched pathways/terms were sorted by their adjusted p-values, that were computed using a Hypergeometric test followed by multiple testing correction via the Benjamini and Hochberg method. (Szklarczyk *et al.*, 2019)

3.20.3. Protein sequence alignment

Genes of interest were translated in Expasy. The resulting amino acid sequences were compared with their paralogs in the species with the highest similarity and in *H. sapiens*, in the web-based tool of EMBL-EBI for pairwise sequence alignments.

3.20.4. *In silico* modelling of protein tertiary structure

The tertiary structure of partial and full length protein sequences of interest, that were obtained via the RNAseq, was modelled using SWISS-MODEL https://swissmodel.expasy.org/interactive

3.21. Synchrotron X-ray Fluorescence (XRF) spectroscopy

The Synchrotron X-ray Fluorescence (XRF) spectroscopy allows for the characterisation of the elemental distribution, *in vivo*, across any biological tissue. Briefly, the procedure is initiated with the introduction of electrons (using an electron gun) into a storage ring within the Synchrotron. The electrons are then accelerated to high speeds and focussed as the electrons pass through dipole (bending) magnets, as well as quadrupole and sextupole magnets. Due to the acceleration experienced by the electrons around the bending magnets, the electrons emit X-rays which are then directed towards the experimental stations where they bombard the sample in question. When a particular atom is hit with this micron-sized X-ray beam, with the energy of this magnitude, an electron from the inner orbital shell of that atom overcomes the nuclear attraction and escapes. In order for the atom to regain stability, an electron from a higher energy orbital shell (i.e. outer shell) moves to the lower energy orbital shell to fill in the vacancy. During the change from a higher energy orbital shell to a lower one, a characteristic fluorescent X-ray radiation is emitted (secondary X-ray photon radiation) which has a specific energy that can act as a unique identifier of the atom from which it had originated. In this way, elemental distribution XRF maps can be produced with high accuracy and precision, depicting the exact composition of the biological tissue.

3.21.1. Sample Preparation and Tissue sectioning

The samples that were used in this experiment were the following: sham-operated worms, 1-week post-decerebration, 4 weeks – 11 weeks post-decerebration, 5 weeks post-hemiganglioctomy and 5 weeks post-hemisectioning. The surgical procedures were carried out as described before. The anterior part of the samples was then fixed, processed and sectioned (6µm) as before. The sections (6µm) were mounted on quartz microscope slides (UQG) and allowed to air dry at room temperature for 24 hours before being stored in a plastic slide holder at room temperature.

3.21.2. XRF experimental procedure

The experiment was conducted at the i18 beamline at the Diamond facility in Oxford. An in-depth description of the instrumental set up is discussed elsewhere (Diaz-Moreno *et al.*, 2018). Briefly, the slides were mounted onto a motorised holder at 45° angle to the X-ray

beam. The incident energy of the beam was set to 10.6KeV in session 1 and 11keV in session 2. The emitted X-ray fluorescence was detected by a dual Vortex ME-4 silicon drift detector system (Hitachi) and positioned at 90° to the beam. 10µm and 3µm beam sizes were used to scan the samples, with the resolution of the elemental maps increasing as the beam size decreased. Dwell times (how much time the beam excited a particular point in the sample) were set to 0.5s and 0.7s for 10µm and 3µm beam sizes, respectively.

3.21.3. Spectra Analysis

The elemental maps were visualised using DAWN 2.14.0. The fitting of the resulting spectra, as well as the elemental quantification, was performed in PyMca 5.4.2.

3.22. Benzidine Assay

A benzidine reaction was used to characterise the distribution of haemoglobin/neuroglobin containing tissues. Samples that had undergone hemiangliooctomy surgery, were prepared for cryosectioning as described in 3.16.5. The cryosections were allowed to dry at room temperature for 24 hours and then stored at 4°C. The benzidine working solution as prepared as follows: 0.5g of benzidine (Merck) of 100ml of 10% acetic acid (dissolved in 1X PBS) for a final concentration of 0.5% benzidine. A 30% H_20_2 solution, in PBS, was prepared for immediate use. The benzidine solution (200µl) was then added to the sections, followed by the addition of 1µl of the 30% H_20_2 solution. The sections were then incubated for 5 minutes. The blue precipitate formed signified the presence of haemoglobin/neuroglobin. The experiment was carried out with *E. fetida* and *E. andrei*, at University of Pecs.

3.23. Terminal deoxynucleotidyl transferase dUTP Nick End Labelling (TUNEL)

Cell apoptosis is a hallmark of regenerative processes and can be studied using Terminal deoxynucleotidyl transferase dUTP Nick End Labelling (TUNEL, Promega), which takes advantage of the fact that cells which undergo programmed cell death exhibit double-stranded nicks in their DNA. Fluorescently labelled nucleotides can, therefore, be ligated and the apoptotic cells detected. The experimental procedure is carried out on formalin-fixed, paraffin-embedded samples. 6µm sections were mounted on Superfrost Plus slides and dried as described above. Tissue sections were deparaffinised by immersing the slides in xylene in a coplin jar for 5 minutes at room temperature, for a total of two washes. The sections were rehydrated by sequential immersion through graded ethanol washes (100%, 90%, 80%, 70%, 50%) for 3 minutes each at room temperature. The samples were then washed in 0.85% NaCl

for 5 minutes at room temperature, followed by 1X PBS wash for 5 minutes at room temperature. The slides were then placed in 4% methanol-free formaldehyde solution in PBS, for 15 minutes at room temperature. The samples were then washed in 1X PBS for 5 minutes, for a total of two washes. Excess PBS was flicked off and the sections digested by adding 20µg/ml (1X PBS was used as the diluent) proteinase K directly onto the sections and incubated for 13 minutes. The slides were then washed in 1X PBS for 5 minutes at room temperature. The slides were then placed back in fresh 4% methanol-free formaldehyde solution, for 5 minutes at room temperature, and washed in PBS for 5 minutes at room temperature. The excess PBS was flicked off and the sections covered with equilibration buffer for 10 minutes. The buffer was then flicked off and the sections covered with the rTdT incubation buffer. The rTdT incubation buffer was prepared as follows: for every 51µl, 45µl equilibration buffer, 5µl nucleotide mix and 1µl rTdT enzyme were mixed thoroughly in a 1.5ml tube. The slides were then incubated in a humidified chamber in the dark at 37^{o}C for 60 minutes, to allow for the incorporation of the fluorescently labelled nucleotides to take place. Following the incubation, the samples were washed in 2X SSC (provided) for 15 minutes at room temperature. In order to eliminate the background signal, the slides were then washed in 1X PBS consisting of 0.1% TRITON X and 5mg/ml BSA for 5 minutes, for a total of three washes, followed by a 5-minute wash in 1X PBS. The excess PBS was flicked off, and the sections were incubated with Hoechst (0.5µg/ml) (i.e. blocking solution was used as diluent) for 5 minutes, to stain cell nuclei. The slides were then washed in 1X PBS for a total of two washes to remove unincorporated Hoechst stain. The excess PBS was flicked off, and the Mowiol mountant was then added onto the sections and covered with a glass coverslip. The samples were analysed immediately under a Nikon Eclipse 2000-S microscope, with a Nikon DS-2Mv camera and the NIS elements software.

3.24. Laser Ablation Inductively Coupled Plasma Mass Spectrometry (LA-ICP-MS)

High-resolution Laser Ablation-Inductively Coupled Plasma-Mass Spectrometry (LA-ICP-MS) imaging was performed on paraffin embedded sections. Paraffin-embedded samples were dewaxed by washing in xylene for 5 minutes (x3) followed by 100% ethanol washes (5 minutes x3), and slides were mounted in the standard microscope slide sample holder of the HelEx II 2-volume ablation cell. An aerosol rapid introduction system (ARIS) was used on the Teledyne CETAC Technologies Inc. Analyte Excite laser ablation system for fast transport of

the aerosol generated from the laser ablation at the sample surface to a Perkin-Elmer NexION350D ICP-MS.

Operational parameters of the Perkin-Elmer NexION350D ICP-MS were tuned, using a NIST SRM 612 glass certified reference material, for maximum sensitivity and low laser-induced elemental fractionation ($^{238}U+/^{232}Th+ \approx 1$). Before imaging, test line scans were conducted on the samples in order to find the optimal operational conditions and data acquisition parameters for high-resolution LA-ICP-MS imaging. The laser energy density of 1.12 J cm^{-2} were selected in order to minimise the signal contribution from the glass microscope slide while still fully ablating the samples. The selected isotopes of interest were ^{111}Cd, and ^{31}P (normalisation purposes), chosen to minimise polyatomic interferences and reduce background signal. The experiment was conducted at the Mass Spectrometry Facility at King's College London in collaboration with Dr. Theodora Stewart, who calibrated and optimised the process.

4. Results

4.1. Characterisation of *Eisenia fetida*: speciation, time-course of regeneration and cell distribution in the neuronal system

4.1.1. Genotypic and phenotypic characterisation of the species, *Eisenia fetida*

Species identification in earthworms has long been a subject of intense debate. Species-specific variation can affect the experimental design and ultimately produce unreliable data, especially in cases of cryptic speciation, where a heterogenous population of worms is used. Initially, steps were taken to ensure that the worms that were used in the experiment were in fact, *Eisenia fetida*. Previous studies have characterised the metabolic phenotype profile of *E. fetida* tissue extracts and coelomic fluid via Nuclear Magnetic Resonance (NMR) spectroscopy and compared it to other earthworms as a means of differentiating the species (Bundy *et al.*, 2002). In addition, a method based on fluorescence was also described by which a distinct metabolic profile of *E. fetida's* coelomic fluid was defined (Albani *et al*., 2003). In this work, the speciation analysis was based on the phenotypic characteristics of *E. fetida* (Sherlock, 2018) as well as molecular barcoding, through Sanger sequencing. These are simple approaches and can be applied in any molecular biology lab, through which the species identity can be reliably assigned.

E. fetida earthworms are characterized by red bands with yellow intersegmental spaces that lack dark pigmentation. However, this is not a unique feature, since this can be observed in other species, such as *Dendrobaena veneta* (Figure 4.1A and B), and thus cannot be reliably used to identify the species. However, the position of the setae, the hair-like bristles located on each segment, differ between the species. Namely, they are more closely paired in *E.fetida* than in *D.veneta*, which is a more reliable way to distinguish them (Figure 4.1C). Interestingly, in England, both *E. fetida* and *D. veneta* are widely used in compost heaps and are often found in mixed cultures across the country.

Initially, for the experiments, earthworms were sourced from commercial suppliers in the UK, that claimed they either sold pure *E. fetida* cultures or in a mixture with *D. veneta*. However, it was apparent that the proportion of *E. fetida* in those cultures was not according as advertised. It was then decided to determine the species identity of earthworms obtained from five commercial suppliers in the United Kingdom marketing the sale of a pure *E. fetida* culture (company A and B) or mixed culture consisting of *E. fetida* and *D. veneta* (company C

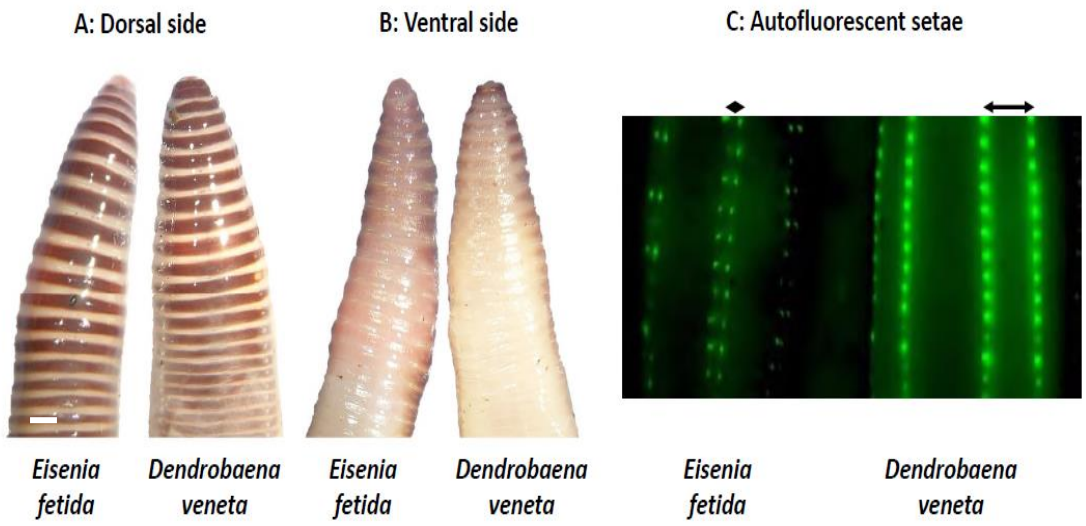

Figure 4.1 Phenotypic characterization of *Eisenia fetida* and *Dendrobaena veneta*. A. The dorsal sides demonstrate the phenotypic similarity, both species being striped with interchanging layers of brown and yellow. B. Setae are positioned on the ventral side where the pigmentation is greatly diminished. C. The setae can be readily visualized by utilizing their intrinsic capacity to autofluoresce (images were digitally captured using a Nikon microscope SMZ800 with blue laser scanning fluorescence (lex = 450–490 nm). The arrows indicate the distance of the setae within each pair; Note the setae are closely paired in *E. fetida* and widely paired in *D.veneta*. Scale bars: 200µm.

to E). Five worms were randomly selected from each company (i.e. 25 worms), and their identity was confirmed by the Sanger sequencing of the cytochrome c oxidase subunit 2 (*coII*), followed by the building of a phylogenetic tree using the *coII sequences* (Figure 4.2). Also, the *coII* sequences of *E. fetida*, *E. andrei*, *Lumbricus rubellus, L. terrestris* and *D. veneta* were included from global locations (obtained either from NCBI or specimens from collaborators) to account for potential sequence variations due to geographical distance. Of all the worms tested, only one clustered with the *Eisenia* group in the tree (Figure 2, node A4). To confirm that this was indeed an *E. fetida* sequence, BlastX showed that the A4 sequence exhibited the highest similarity with an *E. fetida* sequence on NCBI (Accession number; AIL25888.1). Also, the A4 sequence was one of the ten sequences obtained from worms, of which the suppliers claimed that they sold pure *E. fetida*; while the remainder were all *D. veneta*, as indicated by sequence homology on NCBI (Accession number; AIL25877.1). Surprisingly, even though *Eisenia* and *Dendrobaena* species look more phenotypically similar than *Lumbricus*, the tree revealed that *L. terrestris* and *L. rubellus* are more closely related to *Eisenia, than Dendrobaena is*. Also, it is worth mentioning, that *E. andrei* and *E. fetida* do not show an apparent dissociation or split in the tree indicative of a distinct species, as one would expect based on earlier studies (Domínguez *et al.*, 2005), but

instead appear to overlap. Interestingly, cross-breeding experiments have shown that even though *E. andrei* and *E. fetida* are likely to be true species, it is possible to obtain fertile hybrids under specific conditions (Plytycz *et al.*, 2018). The seemingly close association of the two species could be attributed to their isogenic nature, or in fact, some sequences on NCBI could have been reported under a false name; which from what was observed in this work, it is a realistic assumption.

This work was essential in understanding the importance of confirming the species identity prior to any experimental work. Unless stated otherwise in the Materials and Methods section, Professor Molnar kindly provided the worms that were used, in all the experiments, and their species identity was confirmed, following the same methodology as described above (i.e. phenotypic characterisation and genotyping). The identity of these worms was confirmed as *E. fetida*.

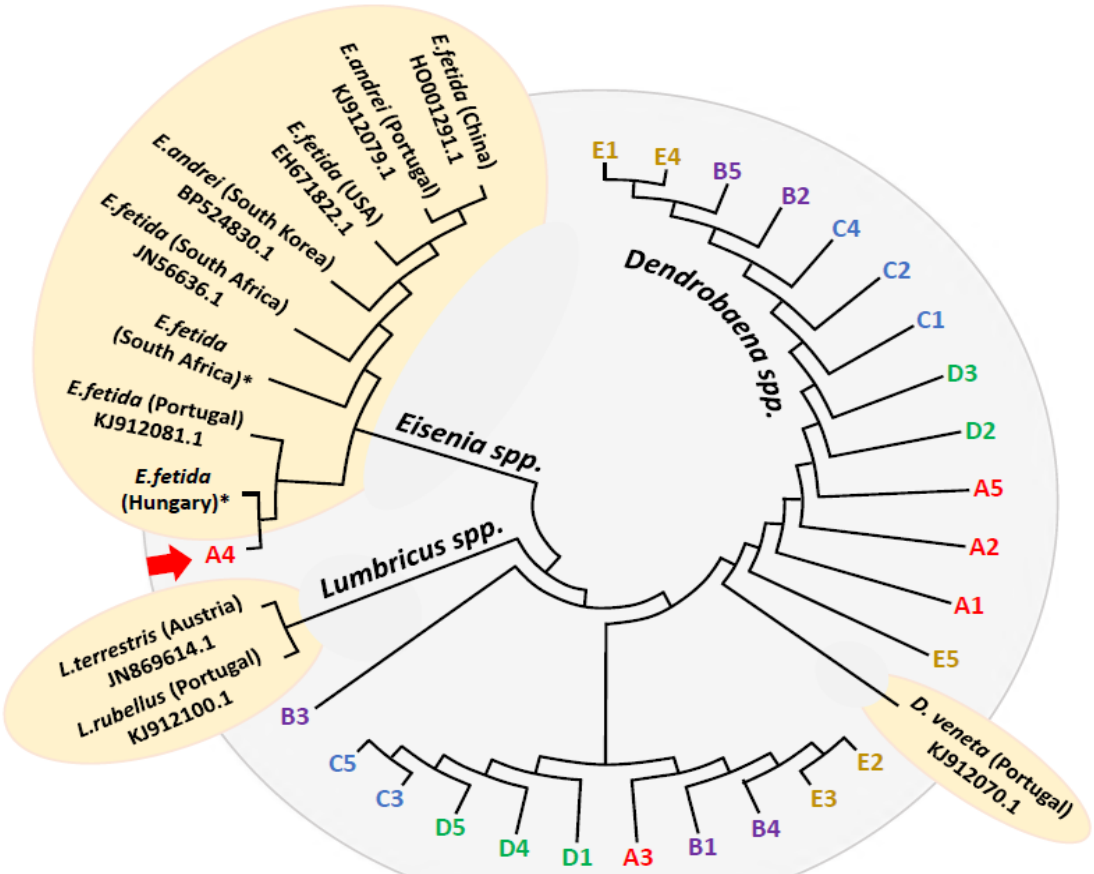

Figure 4.2 Phylogenetic classification of earthworms based on their cytochrome c oxidase subunit 2 (*coII*) sequence. Randomly selected individuals sourced from five UK suppliers claiming to sell either pure *Eisenia fetida* (company A and B) or a mixture of *E.fetida* and *Dendrobaena veneta* (companies C to E) were compared to published reference sequences from NCBI (https://www.ncbi.nlm.nih.gov). The evolutionary relatedness was inferred by using the Maximum Likelihood method and Tamura-Nei model in MEGAX. **E.fetida* obtained from collaborators in South Africa and Hungary, respectively.

4.1.2. Time course of cerebral ganglion regeneration in *Eisenia fetida*

The earthworms, like other species of Annelids, exhibit a remarkable capacity to regenerate their cerebral ganglion (CG) following its surgical removal. Even though there have been studies on CG regeneration, the amount of information in the literature explicitly showing the progression of the regenerating brain in the worm, is lacking. Here, the different stages of CG development following excision are presented (Figure 4.3). In section 3.2 the surgical procedure undertaken to excise the CG from worms was described; for illustration purposes, the excess tissue was removed. In the first 2 weeks following the surgical excision of the

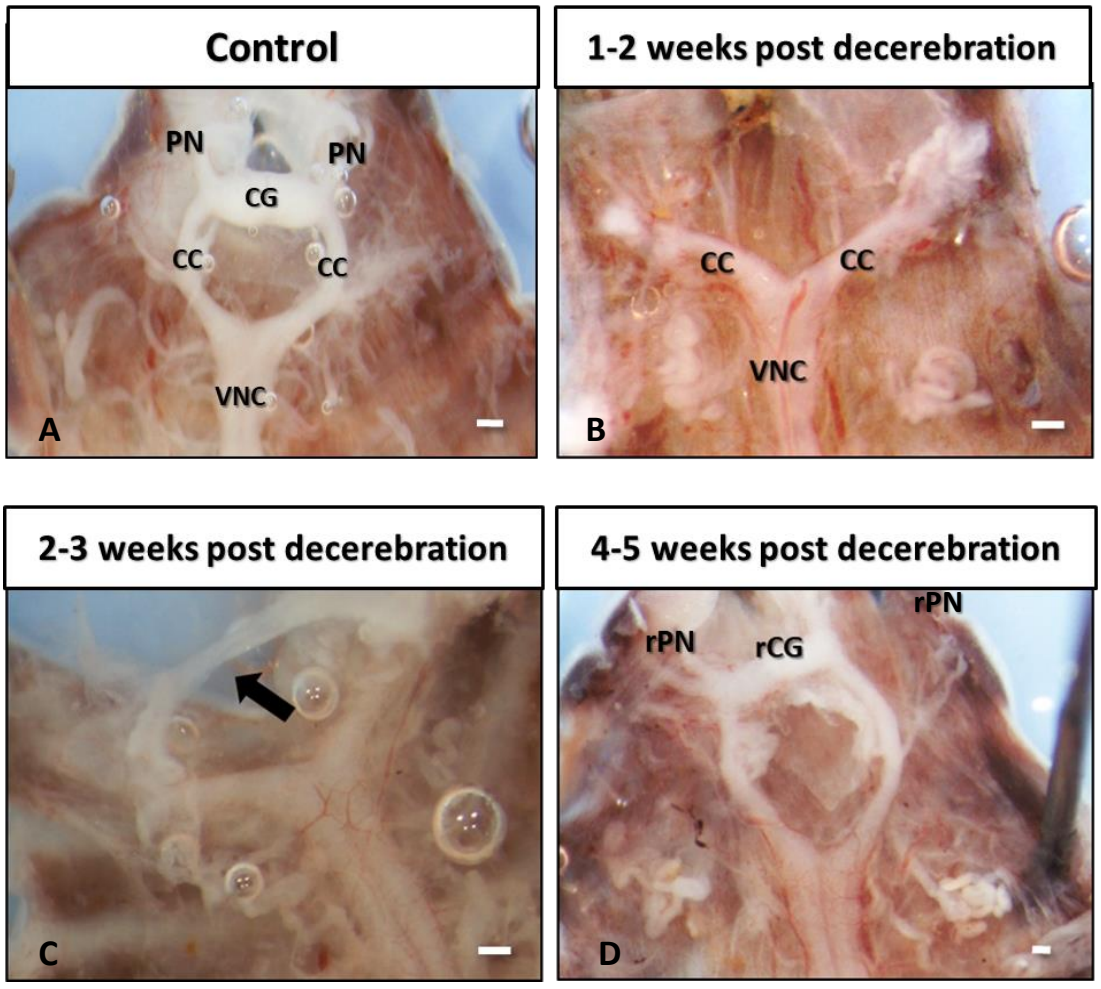

Figure 4.3 Time course of Cerebral Ganglion (CG) regeneration following decerebration. An adult worm is anesthetised via immersion in ice-cold (4-7°C) carbonated water for 3-4 minutes and placed on a dissection mat on its ventral side. The CG was removed and allowed to regenerate as described in section 3.2. A dorsal incision is performed to expose the CG, the Circumpharyngeal Connectives (CC) and Prostomial Nerves (PN). The pharyngeal tissue is carefully removed to reveal the underlying Ventral Nerve Cord (VNC). The first regenerating structure can be identified at week 3, representing a scaffold-like mesh (indicated by the black arrow) at weeks 3 and 4. At week 5 onwards, a distinct regenerated Cerebral Ganglion (rCG) and the regenerated Prostomial Nerves (rPN) can be identified. Images captured via a Nikon DS-2Mv camera. Scale bars: 100µm

brain, a regenerated structure cannot be identified (Figure 4.3B). However, due to the invasiveness in the approach, where the pharyngeal tissue is removed, thin and fragile neuronal structures and axon processes would likely be disrupted and broken down at this time point, and thus would not be visible. At the 3 and 4-week time point (Figure 4.3C), a scaffold-like mesh can be observed, a precursor to the regenerating brain, which will continue to grow and eventually form the regenerated Cerebral Ganglion (rCG), as well as the prostomial nerves (Figure 4.3D). There was a degree of variation in the absolute times at which the brain regenerates, which can be attributed to the individuality of each worm, the age of the worms, as well as the dissecting procedure itself. To account for the individual variation, it is at this stage only possible to indicate a time range rather than an exact time point at which specific regenerative phases were observed. This work did, however, pave the way to define the early and later stages of regeneration in our experimental setting, which was paramount for the downstream experimental conducted.

From these images, preliminary evidence on how the brain develops can be gathered; incremental stages through which axonal processes extend from both the connectives and slowly form the regenerating brain and prostomial nerves. The axons not only extend towards the area of the regenerating brain, but they do so in such a precise manner that can form a neuronal structure resembling the preoperative control brains. The possible avenues that the worm can follow to bring about this remarkable phenomenon are discussed in the next sections.

4.1.3. Histological characterisation of the CNS of *Eisenia fetida*

Before examining the different biochemical pathways that govern the extraordinary regenerative capacity of earthworms, it was imperative to understand how the neuronal system is structured at the cellular level. The cellular distribution within the neuronal system through Hematoxylin and Eosin (H&E) staining, was analysed on formalin-fixed and paraffin-embedded (FFPE) samples. Hematoxylin is a basic deep purple/blue stain (i.e. positively charged) and binds to nucleic acids with high avidity and has been used as the gold standard for labelling cell nuclei. Conversely, eosin is a pink stain which binds to intracellular proteins non-specifically and be used for labelling the cytoplasm. Serial cross-sections (from the anterior to the posterior end) of the CG are presented in Figure 4.4. The CG exhibits an abundant vascular supply that is prevalent within the tissue, and around it, primarily on its dorsal side. The brown staining on the dorsal side of the body wall is indicative

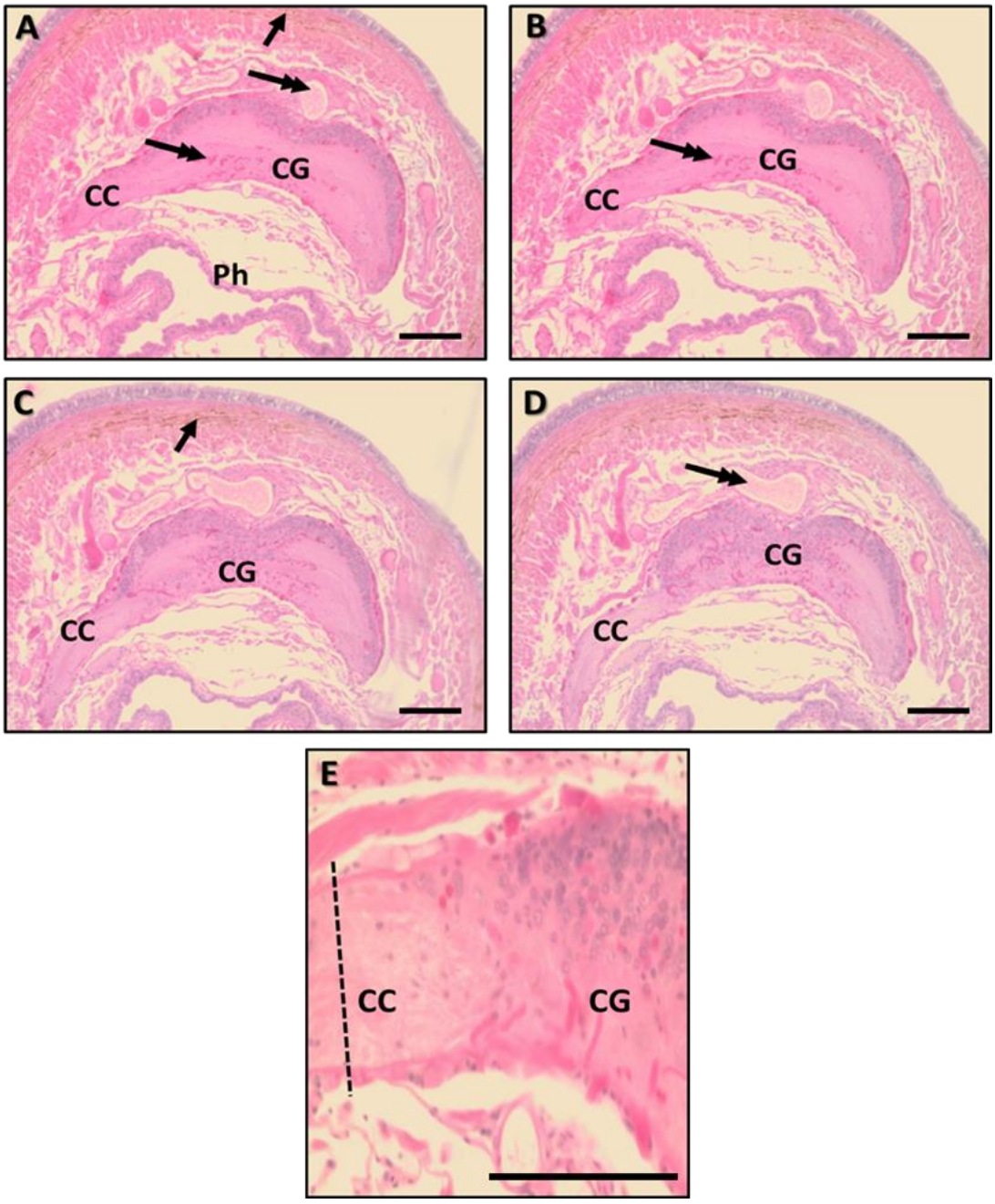

Figure 4.4 Cellular distribution in the CNS and correct cutting level of circumpharyngeal connectives for cerebral ganglion extirpation in *Eisenia fetida*. H&E staining on formalin-fixed paraffin-embedded (FFPE) unharmed samples, demonstrates the cellular distribution in the Cerebral Ganglion (CG), located at the dorsal side of the pharynx (Ph), and in the Circumpharyngeal Connectives (CC). A-D (successive sections). The CG is characterised by a cell-rich region (blue) situated primarily in the periphery. Conversely, the cell count drops within the CC. Dark pigmentation on the dorsal side is indicative of melanin on the worm's body wall (single-headed arrow). The CG displays a rich vascular supply (double-headed arrows) both around and within the tissue. E. Dotted line indicates correct cutting level for CG extirpation, in an area of low cell body presence. Images captured via a Nikon DS-2Mv camera. Scale bars: 100µm.

of the melanin that is found across the earthworm's body. Moreover, cell bodies appear to be situated primarily on the periphery of the dorsal side of the CG, equally on both hemiganglia of the brain. Interestingly, the neuronal tissue of the CG transitions into the circumpharyngeal connectives (CC) at which point the cell distribution pattern is abruptly interrupted, where the cell body count significantly diminished. The difference in cell load between the two neuronal tissues signifies that the CC is not merely a continuation of the brain but in fact, should be considered a distinct part of the CNS with, possibly, specific biological functions. Also, it is worth noting that contrary to the dorsal side, the ventral side of the CG is characterised by a relatively small cell population. The observation that the CG differs in absolute numbers of cells, from the CC, was the foundation from which the dissecting protocol for the removal of the CG was based on. In Figure 4.4E, the difference in cell distribution is shown, alongside with the appropriate cutting level for the precise surgical extirpation of the brain, which is located below the cell-rich region, thus ensuring the complete removal the CG. Moving further down, along the posterior direction, the CCs transition into the SubOesophageal Ganglion (SOG), which is located on the ventral side of the worm (Figure 4.5); the first two ganglia of the Ventral Nerve Cord (VNC) are fused to form the SOG. Similarly to the CG, the density of the ganglion cells is at its highest primarily at the ventral side of the SOG. Furthermore, at the junction between the SOG and CC the density of cells is decreased indicating that the CCs as a whole is a region of a relatively low number of cell bodies.

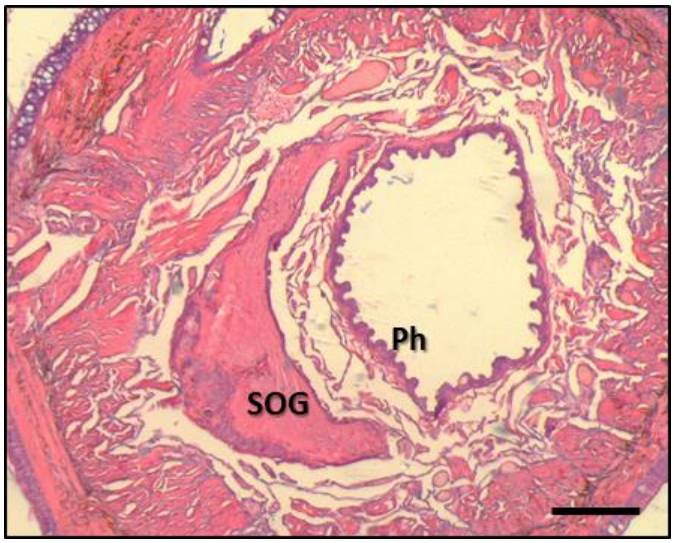

Figure 4.5 Cellular distribution in the Suboesophageal Ganglion (SOG) in *Eisenia fetida*. H&E staining on Formalin-Fixed Paraffin-Embedded (FFPE) unharmed samples, demonstrates the cellular distribution in the SOG, located at the ventral side of the pharynx (Ph). The SOG is characterised by a cell-rich region (blue) situated primarily in the periphery. Images captured via a Nikon DS-2Mv camera. Scale bar: 100µm

4.2. Transcriptomic analysis of regenerating neuronal tissue by RNAseq

The underlying molecular pathways which drive or repress the process of neuronal regeneration in earthworms has never been characterised. Surprisingly, there is a scarcity of information in the literature that focuses on attempting to understand how the earthworms can regulate their intrinsic and extrinsic neuronal environments to achieve neuronal regeneration. In recent years, the emergence of next-generation sequencing techniques coupled with the significant reduction in cost, promises to unravel the mysteries surrounding organisms, which have yet to have their genomes fully sequenced. Here, RNA sequencing (RNAseq) was employed to study the entire transcriptome of the regenerating neuronal tissue. The Circumpharyngeal Connectives (CC), Suboesophageal Ganglion (SOG) and the Ventral Nerve Cord (VNC) of the first 10 anterior segments were studied. To the best of our knowledge, this is the first study where CG regeneration in the earthworm, is specifically targeted for a global transcriptomic analysis. As mentioned above, no earthworm species, including *E. fetida*, have had their genome fully sequenced. However, a recent study was published in which shotgun DNA sequencing and RNAseq was carried out on *E. fetida* (Bhambri *et al.*, 2018), however no large scale sequence information was made publicly available on NCBI, which would have had the potential to be of significant value in the bioinformatics analysis of the transcriptome.

Due to the limited sequence information at available at the time, a *de novo* transcriptome was constructed; which is a sequence scaffold which would represent the different transcripts expressed in the nine samples studied (3 worms per condition; sham, 1 week post-decerebration and 5 weeks post-decerebration). Unlike other techniques, RNAseq does not require any pre-existing knowledge of the organism's genetic make-up or nucleotide sequence and thus one can conduct such experiments with minimal bias, allowing for a more reliable universal interpretation of the results. Since a *de novo* transcriptome had to be assembled, extensive sequence variation within the sample pool would amplify the significance of any errors of the results. When working with an organism for which, unfortunately, there is no centralised 'bank' of the species, a specific strain for experimentation cannot be used. It is inevitable, therefore, that in a heterogenous *E. fetida* population, a significant variation amongst individual worms would be prevalent, even though this can somewhat be minimised with successive rounds of selective breeding within a laboratory setting. To address this issue, the variation was minimised by selecting samples which exhibited a close homology and evolutionary distance. The cytochrome c oxidase

subunit II (coII) was used as a proxy to categorise the worms into groups based on the coII sequence, by conducting a phylogenetic analysis.

The RNAseq generated an extensive list of differentially expressed transcripts present in the regenerating tissue (i.e. CC, SOG and the VNC of the first ten anterior segments). The robust output of the experiment revealed targets and biological processes that appear to dictate the progress of regeneration at specific time points. Even though these results serve as an indicator of what the key genes and biological events are, they are by no means conclusive and should be examined further in targeted biochemical assays. This work aimed to interpret what differentiates the worm in comparison to organisms, including humans, which do not have the capacity for complete restoration of their CNS and use the results to study this phenomenon further. In the following sections, the rationale of the experimental method is presented, followed by a wide-ranging description of the main findings.

4.2.1. Phylogenetic analysis of worms selected for transcriptomic analysis

To conduct the phylogenetic analysis (Figure 4.6), 7 worms were used for each of the three experimental conditions. Firstly, RNA was extracted from the neuronal tissue, followed by total RNA extraction from the pharynx for each of the 21 worms. The pharyngeal RNA was then used for further analysis. A section of the coII transcript (497 bp) was sequenced and

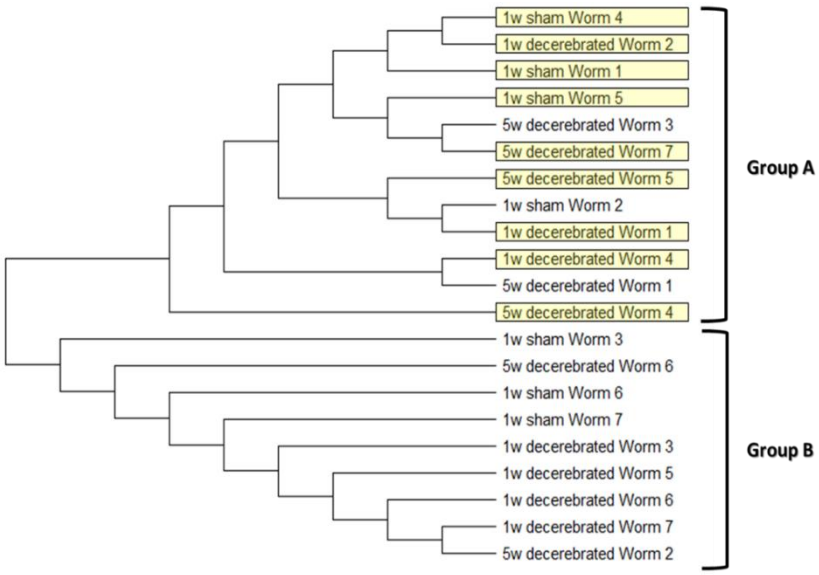

Figure 4.6 Phylogenetic classification of earthworms intended for RNAseq based on their cytochrome c oxidase subunit 2 (*coII*) sequence. Total RNA was extracted from the pharyngeal tissue of 7 worms in each of the three experimental conditions (1w sham, 1w decerebrated and 5w decerebrated). To assess their evolutionary relationship, *coII* was Sanger sequenced, to reveal the presence of two distinct *Eisenia fetida* sub-population amongst the sample pool. The samples that were selected for RNAseq are highlighted. The evolutionary relatedness was inferred by the Maximum Likelihood method and Tamura-Nei model in MEGAX.

used for the construction of the phylogenetic tree. Interestingly, the sequencing analysis revealed the existence of two distinct *E. fetida* sub-populations, group A and B which cluster together. Group A is made up of 12 sequences across all three conditions and Group B is made up of 9 sequences. The pattern of the vast majority of the polymorphisms observed within the sample set is repeated within the members of the same group; an example of this is presented below, where the nucleotide differences are highlighted (Figure 4.7). Following the alignment of all 21 sequences, polymorphisms were identified in 70 positions. From these variations, 61 polymorphisms are consistent differences that are shared amongst the

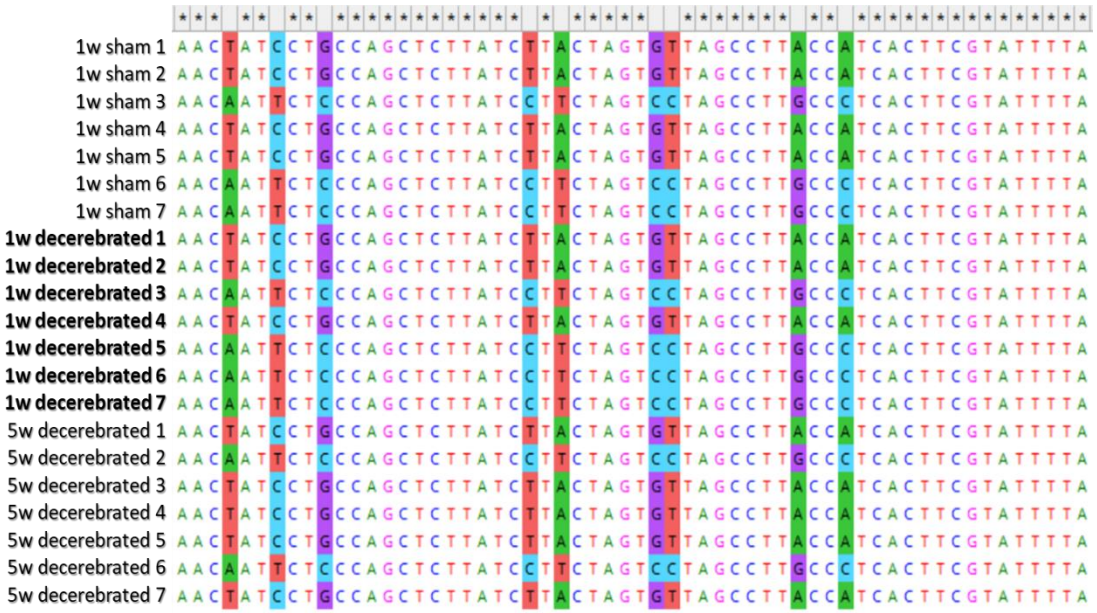

Figure 4.7 Multiple sequence alignment (MSA) of 21 coII sequences in *Eisenia fetida*. The MSA confirmed the existence of two groups within the sample population, each of which exhibits the same genotypic variants across the sequence. The MSA was performed via CLUSTAQ in MEGAX.

members of the same group. Therefore, the presence of two groups, which, evidently, exhibit significant differences between them, led us to decide that in order to simplify the assembly of the *de* novo transcriptome and the bioinformatics analysis of the RNAseq data, the worms to be selected should belong in the same group. In order to decide what group to use, the quality of the RNA and its concentration was also considered, which is described in the following section. The worms that were selected for RNAseq all belonged to Group A.

4.2.2. Quality and quantity assessment of samples used in transcriptomic analysis

RNA was extracted from the regenerating tissue, from a total of 21 worms, 7 individual worms from each experimental condition. Due to the low concentration of total RNA yielded for each sample, which was in the range of 30-80ng/µl, the standard approach (i.e. separation on an agarose gel) to assess the quality and quantity of the RNA could not be followed, as this would result in 'wasting' a lot of material. Therefore, the RNA pico chip was used, which is extremely sensitive to very low amounts of RNA. The original stock of RNA was diluted and loaded onto the RNA pico chip (Agilent Technologies) and analysed in the Agilent 2100 Bioanalyser System. The output included an electropherogram and a gel image of the separated RNA fragments for the 1 week sham (1wS) samples (Figure 4.8), 1 week decerebrated (1wD) (data not shown) and 5 weeks decerebrated (5wD) (data not shown). When total RNA is extracted from most eukaryotic organisms, it is expected that two bands are visible when separated on a gel, corresponding to the 18S and 28S ribosomal RNA.

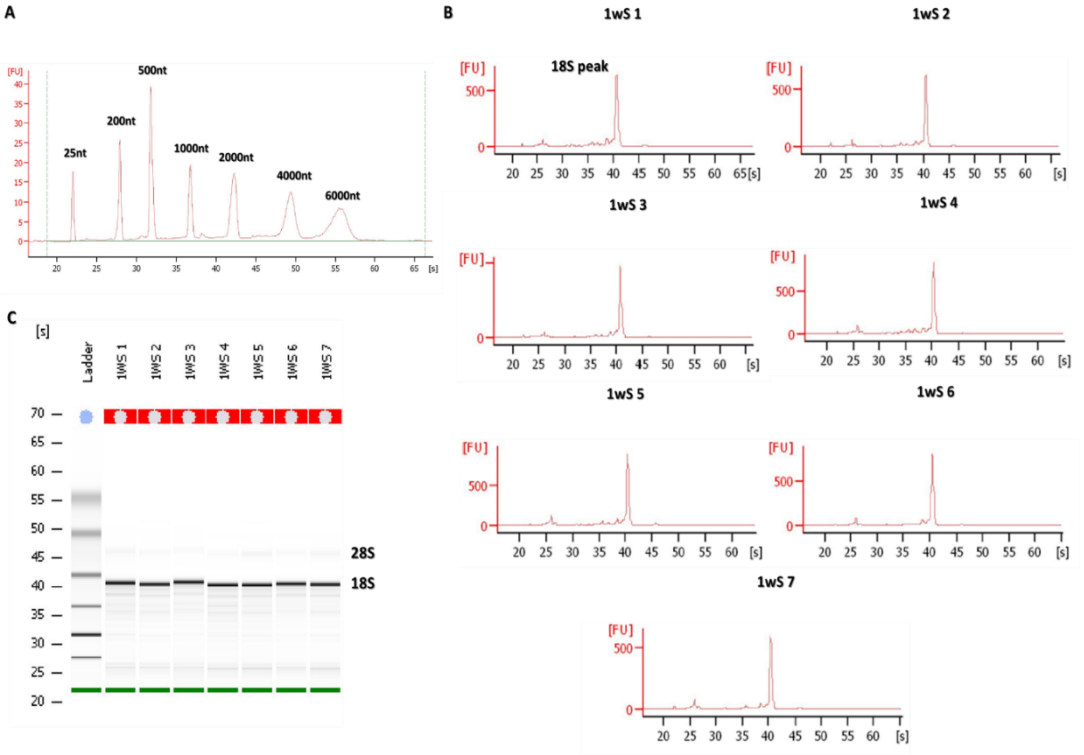

Figure 4.8 Assessment of RNA quality of the seven 1wS samples intended for the RNAseq experiment, using the RNA pico chip. A. The electropherogram of the ladder used in the chip, depicts the migration of nucleotide (nt) fragments of different sizes, in seconds (s) **B.** The electropherograms of the seven samples depict a strong peak close to 1900nt corresponding to the 18S ribosomal subunit; an indication of good quality RNA **C.** The corresponding gel image of all the 1wS samples shows the presence of a strong band, corresponding to the 18S ribosomal subunit. A weak band, corresponding to the 28S, can also be observed. Due to the weak signal by the 28S, an RNA integrity number (RIN) was not specified by the software.

However, the earthworm appears to be different, in the sense that only the 18S ribosomal RNA was highly expressed and prominently visible on the gel of the chip, even though a very faint band representing the 28S could be observed (Figures 4.8C). This agreed with the agarose gel electrophoresis that was routinely implemented to assess the quality of high concentration RNA samples (not shown), where a single band was consistently obtained at the 18S position. Due to the absence of a 28S peak, an RNA integrity number (RIN) was not retrieved by the software. Therefore, the concentration of the samples (Table 4.1) and the integrity of the 18S were relied on in to deduce the quality of the RNA. The concentration of the samples ranged from 24ng/µl (5wD 6) to 74ng/µl (1wD 1), according to the Bioanalyser. Because the quality of RNA was satisfactory across all 21 samples, the underlying reason for selecting the 9 samples was the concentration and the phylogenetic group they belonged to. The best concentration profile amongst the two groups was in Group A, and therefore, 9 samples were selected within that group.

Table 4.1 Concentration of all 21 samples obtained via the RNA pico chip and the RIN number of the 9 samples selected for the RNAseq experiment, obtained through RNA Screen Tape and TapeStation analysis.

RNA sample	Concentration (ng/µl)	RIN
	1wS (control)	
1	58	8.7
2	45	
3	38	
4	67	8.8
5	72	9.1
6	54	
7	44	
	1wD	
1	74	8.7
2	67	9.1
3	46	
4	58	9
5	54	
6	36	
7	49	
	5wD	
1	35	
2	70	
3	33	
4	38	9.4
5	61	9.7
6	24	
7	59	9.2

Therefore, in conjunction with the phylogenetic analysis described above, 9 samples (3 samples for every condition) were selected and sent to Genewiz, for RNA sequencing: for sham (samples 1, 4 and 5), for 1wD (samples 1, 2 and 4) and for 5wD (samples 4, 5 and 7). All samples were of an acceptable concentration and clustered together in the phylogenetic tree, suggesting a close evolutionary relationship. In addition, further quality control analysis was then carried out on the selected samples, using the RNA Screen Tape system, through which the 5S subunit was utilised, through which a good RIN value was obtained for the 9 selected samples (Table 4.1).

4.2.3. General output description of the RNAseq data

Using RNAseq, a comprehensive temporal profile of Regeneration Associated Genes (RAGs) was built, in early (1-week post decerebration) and late (5 weeks post decerebration) time points. This is the first study to specifically define the transcriptomic profile of neuronal tissue and also, focus on CG regeneration in the earthworm. Other studies in the earthworm, have indirectly analysed the neuronal transcriptome through the study of posterior regeneration (Bhambri *et al.*, 2018). However, they extracted RNA from the entire regenerating posterior tissue (a heterogeneous population of different tissue types), which would inevitably lead to false positive and false negatives deductions about neuronal regeneration genes. This methodology ensured that all differentially expressed transcripts identified, are a product of the process of neuronal repair, due to the specificity of the neuronal tissue used.

A total of 286 million sequence reads were obtained for the 9 samples that were used to construct the *de novo* transcriptome, consisting of 311,261 contig sequences. Due to the bioinformatic challenge of assembling a *de nono* transcriptome, it was anticipated that a significant amount of the sequence fragments produced, would not be effectively mapped onto the transcriptome scaffold. An average of 66% of the total sequence fragments was mapped, which was deemed to represent a very satisfactory proportion given the scarcity of sequence information available on *E. fetida*. Nevertheless, this meant that some transcripts and potentially important mediators of neuronal regeneration would not be revealed by this dataset. Using the DESeq2 package, a comprehensive list of significant (adjusted p-value <0.05) differentially expressed (DE) contigs/transcripts was created based on three condition comparisons: sham (control) vs 1 week decerebrated (1wD), 1wS vs 5 weeks decerebrated (5wD) and 1wD vs 5wD. The number of significant DE contigs, both upregulated and downregulated is summarized below (Table 4.2). In the first comparison, of sham vs 1wD, a

Table 4.2 Number of differentially expressed contigs of 1 week (1wD) and 5 weeks (5wD) following decerebration, compared to sham operated worms, and with each other.

	Number of total differentially expressed contigs (n = 3; adjusted p value <0.05)		Number of differentially expressed contigs w/ ID (n = 3; adjusted p value <0.05)	
Condition	***Upregulated***	***Downregulated***	***Upregulated***	***Downregulated***
Sham Vs 1wD	582	657	246	312
Sham Vs 5wD	2761	1013	1239	627
1wD Vs 5wD	4145	1879	1952	1314

total of 1239 DE contigs were identified, of which 582 and 657 contigs were upregulated and downregulated compared to the control, respectively. In the second comparison, of sham vs 5wD, which was a snapshot of the transcriptomic changes taking place at the later time points of regeneration, a 3-fold increase of DE contigs compared to sham vs 1wD, was observed. A total of 3774 DE contigs were identified, of which 2761 and 1013 contigs were upregulated and downregulated respectively, indicative of the intense biochemical and metabolic processes required for the formation of the new neuronal tissue. Lastly, in the third comparison of the two decerebrated samples, 1wD and 5wD, we wanted to gauge how the differences between early and later time points of neuronal regeneration manifest at the transcriptomic level. This comparison created the largest DE contig dataset, with a total of 6024, of which 4145 and 1879 contigs in the 5wD samples, were upregulated and downregulated, respectively, compared to 1wD. This increase in DE contigs was indicative of some being downregulated in 1wD and upregulated in 5wD, and vice versa, which contributed to this observation. Interestingly, this suggests that the variance between 1wD and 5wD, in their transcriptomic profile, is greater than when compared to their control, which follows that the temporal differences in regenerative stages, can have a more profound transcriptomic effect compared to the effect of removing the brain in the first place. In addition, the fact that more transcripts are differentially expressed at 5w compared to 1w, suggests that the regenerative process has not been completed by that time point.

As mentioned above, the availability of *E. fetida* sequences on public databases, such as NCBI, is limited. For this reason, there was an annotation challenge, since most of the transcripts identified have never been reported and uploaded onto NCBI. This was especially true in the context of neurobiology, for which the earthworm has not been the subject of numerous molecular studies. In order to be consistent in how the DE transcripts were annotated, it was decided to annotate them using BLASTx based on the top hit within *Homo*

sapiens sequences (only if that identity was sensibly consistent with the identity obtained in BLASTx across all other species). In cases where there was no identity in *H. sapiens*, but there was a strong homology in other species, that identity was used for annotating the contig. In addition, during the annotation process many contigs that were screened by BLASTx, did not return a homology hit in any species. A breakdown of how many of the DE contigs did not give a hit in BLASTx is described in Table 4.2, where for approximately half of all the DE contigs no sequence similarity was identified. This could be due to a misalignment in the initial bioinformatic composition of the contigs or, more likely, the sequences might be unique to earthworms and may very well explain some of their regenerative capacity; more studies on these sequences are needed to confirm this. To demonstrate this, the top-20 DE contigs (upregulated and downregulated) are presented, which indicates how many of them have successfully been annotated for the three comparisons. In the sham vs 1wD comparison (Table 4.3), only 9 (3 upregulated and 6 downregulated) out of 40 DE contigs were successfully annotated, 11 DE contigs (7 upregulated and 4 downregulated) were annotated in sham vs 5wD (Table 4.4) and lastly 8 DE contigs (5 upregulated and 3 downregulated) were annotated in 1wD vs 5wD (Table 4.5). Overall, contig 8459 exhibited the most robust differential expression, of an 1848-fold upregulation in 1wD vs 5wD. However, the identity of this contig has yet be confirmed. What's more, the top20 upregulated contigs of sham vs 1wD, exhibit on average the lowest magnitude of change, ranging from 56.4 to 268.9 fold

Table 4.3 Top 20 upregulated and downregulated contigs comparing sham vs 1wD as determined by RNAseq, including the fold change and adjusted p value. The contig ID, for those that were annotated, is shown in brackets.

sham vs 1wD

Upregulated			Downregulated		
Contig	*fold change*	*padj*	*Contig*	*fold change*	*padj*
13064	268.9	3.04E-90	22254	-479.3	5.01E-75
7384	257.7	3.75E-59	32021 (*mmel1*)	-155.4	5.81E-42
40056	144.8	9.12E-48	6824 (*atp5a1*)	-145.6	1.29E-38
16501	142.8	8.89E-42	774	-106.0	2.1E-32
24171 (*ptcd2*)	136.1	3.27E-41	55258	-97.7	3.31E-32
8628 (*col1a1*)	118.0	5.09E-42	13382 (*clptm1*)	-87.5	1.77E-28
2431	110.2	3.7E-105	36343	-79.6	2.23E-27
8061	101.3	7.65E-51	56818	-75.0	2.95E-29
24880	89.6	1.65E-32	68393	-58.5	1.16E-23
13296	84.2	9.05E-35	8761 (*golgb1*)	-54.5	7.08E-53
3733	81.3	2.77E-154	10239 (*pdhb*)	-48.8	1.03E-19
25	73.0	1.47E-157	15541	-46.8	2.64E-19
34630 (*trim56*)	70.1	5.55E-40	129862	-43.1	8.16E-19
32980	66.0	6.7E-27	1844	-41.6	1.05E-17
56819	65.1	3.79E-26	28007	-41.5	4.93E-19
9651	64.3	6.13E-72	55586	-40.3	1.62E-17
42205	60.1	4.72E-25	67798	-38.4	3.78E-30
97464	60.0	7.02E-26	61181 (*sidt1*)	-36.7	6.68E-17
58045	57.7	2.69E-28	178682	-35.0	2.38E-17
54226	56.4	2.01E-75	98327	-34.3	2.42E-16

increase. However, the most downregulated contig is 22254 (479.3-fold decrease) which is found in sham vs 1wD; whose identity was also not possible to establish. The tables presented above, serve as an indication of the complex biochemical activity that takes place following the removal of the brain in *E. fetida*.

Table 4.4 Top 20 upregulated and downregulated contigs comparing sham vs 5wD as determined by RNAseq, including the fold change and adjusted p value. Contig ID, for those that were annotated, is shown in brackets.

sham vs 5wD

Upregulated			Downregulated		
Contig	*fold change*	*padj*	*Contig*	*fold change*	*padj*
1436	1128.4	3.0369E-107	22596	-278.7	3.524E-39
82811	379.5	7.33813E-78	43611	-185.7	1.002E-30
264855 (*naga*)	374.8	2.93098E-45	20530	-166.8	3.993E-35
32756 (*gfap/gliarin*)	356.2	4.21856E-39	23105	-164.7	1.101E-30
8628 (*col1a1*)	337.3	3.12641E-44	24093	-153.7	4.409E-32
2137	335.7	1.19592E-43	15417	-152.8	1.519E-25
9660	287.3	8.66447E-39	70163 (*erh*)	-141.9	7.076E-46
47885 (*fcn2*)	275.1	8.85213E-30	25160	-135.6	4.868E-49
48050 (*vim*)	270.6	2.56291E-31	38100	-131.4	8.584E-29
64427	252.3	1.2287E-58	2233	-130.2	3.248E-30
42205	242.2	1.00156E-36	52092 (*washc5*)	-124.2	2.516E-26
36530	237.9	9.18963E-37	105921	-120.9	4.312E-30
77619	226.2	1.13054E-36	50198 (*rapunzel*)	-115.1	9.224E-24
50261	225.3	5.34828E-36	20206	-114.2	3.181E-83
74198	214.9	4.03406E-32	22033	-96.1	9.367E-23
33576 (*tspan9*)	212.1	3.29757E-53	33931	-90.8	8.111E-44
51210	197.5	4.57707E-31	37973	-79.8	2.046E-18
47425	191.6	2.0072E-30	51644	-79.0	1.346E-19
6504 (*fgfr2*)	180.8	3.19904E-41	38528	-77.3	2.516E-26
141	170.9	1.61762E-29	18806 (*zmym1*)	-75.2	5.348E-36

Table 4.5 Top 20 upregulated and downregulated contigs comparing 1wD vs 5wD as determined by RNAseq, including the fold change and adjusted p vlaue. Contig ID, for those that were annotated, is shown in brackets.

1wD vs 5wD

Upregulated			Downregulated		
Contig	*fold change*	*padj*	*Contig*	*fold change*	*padj*
8459	1848.2	1.4082E-121	35495	-189.5	5.337E-29
22947	1060.2	9.25457E-93	6606	-164.5	3.987E-51
1436	967.2	7.4891E-118	13608	-130.2	5.623E-23
82811	817.9	1.73352E-58	52092 (*washc5*)	-128.2	3.539E-24
7077	726.6	1.65784E-63	70163	-109.5	6.552E-35
12410	663.5	8.25351E-54	50198	-102.5	4.992E-20
15644	561.9	1.1546E-49	57354	-98.3	1.222E-26
16947 (*ak1*)	542.1	3.13684E-61	52668	-95.6	9.806E-20
34831	465.0	3.20111E-61	38875	-92.7	2.518E-19
264855 (*naga*)	441.3	7.79287E-44	51644	-87.1	3.97E-22
5362	427.6	2.00468E-59	66655	-86.4	3.53E-18
2137	393.2	3.50708E-42	2974	-86.4	1.484E-51
21951 (*cpa5*)	329.4	3.54442E-39	51628	-79.6	4.002E-18
1663	328.5	1.00963E-44	10545 (*osbpl1a*)	-77.0	8.182E-18
33499 (*myh8*)	311.3	1.65994E-33	32190	-71.7	9.518E-17
1167	273.6	8.32512E-42	52415	-71.2	1.524E-25
14633	262.5	1.18715E-40	28346	-62.1	1.81E-14
62661	254.7	1.72282E-33	70325	-61.7	2.496E-22
9097 (*bicd2*)	252.3	1.02152E-31	47874 (*fuca2*)	-61.3	7.61E-15
18082	251.7	9.91358E-39	54226	-60.6	1.875E-79

Next, the focus shifted into the identification of the significant (padj <0.05) DE contigs whose expression profile persists throughout the regenerative process. Two main observations were made. Firstly, there seems to be compartmentalisation of processes taking place in early (1wD) and late (5wD) time points, indicated by the small overlap of contigs that share the same differential expression profile across the two time points (Figure 4.9). From the cut-off that was set in the analysis, 77 upregulated contigs in the sham vs 1wD (1wD (+)) were identified. In addition, 474 upregulated contigs were identified in the sham vs 5wD (5wD (+));

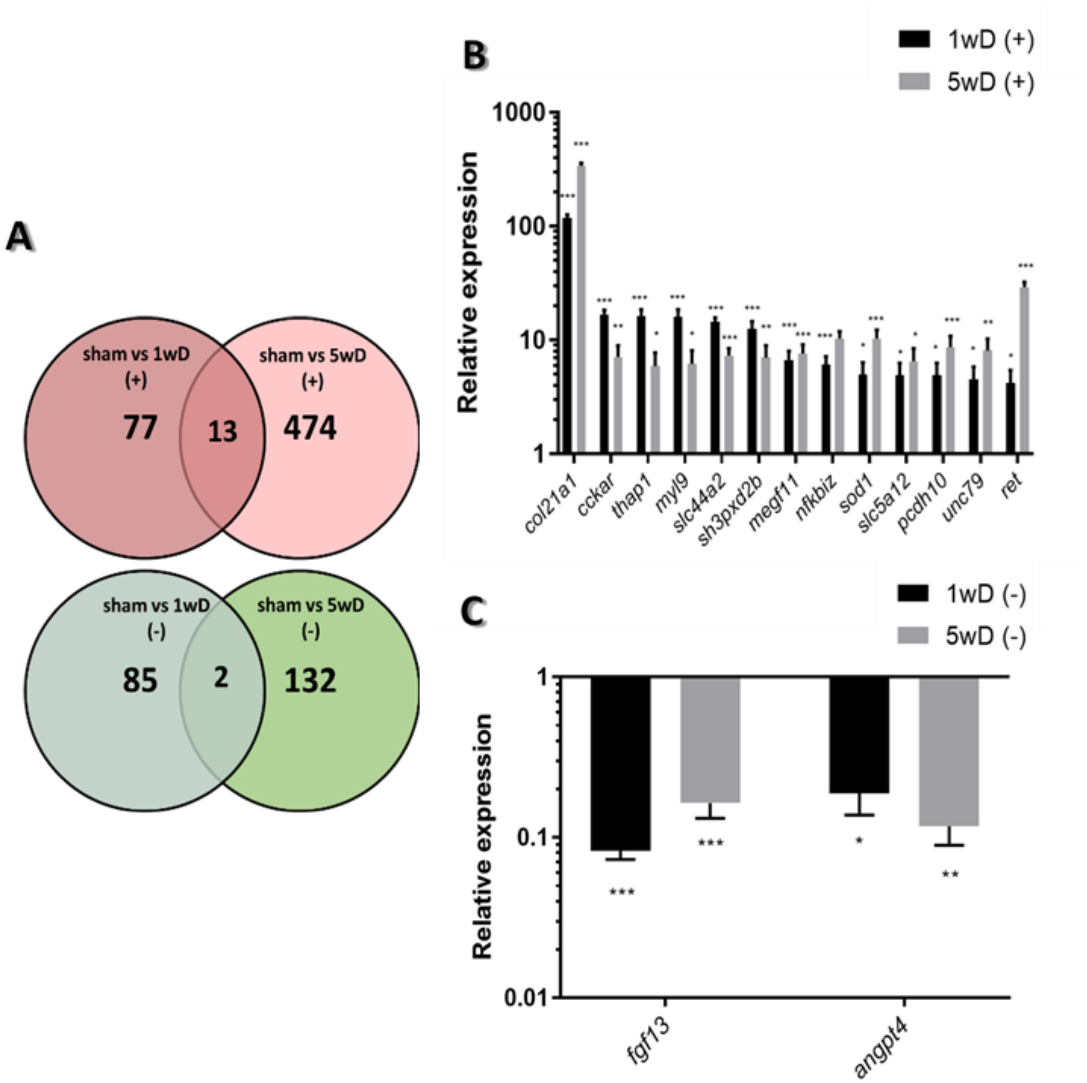

Figure 4.9 Characterisation of contigs which are upregulated and downregulated in both sham vs 1wD and sham vs 5wD in the RNAseq. A. Pie chart depicting the total number of upregulated (+)(red) and downregulated (-) (green) contigs identified in sham vs 1 week post decerebration (1wD; n=77 (+) and n=85 (-)) and sham vs 5wD (n=474 (+) and n=132 (-)), as well as the number of shared contigs between the two datasets (n=13 (+) and n=2(-)). **B.** The relative expression of the 13 shared upregulated contigs that were identified in the RNAseq is presented. The most highly upregulated contig in both datasets was *col21a1*, exhibiting a fold increase of 118 and 337 in sham vs 1wD and sham vs 5wD respectively. **C.** The relative expression of the 2 shared downregulated contigs (*fgf13 and angpt4*) that were identified in the RNAseq. A cut-off 4-fold was set for the detection of differentially expressed contigs. Relative expression represents the log2 fold change of 3 biological replicates ± lfcse (*** padj < 0.001, **padj <0.01, * padj < 0.05)

a significantly higher number of upregulated contigs compared to sham vs 1wD. Only 13 contigs are shared amongst the two datasets suggesting that the primary biological events that take place at 1 week following the removal of the brain, do not persist into the later stages of regeneration. One of the changes that are often associated with regeneration is the reorganisation of the extracellular matrix (ECM) and as such it was no surprise that the highest upregulated gene in both datasets (118 ±8.3 lfcse and 337 ±23.2 lfcse fold increase, in 1wD and 5wD respectively) was the collagen type XXI alpha 1 chain (*col21a1)*, an ECM protein. Another gene in this list, cholecystokinin receptor type A (*cckar*), serves as the receptor for cholecystokinin, an abundant neuropeptide in the mammalian brain. Recently, the importance of CCKAR in neuronal development and migration has been described in mice (Nishimura *et al.*, 2015). It is interesting to see that several genes in this list have not been extensively studied for their role in neuronal regeneration, including SH3 and PX Domain-Containing Protein 2B (SH3PXD2B), which has been shown to degrade the ECM through the interaction with ADAMs (Mao *et al.*, 2009). On the other hand, a gene which has been the subject of study in several biological processes, including neuronal development, is the tyrosine kinase receptor, *ret,* which is enriched in the dataset particularly at 5wD, exhibiting a 29-fold upregulation. The complexity of this process is highlighted by the presence of inflammatory genes, such as NF-kappa-B inhibitor zeta (*nfkbiz)* and free radical scavengers, like superoxide dismutase 1 (*sod1)*. The multi-facet aspect of the regenerative process in earthworms will be discussed further in the following sections. Conversely, there are only 2 contigs which are downregulated in both the 1wD and 5wD time points; one being the fibroblast growth factor 13 (*fgf13),* which is strongly associated with axonal branching, through the polymerisation and stabilisation of microtubules. This finding potentially can contradict studies which have shown that FGF13 can promote axon regeneration in a spinal cord injury (SCI) model (Li *et al.*, 2018), even though the actual function of this protein in the earthworm can vary significantly. The second downregulated gene is angiopoietin-4 (*angpt4),* which has been linked to the negative regulation and inhibition of angiogenesis (Olsen *et al.*, 2006). Angiogenesis is often considered a prerequisite for achieving functional neuronal regeneration (Yu *et al.*, 2016).

The second observation touched upon the notion of isoforms and how they are regulated in this process. There were cases where the same gene ID, was ascribed to different contigs, which seemingly displayed inverse expression profiles to each other, across the time course of regeneration, namely some were shown to be upregulated at 1wD but downregulated at 5wD, and vice versa (Figure 4.10 A and B). It is possible that this phenomenon relates to the

notion that specific genes can both be beneficial or detrimental depending on the point in time they are expressed, and the nature of genes that are co-expressed alongside them, or can indicate the presence of paralogues with distinct functions. The earthworm may also have the capacity to regulate alternative splicing on precursor mRNAs, which gives rise to similar proteins with a slightly distinct function. A noteworthy example is that of receptor-type tyrosine-protein phosphatase sigma (*ptpσ),* where two contigs have been identified as *ptpσ* at the same time point (5wD), of which one is significantly upregulated and the other significantly downregulated. The upregulated contig is characterised by an additional 47 amino acids, in its N-terminus, which constitute an additional fibronectin III (FN3) domain, which is absent in the downregulated contig (Figure 4.10 C).

The work conducted in the project aims to provide a framework to understand what characterises an organism that has mastered neuronal regeneration at the molecular level. Consequently, it is vital to note that the high magnitude of expression change seen for many of the DE contigs, in conjunction with the raw expression data (not shown), highlights the

A

1wD (-)			5wD (+)		
ID	contig	fold change	ID	contig	fold change
ctsc	2267	-24.9	*mrc1*	131286	47.8
pdcd6ip	47685	-15.2	*dpysl5*	1251	41.4
mrc1	122912	-11.4	*piwil1*	71380	40.4
dmbt1	139933	-10.6	*ctsc*	25455	36.7
loxl3	167184	-7.9	*prss12*	308646	32.8
prss12	111372	-5.9	*mrc1*	213815	28.3
dpysl5	3987	-5.7	*asic3*	150530	12.3
cyp2d6	116227	-4.6	*cyp2d6*	126658	8.5
asic3	6033	-4.6	*dmbt1*	78722	6.2
			pdcd6ip	121138	5.8
			loxl3	40620	4.6
			ctsc	18686	4.5
			pdcd6ip	87456	4.1

B

1wD (+)			5wD (-)		
ID	contig	fold change	ID	contig	fold change
trim56	34630	70.1	*zmym1*	18806	-75.2
ttn	59229	26.3	*nphp3*	101511	-50.3
nphp3	40497	20.2	*trim56*	74072	-24.1
trim71	1638	5.4	*trim71*	38103	-10.8
zmym1	27367	4.8	*ttn*	39564	-5.4

C

Figure 4.10 Gene isoforms identified in the transcriptome of *E. fetida*, whch exhibited an inverse expression profile in sham vs 1wD and sham vs 5wD. A. There were nine downregulated contigs in sham vs 1wD whose gene ID also appeared in upregulated contigs in sham vs 5wD and in **B.** Five upregulated gene IDs were shared between the upregulated contigs in sham vs 1wD and downregulated contigs in sham vs 5wD. All the contig sequences that were identified in these comparisons were unique which suggests the presence of isoforms with diverse function. **C.** The RNAseq uncovered two isoforms of *ptpσ* in sham vs 5wD of which one was upregulated, and one was downregulated. Pairwise alignment of their protein sequences revealed an additional 47 amino acids on the N-terminus in the upregulated isoform. The alignment was performed via EMBOSS Needle and a BLOSUM62 matrix.

presence of an 'on/off switch' which is regulated by the removal the cerebral ganglion. The baseline expression levels in the control samples of several contigs are effectively zero, as suggested by the raw counts. Even though an RNAseq experiment is, primarily an attempt to identify differential expression of transcripts in a diverse range of experimental conditions, one should not fail to acknowledge the importance of recognising baseline levels of expression. One can indeed make deductions on the importance of transcripts based on their differential expression profile, but, mistakenly, we are bound to disregard those that maintain a relatively high and constant level of expression across all experimental conditions. The expression of those high-baseline transcripts likely establishes a permissive intrinsic and extrinsic environment in earthworms, in which neuronal tissue can survive and regenerate in the case of injury. This is an underlying theme in this work, which is essential in any endeavour to understand the workings of efficient neuronal regeneration and will be discussed further in later sections.

4.2.4. Gene Ontology (GO) of differentially expressed transcripts

The annotation of the significantly DE contigs revealed how little we currently know about neuronal regeneration in the earthworm. The species to which the top homology hit belonged to was recorded, for every upregulated contig that was annotated in sham vs 1wD and sham vs 5wD (total of 551 contigs) (Figure 4.11). Only 2 contigs matched *E. fetida,* namely

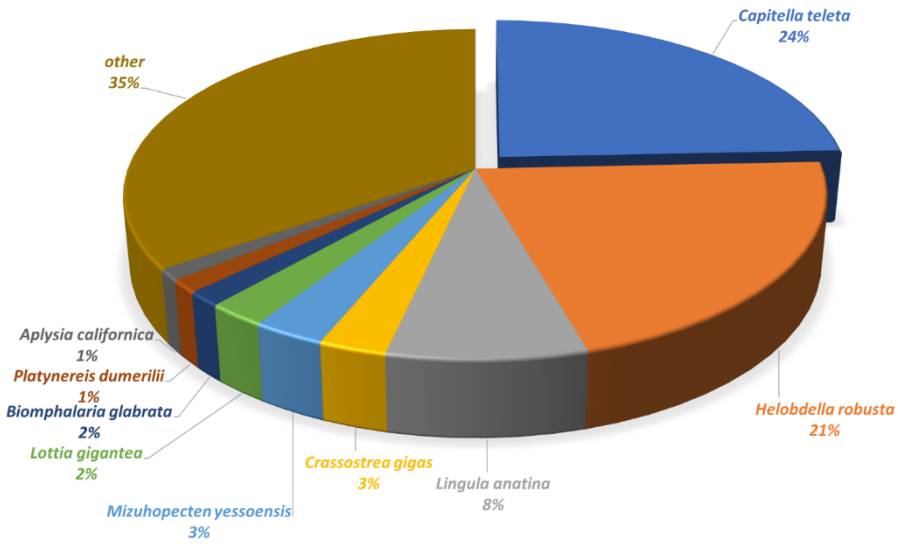

Figure 4.11 Pie chart representation of BLASTx top species hits in upregulated contigs following decerebration. The significantly upregulated contigs in sham vs 1wD and sham vs 5wD, were subjected to BLASTx analysis to identify the species in which the query sequence exhibits the closest homology to. Of the species identified, *Capitella teleta* and *Helobdella robusta* were returned as the top species hit of the sequences examined (24% and 21% respectively).

the ROS scavenger catalase, and neuromacin, a recently characterised neuropeptide in the earthworm, which were upregulated in 1wD and 5wD, respectively.

The species which exhibited the highest sequence similarity to the earthworm was *Capitella teleta,* a segmented annelid worm which was the first marine polychaete to have its genome fully sequenced (Simakov *et al.*, 2013), and thus explaining why 24% of all the contigs matched with this species. The next most similar species (represented by 21% of all contig matches) was the medicinal leech, *Helobdella robusta*, another aquatic annelid which has had its genome fully sequenced. At the time of writing, the complete sequence of the earthworm's genome has not been made available on NCBI, as described at the beginning of the chapter. The present work, therefore, would be a valuable resource for enriching the data banks on available earthworms' sequences, which will serve as a catalyst for a more comprehensive assessment of earthworm molecular biology.

The identification of key transcripts in the process of neuronal regeneration can provide further valuable insights into enriched biological events that take place during regeneration. STRING (Search Tool for the Retrieval of Interacting Genes/Proteins; https://string-db.org/) was used to identify functional enrichments classified into 3 categories: (1) Biological Processes (BP), (2) Molecular Functions (MF) and (3) Cellular Components (CC). Enriched BPs, as the name suggests, include those genes/proteins which act towards bringing about the same biological event. MFs refers to how the effect of these proteins are conveyed and lastly, the CC category refers to the enrichment of the spatial distribution of these proteins, either intracellularly or extracellularly. Up to the 10 most significant enrichments (false discovery rate <0.05) from every category are presented, arising from either the upregulated or downregulated contigs from either sham vs 1wD and sham vs 5wD (GO enrichments produced from the 1wD vs 5wD comparisons are presented in Appendix Figure 7.1). In the upregulated genes in sham vs 1wD (Figure 4.12), the majority of enriched BPs (a total of 73 BPs were enriched) were linked to several developmental processes, as well as the reorganisation of anatomical structures and the cytoskeleton. Moreover, there is evidence from the enriched BPs to support that cells undergo reprogramming in the early stages of regeneration. Interestingly, there was only one BP which was connected to axon growth and neurogenesis, namely the enrichment of the positive regulation of neuron projection development (GO:0010976) (data not shown). The upregulated genes that constituted the enrichment were microtubule-associated protein 1B (*map1b)*, reelin (*reln)*, apolipoprotein E receptor 2 (*apoer2),* semaphorin 5a (*sema5a)*, neurabin-1 (*ppp1r9a)*, and the tyrosine-protein kinase receptor Ret (*ret),* which are thought to contribute towards promoting neurite

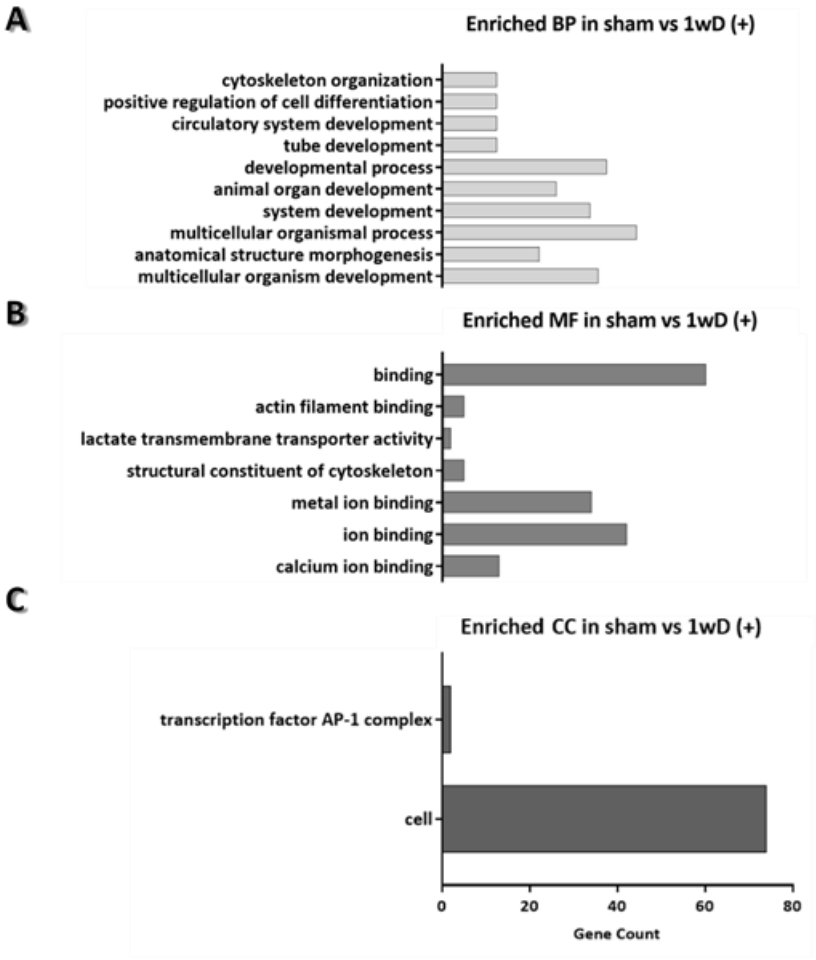

Figure 4.12 Histogram representing the gene ontology classification and functional enrichment of upregulated (+) genes in sham vs 1wD obtained in STRING. A. 10 of the most significantly (false discovery rate <0.05) enriched Biological Processes (BPs) revealed several developmental processes, coupled with structural and cytoskeletal reorganisation. **B.** The 7 enriched Molecular Functions (MFs) revealed that most of upregulated genes are involved in some category of binding, primarily metal and ion binding. **C.** The 2 enriched Cellular Components (CCs) revealed that the majority of the genes associate with the cell. The pro-regenerative AP-1 transcription factor complex is also enriched.

extension and axonogenesis. Less enriched MF were identified than BP, however, 5 out of 7 MF enrichments relate to some category of binding. The 3 most significant MF enrichments refer to metal binding or ion and include the majority of the upregulated genes. Lastly, 2 enriched CCs were identified. Many of the genes associated with the cell. Interestingly, the transcription factor AP-1 complex is also enriched, even though only 2 genes make up that category and that is because, according to GO, the AP-1 complex can only be linked to 5 genes. The AP-1 complex has been studied extensively for its pro-regenerative role following neuronal injury (Sabin *et al.*, 2019).

Metal binding was also enriched in MF for the downregulated genes (Figure 4.13) in sham vs 1wD, as well as hydroxylase and oxidoreductase activity. In contrary to the upregulated

genes, several CC components were significantly enriched highlighting that a lot of the activity of these downregulated genes, were directed at neuronal components indicated by the enriched dendritic and neuronal cell body CC. Also, the enrichments observed suggest that the downregulation of these genes is likely to affect the Extracellular Matrix (ECM), due to their association with collagen and other ECM components. No BP enrichments were identified. It is likely, that in order for the anatomical restructuring to take place, via the action of the upregulated genes, molecular changes in the ECM and its interaction with neuronal components have to occur. This is further supported by enriched Reactome Pathways (not shown), obtained by the downregulated genes in STRING, on ECM

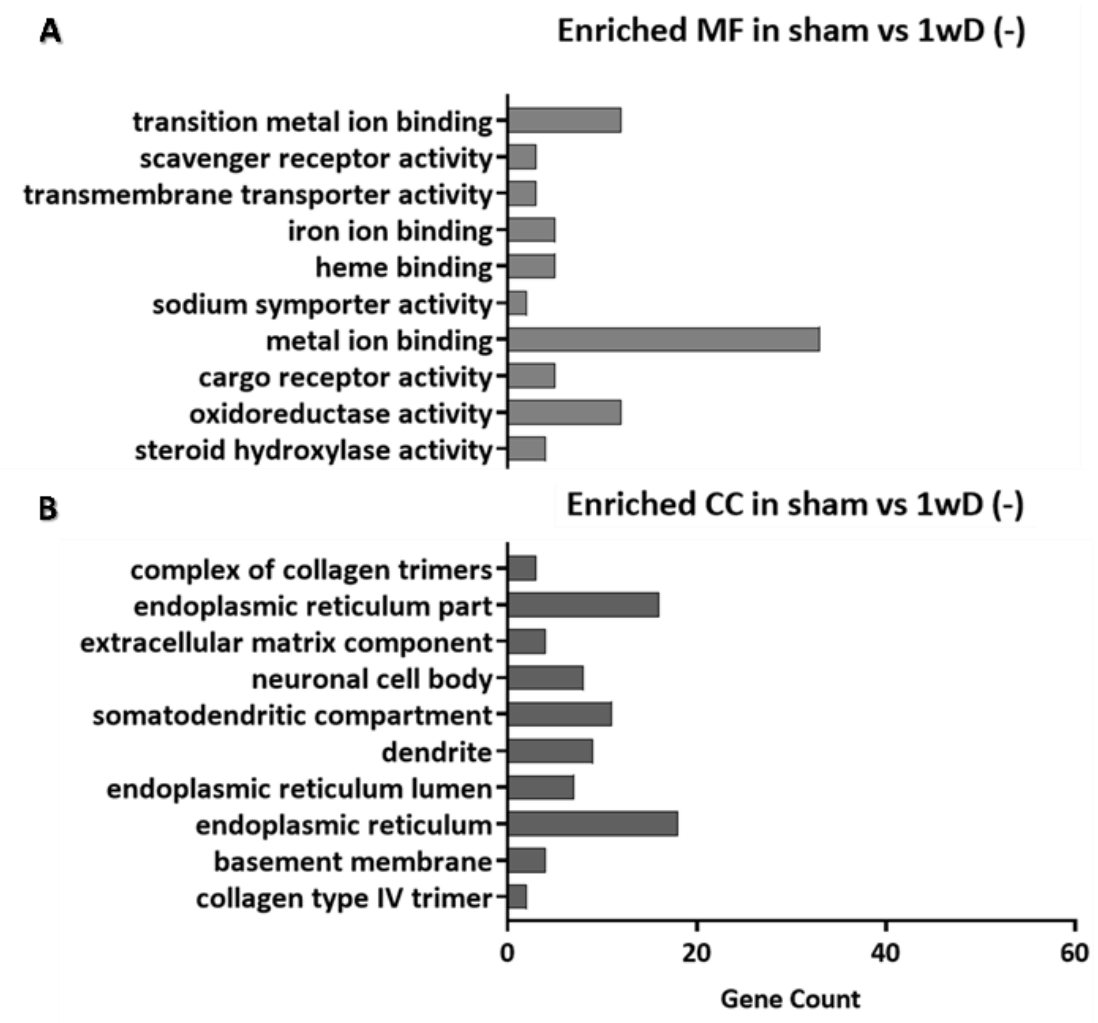

Figure 4.13 Histogram representing the gene ontology classification and functional enrichment of downregulated (-) genes in sham vs 1wD, obtained in STRING. A. The 10 most significantly (false discovery rate <0.05) enriched Molecular Functions (MFs) revealed a strong hydroxylase and oxidoreductase activity as well as metal binding. **B.** The 10 most significantly (false discovery rate <0.05) enriched Cellular Components (CCs) refer to an association with somatodendritic components and the ECM.

proteoglycan interactions (Identifier HSA-3000178), non-integrin membrane-ECM interactions (Identifier HSA-3000171) and laminin interactions (Identifier HSA-3000157).

In the case of sham vs 5wD, significantly more DE contigs were identified and annotated, which resulted in the enrichment of a wide range of gene ontology classifications. The upregulated genes (Figure 4.14) produced a total of 617 significantly enriched BPs, 118 significantly enriched MFs, and 117 significantly enriched CCs, which is indicative of the high biological activity across several pathways at the later stages of neuronal regeneration. A representative sample of 10 of the most significantly enriched GO descriptions is shown for each of the three categories. Firstly, the gene counts for the enrichments are significantly

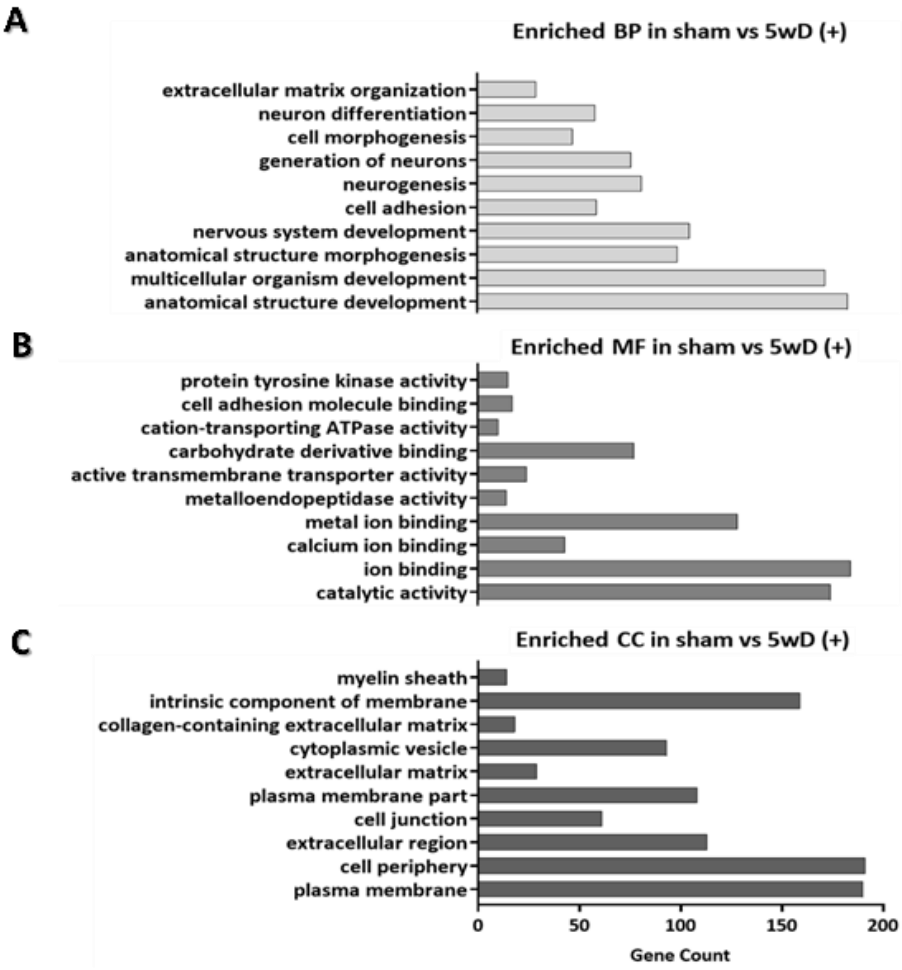

Figure 4.14 Histogram representing the gene ontology classification and functional enrichment of upregulated (+) genes in sham vs 5wD obtained in STRING. A. 10 of the most significantly enriched (false discovery rate <0.05) Biological Processes (BPs) confirmed that this is time point is of intense neurodevelopmental activity and ECM reorganisation. **B.** 10 of the most significantly enriched (false discovery rate <0.05). Molecular Functions (MFs) revealed that most of upregulated genes are involved in some category of binding, primarily metal and ion binding. **C.** 10 of the most significantly enriched (false discovery rate <0.05) Cellular Components (CCs) position a lot of genes/proteins on the cell membrane and the ECM, where they can interact with other cells or the ECM.

higher than that of 1wD. The output from this comparison provides enrichment descriptions based on a larger sample size, which consequently increases the reliability of the output and any conclusions drawn from it. In the BP category, unlike in 1wD, several genes appear to partake in neuronal development, neurogenesis and neuronal differentiation. The prevalence of neurodevelopmental-related processes agrees with the initial observation made on the time-course of CG regeneration, where at 4-5 weeks, the formation of the regenerated CG was observed.

As described above, the involvement of the ECM was observed in the sham vs 1wD as part of the CC enrichment. Here, as part of the enriched BP, several upregulated genes contribute towards the reorganisation of the ECM and anatomical structures indicative of the changes that take place in the extracellular environment that can facilitate neuronal growth. Lastly, as in any regenerative endeavour, cell adhesion is also a prevalent process and comprises the attachments of cells to other cells or an extracellular substrate, such as the ECM. Similar to the upregulated genes in sham vs 1wD, the most significant MF enrichments relate to metal ion binding, as well as metalloendopeptidase activity. The underlying connection of metals in CG regeneration has been studied further and is discussed in more detail in later sections.

Lastly, the analysis of the enriched CC has revealed that most of the upregulated genes/proteins are primarily distributed at the cell membrane and the ECM, enabling them to respond to their dynamic surroundings. Seemingly, this is a time in the regenerative process, which is characterised by active communication between the cellular and ECM components, which work in unison to direct the fate of each molecular piece, which could explain the underlying capacity of earthworms for neuronal repair.

In the downregulated gene pool of the sham vs 5wD group, no enriched BPs were identified. However, the enriched MFs revealed that the decrease in MAP kinase kinase kinase and Jun kinase kinase kinase activity observed in the RNAseq may play a key role (Figure 4.15). Additionally, there is evidence to indicate that there is a decrease in enzymatic activity, disrupting pyrophosphatase and bis(5’-adenosyl)-triphosphatase activity. Lastly, the majority of all the downregulated genes annotated (n=104), appear to be acting intracellularly.

Furthermore, interactions networks were built utilising the genes of interest for each of the experimental comparisons. Understanding the function of individual molecules has been hindered by the limitations in earthworm genetic engineering, namely through targeted gene knockouts, knockdowns or knockins. By constructing these types of gene networks,

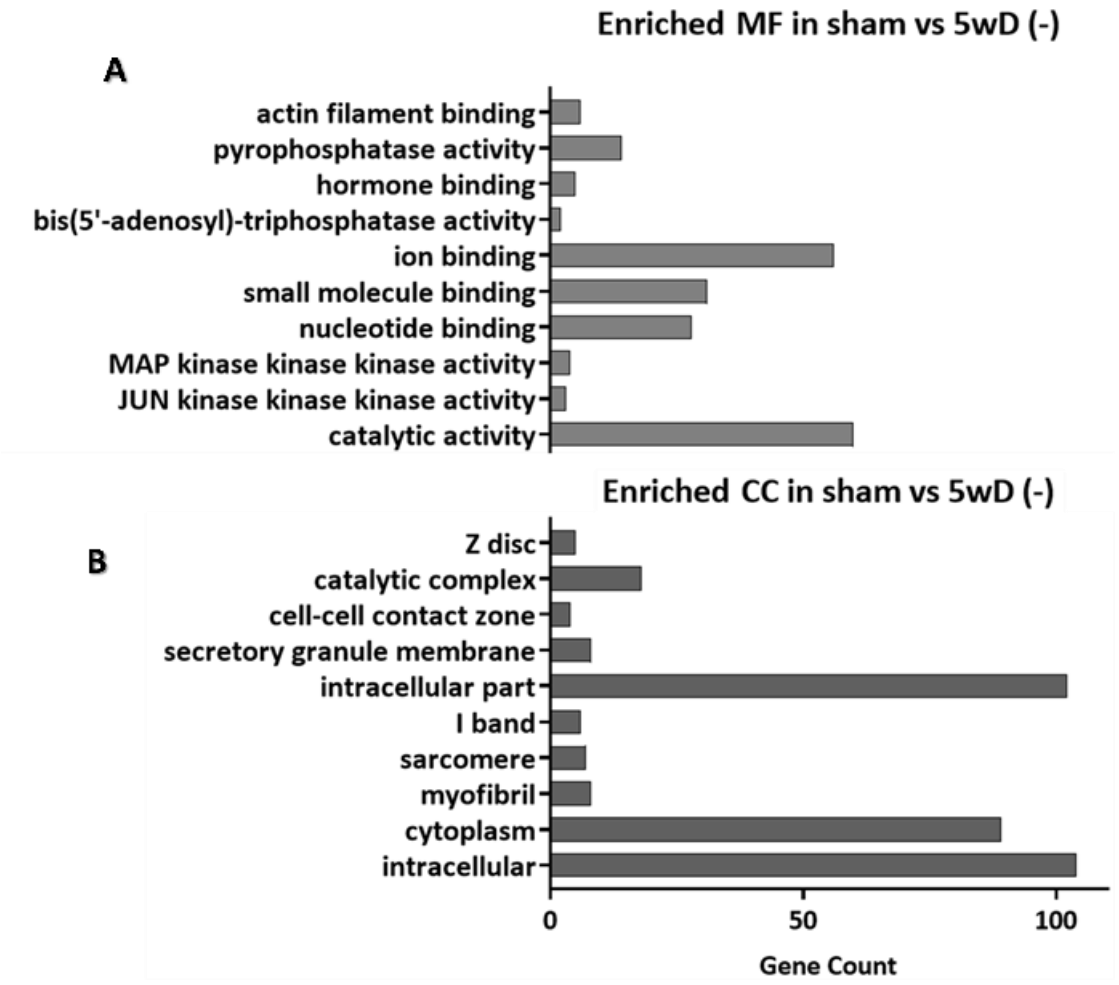

Figure 4.15 Histogram representing the gene ontology classification and functional enrichment of downregulated (-) genes in sham vs 5wD, obtained in STRING. A. The 10 most significantly (false discovery rate <0.05) enriched Molecular Functions (MFs) revealed a MAP and Jun kinase kinase kinase activity amongst the gene pool, as well as enzymatic activity. Ion binding is also prevalent within the gene pool **B.** The 10 most significantly (false discovery rate <0.05) enriched Cellular Components (CCs), suggest that almost all of the downregulated genes annotated (n=104), act intracellularly.

one can begin to appreciate some of the molecular pathways and interactions that are prevalent in the worm and can form the platform from which to study interconnected genes in a more targeted manner, taking confidence of interaction into account.

The networks presented are characterised by protein-protein interaction (PPI) p-value of <0.05, revealing that the genes/proteins in each network interact with each other at a significantly higher magnitude than one would expect from a random set of input proteins from the genome, suggesting that they might share a common biological function. Here, two networks are presented of the upregulated genes from sham vs 1wD and sham vs 5wD, which is an excellent visual illustration for (1) the difference in the number of upregulated genes in each dataset and (2) the comparison of gene ontology enrichments between

datasets. In order to demonstrate this, two of the most significant enrichments common to both datasets were selected (Figure 4.16), namely the anatomical structure morphogenesis and the metal ion binding, both of which are prevalent within their respective gene pools. The number of edges, i.e. connections between the nodes, for both networks far exceeds

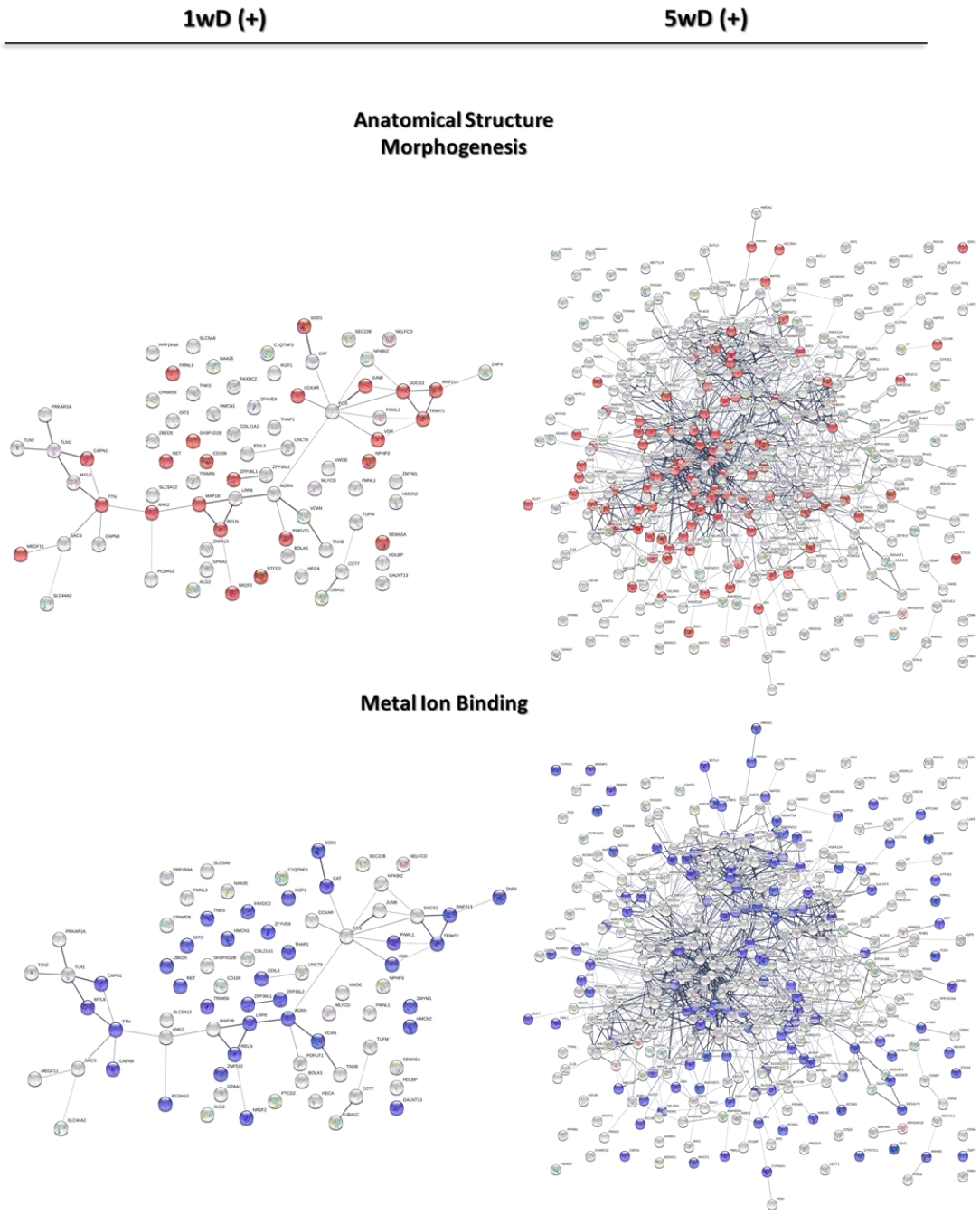

Figure 4.16 Interaction network showing the connections between upregulated genes of sham vs 1wD and sham vs 5wD, in STRING. Highlighted in red are the nodes which play a role in anatomical structure morphogenesis and in blue in metal ion binding; enrichments which are prevalent in the respective datasets. An increase in the number of genes involved in the enrichments is evident at 5wD.

what is expected by a random set of genes; the Protein-Protein Interaction (PPI) enrichment p-value is <0.00617 and <1.0e-16 for sham for 1wD and sham vs 5wD, respectively. Due to the limitations of having to present the network interactions on paper, the names and the connections between nodes cannot be differentiated (See Appendix Figure 7.2). Nevertheless, for the purpose of this work, where the interest lied in identifying differences between time points, precise observations can be made in regard to the absolute number of genes being involved in a particular enrichment. It is apparent that the number of genes in anatomical structure morphogenesis varies immensely amongst the two networks, 23 in sham vs 1wD and 99 in sham vs 5wD. The same is also true for metal ion binding where 34 and 128 genes contribute towards the enrichment in 1wD and 5wD, respectively. Following this approach, we can identify whether a particular gene, which contributes to a gene ontology enrichment, may (or may not) interact with other genes in the dataset. Therefore, this approach can enhance the predictive power when selecting genes for subsequent studies.

The results demonstrate for the first time the multi-facet biological aspects of CG regeneration in *E. fetida*. It is of great importance, however, to remember that the annotations assigned to the contigs, which dictate the subsequent enrichment analysis, are based on sequence similarity and therefore only assume that genes/proteins functions are transferrable to the earthworm. The presence of several members of the same family of proteins can further complicate the analysis. Even though the annotation might indicate one member of that family, the actual function of the protein might resemble more that of a different member of the same family. Moreover, when discussing GO classifications and the effects that DEG exert on a biological system, we do not take into consideration the baseline levels of genes that might also play a crucial role in the regenerative process and the way they interact with their ever-changing environment. These are some of the considerations we should be aware of when moving forward in characterising the molecular pathways and their significance in neuronal regeneration in the earthworm.

4.2.5. Deep dive into the transcriptome to identify isoforms and baseline levels of expression of regenerative and stem cell markers

The analysis of differentially expressed genes in a myriad of biological phenomena has revolutionised our approach towards understanding how biological change is induced. Even though this approach is undoubtedly one which can provide vital information on a biological

system, we should not disregard any transcripts which do not adhere to a differential expression model, as they can unequivocally exert a strong biological effect through their interaction with other genes/proteins. For this reason, it was imperative to get a better grasp on the baseline expression levels of some genes of interest (GOI) that have a prominent place in the neurodevelopmental field and have been shown to partake in neuronal regeneration in some form. Miss Katariina Latvala (Tampere University of Technology, Finland), in collaboration with Mr Thomas Kaminiski (King's College London, UK), built LBlastPycli, a software through which the *E. fetida* de novo transcriptome can be scanned to identify GOIs. The idea that isoforms can behave differently in terms of expression and function through the course of regeneration was briefly discussed above; the example of PTPσ was provided in (Figure 4.10). In total, the transcriptome was scanned and the presence/expression of 35 genes was identified. Surprisingly, for all the GOI that were tested (data not shown), multiple contigs were obtained that share sequence similarity with their respective reference queries.

The primary aim of the initiative discussed in this section, was to identify transcripts that are not differentially expressed in the RNAseq dataset but are still highly expressed throughout the regenerative process. The selection of what transcripts to seek, was based on the enrichments identified in STRING. For instance, the reelin-mediated signalling pathway (GO:0038026) which has been heavily implicated in neuronal regeneration (Pasten *et al.*, 2015), was enriched in the RNAseq dataset. Two components of that pathway, reelin (*reln)* and its receptor apolipoprotein E receptor 2 (*apoer2; a.k.a lrp8)* were identified as being significantly upregulated in sham vs 1wD. Reelin is a large ECM protein and has been demonstrated to play a role in neuronal migration and synaptic plasticity in the CNS (Weeber *et al*., 2002) and axon regeneration in the PNS (Lorenzetto *et al.,* 2008), via the interaction with its receptor APOER2. In the earthworm, like mammals, RELN (810 amino acids) is characterised by reelin domain repeats and central EGF-like domain commonly found in ECM proteins. Interestingly, Microtubule-Associated Protein 1B (*map1b)*, was one of the most highly upregulated genes identified in sham vs 1wD (fold change 34.8), which according to the PPI network (Figure 4.16; also, please refer to Appendix Figure 7.2) forms a first neighbour interaction with both RELN and APOER2 signifying a functional link between these proteins.

According to the GO database, four genes were classified as components of the reelin-mediated signalling pathway: (1) *reln*, (2) *apoer2*¸ (3) *Disabled* homolog 2-interacting protein (*dab2ip)* and (4) Crk-like protein (*crkl)*. The upregulation of *reln* and *apoer2*, therefore, resulted in the enrichment of the pathway. The hypothesis was that if the reelin mediated

signalling pathway was truly involved in the regenerative process, one would expect that all or most its components would be expressed. Therefore, a search was conducted to determine whether the other two components (i.e. *dab2ip* and *crkl)* are also expressed in the earthworm, by scanning the transcriptome. The Accession number for the query sequences that were used for each gene are as follows: *reln* (NP_005036.2), *apoer2* (EAX06742.1), *dab2ip* (AAI46763.1) and *crkl* (CAG30309.1). The results of the sweep are summarised in Table 4.6. Remarkably, not only was it possible to identify the expression of the other two components of the pathway, namely *dap2ip* and *crkl* but also a large number of contigs, 4 and 79 respectively, were seemingly to be highly similar to their query sequences. The full-length protein sequences were also obtained for APOER2 (contig 76648; 728 amino acids), DAB2IP (contig 15887, 1229 amino acids) and CRKL (contig 10722, 271 amino acids), exhibiting high similarity, in terms of the domains present, to their mammalian counterparts (data not shown).

Table 4.6 RNAseq raw counts of the four reelin-mediated signalling pathway components/genes discovered in the transcriptome of Eisenia fetida, via LBlastPycli

Gene ID	Number of contigs identified	contig ID	Significant DEG	Raw counts in RNAseq of the three most significant contigs								
				sham			1wD			5wD		
reln	13	1781	Yes	199	358	263	894	1016	466	713	769	335
		66723	No	76	170	97	288	353	160	366	270	180
		83570	No	45	125	80	210	142	91	155	147	93
lrp8	164	82611	Yes	0	1	0	52	61	91	235	0	83
		76648	No	153	125	164	97	126	110	159	137	143
		13285	No	89	237	160	262	347	83	146	247	197
dab2ip	4	52939	No	84	150	145	212	214	114	111	126	103
		15887	No	734	1023	915	1334	1518	860	1133	1105	1071
		41560	No	741	632	772	685	688	747	595	492	523
crkl	79	10722	No	2040	1359	1872	1281	1563	1488	1597	1320	1345
		24032	No	1435	1273	1585	1528	1475	1331	1178	1097	926
		16723	No	1230	843	1238	1092	1247	1205	1055	835	937

Using *dap2ip* as a proxy, facilitated the assessment of the probability whether these are true isoforms of the proteins or just noise from the sequencing data. Even though all 4 hits were highly similar to the starting query sequence, only 2 (contig_52939 and contig_15887) returned *dap2ip* as the top hit in BLASTx. These two sequences were then translated *in silico* (ExPASy) and aligned. Unlike contig_52939, contig_ 15887 returned a full-length sequence of the DAB2IP. The results (Figure 4.17) indicate that even though these proteins are similar and are labelled with the same identity, they are distinct from one another. The sequences were first aligned to identify the overlapping sequence and then re-aligned to evaluate their similarities. Sequences which are assigned the same annotation but differ significantly in sequence identity is something that is prevalent for many genes within the dataset. Additionally, the RNAseq raw counts were employed in order to establish what the baseline

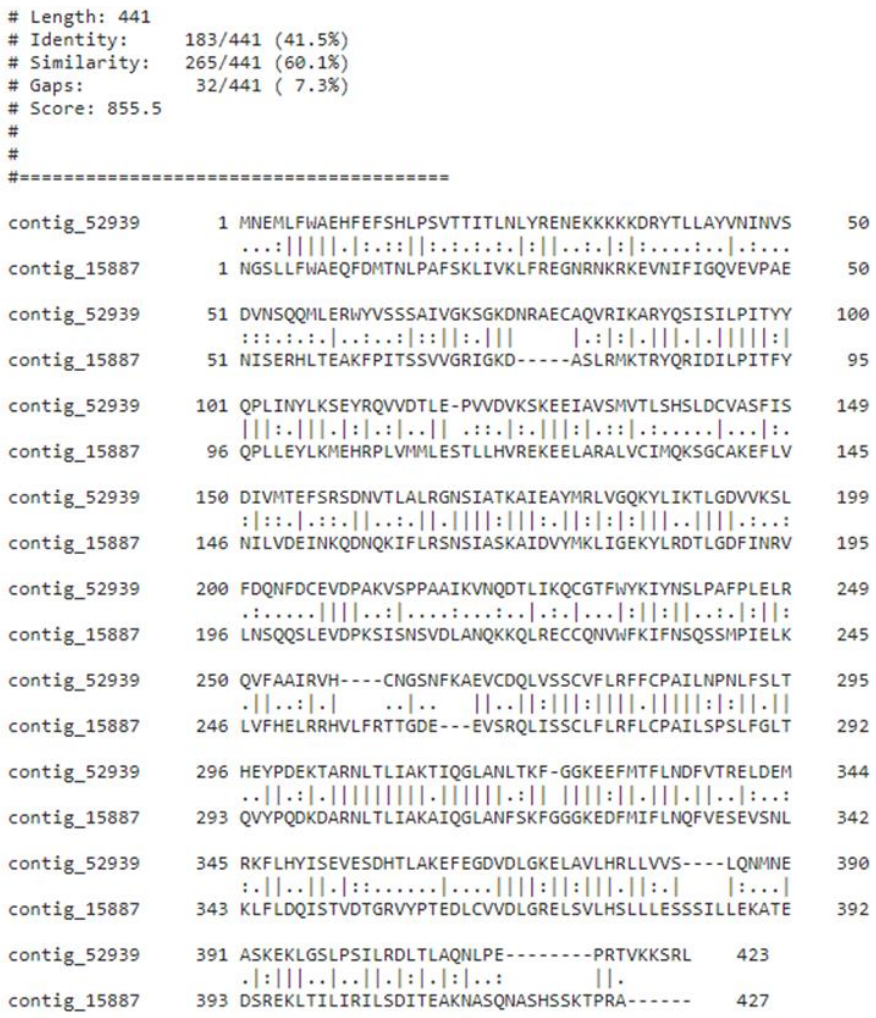

Figure 4.17 Pairwise alignment of two DAB2IP sequences identified via LBlastPycli. The alignment indicates that these two proteins differ significantly and can be considered as isoforms. Alignment was performed using EMBOSS Needle and a BLOSUM62 matrix

level of expression was for the 4 genes in the reelin-mediated signalling pathway. Table 4.6 highlights the raw counts for the 3 most highly similar contigs identified (via LBlastPycli) for each of the 4 genes mentioned above, in the 9 biological replicates used in the experiment. This represents the absolute number of transcripts identified in each earthworm sample and was used to assess what the expression of these genes is during regeneration. Their absolute counts suggest that these genes are expressed constitutively throughout the process, including the sham samples which have an intact brain. It can be concluded, therefore, that all the components, according to GO, of the reelin-mediated signalling pathway are highly expressed in the neuronal tissue of earthworms and can regulate its response to neuronal damage. This exercise was a demonstration of how these tools can be used to describe a biological process in the earthworm accurately and can be potentially applied to all the enrichments that were identified.

Furthermore, via LBlastPycli, a plethora of other Regeneration-Associated Genes (RAGs) was identified. One of the most well-studied aspects of why CNS regeneration fails in mammals is the involvement of the glial scar, which is predominantly comprised of CSPGs. Even though not significantly differentially expressed, here, the CSPGs that were identified in the transcriptome of *Eisenia fetida,* are presented. An ID could only be reliably assigned for two CSPGs, namely aggrecan (*cspg1*; contig 71402) and NG2 (*cspg4;* contig 52329). Moreover, *ptpσ* (contig 96408) and *hb-gam* (contig 1715)¸ were also identified in the transcriptome, of which *ptpσ* was significantly downregulated (discussed further in section 4.3.1), whereas *hb-gam* was highly expressed across all experimental conditions. The RNAseq raw counts for these contigs are presented in Table 4.7. Despite their perceived inhibitory role, *cspg1* and *cspg4* appear to exhibit a high expression profile, including in the regenerating tissue (1wD and 5wD). Immunohistochemical work on NG2 provided additional evidence for its strong

Table 4.7 RNAseq raw counts of cspg1 and cspg4, and cspg-associated genes, namely ptpσ and hb-gam that were discovered in the transcriptome of Eisenia fetida, via LBlastPycli

Gene ID	contig ID	Raw counts in RNAseq								
		sham			1wD			5wD		
cspg1 (aggrecan)	71402	337	247	187	164	196	205	230	161	165
cspg4 (NG2)	52329	140	257	239	297	418	148	171	182	157
ptpσ	96408	19	43	26	1	45	14	0	0	0
hb-gam	1715	25285	16693	18540	25367	24941	21847	18078	14408	13844

expression in the neuronal tissue, including in the regenerating CG at 3wD (see section 4.3.5). On the other hand, *ptpσ* is a cell receptor that is thought to interact with CSPGs and initiate an inhibitory cascade. The RNAseq has demonstrated how its expression levels are low throughout regeneration, particularly at 5wD, where no counts were measured in any of the three biological replicates. Moreover, the RNAseq revealed that one of the proteins, namely HB-GAM, with which CSPGs interact with resulting in disinhibition of regeneration, exhibited a remarkably high expression across all experimental conditions, reaching more than 25,000 counts.

Lastly, due to the evidence that places resident neoblasts in the neuronal tissue in earthworms, as well as their perceived role in neuroregeneration, a transcriptomic scan was

carried out to identify potential neoblast/stem cell markers (Table 4.8). The reference sequence queries, in this case, were based on well-known neoblast sequences from the planarians *Schmidtea mediterranea* and *Schmidtea polychroa*, species of flatworm which have been extensively utilised in regenerative and stem cell research, namely piwi2 (*smediwi-1*), protection of telomeres protein 1 (*smeldob1*), protein arginine N-

Table 4.8 RNAseq raw counts of four neoblast markers that were discovered in the transcriptome of Eisenia fetida utilising planarian reference sequences, via LBlastPycli

Gene ID	Accesion number used for deep dive	BLASTx top hit	Contig ID	Raw counts in RNAseq								
				sham			1wD			5wD		
smedwi-1	Q2Q5Y9.1	piwi2	77891	405	327	649	337	316	321	430	318	497
smedob1	AGG22603.1	protection of telomeres protein 1	156040	15	18	21	13	16	12	17	6	20
prmt5	AEX33822.1	protein arginine N-methyltransferase 5-like	24411	118	154	330	139	153	89	185	93	230
spoltud-1	ACN54319.1	Tudor domain-containing protein 1	8766	293	389	971	419	537	167	784	590	791

methyltransferase 5-like (*prmt5*) and tudor domain-containing protein 1 (*spoltud-1*). The accession numbers for the sequences that were used are Q2Q5Y9.1, AGG22603.1, AEX33822.1 and ACN54319.1 respectively. No differential expression of these neoblasts was observed, however, a high baseline level of expression for 3 out of 4 neoblasts markers was observed across all experimental conditions (*smedob1* is weakly, but consistently expressed throughout the course of regeneration). This finding suggests that resident neoblasts positioned locally within the neuronal tissue can potentially contribute towards the regenerative capacity of the earthworm.

An RNAseq experiment is an attempt to study a biological phenomenon with no preconceptions as to what the output might be which opens the way for a diverse range of discoveries. The analysis of the transcriptome was the best platform from which to build future experimental work and characterise brain regeneration in the earthworm, *Eisenia fetida.* The detailed database that was built, captures the majority of the earthworm's transcripts in control and regenerating neuronal tissue, which in turn has provided valuable insight into the molecular events that drive or repress this process. multitude of pathways and mechanisms that the worm seems to be utilising have been uncovered, in particular ECM remodelling and metal binding, which have been studied further and are discussed in later chapters of the thesis.

4.3. Validation and further characterisation of Regeneration-Associated Genes (RAGs) via quantitative Polymerase Chain Reaction (qPCR) and Immunohistochemistry

Through the RNAseq experiment, a *de novo* transcriptome was built which revealed the transcript sequences of genes, that take part in a diverse range of molecular pathways. The identification of these sequences as potential mediators of neuronal regeneration was undoubtedly one of the biggest contributions of this experiment. However, despite the robustness of the data and the steps taken to minimise variability and the occurrence of false-positive and false-negatives in the results, it was imperative to enhance reliability and reproducibility of the output, through additional molecular techniques. The expression profile of selected gene targets across, all experimental conditions, was individually assessed via qPCR, a technique that has been widely used to study the expression of individual genes. The qPCR analysis added another layer of confidence in the results obtained in the RNAseq and enabled the study of gene expression in additional time points throughout the regenerative process. Below, the validation of the RNAseq via qPCR analysis of DEGs is discussed.

Interestingly, 6 significantly upregulated contigs in sham vs 1wD that were labelled as catalases, an established Reactive Oxygen Species (ROS) scavenger, which posed as an attractive target to study further through qPCR and histological techniques. Furthermore, it was observed that the A Disintegrin And Metalloprotease (ADAM) family holds a prominent place in the RNAseq dataset, particularly at 5wD. It was of high interest, therefore, to study ADAMs further, as a group, to understand how their expression is regulated throughout regeneration. Additionally, there was a strong presence of zinc and iron-linked metalloproteins in the RNAseq dataset (e.g. ADAMs, Matrix Metalloproteases (MMP), Catalase (CAT) and Tripartite Motif-containing (TRIM) proteins), which led to the hypothesis that other metalloproteins could also be playing a role in the regenerative process that did not appear in the RNAseq. Metallothioneins (MT) are metalloproteins which have been the subject of extensive study in earthworms, for their role in metal homeostasis, and as such, it was speculated that they could play a similar role during neuronal regeneration, a hypothesis which was explored further and is discussed below.

4.3.1. RNAseq validation via qPCR

The RNAseq provided us with hundreds of DEG that have the potential to explain what differentiates the worm from mammals within a neuroregeneration context. The expression profile of selected genes at 1wD and 5wD was validated via qPCR using gene-specific oligonucleotide sequences. It is important to note that due to the low RNA concentration of the samples that were used for the RNAseq, those same samples could not be employed for qPCR analysis. Therefore, new biological replicates had to be prepared for the experiment, which introduced some level of variance in terms of the dissection process and the unique genetic makeup of the new worms. Nevertheless, the usage of fresh samples allowed for independent experiments and analysis to take place, which added another layer of confidence on the reproducibility of the results.

4.3.1.1. Sham vs 1wD validation

The transcripts that were selected for further qPCR analysis, included numerous genes, exhibiting both high and low differential expression in order to verify the quality of the RNAseq at both ends of the spectrum. The relative fold change obtained via qPCR for catalase (*cat;* 34.7 ±2.8 SEM, n=3, p<0.001), superoxide dismutase 1 *(sod-1*; 12.8 ±3.2 SEM, n=3, p<0.001*)*, activator protein 1 (*junb*; 2.61 ±0.1 SEM, n=3, p<0.001), cholecystokinin A receptor (*cckar*; 2.5 ±0.3 SEM, n=3, p<0.05), and semaphorin 5A (*sema5a*; 1.7 ±0.2 SEM, n=3, p<0.01) validated the results of the RNAseq at 1wD compared to sham-operated worms: *cat* (17.6 ±2.6 lfcse, n=3, p<0.001), *sod-1* (5.0 ±1.4 lfcse, n=3, p<0.05*)*, *junb* (3.6 ±0.8 lfcse, n=3, p<0.001), *cckar* (16.8 ±1.6 lfcse, n=3, p<0.001), and *sema5a* (4.4 ±1.3 lfcse, n=3, p<0.05) (Figure 4.18). Some of the differences observed in the magnitude of change between the qPCR and RNAseq data can be attributed to the sensitivity of each technique and the variability of the samples in each experiment. The five genes presented exhibit diverse function and potential roles in neuronal regeneration in the earthworm. Firstly, as discussed in the introductory section of the thesis, the enzymes CAT and SOD-1, are both scavengers for ROS. ROS accumulate at neuronal injury sites and contribute to the oxidative stress that is often associated with neuronal damage. It is likely that in the earthworm, *cat* and *sod-1* can serve as neuroprotective molecules while the regenerating tissue is adapting to the damage inflicted upon it as a result of the removal of the brain. The expression profile of *cat* was studied further via qPCR as well through histological techniques and is presented in the next section (4.3.2).

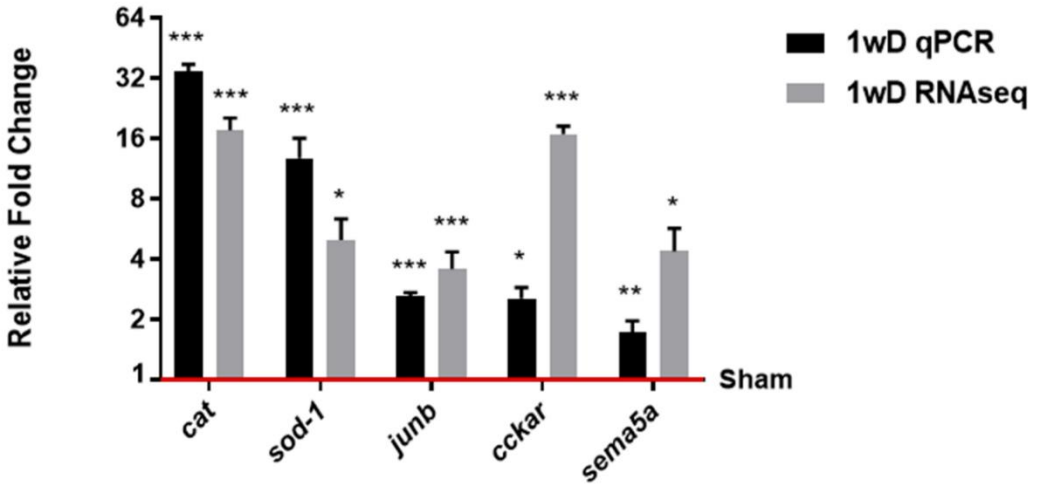

Figure 4.18 RNAseq validation via qPCR for DEGs at sham vs 1wD (*cat*, *sod*-1, *junb*, *cckar* and *sema5a*) on *E. fetida*. Relative expression (compared to sham-operated samples) was determined in RNA that was extracted from regenerating neuronal tissue (i.e. Circumpharyngeal Connectives (CC), Suboesophageal Ganglion (SOG) and Ventral Nerve Cord (VNC) of the first 10 anterior segments) 1 week following decerebration (1wD). Expression values were normalised to *gapdh*. All contigs presented have validated the RNAseq output. Error bars represent the SEM (in qPCR) and the log fold change standard of error (lfcse; in RNAseq). Statistical analysis for the qPCR data was conducted via a 2-tailed t-test and for the RNAseq data via the DESeq2 package (n=3, *** $p < 0.001$, ** $p < 0.01$, * $p < 0.05$)

Next, *junb* expression was selected for validation as it forms the heterodimeric transcription factor, AP-1, vital in neuronal repair. It consists of members of the Jun and Fos family of proteins, which regulates the expression of genes taking part in pro-neuroregenerative processes in the CNS (Raivich, Bohatschek, Da Costa, Iwata, Galiano, Hristova, Abdolrahman S Nateri, *et al.*, 2004). Following decerebration in the earthworm, *junb* expression is significantly upregulated at 1wD, indicative of the molecular changes that are taking place to promote neuronal outgrowth. Interestingly, c-fos, the second component of AP1, is also upregulated as indicated by RNAseq (data not shown). A pilot study was carried out on additional time points following decerebration, to determine how long the AP1-mediated signalling is sustained for (data not shown). Preliminary evidence suggested that the signal is maintained until 3wD, at which point *junb* expression starts to diminish between 3wD and 5wD, which agrees with the time point at which the first regenerated neuronal structures are clearly visible. The decrease in *junb* expression has the potential to inform when the regenerative processes that are taking place in the Circumpharyngeal Connectives (CC) and the SuboesOphageal Ganglion (SOG) have concluded. Note that the protocol adopted for this project did not involve the study of the transcriptome of the regenerating Cerebral Ganglion (rCG) and as such it is likely that AP1-driven regenerative processes are still active within the

rCG, even if they do come to completion in the CC and SOG. However, more work needs to be done to corroborate this finding and to determine the exact location at which AP1 is most active during regeneration.

Moreover, *cckar*, the receptor for the neuropeptide cholecystokinin, was one of the genes which was upregulated at both 1wD and 5wD and as such it is likely that it plays an important role throughout regeneration. Even though the qPCR validated the RNAseq in terms of *cckar* being upregulated, there was a significant divergence in the relative expression between the two experimental techniques, that can be attributed to the poor specificity of the primers, and/or differences in the transcriptome at the same time points between distinct biological samples. It is important to mention at this point, that the primary goal of this project was not to focus on the expression profiles at exact time points, but instead provide an understanding of what genes are likely to play a role in the regenerative process altogether in general.

The last validated gene presented is *sema5a,* which codes for an axon guidance molecule that performs a functionally conserved role in directing the growth of developing axons during regeneration. Sema5A is a protein which is both secreted and embedded in the cell membrane and is considered to be unique amongst other members of semaphorins, in that it contains thrombospondin (TSP) motifs which allow the attachment of neuronal cells to the ECM (Purohit *et al.*, 2014). Sema5A was once thought to contribute to the inability of the CNS to regenerate, due to a perceived inhibitory/repulsive effect on axon growth (Goldberg *et al.*, 2004); however this is not entirely true. Studies have demonstrated that according to the substrate that Sema5A interacts with, that being either Chondroitin Sulfate Proteoglycans (CSPGs) or Heparan Sulfate Proteoglycans (HSPGs), it can serve as a repulsive (through growth cone collapse) or attractive cue, respectively (Kantor *et al.*, 2004). The bi-functionality of Sema5A, according to the environmental composition, is attributed to its two opposing domains, the sema and the TSP domains. The action of sema5a, therefore, adds another layer of evidence to the importance of the constitution of the ECM in the regulation of neuronal regeneration. The upregulation of Sema5A in regenerating neuronal tissue in earthworms is an indication as to how the axons in earthworms, interact with their environment to navigate their way through the interstitial space. Furthermore, it corroborates the findings that it can hold a neuroregenerative potential, unlike what was originally speculated, which is a reminder of the value in studying the transcriptome of species which possess a strong neuroregenerative capacity.

4.3.1.2. Sham vs 5wD validation

As in the case of sham vs 1wD, a diverse range of genes both in function and in the magnitude of differential expression was selected for validation. These were *glial fibrillar acidic protein* (*gfap)*, *Leukocyte cell-derived chemotaxin 1* (*lect1), adam19*, *bmp-1, ptpσ* and *netrin*-1 (*ntn1*). The relative fold change obtained via qPCR was as following: *gfap* (101.5 ±31.3 SEM, n=3, p<0.001), *lect1* (49.3 ±21.2 SEM, n=3, p<0.01), *adam19* (17.1 ±3.3 SEM, n=3, p<0.001), *bmp-1* (3.3 ±0.3 SEM, n=3, p<0.05), *ptpσ* (0.1 ±0.01 SEM, n=3, p<0.01) and *ntn1* (0.7 ±0.05 SEM, n=3, p<0.001) (Figure 4.19). The qPCR data was in agreement with the RNAseq in which the following was obtained: *gfap* (356.1 ±26.0 lfcse, n=3, p<0.001), *lect1* (144.0 ±11.3 lfcse, n=3, p<0.001), *adam19* (23.1 ±3.6 lfcse, n=3, p<0.001), *bmp-1* (29.9 ±4.1 lfcse, n=3, p<0.001), *ptpσ* (0.04 ±0.006 SEM, n=3, p<0.001) and *ntn1* (0.15 ±0.04 SEM, n=3, p<0.001).

GFAP is an intermediate filament (IF) protein which is a structural component of the cytoskeleton. It is highly expressed in the CNS and in glial cells, particularly astrocytes and is often utilised as a marker for the identification of glial cells and reactive gliosis (Fernández-Klett and Priller, 2014). Moreover, qPCR data on the expression of *gfap,* suggests that the glial cell population is increased as early as 3 days following decerebration (data not shown).

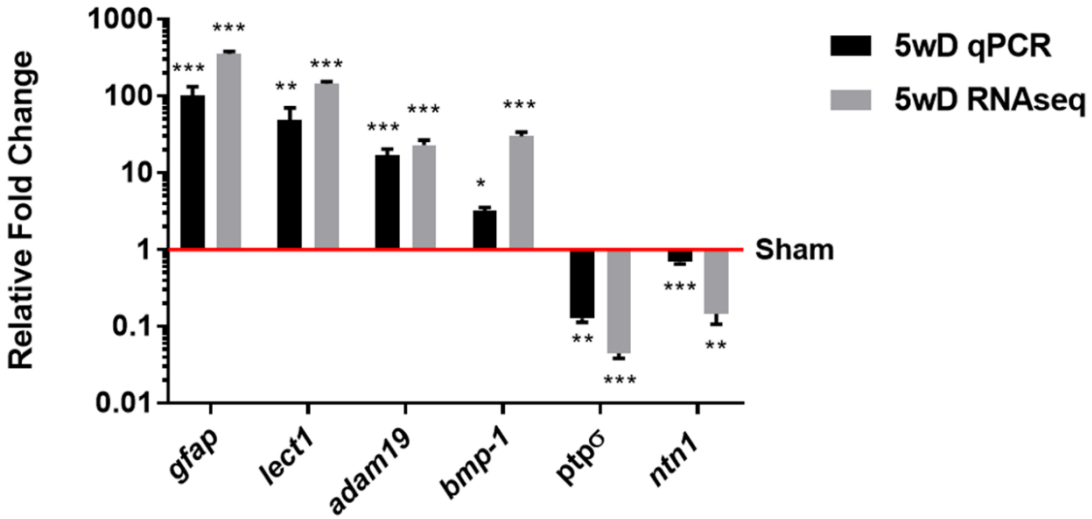

and *ntn1*) in *E. fetida*. Relative expression (compared to sham-operated samples) was determined in RNA that was extracted from regenerating neuronal tissue (i.e. Circumpharyngeal Connectives (CC), Suboesophageal Ganglion (SOG) and Ventral Nerve Cord (VNC) of the first 10 anterior segments) 5 weeks following decerebration (5wD). Expression values were normalised to *gapdh*. All contigs presented have validated the RNAseq output. Error bars represent the SEM (in qPCR) and the log fold change standard of error (lfcse; in RNAseq). Statistical analysis for the qPCR data was conducted via a 2-tailed t-test and for the RNAseq data via the DESeq2 package (n=3, *** p < 0.001, ** p < 0.01, * p < 0.05)

The expression of *gfap*, therefore, suggests that the glial cell population during neuronal regeneration is dynamic and highly responsive to neuronal damage. Due to the neuroregenerative capacity of the earthworm, the upregulation of *gfap* must be perceived as advantageous towards efficient regeneration.

One of the aims of the RNAseq was to identify novel genes that are not associated with neuronal regeneration. An example of this includes *lect1*, one of the most highly upregulated genes in the RNAseq dataset, which has been studied for cancer, heart disease and cartilage regeneration (Zhu *et al.*, 2019); however, there have not been in any studies which address its role in neuronal regeneration. As discussed above, one of the observations that was made in the RNAseq was the prevalence of genes that have a role in ECM reorganisation, which includes the metalloproteases *adam19* and *bmp-1*, which highlights one of the main reasons why these genes were selected for validation. Their role in neuroregeneration was discussed in the introductory section of the thesis. Remarkably, there were nine members of the ADAM family of metalloproteases that were differentially expressed at sham vs 5wD in the RNAseq dataset and were studied further to establish their expression profile across additional time point following decerebration (see 4.3.3). Also, two of the genes that were validated, *ptpσ* and *ntn1,* were downregulated. The receptor *ptpσ* along with its interaction with CSPGs are considered to contribute to the regenerative failure of the CNS and have been extensively explored within this context (see introductory section). Even though in this study CSPGs have been shown to be highly expressed in the CNS during regeneration, their binding to *ptpσ*, and the initiation of a downstream inhibiting signalling cascade is likely to be diminished as *ptpσ* is downregulated. This can be one of the fundamental differences as to how the earthworm regulates the intrinsic capacity of neurons to enable regeneration. Furthermore, the downregulation of *ptpσ* and the potential effect this can have on the inhibitory effect of CSPGs, led us to search for a protein (via LBlastPycli) which has recently been shown to bind and inhibit the interaction of CSPGs with *ptpσ* (Paveliev *et al.*, 2016). HB-GAM or pleiotrophin is secreted by neurons and glial cells and has been shown to promote neuronal growth by binding to CSPGs the cell surface receptor, glypican-2 (Figure 1.1). As described earlier, *hb-gam* was not only identified in the neuronal transcriptome of *E. fetida* (contig 1715) but it also exhibited a remarkably high level of expression in all the experimental conditions (including controls) – a table of *hb-gam* RNAseq raw counts was presented in section 4.2.5. The high baseline was later confirmed in qPCR studies (data not shown) as well which was almost at par with that of *gapdh*, even though there was no significant difference between control and decerebrated samples. This finding gives rise to a multitude of questions, as to

what the function of HB-GAM in *E. fetida* is and whether the CNS in earthworms is primed to promote regeneration ubiquitously, by blocking the inhibitory effects of CSPGs.

Lastly, *ntn1* is an axon guidance molecule that is primarily secreted and similarly to Sema5a, it can act as a chemoattractant or chemorepellent for growing axons, depending on several factors including the ECM composition. In this study, despite showing that *ntn1* is downregulated at 5wD, it was also observed that it is highly and constitutively expressed in the CNS of the earthworm, even in control samples. Moreover, due to its role in axon guidance, it was hypothesised that netrin might also be expressed by neighbouring tissues, to direct the growth of regenerating axons suitably in order to regenerate the CG. Surprisingly, qPCR work on pharyngeal tissue samples of both sham-operated and decerebrated worms revealed that *ntn1* is also expressed in the pharynx (data not shown) and thus it likely has the capacity to guide axons to its dorsal side for the formation of the regenerated brain. Additional work, using an *in situ* approach, needs to be performed to characterise the distribution of netrin and other axon guidance molecules across neuronal and adjacent tissues to uncover how growing axons reach their destination in such a precise manner.

It is important to note that only a subsection of DEGs was selected for validation, and therefore this can only increase the confidence of the results obtained in the RNAseq. It also provides the means to assess the reproducibility of the results through different experimental techniques but cannot claim to provide accurate and valid expression data for the entire transcriptome.

4.3.2. Catalase expression during neuronal regeneration revealed a strong induction and demonstrated high activity in and around regenerating neuronal tissue

As discussed above, catalase was one of the genes that was highly upregulated at 1 week following decerebration. Its protective role against free radicals is one that is speculated to play a crucial part in the early stages of regeneration and as such its expression and distribution was assessed further through qPCR and DAB (3,3'-diaminobenzidine) staining (Figure 4.20). The qPCR (Figure 4.20A)revealed that catalase is upregulated from day 3 (7.4 ±1.4 SEM, n=3, $p<0.05$) until week 3 following decerebration (1.6 ±0.6 SEM, n=3, $p<0.001$), while it achieves its highest induction at 1-week post brain removal (29.0 ±1.7 SEM, n=3,

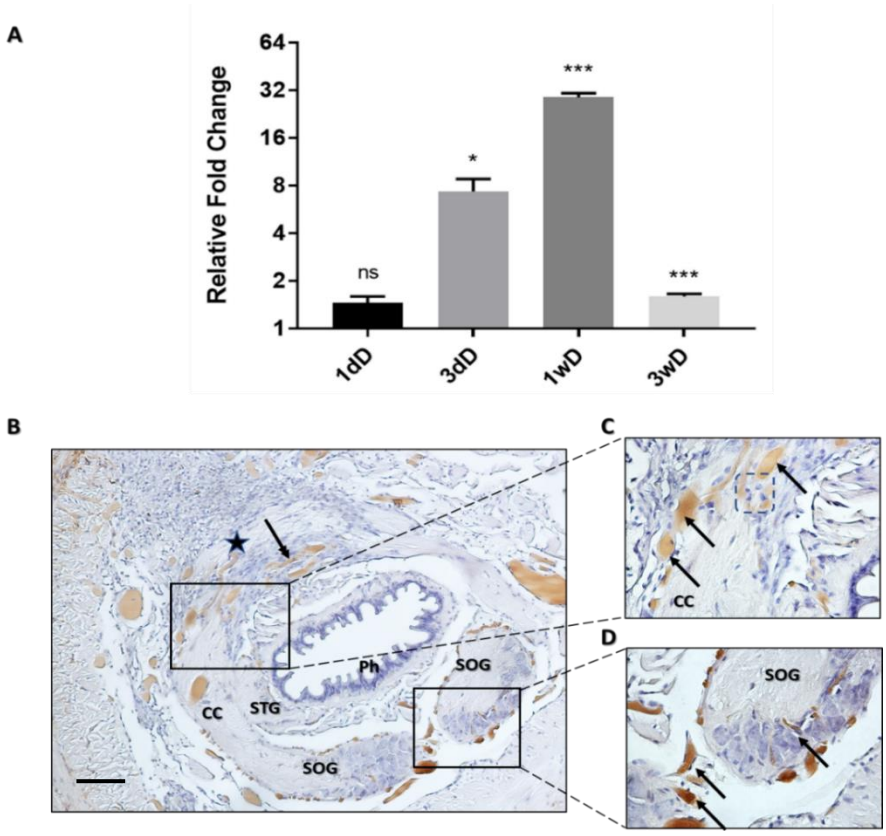

Figure 4.20 Catalase relative expression and distribution in regenerating neuronal tissue during CG regeneration. A. Relative expression (compared to sham-operated samples) was studied via qPCR in RNA that was extracted from regenerating neuronal tissue (CC, SOG and VNC) across four tme points (1 day post decerebration (1dD), 3 days post decerebration (3dD), 1 week post decereration (1wD) and 3 weeks post decerebration (3wD)). A strong induction of was observed from 3dD until 3wD. Statistical analysis was carried out via a 2-tailed t-test and error bars represent the SEM (n=3, *** $p < 0.001$, * $p < 0.05$). **B.** Histochemical characterisation of catalase activity, via DAB, was performed on 1wD samples in paraffin cross sections (6µm). The anatomical structure that is the proudct of growing axonal processes is marked by the star. **C.** Catalase activity was predominately associated with capillaries at the tip of the regenerating connective. A group of neoblasts were identified at the tip of the connective (dotted square). **D.** Likewise, catalase activity was also prevalent at the periphery of the SOG. CG; Cerebral Ganglion, CC; Circumpharyngeal Connectives, STG; Stomatogastric Ganglion, SOG; Suboesophageal Ganglion, Ph; Pharynx. Scale bars: 100µm

p<0.001), potentially signifying the period in which the neuronal tissue is vulnerable to ROS damage. There was no significant change in the relative expression of catalase at 1 day following decerebration. Since catalase is a peroxidase enzyme, it can partake in the oxidation of DAB, which is commonly used as a chromogenic substrate in ImmunoHistoChemistry (IHC), resulting in false-positive staining. Consequently, one of the steps in performing immunohistochemistry on paraffin sections is to block the endogenous peroxidase activity, through the incubation of the section with H_2O_2. Here, the sections were not saturated with H_2O_2, which did not block the intrinsic peroxidase activity, thus employing the enzymatic capacity of catalase to oxidise DAB. This approach was utilised as a proxy for

catalase distribution in cross-sections of the regenerating tissue. The time point exhibiting the strongest induction of catalase, i.e. 1wD, was employed for the study of catalase distribution. Firstly, as expected, catalase was predominantly found in the capillaries which innervate the neuronal tissue, near to both the regenerating connectives (Figure 4.20C) and the SOG (Figure 4.20D). A group of stem cell-like neoblasts were identified at the tip of the regenerating connectives, indicative of the presence of a blastema (Figure 4.20C; marked by the dotted square). Catalase activity was also observed within the neuronal tissue itself primarily within the SOG. Additionally, there is a high volume of undifferentiated cells situated near the regenerating connectives dorsally of the pharynx where the regenerated CG (rCG) will eventually reside. Also, an anatomical scaffold, or neuropil, is formed by axonal processes stemming from the CC (marked by the star), which is an interlaced network of fibres that will form the central part of the CG. Interestingly, this specific biological process was enriched in sham vs 1wD. This suggests that either the number of DEG present in this comparison were not sufficient to produce an enrichment or that cells, not found in the CC and the SOG, contribute to the formation of this scaffold. Moreover, a large number of undifferentiated cells present near the regenerating connectives can be indicative of a high metabolic activity, which is naturally accompanied by the production of ROS, a hallmark of any regenerating tissue. The presumed production of ROS and their toxic effects can be counteracted by catalase activity in the capillaries, which innervate the surrounding cells (Figure 4.20B; marked by the double-headed arrow) and the tip of the regenerating connectives (Figure 4.20C). Further work needs to be conducted to study the activity and distribution of catalase in a more targeted and specific manner.

4.3.3. ADAMs are highly upregulated during neuronal regeneration

To the best of our knowledge, the family of A Disintegrin And Metalloprotease (ADAM) have never been studied in earthworms within a neuroregenerative context. Here, the expression of 5 members ADAMs (*adam8, adam12, adam19, adam28* and *adamts2)*, which were differentially expressed at 5wD in the RNAseq, was evaluated further via qPCR across four time points following decerebration, 1wD, 3wD, 4wD and 5wD. ADAMs' expression was validated as being significantly upregulated throughout regeneration over a course of 5 weeks, including 1 week following the removal of the brain unlike what the RNAseq has shown (Figure 4.21). To investigate this inconsistency, the ADAMs RNAseq raw counts were assessed (Table 4.9), which demonstrate the expression of all the ADAMs identified for each biological replicate in each experimental condition. In the RNAseq experiment individual

Table 4.9 RNAseq raw counts of differentially expressed genes in the ADAM family

RNAseq raw counts									
ID	Sham			1wD			5wD		
ADAM8_contig 274492	1	1	1	0	1	1	172	24	71
ADAM10_contig 88163	7	6	18	55	30	12	73	68	136
ADAM12_contig 36723	0	1	0	47	0	2	72	61	204
ADAM19_contig 167825	0	1	0	10	0	0	29	34	86
ADAM21_ contig 102187	4	1	6	8	5	0	25	13	28
ADAM28_contig 169508	0	0	0	2	0	0	23	28	43
ADAMTS2_contig 50247	0	0	0	31	0	0	58	18	72
ADAMTS6_contig 84285	0	0	0	153	0	2	376	80	290
ADAMTS12_contig 94713	1	4	4	87	9	6	43	21	92

worms were used to represent a distinct biological replicate. Even though there was no significant differential expression of ADAMs at sham vs 1wD based on the three biological replicates, the raw RNAseq counts portray an increased level of expression in one of the three biological replicates in 1wD. The difference between the RNAseq and qPCR in terms of ADAM expression at 1wD is probably due to the pooling of samples that was carried out for qPCR, in order to extract a satisfactory amount of RNA. In the qPCR methodology, each pool of samples represented a single biological replicate, and consequently, any variation in expression amongst the samples (as in the RNAseq) which comprise the pool, would be amplified. Moreover, not all ADAMs identified in the RNAseq were validated (i.e. *adam10*, *adam21*, *adamts6* and *adamts12*), due to issues with primer specificity and reproducibility of results. However, their involvement cannot be disregarded at this point, and further experimental work is needed. The expression levels of the ADAMs which were validated via qPCR is described below.

For ***adam8***, robust differential expression was observed in all the time points tested following decerebration, apart from 1wD. The highest induction was seen at 3wD (52.1 ±17.0 SEM, n=3, $p<0.001$), followed by a small decrease at 4wD (18.8 ±8.2 SEM, n=3, $p<0.001$), before increasing again at 5wD (37.2 ±20.1 SEM, n=3, $p<0.001$). The differential expression values obtained via qPCR in the later stages of regeneration (i.e. 3wD to 5wD) closely reflect that of the RNAseq obtained at 5wD (22.0 ±3.4 lfcse, n=3, $p<0.001$). For ***adam12***, significant differential expression was observed in all the time points tested following decerebration. As in the case of *adam8*, the time point which displayed the strongest differential expression compared to sham-operated worms was 3wD (80.4 ±38.6 SEM, n=3, $p<0.001$). Conversely, the expression of *adam12* in the other time points was lower than 3wD but in general of similar level; 1wD (8.69 ±3.5 SEM, n=3, $p<0.01$), 4wD (7.3 ±2.1 SEM, n=3, $p<0.01$) and 5wD (8.8 ± 1.2 SEM, n=3, $p<0.001$). The strong induction detected in the qPCR was also evident in the RNAseq at 5wD (40.9 ±5.3 lfcse, n=3, $p<0.001$). Next, for ***adam19***, significant differential

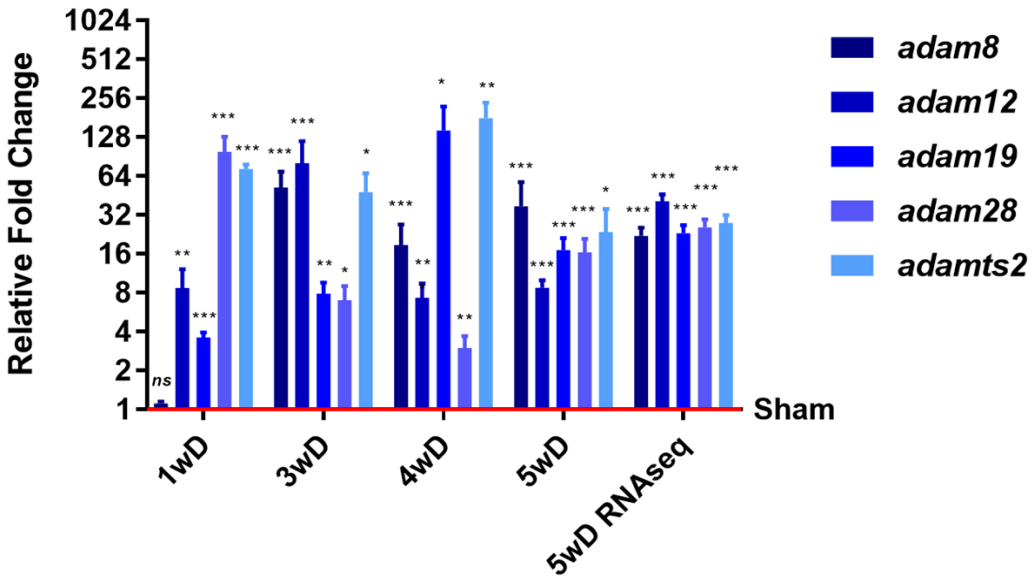

Figure 4.21 Relative expression of genes in the ADAM family (*adam8, adam12, adam19, adam28,* and *adamts2*) in regenerating neuronal tissue during Cerebral Ganglion (CG) regeneration. Relative expression (compared to sham-operated samples) was studied via qPCR in RNA that was extracted from regenerating neuronal tissue (CC, SOG and VNC) across four tme points (1wD, 3wD, 4wD and 5wD). High degree of upregulation was obtained across all the time points examined, for all the genes tested which validated the results obtauned in the RNAseq at sham vs 5wD. The only exception was *adam8* at 1wD, in which no significant differential expression was identified. Expression values in qPCR were normalised to *gapdh*, statistical analysis was carried out via a 2-tailed t-test and error bars represent the SEM (n=3, *** p < 0.001, **p <0.01, * p < 0.05). For the RNAseq data error bars represent the lfcse and statistical analysis was carried out via the DESeq2 package (n=3, *** padj < 0.001).

expression was observed in all the time points tested following decerebration. At 4wD *adam19*, showed a remarkably high induction (144.2 ±76.3 SEM, n=3, p<0.05), however it also showed high variability amongst the biological replicates. The lowest level of upregulation was seen at 1wD (3. 6 ±0.3 SEM, n=3, p<0.001) and 3wD (7.9 ±1.7 SEM, n=3, p<0.01). At 5wD (17.1 ±4.1 SEM, n=3, p<0.001) the expression levels were analogous to those obtained in the RNAseq (23.1 ±3.6 lfcse, p<0.001). In contrast to the ADAMs already discussed, ***adam28*** exhibited the strongest induction at 1wD (98.2 ±31.2 SEM, n=3, p<0.001), followed by a decrease in the level of induction at 3wD (7.0 ±1.9 SEM, n=3, p<0.05) and 4wD (3.0 ±0.7 SEM, p<0.01), before increasing at 5wD (16.4 ±4.6 SEM, n=3, p<0.001). The qPCR results for 5wD validated the results in the RNAseq (25.6 ±3.9 lfcse, n=3, p<0.001). Lastly, for ***adamts2***, even though a significant and robust differential expression was observed in all the time points tested following decerebration, it was a gene which exhibited greater variation in its expression profile amongst the biological replicates, compared to its ADAM counterparts. At the early stages of regeneration, i.e. 1wD, a high induction was detected (72.4 ±6.3 SEM, n=3, p<0.001), which was maintained through 3wD (48.1 ±19.0 SEM, n=2,

p<0.01), 4wD (179.2 ±58.3 SEM, p<0.01) and 5wD (23.7 ±11.9, n=3, p<0.05). The general pattern of upregulation seen in the qPCR resembled the results of the RNAseq (27.8 ±4.2 lfcse, n=3, p<0.001).

ADAMs can regulate cell-cell and cell-ECM interactions, as well as induce ECM remodelling through selective digestion of ECM components. Functional domains on the proteins (see section 2.5.5.2) allow the ADAMs to carry out these specialised roles, which have been the subject of intense scrutiny in developmental neurobiology. In the present study, nine ADAMs were identified as being differentially expressed during regeneration of which five were validated (at the time of writing). The validated ADAMs and ADAM10 were then subjected to further analysis of their protein sequence, which established the domains that are present in each member of the family, hence inferring their function in the earthworm (Appendix Figures 7.3 and 7.4). Note that ADAMTS2 did not return any conserved domains and is not presented. The adamalysin and the disintegrin domains were identified in all ADAMs, while the prodomain was identified only in ADAM8 and ADAM10. Partial protein sequences were derived from the transcriptome for all the ADAMs examined, except for ADAM10 (contig 88163; Appendix Figure 7.4) for which a full-length sequence was obtained (875 amino acids). ADAM10's protein sequence exhibited limited similarity to its mammalian counterparts.

The results from the RNAseq and qPCR demonstrated that several members of the ADAM family are upregulated throughout CG regeneration in the earthworm. However, through these experimental techniques, one cannot identify the spatial distribution on the neuronal tissue itself. Immunohistochemistry (IHC) was employed to study the localisation of ADAM proteins in neuronal tissue in *E. fetida*. Due to the limited availability of earthworm-specific antibodies, the antibody that was utilised for this purpose (kindly provided by Professor Jörg-Walter Bartsch), was initially designed to be directed against the prodomain (more evolutionary conserved than other domains) of ADAM10 in mice. To assess the similarity of the prodomains between the mouse and the earthworm, further analysis on the prodomains of the *Mus musculus* ADAM10 (NP_031425.2; 94 amino acids) and the *E. fetida* ADAM10 (contig 88163; 93 amino acids) and ADAM8 (contig 274492; 101 amino acids) (Figure 4.22A and B) was carried out, firstly by identifying the domains in BLASTx, followed by the pairwise alignment of the target sequences. The investigation revealed that the ADAM10 prodomain of *M. musculus* varies considerably to that of *E. fetida*'s ADAM10 (similarity: 53.6%; identity: 34.0%) and ADAM8 (similarity: 37.2%; identity: 21.2%), which suggests that if the anti-ADAM10 antibody can bind to ADAM10 in earthworms, it also has the potential to bind to

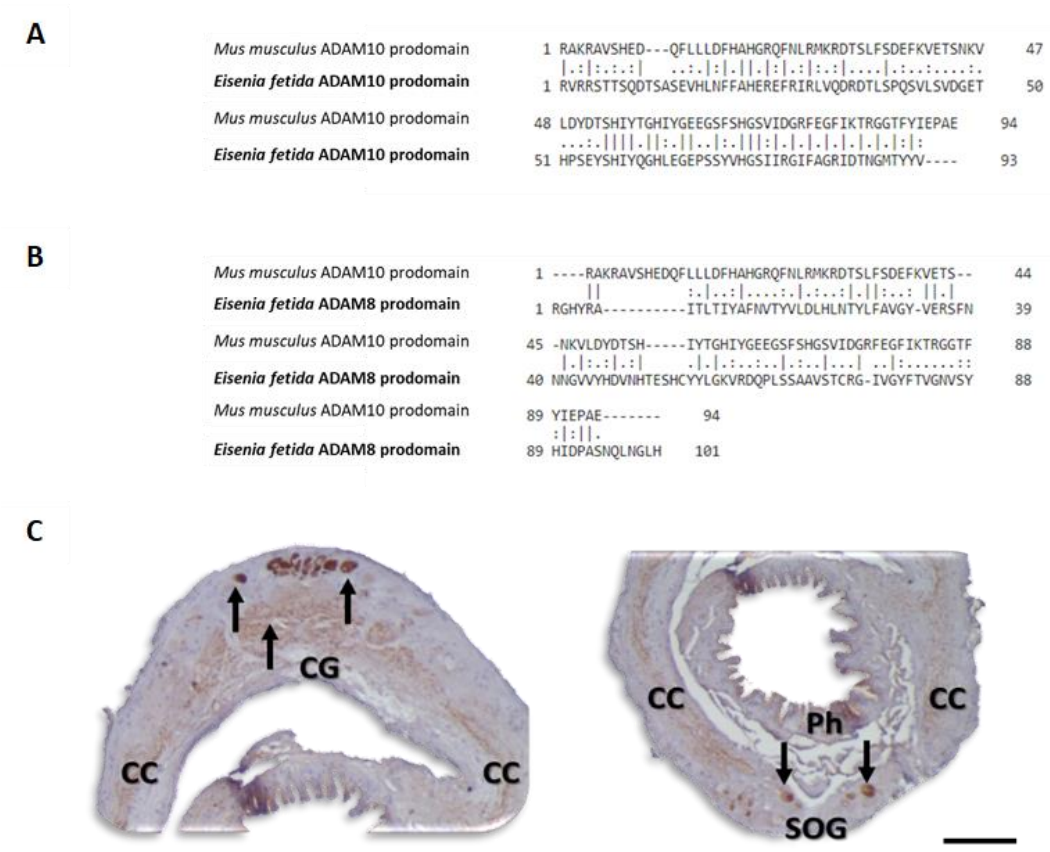

Figure 4.22 ADAMx characterisation via IHC. Pairwise Sequence Alignment (PSA) of the prodomain of Mus musculus ADAM10 (NP_031425.2) revealed low similarity against the prodomain sequence of E. fetida ADAM10 **(A)** and ADAM8 **(B)**. The analysis suggests that the antibody directed against the prodomain of mouse ADAM10 has the potential to bind to other ADAM epitopes in earthworms. **C.** IHC directed against the prodomain of ADAMx revealed the presence of the protein in the cells of both the Cerebral Ganglion (CG) and the Suboesopharyngeal Ganglion (SOG) (marked by the black arrows) as well as in axonal processes and/or secreted into the ECM. The alignments were conducted on the web-based software, EMBOSS (https://www.ebi.ac.uk/Tools/psa/). Scale bars: 100µm

the epitopes of other ADAMs as well. Consequently, the signal obtained is likely to represent a combination of more than one member of the ADAM family, and as such will be referred to as ADAMx hereafter. The IHC, enabled the characterisation of the spatial distribution of ADAMx (Figure 4.22C) in neuronal tissue in the earthworm. ADAMx-positive cells were identified on the dorsal side of the CG and SOG. Likewise, signal positivity was also identified in the axons and/or ECM distributed across the CG and the CC, indicating the secretion of ADAMx. The use of antibodies originally designed for species other than the earthworm can be associated with issues of non-specificity, and as such, this work on ADAMx distribution is not conclusive and can only serve as an indication of the expression and localisation of the proteins. Although there are specificity issues, this is a powerful tool to elucidate, generally, ADAM's involvement in regeneration.

4.3.4. Metallothionein-2 is upregulated during neuronal regeneration and is expressed in both the cerebral and the suboesophageal ganglia

In the results discussed thus far, the involvement of metals through their association with upregulated proteins has been prevalent. It was conjectured, therefore, that additional metalloproteins, may play a prominent role during neuronal regeneration. Metallothionein 2 (MT2) is a protein which has been the subject of several toxicological studies in earthworms; however, its role in neuronal tissues has yet to be elucidated. MTs are low molecular weight cysteine-rich proteins, which can serve as molecular chaperones for the transportation of zinc and as such can regulate zinc homeostasis in neuronal systems. They have also been demonstrated to adopt a protective role against oxidative stress during neuronal injury. Their multi-faceted roles make MTs a promising target to study within a neuroregenerative context in the earthworm.

Firstly, the expression of *mt2* across regeneration was determined via qPCR (Figure 4.23A), which revealed that it is moderately upregulated as early as the first day following the removal of the brain (1dD) (2.6 ±0.5 SEM, n=3, $p<0.01$) and peaks at 3dD (4.1 ±0.3 SEM, n=3, $p<0.001$) before decreasing at 1 week post decerebration (1wD; 3.2 ±0.2 SEM, n=3, $p<0.001$) and 3wD (1.7 ±0.2 SEM, n=3, $p<0.05$). No significant differential expression was evident at 5wD, suggesting that it is no longer required in the latter stages of regeneration, which coincides with the time that the first neuronal structures begin to appear (i.e. 3-4 weeks following decerebration; see section 4.1.2).

Following the finding that MT2 plays a role during neuronal regeneration in the worm, the localisation of the protein across the neuronal tissue was explored further via IHC and immunofluorescence (IF). An earthworm specific antibody against MT2 was employed to study its distribution. Previous studies have demonstrated that MT2 is induced in the gut epithelium in earthworms following exposure to the toxic metal cadmium (Cd), which was utilised to determine the quality and specificity of the antibody. The worms were exposed to 200mg Cd /kg soil for 20 days, at which point the gut was tested for MT2 positivity, that resulted in a strong positive signal indicative of the specificity of the antibody (Figure 4.23B). For the purposes of enhanced visual representation, it was decided to perform immunofluorescence (IF) to determine the spatial distribution of MT2. Initially, triple labelling was carried out with Hoechst stain (marker for cell nuclei), anti-β-tubulin antibody (a marker for neuronal microtubules) and anti-MT2 for all subsequent experiments. However, for the simplicity and clarity of the data presented, a single

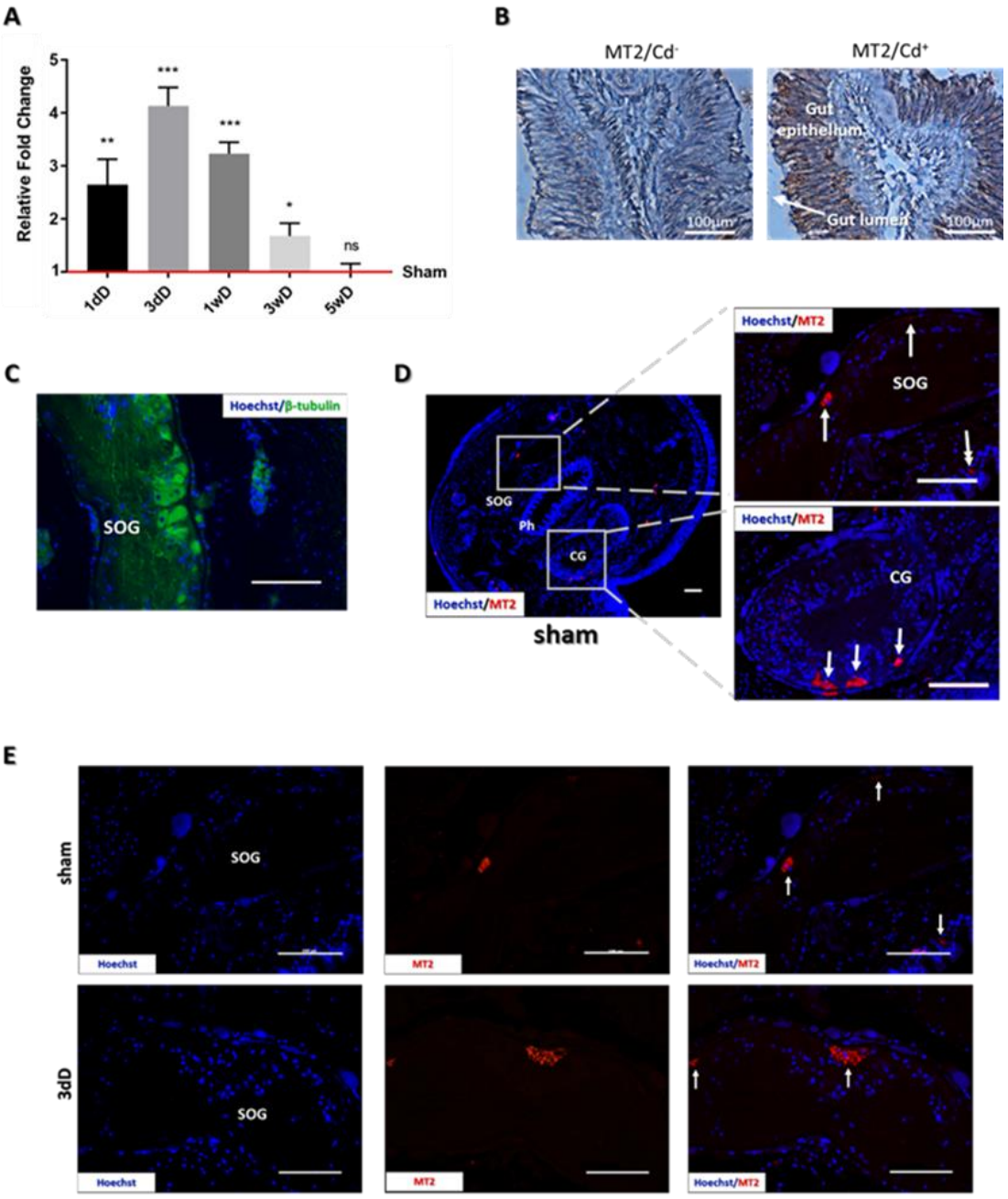

Figure 4.23 Metallothionein-2 (*mt2*) relative expression and distribution in the SubOesophageal Ganglion (SOG) during Cerebral Ganglion (CG) regeneration. A. Relative expression (compared to sham-operated samples) was studied via qPCR in RNA that was extracted from regenerating neuronal tissue (CC, SOG and VNC) across five time points (1dD, 3dD, 1wD, 3wD and 5wD). Significant upregulation of *mt2* was observed in 1dD to 3wD before returning to baseline levels at 5wD. Statistical analysis was carried out via a 2-tailed t-test and error bars represent the SEM (n=3, *** $p < 0.001$, ** $p < 0.01$, * $p < 0.05$). **B.** Paraffin sections of the gut of control and cadmium-exposed (200mg/kg of soil) worms were processed for MT2 immunohistochemical (IHC) labelling. Strong induction of MT2 was identified in the gut epithelium of cadmium-exposed worms. **C.** IHC labelling of β-tubulin marks the presence of neuronal components in the SOG (green) and Hoechst staining marks the cell nuclei (blue). **D.** IHC labelling revealed the regions in the control SOG and control CG that MT2 is expressed (red). **E.** IHC labelling on decerebrated samples confirmed the results of the qPCR, which showed a higher degree of MT2-positivity. Scale bars: 100µm

representative image of β-tubulin is shown (Figure 4.23C) to confirm the presence of neuronal components in the SOG. MT2 is expressed in both the SOG and the CG in sham-operated worms, primarily on the periphery of the ganglia, where the majority of the cell population is situated (Figure 4.23D). In the SOG, a large hotspot of MT2 was observed at the midline of the fused ganglia towards its ventral side, whereas in the CG MT2-positivity was observed towards the edges of the ganglia.

Additionally, in the cross-sections shown, MT2 positive cells were identified in the pharyngeal epithelium. Next, the SOG was examined further for any variations in distribution compared to control samples, at 3 days post-decerebration which exhibited the highest induction in the qPCR (Figure 4.23E). The distribution pattern of MT2 does not seem to change following decerebration, however, the elevated level of MT2 positivity at the midline of the SOG, suggests that MT2 is induced not only at the transcriptomic level but also at the translational level, during neuronal repair in *E. fetida*.

To the best of our knowledge, this is the first study to examine how metallothionein-2 responds to neuronal damage in earthworms. The results suggest that MT2 is highly expressed in the CNS of earthworms and is upregulated for a period of 3 weeks following decerebration. The discovery that a wide range of metalloproteins, including metalloproteases such as ADAMs or molecular chaperones such as MT2, are differentially expressed during regeneration, suggests that metal homeostasis plays a central role during this phenomenon in the earthworm. The hypothesis was studied further at the Diamond Light Source (DLS), the UK's national Synchrotron facility located at the Harwell Science and Innovation Campus in Oxford, which enabled the characterisation of metal distribution across regenerating tissue in *E. fetida*. The results of this endeavour are presented in section 4.4.

4.3.5. NG2 expression in control and regenerating neuronal tissue suggests a growth promoting function

The inhibitory role of CSPGs in neuronal regeneration has been extensively investigated, including NG2 (CSPG4) (Filous *et al.,* 2014). In section 4.2.5, the baseline levels of expression of NG2 was determined and showed that it was expressed in control and regenerating neuronal tissue (Table 4.7). The presence of NG2 in these tissues was verified via IHC, which revealed that besides exhibiting a strong expression in the CC and SOG (Figure 4.24A), as the

RNAseq suggested, it was also expressed in control CG and regenerated neuronal anatomical structure (neuropil) that was formed 3 weeks following the removal of the brain (Figure 4.24B). As a transmembrane protein, NG2 co-localised with cell bodies at the periphery of both the control CG and SOG, as well as in the ECM and/or axonal processes. The cell density in the regenerated structure was low and as such NG2 positivity was not associated with cell bodies, but with the ECM and/or axons instead.

As with the case of ADAMx distribution in neuronal tissue, a non-specific antibody was used to assess the expression of NG2. However, there is evidence to support that the antibody targets CSPGs specifically, since NG2 positivity was limited to the neuronal tissue of the worm. Nevertheless, the work conducted here is not conclusive and can only serve as a strong indication of CSPG presence in the neuronal tissue of *E. fetida* at this point.

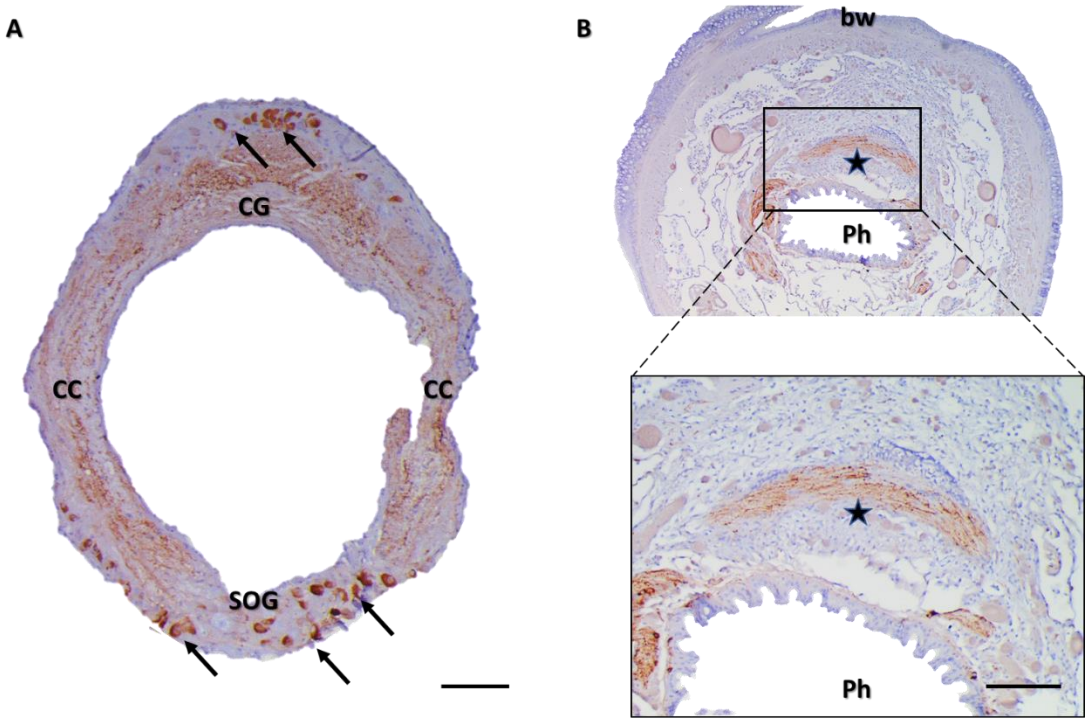

Figure 4.24 NG2 distribution in control and regenerated neuronal tissue in *E. fetida*. A. IHC labelling revealed NG2-positivity associated with cell bodies in the CG and SOG (marked by the arrows), as well as in axonal processes and/or secreted into the ECM. **B.** NG2 positivity was detected in the regenerated neuronal structure (neuropil) at 3 weeks following decerebration (marked by the star), associated with the ECM and/or developing axonal processes. There was no NG2 positivity associated with cell bodies. Scale bars: 100µm. *CG; Cerebral Ganglion, CC; Circumpharyngeal Connectives, SOG; SubOesophageal Ganglion, bw; body wall, Ph; Pharynx*

4.3.6. Rapid Amplification of cDNA Ends (RACE)

The work carried out on the RNAseq enabled the identification of thousands of transcripts and their sequences. However, since only 66% of the total contigs were mapped onto the *de novo* transcriptome, many genes remain to be identified and for many that have been identified, only a partial transcript sequence was obtained, on which their identity was based. To address this issue, two RACE libraries (one 5' RACE and one 3' RACE) were constructed through which the full-length transcript sequences of genes of interest (GOIs) could be determined. A full-length sequence adds more confidence into the identity of the contigs and ultimately provide more information on their protein structure and function. The process of generating the full-length sequences from the RACE libraries was carried out in two separate reactions (see section 2.13 for more details on the methodology). One which produced the 5' RACE amplicon (generated via the antisense primer and the UPM, utilising the 5' RACE library as a template) and one which produced the 3' RACE amplicon (generated via the sense primer and the UPM, utilising the 3' RACE library as a template), that ultimately represented the 5' end and the 3' end of the transcript sequence, respectively. Attempts were made to extract the full-length sequences of numerous GOIs, including but not limited to, ADAMs, *ptpσ,* MMPs, *sema5a* and *ntn1,* however these did not return satisfactory results and are not presented. This can be attributed to several factors, mainly due to the low abundance of some of the transcripts present in the libraries or the hard-to-detect small amplicons produced via the sense and antisense primers. Nevertheless, the full-length transcript sequences of the following three GOIs were obtained: *coII* (which served as the gene in phylogenetic studies), *gapdh* (which served as the reference gene in all the qPCR experiments) and *mt2* (which was upregulated during neuronal regeneration). The 5' and 3' RACE amplicons (5'R and 3'R) were cloned in pGEMT-easy vectors and cultured in competent bacteria (*E. coli;* DH5a). Three individual bacterial colonies were selected for each product, for each gene (i.e. 18 colonies), from which the plasmids were isolated and then screened for the presence of the insert via PCR (T7 and SP6 promoter primers were used that flanked the position of the cloned insert) and finally ran on a 1% agarose EtBr gel (Figure 4.25). Of the 18 colonies examined, only lanes 2b and 6b two did not show the presence of the insert, which represented one colony of the 3'R amplicons for *coII* and *mt2*. Plasmid (a) for each gene was selected for further analysis via Sanger sequencing. The 5'R amplicon size (excluding the UPM primer and the vector flanking sequences) for *coII, gapdh,* and *mt2* were 530bp, 754bp and 363bp, respectively. In contrast, the 3'R amplicon size (excluding the UPM

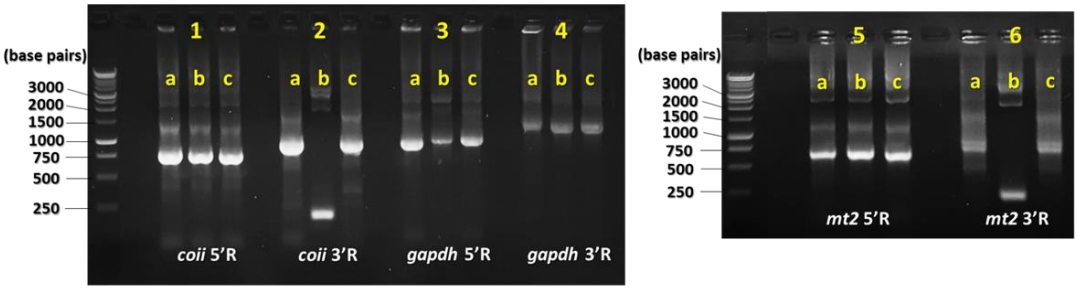

Figure 4.25 Detection of cloned RACE product inserts (5' or 3' RACE) in pGEMT-easy vectors via PCR, for *coII, gapdh* and *mt2*. The flanking region of the cloned insert position was amplified via PCR by T7 and SP6 promoter primers. The resulting amplicons were subjected to electrophoresis on a 1% agarose gel containing ethidium bromide. Amplicons were visualised under ultraviolet light. Three colonies were investigated for the presence of the insert for each of the sequences. All the plasmids investigated across the three genes (n=18), confirmed the presence of their respective inserts, except 2.b and 6.b, which corresponded to the 3'RACE products of *coII* and *mt2*. L = 1kb DNA ladder

primer and the vector flanking sequences) for *coII, gapdh* and *mt2* were 687bp, 1032bp and 427bp, respectively. The overlapping of the 5'R and 3'R amplicons enabled the characterisation of the complete transcript sequence for each gene (*coII;* Figure 4.26, *gapdh*; Figure 4.27, *mt2*; Figure 4.28). The complete transcript sequence obtained for *coII* was 720bp, which translated to 230 amino acids. As for *gapdh*, the largest of the three genes, its nucleotide sequence was 1660bp, of which 583bp constituted the 3' untranslated region (UTR) and its protein sequence was 334 amino acids. Lastly, *mt2* produced a transcript

```
atg gga atg cca aat tga ggt caa gta ata ttt caa gac gcc gca tct tct gtg ata ctc
M   G   M   P   N   W   G   Q   V   M   F   Q   D   A   A   S   S   V   M   L

cat tta att tcc ttt cac gat cac aca ctt cta gtt cta aca cta gtc tta aca gtc gtg
H   L   I   S   F   H   D   H   T   L   L   V   L   T   L   V   L   T   V   V

ggc tat gcc cta ctt gct cta atg cta aat aag tac tta aac cgt tat att cta gaa gct
G   Y   A   L   L   A   L   M   L   N   K   Y   L   N   R   Y   I   L   E   A

caa aca gtt gag aca gtt tga act atc ctg cca gct ctt atc tta cta gtg tta gcc tta
Q   T   V   E   T   V   W   T   I   L   P   A   L   I   L   L   V   L   A   L

cca tca ctt cgt att tta tat att aca gat gag gta agt cag cca tct tta acc gta aaa
P   S   L   R   I   L   Y   I   T   D   E   V   S   Q   P   S   L   T   V   K

aca atc ggg cac caa tga tac tga agt tat gaa tac acc gac ttc ata aac gta gaa ata
T   I   G   H   Q   W   Y   W   S   Y   E   Y   T   D   F   M   N   V   E   M

gat tcc tat ata ctt ccc acc acc gac cta atg ccc ggg gac tat cgc cta cta gaa gtt
D   S   Y   M   L   P   T   T   D   L   M   P   G   D   Y   R   L   L   E   V

gat aac cga ata gtt gtt cca ata cag cta gaa att cga ata cta atc acc gct gca gac
D   N   R   M   V   V   P   M   Q   L   E   I   R   M   L   I   T   A   A   D

gtg att cac tca tga act gtt cct gta cta ggt gta aaa gta gat gcc gtt cct gga cga
V   I   H   S   W   T   V   P   V   L   G   V   K   V   D   A   V   P   G   R

tta aat caa att ggt ttt acc acc tca caa cct gga atc ttc tac gga caa tgt tca gaa
L   N   Q   I   G   F   T   T   S   Q   P   G   I   F   Y   G   Q   C   S   E

atc tgt ggt gct aac cac tcc ttt atg cca atc gcc gtt gaa gcc att aac act aaa tct
I   C   G   A   N   H   S   F   M   P   I   A   V   E   A   I   N   T   K   S

ttc ata aaa tga gtc tca aac ttt gat aat taa aaa aaa aaa aaa aaa aaa aaa aaa aaa
F   M   K   W   V   S   N   F   D   N   -
```

Figure 4.26 Full length transcript and protein sequence of *coII* in *Eisenia fetida*, derived from RACE. The complete transcript sequence (720 nucleotides) was obtained by Sanger sequencing of the 5' and 3' RACE products. *In silico* translation (230 amino acids) of the transcript sequence was carried out on the online software ExPASy.

sequence of 604bp and, as expected, a relatively short protein sequence of 80 amino acids, of which 21 were cysteines (Cys, C). A feature of *E. fetida*'s MT2 sequence, which is not shared by all the earthworms in the Annelida phylum, is the presence of 3 consecutive Cys residues starting at position 22 of the protein (marked by the dotted line in Figure 4.28).

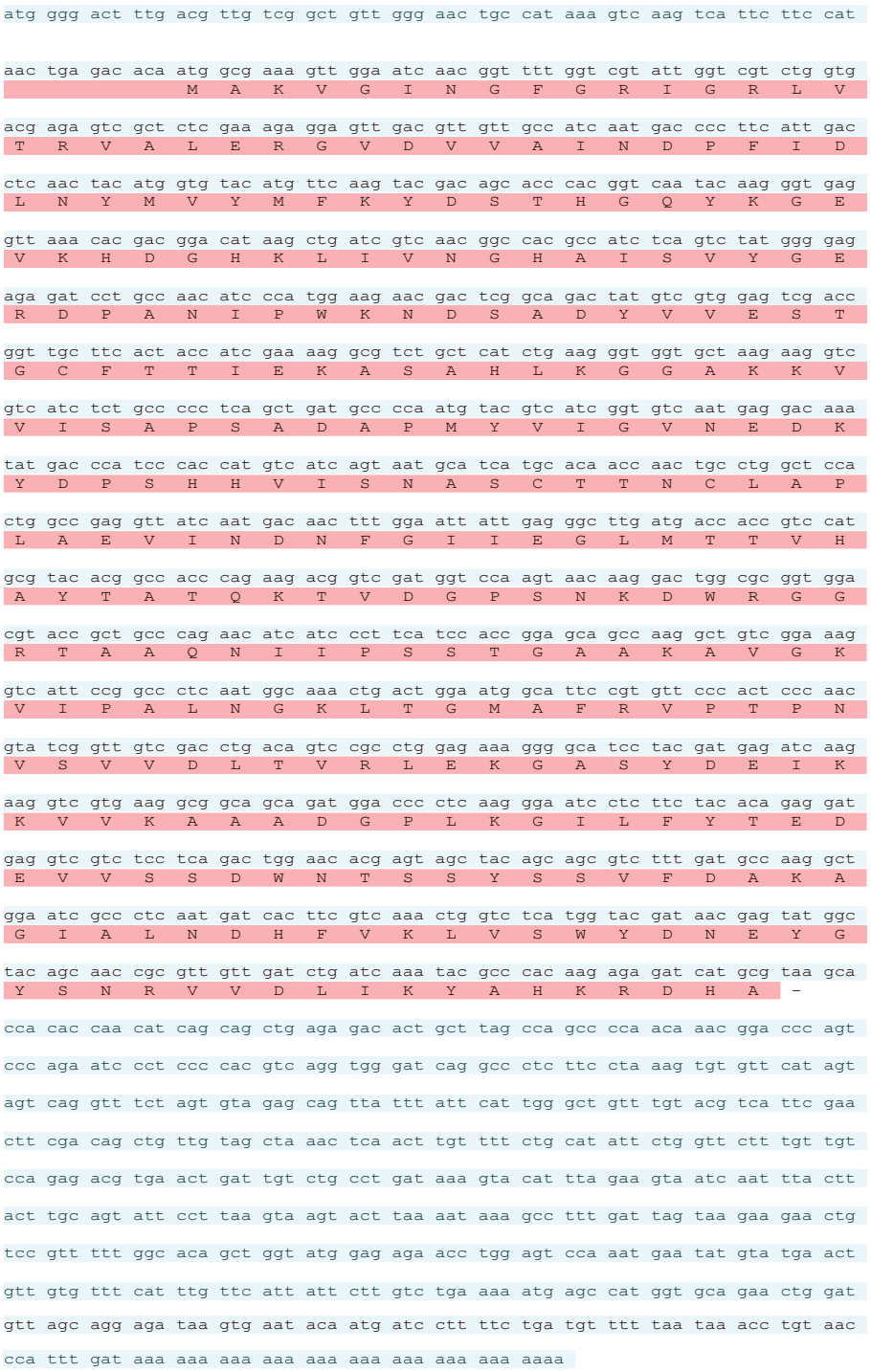

Figure 4.27 Full length transcript and protein sequence of *gapdh* in *Eisenia fetida*, derived from RACE. The complete transcript sequence (1660 nucleotides) was obtained by Sanger sequencing of the 5' and 3' RACE products. *In silico* translation (334 amino acids) of the transcript sequence was carried out on the online software ExPASy.

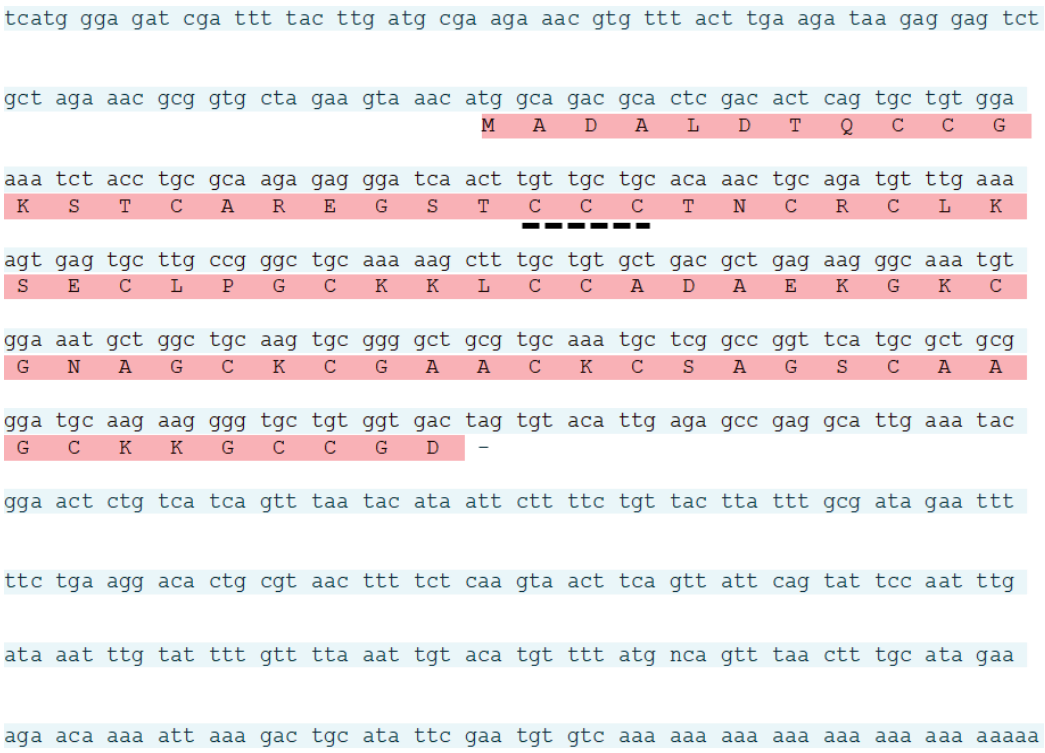

Figure 4.28 Full length transcript and protein sequence of *mt2* in *Eisenia fetida*, derived from RACE. The complete transcript sequence (604 nucleotides) was obtained by Sanger sequencing of the 5' and 3' RACE products. *In silico* translation (80 amino acids) of the transcript sequence was carried out on the online software ExPASy. The characteristic triple cysteine (C) of the MT2 protein present in *E. fetida*, is marked by the dotted line.

Indeed, multiple sequence alignment of the MT2 protein sequences between the *E. fetida* sequence identified in this study and its ten most similar MT2 protein sequences in annelids (identified by BlastP), revealed that only three earthworms share the triple cysteine feature with *E. fetida*: these are *Eisenia andrei, Aporrectodea caliginosa* and *Allolobophora chlorotica* (Figure 4.29A). The similarity of the MT2 sequences is also reflected by the phylogenetic analysis performed (Figure 4.29B), in which the four species of earthworms (including *E. fetida*) form a cluster, suggesting a close evolutionary relationship. The role of metallothioneins in metal homeostasis, protection against ROS and serving as a buffering medium against toxic metals can all be traced back to the interactions with cysteine residues in the protein. The triple cysteine, therefore in *E. fetida*, can provide some answers as to why it exhibits higher resiliency against toxic compounds, compared to other species of earthworm, described in section 4.1. It would be of value, therefore, if further toxicological studies were conducted in which the responses of earthworms which possess the triple

cysteine, were evaluated against those that do not. Establishing the full-length sequences of other GOIs (e.g. ADAMs and other metalloproteins and axon guidance molecules amongst other RAGs), would enhance the confidence of the annotations assigned to these contigs and ultimately deduce their presumed function more accurately.

A

```
Polypheretima_elongata_ACA60735.1      --MSDNTKCCGKTTCPREDSKCVCPNCQCAKDNCPPNCDKNCCASAGCGS-AKCGNANCK   57
Metaphire_californica_ACD84579.1       --MSDTTKCCGKAACPREDNQCVCPNCQCPKGECPPNCDKNCCGSAGCGS-AKCGNANCK   57
Pontoscolex_corethrurus_ACD84582.1     MSDACVTKCCGKPECPREGGKCACANCKCTKEECLPHCHKNCCADAGCGAAAKCGNANCK   60
Lumbricus_friendi_ADW27175.1           ------------------GSTCACSKCRCPKDDCLPNCKKLCCADA------QCGDAGCS   36
Lumbricus_rubellus_                    MADALNTQCCGNKTCPREGSTCACSKCRCPKDDCLPNCKKLCCADA------QCGNAGCS   54
Lumbricus_terrestris_CAA09056.1        ------TQCCGNKTCPREGSTCACSKCRCPKDDCLPNCKKLCCADA------QCGNAGCS   48
Lumbricus_castaneus_CAA09057.1         ------TQCCGFDACPRRGAACACTNCRCLKSECSPNYRKLCCADS-Q---GKCGNAGCK   50
Allolobophora_chlorotica_ADK62365.1    --------------------TCCGKCRCLKTECPPNCKKNCCADA-Q---GKCGNASCK   36
Aporrectodea_caliginosa_ANS56713.1     --------------------TCCGNCRCLKSECPPNCKQLCCADAEK---GKCGNASCK   37
Eisenia_fetida*                        MADALDTQCCGKSTCAREGSTCCGNCRCLKSECLPGCKKLCCADAEK---GKCGNAGCK   57
Eisenia_andrei_AKJ51798.1              --------------------CCGNCRCLKSECLPGCKKLCCADAEK---GKCGNAGCK   36
                                                            * * :*:* * :* *   : **..:     :**:*.*.

Polypheretima_elongata_ACA60735.1      CGADCKCTGGPACATECVKGSCK-   80
Metaphire_californica_ACD84579.1       CGADCKCVGGPACATECAKGSCK-   80
Pontoscolex_corethrurus_ACD84582.1     CGANCQCKPGA-CTEGCKQGCCAD   83
Lumbricus_friendi_ADW27175.1           CGAAFKCAAGS-CASGCKKGWCG-   58
Lumbricus_rubellus_                    CGAACKCAAGS-CASGCKKGCCAD   77
Lumbricus_terrestris_CAA09056.1        CGAACKCAAGS-CASGCKKGCCGD   71
Lumbricus_castaneus_CAA09057.1         CGAACKCAAGA-CASGCKKGCCGD   73
Allolobophora_chlorotica_ADK62365.1    CGASCKCAAGS-CAAGCKKGCCG-   58
Aporrectodea_caliginosa_ANS56713.1     CGAACKCAAGS-CASGCKKGCCG-   59
Eisenia_fetida*                        CGAACKCSAGS-CAAGCKKGCCGD   80
Eisenia_andrei_AKJ51798.1              CGAACKCSAGS-CAAGCKKGCCGD   59
                                       *** .*  *  *:  * :* *
```

B

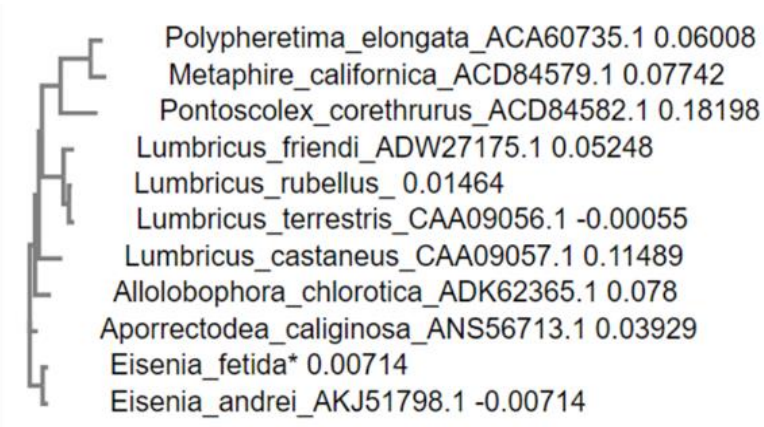

Figure 4.29 Identification of earthworm species which possess a triple cysteine in their metallothionein-2 (MT2) protein sequence. A. The ten MT2 sequences in annelids, which exhibited the highest similarity to the MT2 that was identified through RACE, were subjected to multiple sequence alignment (MSA). The analysis revealed that other than *Eisenia fetida,* three earthworm species (*Eisenia andrei, Aporrectodea caliginosa and Allolobophora chlorotica),* also possessed the triple cysteine in the protein. **B.** The evolutionary relatedness of the species which possessed the triple cysteine, was confirmed via phylogenetic analysis by the Neighbour Joining Method. The MSA and phylogenetic analysis were conducted on the EMBL-EBI online software **https://www.ebi.ac.uk/Tools/msa/clustalo/**

4.4. X-ray Fluorescence (XRF) spectroscopy revealed the time-resolved involvement of iron, calcium and zinc trafficking during cerebral ganglion regeneration

The analysis of the transcriptome during neuronal regeneration in the earthworm provided a framework from which to develop our understanding of what regulates this process. A central discovery in this study was the detection of several upregulated metalloproteins, primarily associated with zinc and iron. Due to the important part that metal homeostasis holds in neuronal regeneration and in conjunction with the aforementioned induction of metalloproteins, here, for the first time, the metal composition of control and regenerating neuronal tissue in *E. fetida* was determined by employing X-ray Fluorescence (XRF) spectroscopy, at Diamond Light Source (DLS) i18 beamline. XRF is a powerful and sensitive technique which can determine distinct elemental distributions at high spatial resolution.

XRF is based around the unique makeup of atoms of different elements, which are bombarded by high energy X-ray beams. A description of the method is described in section 3.21 and is also presented here for more expedient referencing purposes. The generation of the X-rays is initiated with the introduction of electrons (using an electron gun) into a booster ring, where they accelerate and build up energy, before entering the storage ring within the Synchrotron (Figure 4.30A). The electrons are then accelerated and focussed as they pass through dipole (bending) magnets, as well as quadrupole and sextupole magnets. Due to the acceleration experienced by the electrons around the bending magnets, the electrons emit

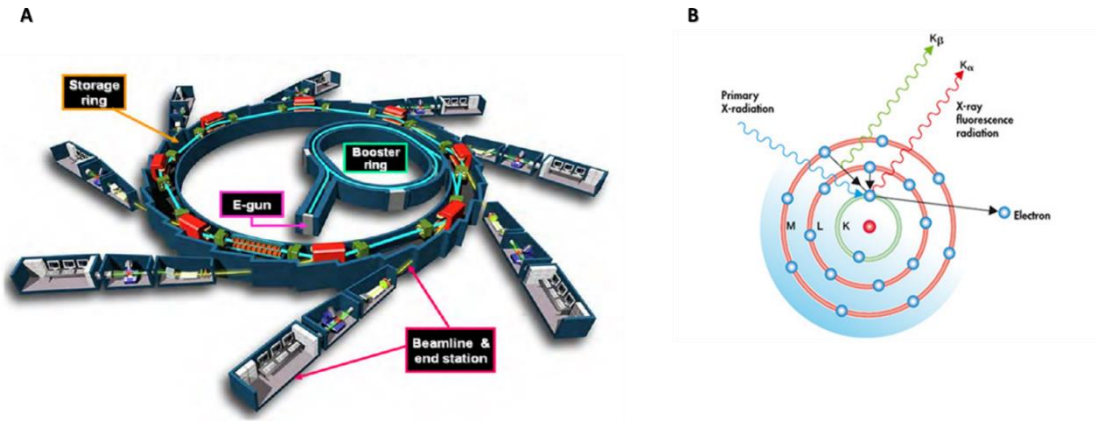

Figure 4.30 Synchrotron radiation underlying principles. A. Electrons produced by an electron gun are accelerated and build up energy within the booster and storage rings. The accelerated electrons emit X-rays which are directed into experimental stations and interact with the sample. **B.** X-ray energy forces an inner electron (K-shell) to escape the nuclear attraction. Outer shell electrons (L or M) then migrate into the inner shell to restore stability. In the process, X-ray fluorescence radiation is emitted that is unique to each element and can be exploited to determine the elemental composition of the sample.

X-rays which are then directed towards the experimental stations where they bombard the sample in question (Figure 4.30B). When an atom is hit with this micron-sized X-ray beam, with the energy of this magnitude, an electron from the inner (K-shell) orbital shell of that atom overcomes the nuclear attraction and escapes. In order for the atom to regain stability, an electron from a higher energy orbital shell (i.e. outer shell), either from the M- or L-shells, moves down to the lower energy orbital shell to fill in the vacancy. During the transition of the electron from a higher energy orbital shell to a lower one, a characteristic fluorescent X-ray radiation, of specific energy, is emitted (referred to as secondary X-ray photon radiation) that can serve as a unique identifier of the atom from which it had originated. Two secondary X-ray photon radiations can be produced by an atom, Kα or Kβ, which are the result of electron migration from an M and L-shell respectively. Next, trough the identification of the origin of the secondary X-ray on the sample, the elemental composition of a micron-sized area within the neuronal tissue can be determined. In the same way, the entire sample is analysed, through which a 2D elemental distribution XRF map is constructed. In addition to determining what the metal distribution was in the samples, the quantity of those metals was also established through the XRF measurements of calibrated standards provided by the DLS. All the experiments conducted were carried out on paraffin wax sections as described in section 3.16.

XRF was performed on sham-operated samples and decerebrated samples across a range of time points (1wD, 4wD, 5wD, 6wD, 7wD, 8wD and 10wD) and with two beam sizes in increasing level of resolution: (1) 10µm and (2) 3µm. The primary aim of the study focussed on identifying changes in the distribution of iron, calcium and zinc metals which have been linked to neuronal regeneration in other species. It is important to mention that the XRF experiments took place across two sessions at the facility and the following results will be presented in the same way to reflect this, in order to describe the scientific rationale of the work. The resulting spectra and the maps obtained from DAWN for each XRF scan were fitted in PyMca in order to test for the accuracy and reliability of the output. A representative fitting obtained in each session is presented below (Figure 4.31).

At least three individual worms were used at each time point; a representative 10µm XRF map is presented from each (Figure 4.32). Firstly, it was interesting to establish that metal distribution in a typical CNS environment follows a similar pattern to cellular distribution within the tissue, in that the periphery of both the CG and SOG produced the strongest signal for all three metals in the CNS, and less so in the connectives. Iron hotspots appear to localise in the periphery of the CG and the SOG at much higher levels than in neighbouring tissues.

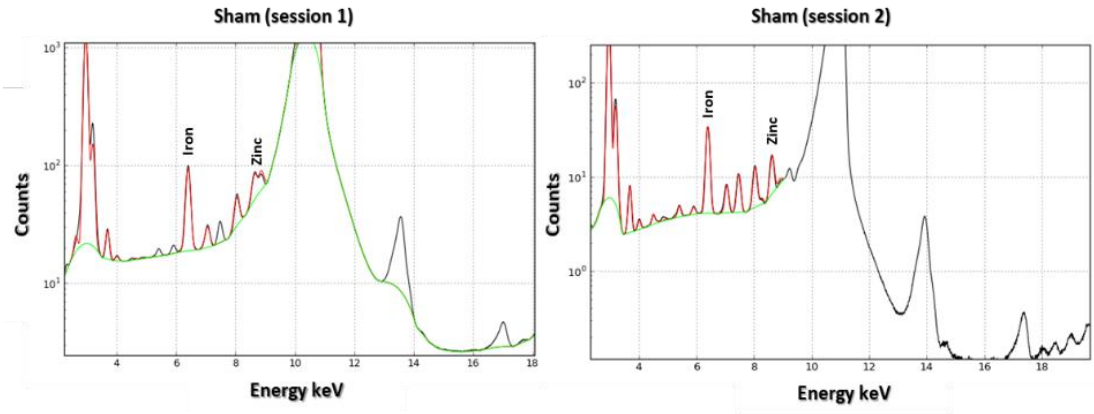

Figure 4.31 Fitting of the XRF spectra. The resulting spectra from the XRF experiments (black) in session 1 and 2 were fitted (red) which demonstrated a good quality and reliability of the results. The energy corresponding to iron (6.4keV) and zinc (8.6keV). Fitting was carried out in PyMca.

Also, evidence from the 1wD and 4wD suggest that there is an influx of iron into and around the regenerating connectives. Moreover, one of the most thought-provoking findings made in this study was the discovery that the regenerated Cerebral Ganglion (rCG), seen at 4wD and 5wD, is largely devoid of iron especially when compared to control CG. The rCG on the iron maps are indicated by the dotted lines. Interestingly, at 4wD, high levels of iron in the CC are abruptly interrupted (double-sided arrow), transitioning into the rCG that is characterised by low levels of iron. This transition takes place at the point where the decerebrating incision was originally performed. In addition, the low levels of iron in regenerated tissue was also detected at 1wD, on axonal processes (marked by the star) which extend from the connectives. Calcium distribution, on the other hand, does not change during regeneration and its levels, unlike iron, appear to be replenished in the periphery of the regenerated brain at 5wD, resembling the control CG.

In sham-operated worms, there were no zinc hotspots associated with the neuronal tissues and, except for the body wall, zinc is evenly distributed across all the different tissues present on the section, including the CNS. In contrast, in 1wD samples, a high zinc influx was observed closely associated with the regenerating circumpharyngeal connectives (CC) in and around the tissue, a phenomenon that was not evident in the latter stages of regeneration (4wD and 5wD). Zinc, iron and calcium appear to co-localise in these hotspots. Moreover, zinc levels in the rCG at 5wD appear to be replenished and follow a similar distribution pattern to the control CG. The accumulation of zinc at 1wD samples was studied further under a 3µm beam diameter from which an enhanced spatial resolution of the zinc hotspots was obtained. All the 1wD samples that were scanned with the 3µm beam are presented below along with a

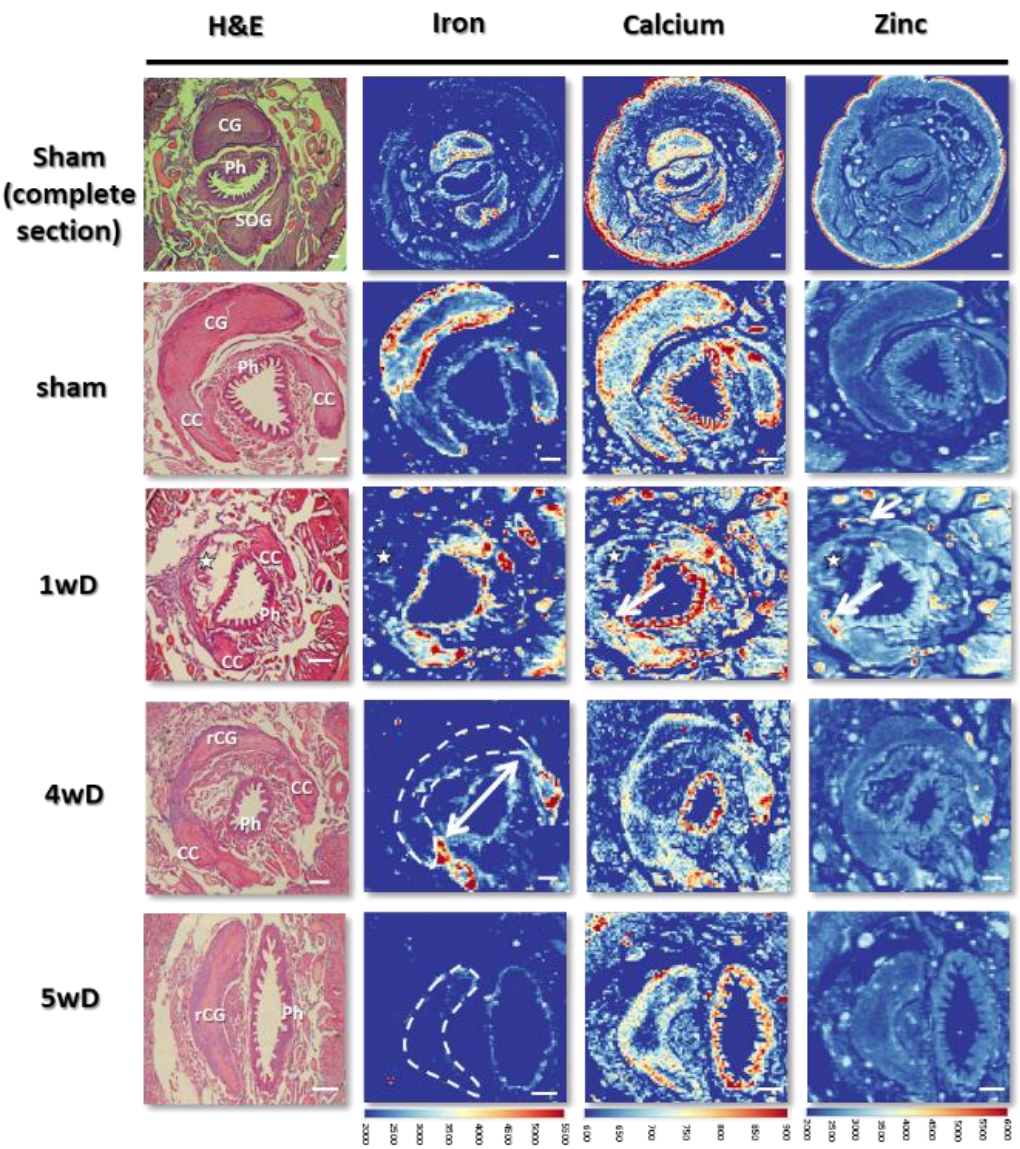

Figure 4.32 XRF heatmaps depicting the distribution of iron, calcium and zinc in control and regenerating neuronal tissue in *Eisenia fetida*. XRF scans (10µm) were performed on paraffin cross-sections (6µm) of sham operated samples, 1wD, 4wD and 5wD. The maps demonstrate that metal distribution follows the pattern of cellular distribution in neuronal tissue identified in H&E. Lower levels of iron were detected in rCG at 4wD and 5wD compared to control CG. Accumulation of zinc was observed at 1wD, associating with the tip of CC. The incident X-ray beam energy was set to 10.6keV and the maps were produced in DAWN 2.14.0. Scale bars: 100µm. *CG; Cerebral Ganglion, CC; Circumpharyngeal Connectives, rCG; regenerated Cerebral Ganglion, Ph; Pharynx, SOG; Suboesophageal Ganglion*

representative XRF map of sham-operated samples (Figure 4.33). These once again demonstrated that, contrary to sham samples, pockets of high zinc load associated with the CCs (marked by the arrows) in the early stages of regeneration. The results of the first session at Diamond provided evidence to support the hypothesis that zinc homeostasis, particularly at the early stages of neuronal injury, plays a role in regeneration in the earthworm. What is more, iron levels in the regenerated brain were significantly lower compared to its control

counterpart, which was remarkably consistent across all the samples tested and demonstrates that the brain has not yet fully regenerated at 5wD. The next step in the investigation focussed on answering two main questions: (1) Does the brain continue to regenerate past 5wD and eventually restores its iron levels and (2) if so, how many weeks does this happen in? These questions were answered during the second session at Diamond, at which significant emphasis was given in determining the quantity of the metals in the

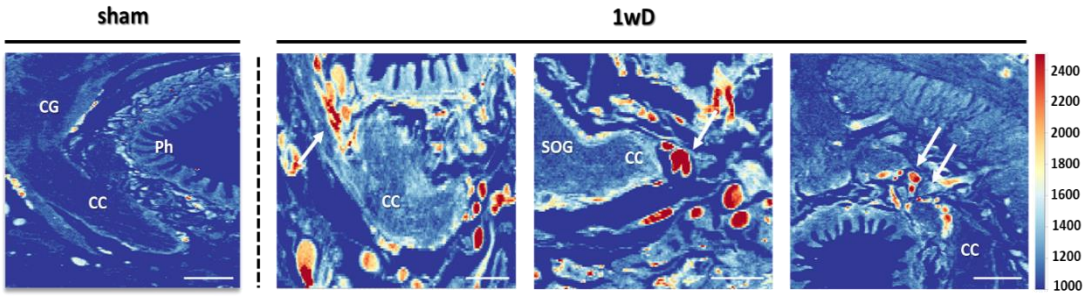

Figure 4.33 XRF heatmaps depicting the distribution of zinc in control and regenerating neuronal tissue in *Eisenia fetida*. XRF scans (3µm) were performed on paraffin cross-sections (6µm) of sham operated samples and 1wD. The maps demonstrate that zinc accumulates near and within the regenerating connectives (marked by the arrows). X-ray beam energy was set to 10.6keV and the maps were produced in DAWN 2.14.0. Scale bars: 100µm. *CG; Cerebral Ganglion, CC; Circumpharyngeal Connectives, Ph; Pharynx, SOG; Suboesophageal Ganglion*

neuronal tissue with calibrated standards. New samples were examined during this set of experiments, in an attempt to also replicate results from the first session. As before, at least three individual worms were used at each time point and a representative 10µm XRF map is presented from each (Figure 4.34). At 5wD, iron levels in the rCG were negligible compared to the control, thus validating the previous results obtained during the first session. Iron levels exhibited a small increase at 6wD in the rCG compared to 5wD, followed by a steady increase until week 10 after the removal of the brain, in which iron was present at similar levels to the control brain both in quantity and distribution within the tissue. The results suggest that the brain continues regenerating and developing past the 5th week following decerebration, as indicated by the increasing levels of iron. Therefore, assessing the distribution of iron in regenerating tissue can serve as an indication for the functional recovery and complete regeneration of the brain in the earthworm.

Additionally, an experimental protocol was devised in which only one ganglion of the brain was removed, termed hemiganglioctomy, in order to show, within the same brain, differences in iron content between the control and regenerated tissue. Firstly, consistent with previous findings (unpublished), it was shown that the existing neuronal tissue (i.e. CG

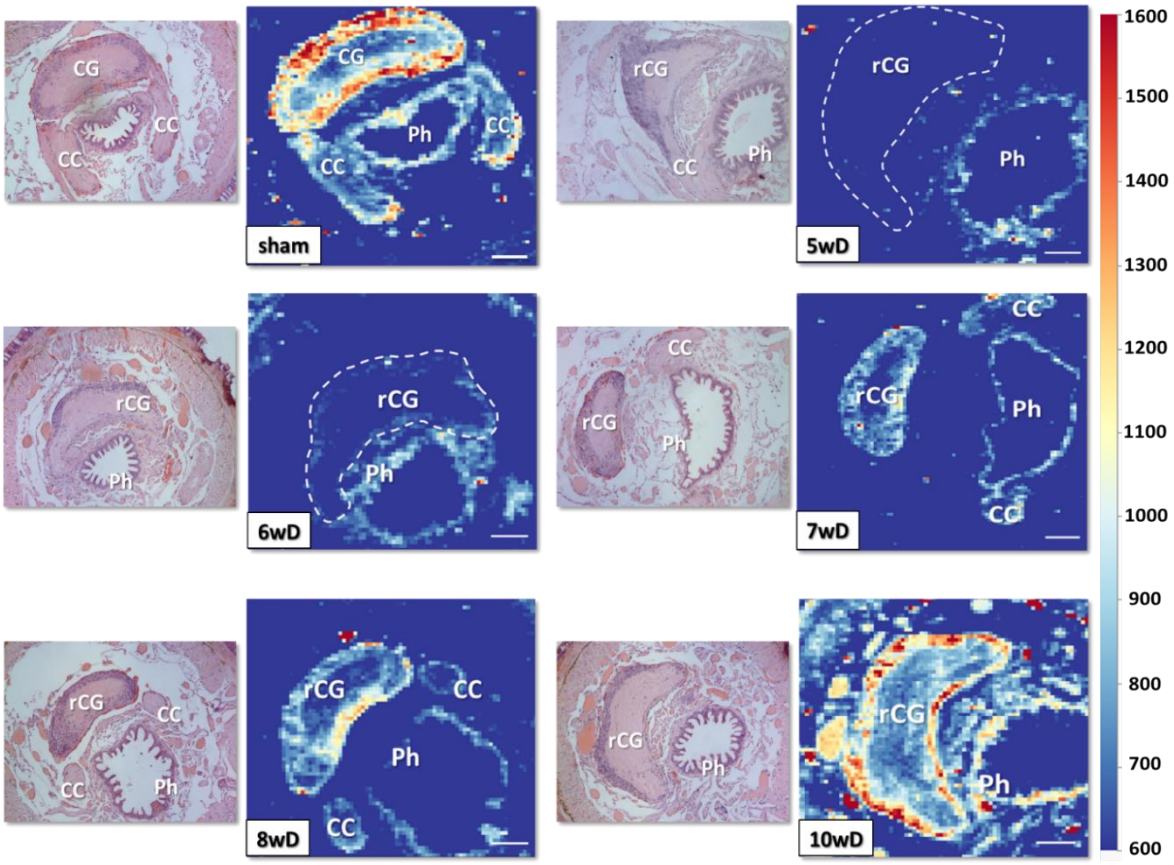

Figure 4.34 XRF heatmaps depicting the distribution of iron in control and regenerating neuronal tissue in *Eisenia fetida*. XRF scans (10µm) were performed on paraffin cross-sections (6µm) of sham operated samples, 5wD, 6wD, 7wD, 8wD and 10wD. The maps demonstrated that iron levels in the rCG from 5wD to 8wD are diminished. At 10wD iron levels appear to return to similar levels as in the control brain. Corresponding H&E images for each map, suggest that iron levels are not directly proportional to the anatomical development of the brain. The incident X-ray beam energy was set to 11keV and the maps were produced in DAWN 2.14.0. Scale bars: 100µm. *CG; Cerebral Ganglion, CC; Circumpharyngeal Connectives, rCG; regenerated Cerebral Ganglion, Ph; Pharynx*

ganglion) can integrate incoming regenerating axons, to replace the excised ganglion (Figure 4.35). Secondly, this work provided additional evidence to support that low iron levels is a characteristic of the regenerated tissue since the regenerated ganglion (rG) and the regenerated circumpharyngeal connective (rCC) exhibited lower iron levels compared to their control counterparts. An image where the intensity range was adjusted is also presented so that the differences in iron levels are more distinct.

To further demonstrate the difference in iron levels, the absolute amount of iron between control and regenerated brains was quantified in PyMca for all the XRF maps produced. Here, for simplicity purposes, representative results for the quantification of iron is presented for the sham, 6wD, 8wD and 10wD XRF maps in Figure 4.36. It is important to remember that the quantification was based on 6µm sections, and it is likely that a different thickness would

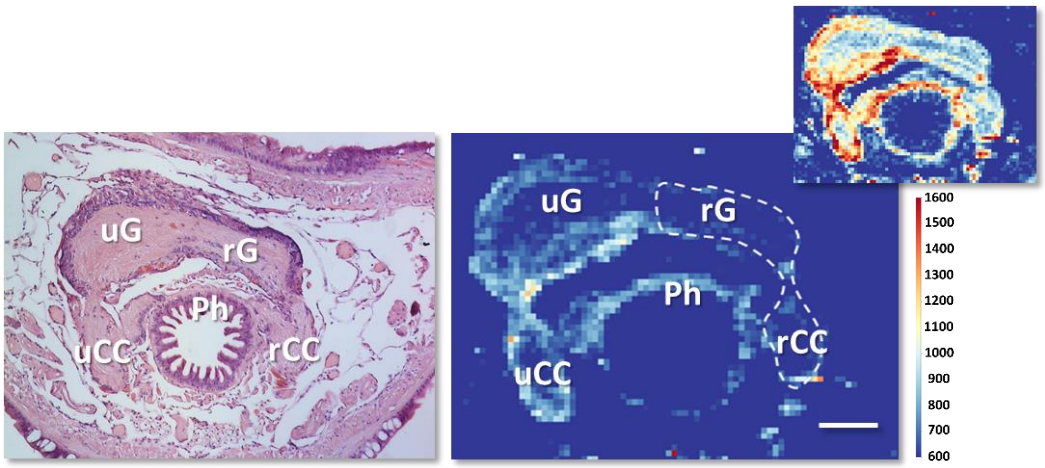

Figure 4.35 XRF heatmap depicting the distribution of iron in the CG following hemiganglioctomy in *Eisenia fetida*. XRF scans (10µm) were performed on paraffin cross-sections (6µm), of samples 5 weeks following hemiganglioctomy. The rG and rCC were characterised by low iron levels when compared to their uncut counterparts. The corresponding H&E image demonstrates that the rG is smaller but equally rich in cellular presence. The incident X-ray beam energy was set to 11keV and the maps were produced in DAWN 2.14.0. Scale bars: 100µm. *uG; uncut Ganglion, uCC; uncut Circumpharyngeal Connectives, rG; regenerated Ganglion, rCC; regenerated Circumpharyngeal Connectives, Ph; Pharynx*

show different results. Iron levels were quantified at the most dorsal side of the CG within the area specified. Analysis of the control CG (Figure 4.36A) demonstrated that the concentration of iron per data point ranged between 250ppm and 650ppm. Also, the average concentration per data point across all the control CG biological replicates tested was 583.1ppm (±88.4 SEM, n=3) (Figure 4.36E). On the contrary, the amount of iron in regenerated brains was significantly decreased compared to the control. In the 6wD rCG depicted here, iron levels were between 170ppm - 230ppm, and a collective average of 224.2ppm per data point (±14.3 SEM, $p<0.01$ vs control CG, n=3) was obtained in all the samples tested, equivalent to a more than two-fold decrease compared to the signal measured in control CG. Next, there was a small increase in iron levels at 8wD rCG, ranging from 230ppm to 400ppm, with an average concentration of 246.1ppm per data point (±11.7 SEM, $p<0.01$ vs control CG, n=3). Moreover, the brain appeared to replenish its iron content at 10wD and returned to levels not dissimilar to those observed pre-operation (300ppm - 600ppm, averaging 389.3ppm ±28.0, n=3). Lastly, all the XRF maps across all the experimental conditions in session 2 were subjected to further analysis in ImageJ, where the whole brain was investigated in terms of iron content (Figure 4.36F). The results were in close agreement with the work conducted in session 1, namely confirming that the signal in control CGs was substantially stronger than in rCGs of 6wD, 7wD, and 8wD. No significant difference was identified at 10wD highlighting the complete restoration of iron levels in the regenerated

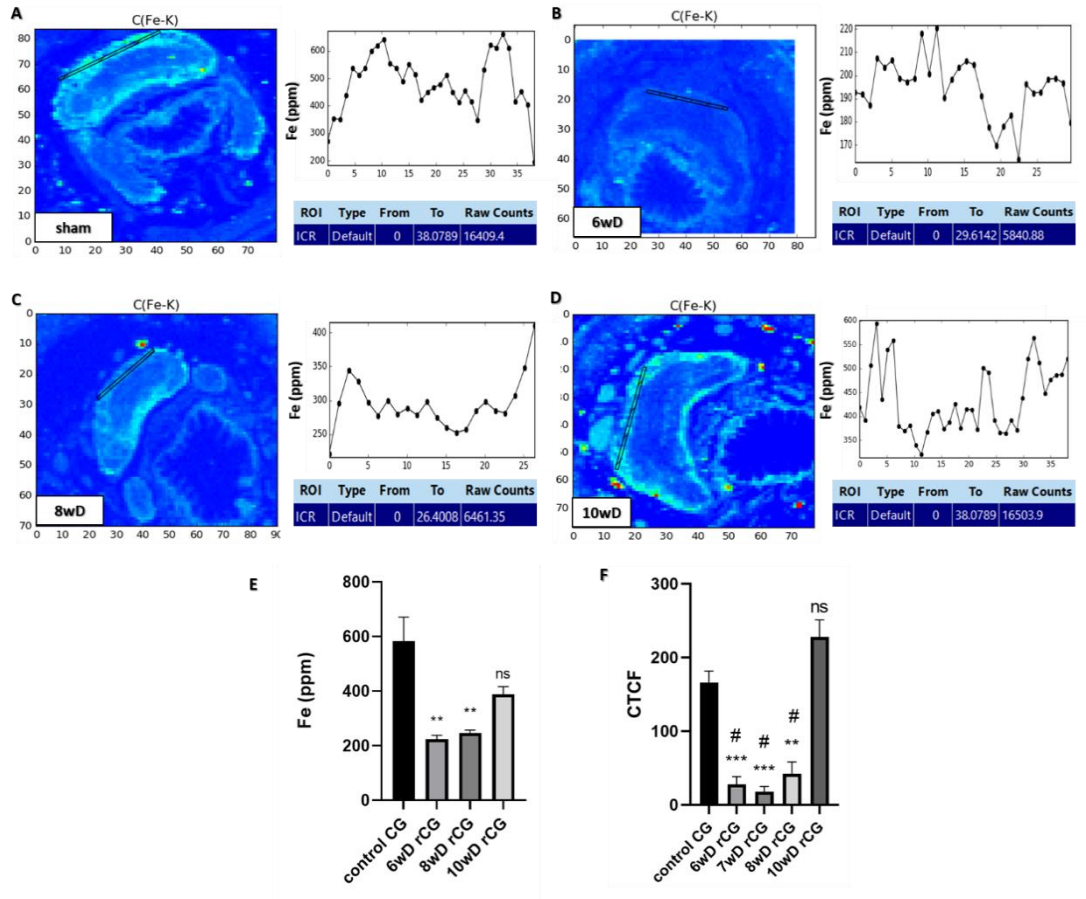

Figure 4.36 Quantification of iron in the most dorsal side of either control or regenerated CG in *Eisenia fetida*, via XRF. A. Iron concentration (ppm) in sham operated worms, per data point within the region of interest (marked by the rectangle), ranged between 250ppm and 650ppm. Weaker iron signal was detected in the rCG, at **(B)** 6wD and **(C)** 8wD, indicative of a lower iron concertation in regenerated tissue. **D.** Iron signal was restored at 10wD, similar to preoperative brain **E.** The collective average of iron concentration across all the biological replicates examined (n=3 per condition), demonstrated that the rCGs in 6wD and 8wD were characterised by a more than 2-fold decrease in iron levels compared to the control CG. There was no significant difference in iron content between control CGs and 10wD rCGs. **F.** ImageJ analysis investigated the iron signal obtained across the entire brain of all the biological replicates examined (n=3 per condition), which revealed that iron signal in regenerated CGs in 6wD and 8wD, were significantly lower than control and 10wD CGs. The incident X-ray beam energy was set to 11keV and the quantification was performed in PyMca. Statistical analysis was carried out via a 2-tailed t-test and error bars represent the SEM (n=3, *** $p < 0.001$, **$p < 0.01$ vs control CG; # $p<0.001$ vs 10wD CG). *CG; Cerebral Ganglion, rCG; regenerated Cerebral Ganglion; CTCF; Corrected Total Cell Fluorescence*

brain. The work carried out thus far showed that the signal in XRF maps offers a reliable representation of iron concentration in the brain and other neuronal tissue.

Moreover, a representative image of a control CG depicts the concentration of the three most abundant metals (Figure 4.37 A: iron, B: calcium, C: zinc), which demonstrated that iron was the most concentrated metal, followed by calcium then zinc. The average concentration per data point across all the control CG biological replicates for iron, calcium and zinc were 583.1ppm (±88.4 SEM, n=3); 341.3ppm (±33.8 SEM, n=3); and 75.0ppm (±4.65 SEM, n=3),

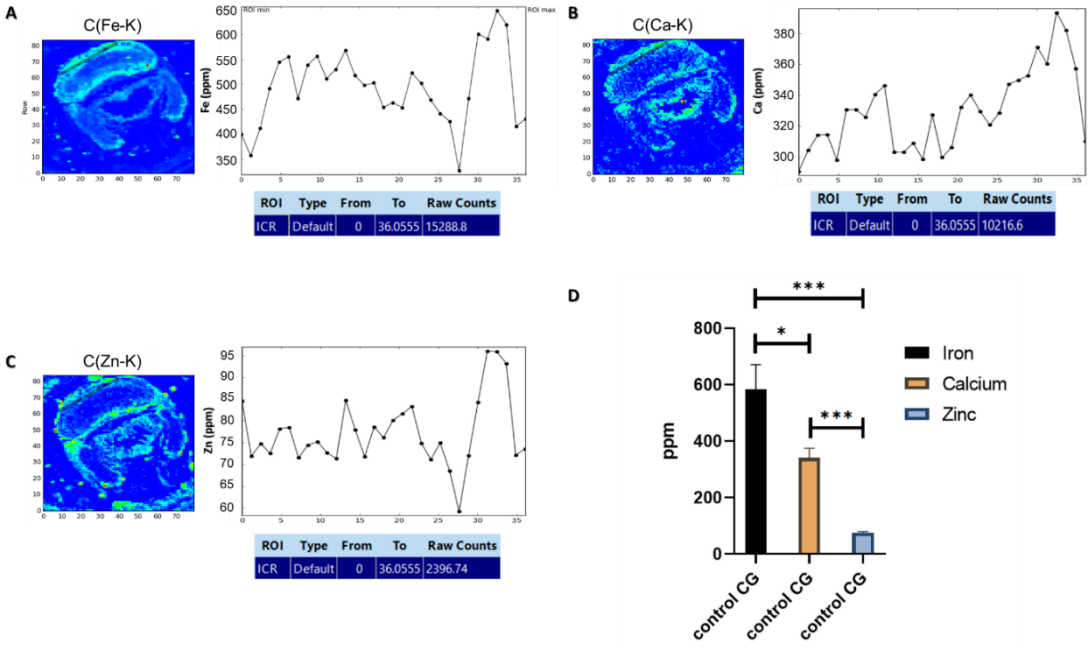

Figure 4.37 Quantification of iron, calcium and zinc in the most dorsal side of control CG in *Eisenia fetida*, via XRF. Of the three metals, **A.** iron was the most concentrated, followed by **B.** calcium then **C.** zinc. A more than 5-fold difference in the concentration range was detected for iron compared to zinc. **D.** The collective average concentration within the region of interest in the control CGs, uncovered a significant difference of iron and calcium compared to zinc ($p<0.001$). Also, the levels of iron were significantly higher than calcium ($p<0.05$). The incident X-ray beam energy was set to 11keV and the quantification was performed in PyMca. Statistical analysis was carried out via a 2-tailed t-test and error bars represent the SEM (n=3, *** $p < 0.001$, *$p < 0.05$). *CG; Cerebral Ganglion, rCG; regenerated Cerebral Ganglion*

respectively (Figure 4.37D). Both iron and calcium were significantly more concentrated than zinc ($p<0.001$), as was the difference between iron and calcium

No significant difference in metal concentration was identified between the ventral and dorsal side of the brain within the same experimental condition. Interestingly, the reduction in iron levels within the regenerated brain does not appear to apply to all metals, since the levels of calcium and zinc across all the regenerated brains tested did not demonstrate any significant decrease, when either the dorsal or the ventral side were measured (Figure 4.38).

Note that the concentration of iron across all the experimental conditions (control CG, 6wD CG, 8wD CG and 10wD CG; Figure 4.36), as well as the concentration of calcium and zinc in the control CG (Figure 4.37) on the dorsal side of the brain, were discussed previously and the reader is advised to refer to the text above. On the dorsal side at 6wD within the region tested, the average concentration of calcium and zinc was 362ppm (±26.8 SEM, n=3) and 73.2ppm (±4.4 SEM, n=3), respectively. At 8wD the average concentration of calcium and zinc was 303.9ppm (±2.6 SEM, n=3) and 70.8ppm (±3.3 SEM, n=3), respectively. Finally, the

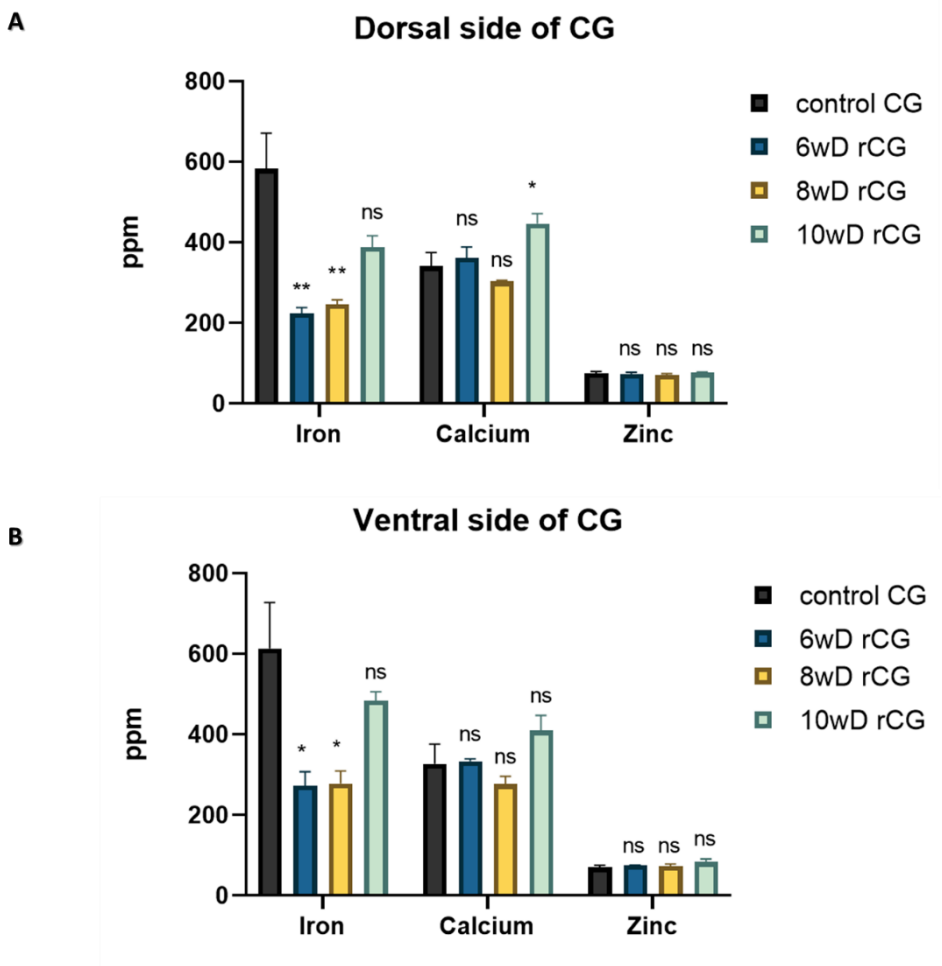

Figure 4.38 Quantification of iron, calcium and zinc in the dorsal and ventral side of control and regenerated CGs in *Eisenia fetida*, via XRF. A. Iron was the only metal which exhibited a significant decrease in concentration within the anterior side of rCGs at 6wD and 8wD ($p<0.01$). No significant difference was observed for calcium or zinc between control and rCGs at any time point. **B.** Iron concentration was also decreased on the ventral side of rCGs compared to control CGs, but not calcium or zinc. The incident X-ray beam energy was set to 11keV and the quantification was performed in PyMca. Statistical analysis was carried out via a 2-tailed t-test. The concentration (ppm) data is presented as the mean ±SEM (n=3, **$p<0.01$, *$p<0.05$). *CG; Cerebral Ganglion, rCG; regenerated Cerebral Ganglion*

levels of calcium and zinc in the regenerated brains at 10wD was 447.3 (±24.2 SEM, $p<0.05$ vs control CG, n=3) and 76.6 (±2.02 SEM, n=3). Equally, on the ventral side the concentration of the metals was similar to that of the dorsal side: in the control CG, within the region tested, the average concentration of iron, calcium and zinc was 613.5ppm (±113.8 SEM, n=3), 326.8ppm (±49.4 SEM, n=3) and 70.3ppm (±4.6 SEM, n=3), respectively. At 6wD the average concentration of iron, calcium and zinc was 273.0ppm (±34.4 SEM, $p<0.05$ vs control CG, n=3), 333.4ppm (±6.2 SEM, n=3) and 75.0ppm (± 0.9 SEM, n=3), respectively. Moreover, the average concentration of iron, calcium and zinc on the ventral side of the brains tested at 8wD, was 278.4ppm (±31.0 SEM, $p<0.05$ vs control CG, n=3), 276.8ppm (±19.5 SEM, n=3) and 73.1ppm (± 5.4 SEM, n=3), respectively. Lastly, as described in Figure 4.36, at 10wD iron

levels were replenished, when the dorsal side of the regenerated brains was evaluated. Likewise, examination of the ventral side yielded similar results in which iron levels, within the region tested, were 484.7ppm (±21.9 SEM, n=3). In addition, as with earlier time points, no changes in calcium and zinc levels were observed, which exhibited a concentration of 410.1ppm (±37.7 SEM, n=3) and 83.2ppm (±7.5 SEM, n=3), respectively.

The finding that calcium and zinc were present at the same levels in both the control CG and rCG but iron was not, can serve as an indication that changes in metal distribution are not universal and should not be perceived as a way to assess the progression of CG regeneration, but rather of a functional importance. It is also worth noting that zinc concentration, even though it is found at lower levels than the other metals overall, is more tightly regulated as suggested by the minor fluctuations in concentration across all the samples tested during regeneration.

The XRF experiments were the first attempt to characterise the time-resolved involvement of metals during cerebral ganglion regeneration and their differential distribution throughout this phenomenon. The findings indicate that both zinc and iron play an active role during this process and they should be studied more closely to understand how they are functionally contributing towards achieving efficient regeneration.

4.4.1. Laser Ablation-Inductively Coupled Plasma-Mass Spectrometry

In light of a recent study, in which the authors observed enhanced tail regeneration following amputation in cadmium-exposed earthworms (Rorat *et al.*, 2017), the accumulation of administered cadmium was evaluated (Figure 4.39) in unharmed neuronal tissue following a 20-day soil exposure (200mg Cd / kg). The XRF work on iron, calcium and zinc in the neuronal tissue of the earthworm, revealed the time-resolved changes in distribution and concentration of the metals that take place during neuronal regeneration. Even though the respective characterisation of cadmium was not feasible via XRF, this was achieved through high-resolution Laser Ablation-Inductively Coupled Plasma-Mass Spectrometry (LA-ICP-MS) on paraffin cross-sections. The experiment was carried out in order to understand whether cadmium can also play a part in neuronal regeneration through its accumulation in the tissue. The isotopes that were selected for this study were ^{111}Cd (one of the most stable isotopes of the metal) and ^{31}P (phosphorus; which was utilised for normalising and referencing purposes). It is important to note that the aim by adopting this approach was not to obtain an absolute quantification measurement for cadmium, but rather characterise the distribution of the metal across the section. In the CG and SOG, phosphorus was localised in

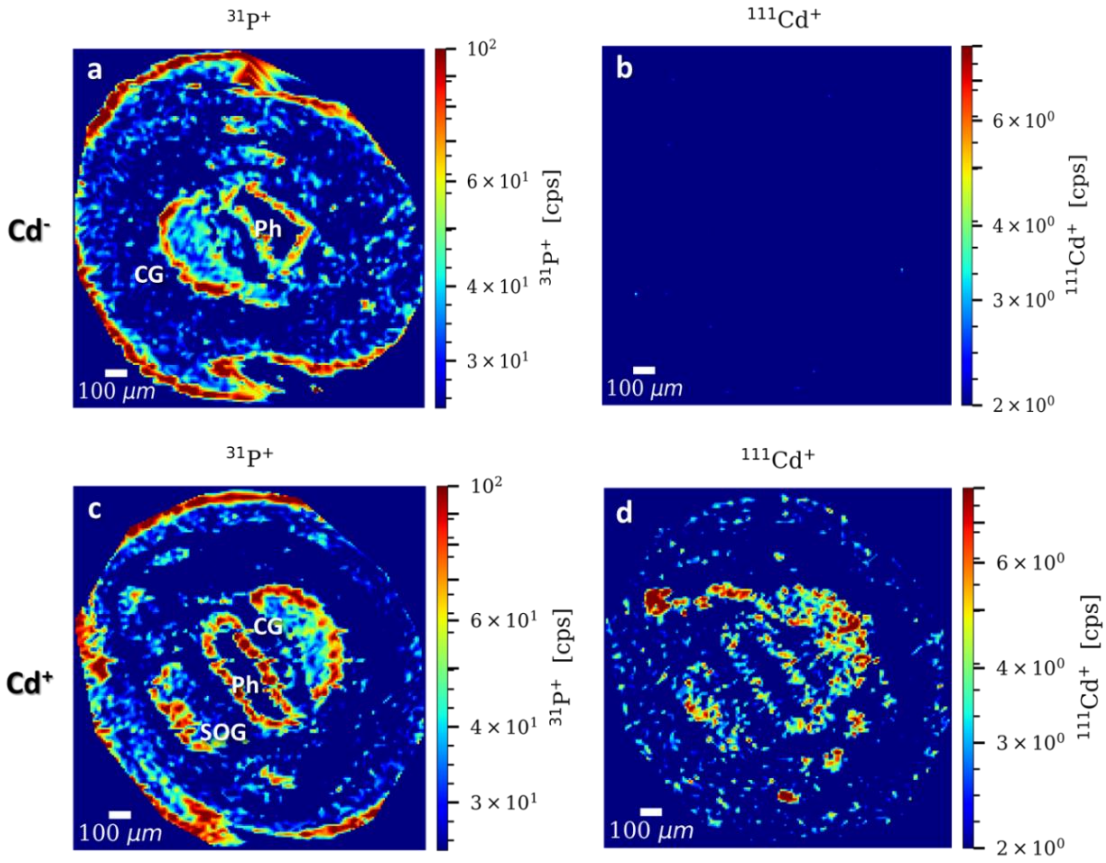

Figure 4.39 LA-ICP MS images of cadmium in unharmed *Eisenia fetida*. The accumulation of cadmium (isotope 111) **(b)(d)** in neuronal tissue, following a 20-day exposure (200mg/kg of soil) was determined via LA-ICP MS. The characterisation of the distribution of phosphorus (isotope 31) **(a)(c)** was utilised for calibration and referencing purposes. Cadmium build-up was observed in both the SOG and CG. Scale bar: 100µm. *CG; Cerebral Ganglion, SOG; Suboesophageal Ganglion, Ph; Pharynx*

the periphery of the tissue (Figure 4.39 a+c), which paralleled the distribution of iron, calcium and zinc observed in the XRF experiments. As a positive control, the gut of cadmium-exposed worms was scanned which demonstrated a widespread accumulation of cadmium across the gut epithelium, as expected, (Data not shown) and served as a reference point of the degree of accumulation in the neuronal tissue. Limited amounts of cadmium were found on the body wall; however, heavy cadmium build-up was detected in both the CG and SOG as well as pharyngeal tissue, in similar levels (Figure 4.39d). Also, cadmium appeared to be universally distributed across the neuronal tissue even in regions of low cell count. No cadmium signal was detected in the negative control (Figure 4.39b), in which the worms were not exposed to the metal.

4.4.2. Benzidine assay for the detection of iron-rich neuroglobin

The results at Diamond revealed that iron levels in the regenerated brain are significantly lower compared to the controls. However, the nature of iron and the proteins it may associate with in the brain remains unclear. The difference in iron can be attributed to several factors: (1) lower total cell number in rCG, even though this can be refuted by the fact that calcium and zinc levels remain the same in regenerated brains, (2) the vasculature innervating the brain has yet to fully form, and thus haemoglobin deficit results in iron deprivation in the area, (3) iron might be inhibitory towards CG development, possibly via ferroptosis, or (4) certain neuroglobin/iron-rich pockets within the brain have yet to differentiate. A benzidine assay was employed to address the latter and detect neuroglobin-rich areas in neuronal tissue (Figure 4.40). A hemiganglioctomy was performed by which only one ganglion was excised and allowed to regenerate as discussed previously. Cryosections of the CG, demonstrated that a benzidine-positive signal co-localised with the cellular and iron distribution, as observed previously, in the uncut Ganglion (uG). In contrast, the rG exhibited low benzidine positivity which agreed with the observations made in the XRF experiments.

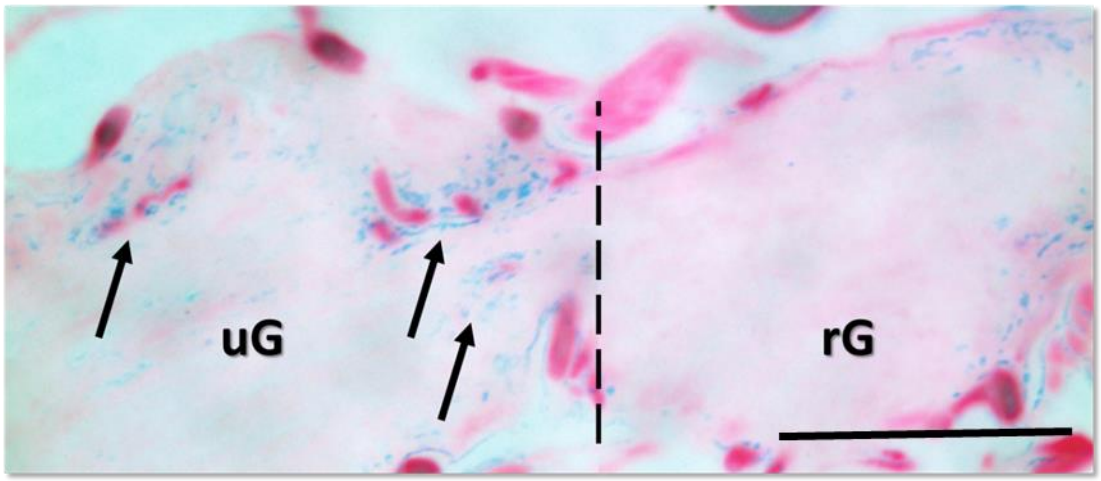

Figure 4.40 Benzidine assay for the detection of neuroglobin in the CG of earthworms. Benzidine positivity is an indication for the presence of iron-rich neuroglobin and was employed to examine the differential distribution of iron in regenerated neuronal tissue. The assay was performed on cryosections in which a stronger and more widespread signal was detected in the uG compared to the rG, 5 weeks following hemiganglioctomy. Dotted line marks the point of where the uG connected to the rG. Scale bars: 100µm. *uG; uncut Ganglion, rG; regenerated Ganglion*

4.4.3. Terminal deoxynucleotidyl transferase dUTP Nick End Labelling (TUNEL) revealed apoptotic activity in both the control and regenerated Cerebral Ganglion (CG)

A characteristic of neuronal systems is the process of apoptosis, or Programmed Cell Death (PCD), which is a prerequisite for healthy and functional development in both vertebrates and invertebrates (Yamaguchi and Miura, 2015). PCD has been described to play an essential role in shaping anatomical structures by eliminating surplus cells, regulating the total cell number within the tissue and filtering out those cells which are damaged and/or defective. The discoveries derived from the RNAseq and X-ray fluorescence spectroscopy revealed that regeneration has not reached completion when a brain, which is morphologically similar to the control, is formed, but rather it continues its development for several weeks thereafter. It is likely, therefore, that the regenerated brain undergoes structural changes throughout this time. To test this, the apoptotic profile of the regenerated brains was assessed via the Terminal deoxynucleotidyl transferase dUTP Nick End Labelling (TUNEL) method. TUNEL utilises the double-stranded DNA breaks that occur naturally during apoptosis and inserts a fluorescently-labelled uracil nucleotide directly onto the 3' terminus of the DNA break. The insertion of the nucleotide allows for the identification of cells which are undergoing PCD.

In the same way as in other experiments, TUNEL was performed on 6µm paraffin wax cross-sections. In agreement with other species (Paveliev *et al.*, 2016), a baseline level of apoptosis is seemingly taking place in the control brains (Figure 4.41a, b, c). All the control CGs tested, either in intact or sham-operated worms, showed minimal apoptotic activity, in which one or two cells per section (marked by the arrows) resulted in TUNEL positivity ($TUNEL^+$). In addition, the dissection protocol itself appears to be highly damaging to the surrounding tissue, as many $TUNEL^+$ cells were identified at the site of the dorsal incision, just 3 hours following the procedure. At 3 weeks however (Figure 4.41d), when the body wall was repaired, no $TUNEL^+$ cells were present at the site of incision. Also, 3wD low levels of apoptosis were observed around the anatomical structure made up by the growing axons, even though the area was characterised by a highly dense population of cells. This was also the case for the circumpharyngeal connectives (CC) in which almost no apoptotic cells were identified (data not shown). On the contrary, the regenerated brain, however, demonstrated stronger apoptotic activity compared to the control brain. At 5wD, cells were shown to undergo PCD at the junction of the CCs and the regenerated CG (rCG) (Figure 4.41e). From that point onwards, all the time points examined, revealed numerous $TUNEL^+$ cells mainly at the periphery of the rCG, towards the dorsal surface.

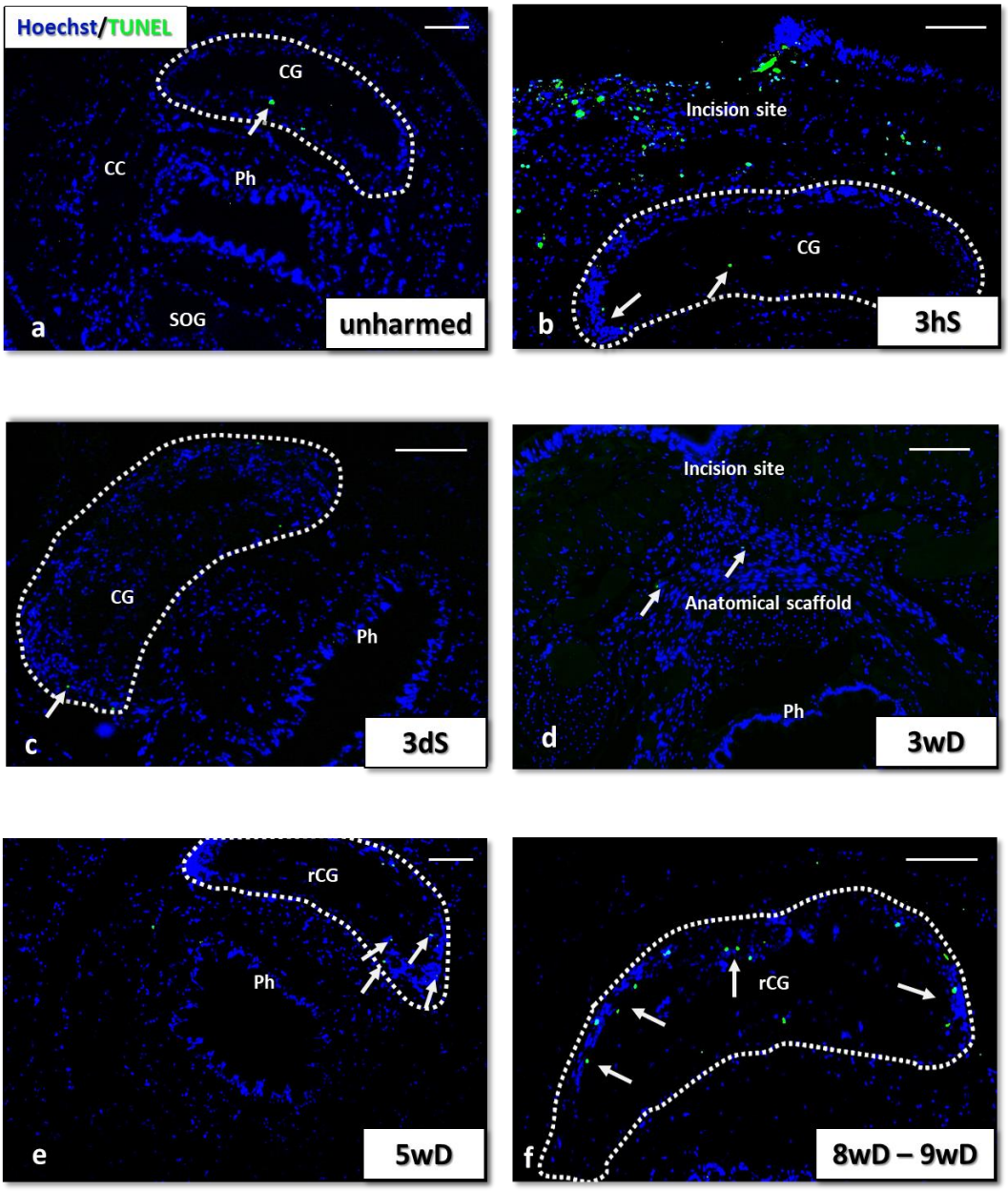

Figure 4.41 Detection of apoptotic cells in CG in *Eisenia fetida*. TUNEL assay was performed on paraffin cross-sections (6µm) of unharmed, sham-operated and decerebrated samples. The CGs were examined by fluorescence microscopy to identify TUNEL$^+$ cells (green). A baseline level of apoptotic cells (marked by arrows) were detected in control brains, in worms which were either **(a)** unharmed or **(b)(c)** had undergone sham surgery. Strong apoptosis characterised the body wall of worms at **(b)** 3 hours following sham surgery (3hS). In regenerated brains **(e) (f)**, TUNEL$^+$ cells were detected in the periphery of the tissue. Hoechst staining marked the cell nuclei (blue). Images were digitally captured using a Nikon Eclipse 2000-S fluorescent microscope and DS-2Mv digital camera. Scale bars: 100µm. *CG; Cerebral Ganglion, rCG, regenerated Cerebral Ganglion, Ph; Pharynx, SOG; Suboesophageal Ganglion*

5. Discussion

The inability of the CNS to spontaneously regenerate and restore function following neuronal trauma results in debilitating conditions in cases of Spinal Cord Injury (SCI), stroke, Parkinson's Disease (PD), Alzheimer's Disease (AD) amongst many others. Understanding the underlying molecular events which drive or repress the process of neuronal regeneration, has been the 'holy grail' of modern neuroscience. Model organisms which possess the ability to regenerate fully any part of their nervous system, provide insights into the complex and multivariate workings of neuronal networks. Here, the earthworm *Eisenia fetida* was employed, which can regenerate its Cerebral Ganglion (CG) - loosely defined as the brain of the worm – within weeks of its surgical removal. The regenerative process was assessed through a range of experimental techniques that covered a multitude of disciplines. The results of this endeavour are discussed below. The multidisciplinary work conducted in this project hopes to set out a framework from which future work can be built on and establish the earthworm as a model organism in developmental neurobiology.

5.1. Addressing the issue of cryptic speciation is of paramount importance in earthworm experiments

At the beginning of this project, the decision was made to work with *E. fetida*, an earthworm species which has been widely exploited as a model organism in toxicological studies, under the Organization for Economic Co-operation and Development (OECD) guidelines. Initial attempts to source the earthworms from commercial suppliers in the UK, that claimed to provide *E. fetida* either in pure or mixed cultures, revealed that the majority of the worms were *Dendrobaena veneta*. A heterogeneous population of *E. fetida* and *D. veneta* is often preferred in compost heaps and as such it is not surprising that it is difficult to obtain a pure *E. fetida* culture. The identity of the species was confirmed through phenotypic characteristics (Figure 4.1), primarily assessing the distance of the paired setae, and molecular barcoding via cytochrome c oxidase subunit 2 (*coII)*. Of the 25 worms tested across five suppliers, only 1 worm proved to be *E. fetida* (Figure 4.2). Due to the phenotypic similarities exhibited between *D. veneta* and *E. fetida*, identification of the species via genotyping provides more reliable and conclusive results. Misidentification of phenotypically similar species can potentially have significant downstream ramifications on experimental design and most importantly on the interpretation of the results.

Different species of earthworms have been demonstrated to exhibit high variance in their responses to toxic substances, as part of the OECD testing. For example, the mortality rate of *E. fetida* and *D. octaedra* challenged with the phosphorothioate insecticide Fenitrothion differ, with *E. fetida* being eight times less sensitive to the compound than *D. octaedra* (Addison and Holmes, 1995). *E.fetida* is also less susceptible to exposures of anaesthetics, glyphosate and the cholinesterase-inhibiting pesticide carbaryl than *Dendrobaena veneta* (Stenersen *et al.*, 1992; Jarmuł-Pietraszczyk and Jastrzębska, 2012). Interestingly, there are also noticeable variations in the speed at which different species of earthworms can regenerate their cerebral ganglion (CG) (Koritsánszky and Hartwig, 1974; Lubics *et al.*, 2002; Molnar *et al.*, 2015). Species-specific variation can, therefore, have a significant impact on the reproducibility of the experimental results, as it can produce unreliable data, especially in cases of cryptic speciation.

The underlying differences in response to toxic compounds and the time course of neuronal regeneration are thought to be attributed to the distinct molecular makeup that defines each earthworm species. For example, the full-length sequence of metallothionein-2 (*mt2*) in *E. fetida*, that was obtained through Rapid Amplification of cDNA Ends (RACE) (Figure 4.27), revealed a characteristic feature in the protein where three cysteines were present in successive order towards the N-terminus. Even though metallothioneins are defined by a large proportion of cysteines (up to 30%), the triple-cysteine feature was only found in 3 other species out of the 10 most similar sequences to *E. fetida*'s MT2 (Figure 4.28). Metallothioneins have been demonstrated to be involved in the protection against Reactive Oxygen Species (ROS) (Sato and Kondoh, 2002) and heavy metals, such as cadmium (Stürzenbaum *et al.*, 2001). Metallothioneins can act as cadmium chelators through the binding of the cysteine residues to the heavy metal, displacing zinc in the process. Recent studies have also highlighted that metallothionein expression is induced in earthworms after exposure to antibiotics (Guo *et al*., 2014) and microplastics (Prendergast-Miller *et al.*, 2019).. At the time of writing, there has not been a study which specifically addresses how different species, possessing the triple cysteine, respond when exposed to environmental stressors. This is beyond the scope of a neuroregeneration project, nevertheless, it will be of value to toxicology studies and as such should be explored further.

5.2. RNAseq revealed higher activity in the late stages of regeneration

Uncovering the molecular events that characterise the process of neuronal regeneration in earthworms was achieved by investigating the transcriptome of the regenerating tissue (Circumpharyngeal Connective (CC), SubOesophageal Ganglion (SOG) and the Ventral Nerve Cord (VNC)) through RNAseq. The affordability of next-generation sequencing in recent years has enabled the study of organisms, at the molecular level, for which limited genetic information exists. Here, a total of 286 million sequence reads were obtained across 9 samples in three experimental conditions, sham-operated worms, 1 week following the removal of the CG (1wD and 5 weeks following the removal of the CG (5wD). The sequence reads were used to construct the *de novo* transcriptome, consisting of 311,261 contig sequences. Differential expression analysis was carried out in DESeq2 which revealed thousands of Differentially Expressed Genes (DEGs) during regeneration (Table 4.2). Transcriptomic analysis revealed a diverse range of RAGs and molecular pathways in early and late time points of CG regeneration. The fact that a larger number of DEGs was detected at sham vs 5wD compared to sham vs 1wD, is an indication of a higher neuroregenerative activity at the later time points of regeneration. This coincides with the period at which the first regenerated structure becomes apparent (Figure 4.3). Also, it worth noting that the high activity observed at 5wD suggests that regeneration is not completed when the regenerated CG (rCG) is formed. This was also supported by XRF experiments and will be discussed in more detail below. In addition, it was surprising to see that from the thousands of DEGs identified, a large proportion of them (almost 50%) had no known orthologs following a BLAST search (Tables 4.2-4.5), pointing towards the presence of, not only earthworm specific genes, but to *E. fetida* specific genes which are predicted to play a crucial role in promoting neuronal regeneration. Other studies have also highlighted species-specific genes in Annelids. Transcriptomic analysis of posterior regeneration in *E. fetida* showed that 315 of almost 10,000 upregulated genes did not exhibit any similarity to a known sequence (Bhambri *et al.*, 2018). Subtractive hybridisation experiments on regeneration in *Enchytraeus japonensis*, isolated 165 sequences which were upregulated of which 86 remained unidentified (Myohara *et al.,* 2006). Furthermore, analysis of expressed sequence tags (ESTs) associated with the anterior regeneration in *Perionyx excavatus,* also discovered novel genes that are differentially expressed in this process (Cho *et al.*, 2009). Considering these investigations, in conjunction with the current study, it is likely that unique genes partake during regeneration and serve a very precise role, which can be one of the most important

differences between Annelids and mammals. Further characterisation of the unknown sequences, either by studying their protein sequences and their domains to predict their function or by assessing their expression profile in different time points during regeneration, was beyond the scope of this project. However, assigning a function to these 'orphan' genes can provide a more comprehensive overview of what makes the earthworms special within a neuroregenerative context, and thus should be explored in more detail in the future.

A small overlap of DEGs was detected between sham vs 1wD and sham vs 5wD, suggestive of the presence of distinct phases of biological events, which are characterised by the expression of a different set of genes. Of the upregulated contigs, only 13 were present in both datasets whereas only 2 were shared between the two downregulated datasets. This agrees with what we know about the multicellular response that defines neuronal tissue following injury (Burda and Sofroniew, 2014). The response elicited by the CNS is characterised by overlapping phases of cell death and inflammation, tissue replacement and tissue remodelling. The small number of overlapping DEGs can be attributed to the degree of progression of regeneration in the time points tested. There is a 4-week difference in the extent at which regenerative processes have progressed between the two datasets (i.e. from 1wD to 5wD). This period is long enough for any overlap observed in both the genes expressed and molecular events taking place, to diminish. The specific Gene Ontology (GO) enrichments that were identified in the two time points are discussed below.

5.3. ECM remodelling plays an essential role during CG regeneration in *Eisenia fetida*

The regenerating tissues examined, showed that a large number of upregulated genes were associated with the reorganisation of the ECM. We now know that efficient and functional neuronal regeneration is a multifaceted phenomenon which is highly dependent on the environment in which the regenerating tissue resides. This was first demonstrated in grafting experiments where CNS neurons were able to regenerate and grow within a PNS extracellular matrix (David and Aguayo, 1981), which provided evidence that the ECM can dictate whether a neuron can regenerate or not. The ECM itself is composed of a range of structural proteins including collagen, laminin and CSPGs, which interact with integrin receptors on neuronal cell membranes and regulate axon pathfinding (Myers *et al.,* 2011). The expression of several different collagen genes was highly induced, mainly at the 5wD time point, highlighting the capacity of regenerating tissue to produce and maintain its own

ECM. In fact, *col21a1* (contig 8628*)* is one of the genes that was upregulated in both 1wD and 5wD (Figure 4.9). The secretion of collagens has been demonstrated to play a principal role during PNS regeneration in mammals, serving as a docking site and a way to guide growing axons (Chernousov *et al.,* 2008). The expression of collagen across the 5-week period suggests that the rebuilding of the ECM is initiated as early as 1 week following the removal of the brain. Even though no ECM related enriched Biological Processes (BPs) were identified at 1wD, there is evidence to suggest that restructuring of the ECM begins at the early stages of regeneration. Changes in anatomical structure and cytoskeletal organisation were predicted based on the upregulated genes at 1wD, whereas the enriched Cellular Components (CCs) obtained from the downregulated genes, revealed an association with the ECM (Figures 4.12 and 4.13), suggesting that the worm undergoes an intense structural and cytoskeletal reorganisation in the early stages of regeneration, in preparation for the subsequent neuronal development. The ECM changes that are likely in place during the early stages of regeneration in the earthworm, agree with the characteristics of the first response phase after neuronal injury in mammals (Burda and Sofroniew, 2014), which include collagen production and ECM formation. The ability of organisms to restore lost body parts appears to be largely reliant on the regulation of their ECM. A recent study on posterior regeneration in *E. fetida* also identified an over-representation of ECM-related genes (Bhambri *et al.,* 2018), whereas limb regeneration in the lizard *Podarcis muralis* was demonstrated to be regulated by the action of ECM proteins (Vitulo *et al.*, 2017).

Moreover, the RNAseq did not only reveal that formation of the ECM is taking place during CG regeneration but most importantly that the regenerating tissue can remodel the ECM through the action of metalloproteases, including ADAMs, MMPs and BMP1, at the later stages of regeneration (i.e. 5wD). The large and insoluble ECM components can be targeted for proteolytic degradation which transforms the ECM into a biologically active environment (Mott and Werb, 2004). In total, the high expression of more than 15 metalloproteases was detected, which suggests that they target a wide range of molecules and they work in unison to promote neuronal regeneration. Furthermore, it is important to highlight that the gene expression profile of the regenerating CCs, SOG and the VNC and not the regenerated CG was assessed via RNAseq. Consequently, the discovery that these metalloproteases are highly expressed, at a period where a regenerated brain has already developed, suggests that the ECM changes are taking place in either or all of the tissues mentioned above. Based on the large number of DEGs identified, we can also speculate that ongoing CG regeneration is largely driven by the biological events that are initiated at the CC and the SOG, even after

the formation of the first regenerated structure. A previous study on CG regeneration in *E. fetida*, investigated the rebuilding of the serotonergic system in the CG (Lubics *et al.,* 2002) and supports the above mentioned hypothesis. The authors labelled serotonergic neurons through a serotonin antiserum and demonstarted that the number of cells in the SOG was lower than in control animals throughout the time period that this was examined (i.e. 70 days post decerebration). The lower cell number provided evidence that undifferentiated cells migrate from the SOG towards the tip of the regenerating CCs and as such structural modifications must take place in order to facilitate this process.

5.4. Regenerative signalling: Reelin-mediated signalling and the non-canonical AP-1$^{cFos/JunB}$ regulate CG regeneration

Transcriptomic analysis of regenerating tissue has uncovered a multitude of molecular events in play, based on the DEGs identified. More than 700 BPs, 100 MFs and 100 CCs were enriched across all the datasets analysed, ranging from ECM reorganisation, neuronal cell dedifferentiation and neurogenesis to metal ion binding and blood vessel formation. Due to time constraints, it was not possible to examine all more comprehensively and describe the genes that are involved in each. Nonetheless, an enriched BP and CC were analysed further, namely the reelin-mediated signalling pathway and the transcription factor AP-1 complex, respectively, since their background gene count, according to the GO database, was relatively low compared to other enrichments (four in reelin-mediated signalling pathway and five for the AP-1 complex), which allowed for a more comprehensive analysis and evaluation of its significance.

Of the four possible components of the reelin pathway, two were shown to be upregulated at 1wD (reelin *(reln*) and apolipoprotein E receptor 2 (*apoer2*)). This observation led to the inspection of the transcriptome to identify the other two, specifically the disabled homolog 2-interacting protein (*dab2ip*) and crk-like protein (*crkl*). All components of the pathway were expressed across all the time points tested (Table 4.6). Surprisingly, *reln, dab2ip,* and *crkl* exhibited a relatively high level of expression, supporting that reelin mediated signalling is, in fact, crucial not only during regeneration, as indicated by the upregulation of *reln* and *apoer2*, but for the normal function of the earthworms CNS as well.

Domain analysis of RELN via BLASTx revealed a similar structural organisation as the mammalian versions, which contain reelin-domain repeats and a central EGF-like domain.

The other three components of the pathway also exhibited strong similarity with their mammalian counterparts, which can be an indication that these proteins have a comparable function in the earthworm as well. This is the first characterisation of these proteins in earthworms, which have been recently described as developmental regulators in neuronal systems. There is evidence to support that they can regulate the development and migration of neurons in the CNS. The expression of *reln*, *apoer2* and *dab1*, were detected in transplanted Neural Stem-Progenitor Cells (NSPCs), that were able to migrate towards the injured motor cortex in mice, which improved their motor function (Arimitsu *et al.*, 2019). This provides evidence to suggest that the environment of the CNS can be accommodating to neuronal growth given the right conditions. In the same study, unlike the earthworm, a moderate amount of *reln* expression was observed in the damaged cortex, when no NSPCs were transplanted.

Furthermore, reelin signalling has been studied PNS regeneration. In *reln* knockout mice, termed reeler mice, axon regeneration was severely impaired (Lorenzetto *et al.*, 2008). In addition, the results obtained here, corroborate previous findings, which provided evidence of induction in the expression of both *reln* and *apoer2* (Pasten *et al.*, 2015). Moreover, the authors showed that reelin can induce cytoskeletal changes and regulate Schwann Cell (SC) migration, through its interaction with APOER2, a process that has been deemed crucial for efficient PNS regeneration (Pasten *et al.*, 2015).

It has already been discussed that cytoskeletal organisation is an enriched BPs in sham vs 4.16) revealed that Microtubule-Associated Protein 1B (MAP1B) was also upregulated, which formed first neighbour connections with both RELN and APOER2, suggesting a functional link amongst these proteins. MAP1B is a neuron-specific protein which associates with microtubules. Reelin has been proposed to initiate a signalling cascade that starts with its binding to APOER2, resulting in the phosphorylation of DAB1P. CRKL associates with DAB1P through which downstream signalling cascades are mediated, including the phosphorylation of MAP1B (González-Billault *et al.*, 2005; Park and Curran, 2008). Post-translational modifications on MAP1B via reelin-signalling pathways have been suggested to play a significant role in neuronal migration. In fact, abrogation of MAP1B activity in mutant mice resulted in neuronal migration deficits. MAP1B phosphorylation induced by reelin was detected in developing mice brains (embryonic and postnatal), highlighting how reelin is required to orchestrate the normal development of the CNS (González-Billault *et al.*, 2005). Co-expression of *map1b* with reelin pathway components in the earthworm, further supports that reelin-mediated signalling is expected to contribute towards regulating cellular

migration of either undifferentiated neurons, glial cells or to help drive neurite extensions, within the regenerating tissue.

The second enrichment of interest that was identified at 1wD was the AP-1 transcription factor (TF) complex. AP-1 is primarily a heterodimer which can be composed of a variety of proteins from the Jun (c-Jun, JunB, JunD) and Fos (c-Fos, FosB, Fra-1, and Fra-2) families (Raivich *et al.,* 2004). In the transcriptome of *E. fetida,* both *junb* and *c-fos* were upregulated at 1wD, signifying that AP-$1^{cFos/JunB}$ TF complex plays a role during the early stages of CG regeneration in earthworms. The different combinations which make up the AP1 transcription factor complex, regulate the expression of genes across a range of biological processes, including cell differentiation, proliferation and apoptosis, and as such it has been studied extensively in oncology, as well as an inducer of neuronal regeneration (Vanňhara and Šmarda, 2006; Fernandes *et al.*, 2013). Early response to neuronal injury has been shown to be elicited by the activity of the AP-1 transcription factor (Herdegen and Leah, 1998). In mice, PNS regeneration depends on the expression of c-Jun (part of the AP-1 heterodimer) for achieving long-distance axonal regeneration, as knocking out neuronal c-Jun results in reduction of regenerative speed and failure of axons to reconnect to their peripheral targets (Ruff *et al.*, 2012). In addition to the neuronal components of the PNS, abrogation of c-Jun in the glial cell population, specifically Schwann cells, has also been shown to hinder axonal regeneration (Arthur-Farraj *et al.*, 2012; Fontana *et al.*, 2012). Genetically modified Schwann cells overexpressing c-Jun displayed enhanced migration and proliferating capabilities while enhancing neurite growth from DRG tissue explants (Huang *et al.*, 2015). Efficient Schwann cell proliferation results in the formation of 'bands of Büngner', which are important in guiding the growing axon. The time at which c-Jun is expressed appears to be of high importance to the regenerating process since it can suppress myelination at high levels (Fazal *et al.*, 2017) resulting in a reversion into a dedifferentiated phenotypic state.

A substantial body of scientific literature has discussed the role of c-Jun as the primary component of AP-1-related neuroregenerative processes. However, the RNAseq revealed that it is JunB and not c-Jun that was upregulated during CG regeneration in the earthworm. The biological effect JunB and c-Jun exert when combined with Fos proteins to form AP-1 can be widely different, even though they belong to the same family. The ability of JunB to activate gene expression is significantly weaker than that of c-Jun, largely due to differences in the amino acid sequence at their DNA-binding domains (Deng and Karin, 1993). The

difference between the two Jun proteins was recently highlighted in a study, where axolotls were utilised to study spinal cord regeneration (Sabin *et al.*, 2019). In agreement with the results presented here, the authors performed spinal cord ablations, which resulted in upregulation of the non-canonical AP-1$^{cFos/JunB}$ in the glial cells of the regenerating tissue. Interestingly, expression of the canonical AP1$^{cFos/c\text{-}Jun}$ was linked to glial scar formation and defective axon regeneration, whereas the expression of the non-canonical AP-1$^{cFos/JunB}$ promoted regeneration, partly by repressing the build-up of a glial scar. Therefore, it can be proposed that as in the axolotl study described above, due to the diverse cell population in the tissues investigated, it is possible that AP-1$^{cFos/JunB}$ was expressed in the glial cells of the regenerating tissue. This notion is supported by preliminary qPCR evidence that showed an induction of *gfap* as early as 3 days post decerebration (data not shown). Despite the induction of *gfap* however, the earthworm appears to be in a position where it can either mitigate or completely abolish any inhibitory effects resulting from a glial scar, or it can prevent one from forming all together. Further studies are needed to address these questions and solidify the position of earthworms, as a model organism in neurobiology.

Lastly, it is important to mention that the induction of AP-1$^{cFos/JunB}$ was detected at 1wD but not at 5wD. This suggests that the regenerative signalling brought about by AP-1 is completed, but only at the CC, SOG and VNC, since the expression profile of the regenerated CG was not investigated. Since we know that regeneration in the CG has not yet fully completed at 5wD, as a large number of DEGs at this point seem to indicate, it is reasonable to assume that AP1-mediated signalling is active elsewhere, most likely in the rCG itself. It has also been suggested that CG regeneration is a phenomenon which does not rely solely on the CCs, SOG and/or the VNC, but rather that it can be driven by migrating neurons from the body wall or pharyngeal plexus (Csoknya *et al.*, 2003a) and as such their role in regenerative signalling should be evaluated further.

5.5. Induction of *gfap,* and presence of CSPGs, suggests that glial cells are advantageous towards achieving complete neuronal regeneration

The current dogma of developmental neurobiology states that one of the main inhibitory barriers which prevent regeneration in the CNS in mammals is the formation of a glial scar. Even though there are studies which have demonstrated how minimal glial scar formation can enhance regenerative capacity of DRG neurons (Davies *et al.,* 1997), there are conflicting studies which have proposed the opposite, predicated on evidence that minimal inflammation and glial scarring does not lead to axon growth (Canty *et al.*, 2013). The authors stated that the glial scar might not be the primary reason why regeneration fails in the CNS. In fact, a recent study went on to suggest that preventing a glial scar from forming, can also reduce the growth of axons (Anderson *et al.*, 2016). Moreover, GFAP and Vimentin (VIM) are cytoskeletal components of glial cells which are upregulated following neuronal injury, in the PNS and CNS, and as such has been often utilised as a marker for their identification (Yang and Wang, 2015). There are several studies which have selectively knocked out either or both of these genes and have observed significant neurite growth and functional recovery following CNS injury (Menet *et al.*, 2003; Brenner, 2014). Here, an induction of *gfap* (Figure 4.20) (and *vim;* data not shown) was also observed following CG extirpation, but it contradicts the premise that *gfap* and *vim* are detrimental to neuronal growth, since the earthworm is defined by its ability to fully regenerate neuronal tissue. The induction of *gfap*, therefore, suggests that glial cells are highly active and proliferate during CG regeneration, which are likely to play a significant role in promoting regeneration. It is probable therefore, that a glial scar does not form and if it does, its composition might be such which protects neurons from further damage, and at the same time allows the growth of axons.

One of the main components of the glial scar are CSPGs which are deposited at the site of injury (McKeon *et al.,* 1999; Jones *et al.,* 2003a; Tang *et al.,* 2003). There is a plethora of studies in mammals that have demonstrated CSPGs are in fact upregulated after spinal cord injury and contribute towards the inhibition of neuronal regeneration (McKeon *et al*., 1995; Gilbert *et al.,* 2005; Wang *et al.,* 2008). However, CSPGs-mediated inhibition can be overcome under the right conditions, which create a permissive environment for specific subsets of neurons (Inman and Steward, 2003). Also, more recently, expression of CSPGs have been linked to neurogenesis in the hippocampus (Yamada *et al.*, 2018) and promote the proliferation of neural stem cells (NSCs) (Purushothaman *et al.*, 2012). Transcriptomic analysis of control and regenerating tissue revealed that both *cspg1* (aggrecan) and *cspg4* (NG2) were moderately expressed consistently across the three time points tested (sham, 1wD and 5wD) even though no differential expression was observed (Table 4.7). Regarding NG2, there is conflicting evidence on its role on axonal growth. Studies on $NG2^{+}$ cells have

highlighted its role in entrapping growing axons, thus contributing to their failure to extend past the glial scar (Filous *et al.,* 2014). Remarkably, however, high levels of NG2 were identified in SCI (i.e. CNS) (and in sciatic nerve) lesions, which was strongly associated with axons growing through implanted grafts demonstrating the NG2, can be growth promoting in the CNS (Jones *et al.*, 2003). Furthermore, the authors also identified a co-localisation with laminin at the lesion sites which supports the notion that axon growth is characterised by a diverse milieu of growth promoting and inhibitory molecular substrates. The IHC work conducted, characterised the distribution of NG2 in both control and regenerated neuronal structures in the earthworm (Figure 4.24). We identified a strong presence of NG2 in the regenerated structure which confirms that growing axons can be associated with high levels of CSPGs, namely NG2, and regenerate highly complex neuronal systems under high precision.

In the light of these results, two closely associated genes to CSPGs were investigated, namely *ptpσ* and *hb-gam*. The inhibitory effects of CSPGs have been strongly associated with the interaction with PTPσ, which initiates a downstream signalling cascade that leads to the dystrophic state of growing axons, a leading cause of regenerative failure. Downregulation of *ptpσ* was observed (Figure 4.20) at the later stages of CG regeneration, which provided evidence to support that, like mammalian systems (Lang *et al.*, 2015; Yao *et al.*, 2019), it exerts an inhibitory role on neuronal regeneration and as such the earthworm has the capacity to minimise its expression and achieve restoration of its CG. It is likely to assume that the downregulation of *ptpσ* lessens the impact of the inhibitory effect, if any, exerted by the CSPGs. Moreover, *hb-gam* was a gene of high interest due to its role in binding to CSPGs preventing their interacting with PTPσ, resulting in axonal growth (Figure 2.1). The expression levels of *hb-gam* across all the experimental conditions examined (i.e. sham, 1wD and 5wD) were remarkably high (Table 4.7). Significantly stronger expression of *hb-gam* was previously seen in the brains of early postnatal rats, compared to embryonic or adults brains (Merenmies and Rauvala, 1990b). Here, the example of *hb*-gam in conjunction with the high baseline expression of resident neoblast markers (Table 4.8), provides strong evidence to suggest that the earthworm has evolved adaptations to enable rapid responses following neuronal damage, thus priming itself for regeneration. The results from this study can be an indication of how the strong presence of *hb-gam* and the downregulation of *ptpσ,* work in unison to offset any negative effects of CSPGs and/or the glial scar.

It is important to appreciate that the phenomenon of neuronal regeneration depends on a multitude of factors. For example, the identification of CSPG expression in both regenerating

and regenerated neuronal tissue can be attributed to the concept of the relative ratios at which growth-promoting and growth-inhibitory factors are co-regulated at any one point during regeneration. The earthworm has likely achieved a fine balance where it can maximise the beneficial and minimise the detrimental effects of the proteins involved, in a game of molecular 'tug-of-war'.

5.6. The ADAMs family of metalloproteases are strongly induced in the first 5 weeks following decerebration and are co-expressed with Notch signalling components

The expression of nine ADAMs or ADAMTS was significantly induced at 5 weeks following the removal of the CG according to the RNAseq data (Table 4.9), however at the time of writing five (*adam8, adam12, adam19, adam28, adamts2)* were also validated via qPCR (Figure 4.21). Little or no expression was detected in RNAseq and qPCR, in sham operated worms. The results showed that there was a strong upregulation throughout the first 5 weeks after the brain had been surgically removed. ADAMs are metalloproteases consisting of domains which enable them to interact with a diverse range of substrates within the ECM, as well as cell membrane receptors (Blobel *et al.*, 1992; Iba *et al.*, 1999; White, 2003). They exert a proteolytic effect upon their targets via the disintegrin domain which is characteristic of all ADAMs. In fact, analysis of the earthworm ADAM sequences revealed that they share remarkable similarities in terms of the domains that are present (Appendix Figure 7.3 and 7.4) and as such their function in the earthworm can be reliably inferred, based on the work carried out on mammalian species. ADAMs have been shown to regulate cell-cell interactions, cell-ECM interactions as well as induce ECM remodelling through selective digestion of ECM components. They can interact with cell membrane receptors of the integrin family, via the disintegrin domain (White, 2003) and also to syndecan proteoglycans and fibronectin in the ECM, through their adhesive domain, or cysteine domain (Gaultier *et al.*, 2002). Integrins are known to be the primary cellular receptors for ECM components, through which the ECM can actively exert a biological effect on cells (Hynes, 2002). The binding of ADAMs to both integrin and ECM components, therefore, has been suggested to be the underlying reason why they can proteolytically cleave integrin-ECM interactions, resulting in ECM remodelling, a pre-requisite for neuronal regeneration. Due to the presence of both the disintegrin and cysteine domains in earthworms' ADAMs (apart from ADAM10

which does not have a cysteine domain), we can deduce that they can also manipulate the ECM in a comparable way. Furthermore, the fact that ADAM expression is induced throughout the first 5 weeks of CG regeneration (at least for the five genes validated) is an indication that ECM remodelling via ADAMs contributes towards neuronal growth in earthworms. Moreover, several other types of metalloproteases were upregulated as indicated by RNAseq, including MMPs and BMP1, which was also validated via qPCR.

In addition to ADAMs' role in remodelling the ECM, studies have uncovered motifs that serve as docking sites for SH3 domain-containing proteins. Similarly, specific amino acids can be targeted for phosphorylation by serine-threonine and/or tyrosine kinases (Seals and Courtneidge, 2003). The phosphorylated residues can then serve as docking sites for SH2-containing proteins. Interestingly, the transcriptome identified such proteins, namely SH3 domain-containing protein (SH3PXD2B), which can bind to ADAMs and was highly upregulated at 5wD. The identification of SH3PXD2B provides evidence that earthworm's ADAMs can also serve as binding sites for the assembly of complexes (Seals and Courtneidge, 2003) having distinct functions that may prove to be essential in neuronal regeneration. ADAMs can also be considered as sheddases, in that they have the capability to proteolytically cleave and shed the ectodomain of transmembrane precursor proteins, such cytokines, membrane-associated growth factors (Blobel, 2005). The cleavage of these domains are of significant biological relevance in a diverse range of pathways (Seals and Courtneidge, 2003; Scharfenberg *et al.*, 2019).

For example, Notch signalling is possibly one of the most well-studied pathways, linked to neurogenesis, in which the notch receptor undergoes ectodomain shedding by ADAM10, in a process known as Regulated Intramembrane Proteolysis (RIP) (Groot and Vooijs, 2012; Ma *et al.*, 2013). Upregulation of both *notch* and *adam10* were identified at the later stages of regeneration via RNAseq. Also, ADAM12 has been shown to be involved in Notch signalling, either indirectly via the proteolytic activation of ADAM10 or directly by shedding the ectodomain of delta-like 1 (DLL1), a ligand for Notch receptor (Dyczynska *et al.*, 2007; Tousseyn *et al.*, 2009), which was also upregulated at the later stages of regeneration according to the RNAseq dataset. In fact, it has also been suggested that ADAM10 activity, might be a rate-limiting step for the initiation of Notch signalling. Morever, ADAM10-Notch signalling has been shown to regulate gliogenesis and neuronal growth in the developing cortex in mice (Ma *et al.,* 2013), that can be linked to the presumed induction of glial cells during regeneration discussed above. The co-expression of Notch components and several members of the ADAM family supports the view that Notch-mediated signalling plays a

significant role in CG regeneration in *E. fetida.* Additionally, there are several lines of evidence to implicate ADAM19 with the ectodomain shedding of NeuReGulin-1 (NRG1), which is one of the main glial cell growth factors implicated in glial cell development (Garratt *et al.*, 2000; Yokozeki *et al.*, 2007). As such, in the PNS, ADAM19 was demonstrated to play a crucial role in the differentiation of Schwann cells and the remyelination of neurons following nerve injury (Wakatsuki *et al.*, 2009). Lastly, studies have also highlighted the importance of another member of ADAMs in neuronal regeneration, namely ADAM8, which is another example of the wide range of substrates these metalloproteases can target and regulate their activity. ADAM8 can shed the ectodomain of the neural cell adhesion molecule Close Homologue of L1 (CHL1), a soluble domain that can promote axon growth (Naus *et al.*, 2004). These findings place ADAMs at the centre stage of neuronal regeneration in earthworms. However, the exact pool of substrates that ADAMs can potentially target in earthworms, remains to be determined.

5.7. Neuronal protection from oxidative stress is essential for CG regeneration

Oxidative stress is often associated from the accumulation of Reactive Oxygen Species (ROS) which can lead to neuronal death, and has been associated with the onset of neuronal diseases (Vaudry *et al.*, 2002; Ying *et al.*, 2002; Serrano and Klann, 2004; Kumar *et al.*, 2012). The CNS is particularly vulnerable to oxidative stress, due to a high demand for oxygen and the presence of high levels of PolyUnsaturated long-chain Fatty Acids (PUFAs), both of which contribute towards the generation of free radicals (Bélanger *et al.*, 2011; Bazinet and Laye, 2014). One of the defences that the CNS can raise against oxidative stress, comes through astrocytes and the expression of free radical scavengers such as Catalase (CAT) and Superoxide Dismutase 1 (SOD1). Here, both *sod-1* and *cat* have been differentially expressed at 1 week following decerebration in RNAseq (Figure 4.18). Moreover, *cat* was shown to be induced as early as 3 days following the removal of the brain and maintained at high levels until the 3rd post-operative week. Histochemical characterisation of catalase in and around regenerating tissue (Figure 4.20), revealed a strong activity, that was primarily associated with the vasculature innervating the tip of the circumpharyngeal connectives and the area surrounding axonal processes which would eventually form the central part of the regenerated CG. The discovery of strong catalase activity at these sites is indicative of the

build-up of ROS, which suggests that the earthworm can regulate and alleviate any negative effects of ROS, particularly at earlier time points of regeneration, which seems to be the time when neuronal components are at their most vulnerable. Interestingly, the neuroprotective ability of catalase has been the subject of translational research, however classical methods to administer catalase to the CNS as a therapeutic is hindered by poor uptake and inefficient delivery systems (Jaffer *et al*., 2011). However, more recently, there have been attempts to overcome these issues, namely through nanoparticle-mediated delivery of catalase, which protected neurons from DNA and mitochondrial damage *in vitro* (Singhal *et al.,* 2013). In addition, the administration of *sod-1* has also been shown to promote the differentiation of Neural Stem Cells (NSCs) and improve functional recovery following traumatic brain injury (TBI) in rats (Jia *et al.*, 2018). The critical role of *sod-1* in healthy neuronal function has been highlighted in studies where mutations induced on SOD-1 resulted in neuronal pathologies, including Amyotrophic Lateral Sclerosis (ALS) (Papadeas *et al*., 2011). It is probable, therefore, that the defence mechanisms that the earthworm employs against oxidative stress utilise both CAT and SOD-1. The capacity of the earthworm to protect its neurons through ROS scavenging, can be a critical differentiator when compared to other species and have the potential to serve as a predictive marker for the degree of success in neuronal regeneration.

The induction of *cat* and *sod-1* coincided with the induction of metallothionein 2 (*mt2)* during the same time period (Figure 4.23). Metallothioneins are cysteine-rich, low molecular weight metal-binding proteins. To the best of our knowledge, this is the first study to identify metallothionein linked to neuronal systems in *E. fetida* and also demonstrate that it is upregulated during neuronal regeneration. As in the case of *cat* and *sod-1, mt2* has been shown be highly expressed by glial cells in the CNS and play a neuroprotective role against ROS (Waller *et al.*, 2018). Recently, upregulation of *mt2* was observed in a SCI rat model (Stephens *et al.*, 2018) and in astrocytes in a mouse model (Anderson *et al.,* 2016), further supporting that glial cells can positively contribute towards neuronal regeneration. Due to the heterogeneity of the tissue sample used for RNAseq, it is possible that *cat, sod-1* and *mt2* are all expressed by glial cells in the earthworm CNS. Metallothioneins appear to promote neurite outgrowth and accelerate wound healing following cortical injury in rats (Chung *et al.*, 2003b) as well as in an *in vitro* setting (Køhler *et al.*, 2003b), which has been suggested to be mediated by the interaction with the megalin receptor (Fitzgerald *et al.*, 2007).

The induction of *mt2*, *cat* and *sod-1* is indicative to a response to oxidative stress. One of the defence mechanisms that earthworm employ to combat the effects of free radicals are

through coelomocytes, immunocompetent cells in earthworms, which can express superoxide dismutase, catalase and metallothionein (Stürzenbaum *et al.*, 2001; Homa *et al.*, 2010; Homa, 2018). It is well established that coelomocytes can migrate to the site of injury and can contribute towards raising an antioxidant immune response, which in the case of neuronal trauma can provide a rapid protection to damaged neurons. Indeed, previous studies in *E. fetida*, have demonstrated that a few days following brain extirpation, coelomocytes flood the area where the brain was previously situated (Csoknya *et al.*, 2003b). It is conceivable, therefore, that the upregulation of *mt2, cat* and *sod-1* is due to the accumulation of these coelomocytes, that can associate with or even integrate into the regenerating neuronal tissue.

In light of the identification of the induction of three established neuroprotective components of neuronal systems, an anti-oxidative stress mechanism is proposed which is initiated at the early stages of regeneration in *E. fetida*, which is regulated by accumulating glial cells, coelomocytes or both in the regenerating tissue and ultimately protects neurons from the further injury.

5.8. Differential distribution of zinc and iron in regenerating neuronal tissue

A diverse range of metals accumulate in neuronal tissues serving a key role as cofactors contributing to the normal physiology. As already discussed, several DEG associated with metals (e.g *adam, mmp, mt2, sod-1)* were identified, resulting in the enrichment of Molecular Functions (MFs) pertaining to metal ion binding, suggesting that metal homeostasis would need to be tightly regulated in order to depend on a high volume of metalloproteins during neuronal regeneration.

MT2, besides playing an important part in providing protection against oxidative stress during neuronal regeneration, it has been demonstrated to contribute towards zinc trafficking and homeostasis serving as a molecular shuttle protein (Maret, 1994). The differential expression of *mt2* during neuronal regeneration in the earthworm, which was highlighted previously (described in 5.7), can also serve as an indication for the change in cellular demand for zinc and other metals during CG regeneration. To investigate this hypothesis, paraffin sections of control and regenerating samples were examined via XRF at DLS. Firstly, it was found that unlike control samples, zinc-rich pockets associated with the

regenerating circumpharyngeal connectives (Figures 4.32 and 4.33) at 1 week following decerebration. This coincided with the upregulation of genes in the ADAMs family (Figure 4.21), zinc-based metalloproteases which are active in remodelling the ECM. The role of zinc in the survival of neurons and regeneration has been somewhat the subject of controversy since it is characterised by a bimodal action. It can indirectly combat the detrimental effects of oxidative stress (Oteiza *et al*., 1990; Verstraeten *et al*., 2004; Mackenzie *et al*., 2006; Bousleiman *et al*., 2017), however at the same time excessive zinc influx at optical nerve injury sites has been shown to contribute significantly in inhibiting neuronal survival and axon regeneration in mice (Li *et al*., 2017). This conflicting paradigm highlights the importance of achieving the desired balance in the amounts of zinc in regenerating tissue, which evidently appears to have been achieved by the earthworm. Nevertheless, previous studies have discussed the importance of zinc in promoting the proliferation and differentiation of stem cells towards adopting a neuronal fate (MacDonald, 2000; Moon *et al.*, 2018). Here, the presence of resident neoblasts have been identified both in control and regenerating tissue (Table 4.8), as well at the tip of the regenerating CCs at 1wD (Figure 4.20C). As such it is pertinent to speculate that zinc influx can influence the development of neoblasts and the growth of axons emanating from the connectives. Furthermore, zinc accumulated in capillaries that developed near the regenerating CCs at 1wD. As discussed previously, ROS scavengers, namely CAT and SOD1, are likely to exhibit neuroprotective effects during this process. It is likely therefore, that the strong zinc presence observed in the capillaries is associated with SOD1 and as such can implicate the vasculature around the neuronal tissue in protecting against oxidative stress. Even though XRF is a powerful tool in the characterisation of the distribution of metals, such as zinc, however it does not inform on the ligand environment of zinc. In other words, whether the signal obtained originates from free zinc or bound to other elements which would indicate the composition and nature of the compound. To further understand the role of zinc therefore, X-ray Absorption Near Edge Structure (XANES) was performed on cryo- and paraffin sections at the DLS, to describe the ligand environment of zinc, however, the analysis of the results is currently ongoing.

Next, iron also exhibited differential distribution during regeneration. The regenerated CGs (rCGs) were examined and revealed significantly lower levels of iron from 4wD until 10wD, at which point the iron levels were restored analogous to that of the control brains (Figures 4.32, 4.34 and 4.35). This was also demonstrated through distribution maps, in addition to absolute quantification of iron at the dorsal and ventral sides of the control and regenerated

brain (Figure 4.37 and 4.38). Even though the underlying reasons for this observation cannot be conclusively determined, different explanations are described below.

A possible, but unconvincing, reason for the large decrease in iron levels can be attributed to the lower number of neuronal cells that form the rCG, which agrees with previous observations made by Csoknya and colleagues, who demonstrated that there is a steady increase in the total number of cells in the rCG, including dopaminergic and serotonergic cells, until the 80th post-operative day (Csoknya *et al*., 2003). Therefore, it is feasible that the decrease in iron is directly linked to the number of cells. However, the above claim can be refuted based on two observations. Firstly, the cell density, as indicated by H&E staining of the same sections that were used in the XRF experiments, (Figure 4.34), demonstrated a similar cell density and distribution in the rCG, as early as 6 weeks post-decerebration, compared to the control CG. Although the cell density appeared to be similar, iron levels were significantly different. The second line of evidence which contests the total cell amount hypothesis, is based on fact that the levels of calcium and zinc measured in the rCG were analogous to those in the control CG. This can be indicative of a comparable cell density, especially since the distribution pattern of the two metals (data not shown) is akin to the control CG and co-localises with the cellular distribution. Despite the fact the total cell density in rCGs is comparable to the control CGs, we wanted to assess whether specific subsets of iron-rich neurons or the vasculature innervating the brain have yet to develop. A benzidine assay was performed which revealed that there was a significant decrease in the accumulation of haemoglobin/neuroglobin in regenerated neuronal tissue (Figure 4.40). This most likely pertains to neuroglobin-containing neuronal components which have not fully developed.

Furthermore, as in the case of zinc, iron has been the subject of controversy regarding its contribution in healthy neuronal function and during neuronal regeneration. There is a plethora of studies which have discussed a positive role for iron and highlight its role in learning and memory (Jorgenson *et al.,* 2003; Jorgenson *et al*., 2005; McEchron *et al*., 2005), as well as synaptic plasticity (Serrano and Klann, 2004; Hidalgo *et al*., 2006; Muñoz *et al*., 2006; Kemmerling *et al.,* 2007). On the contrary, excessive levels of iron have been shown to be highly toxic to neuronal and glial cells alike (Kress *et al*., 2002) and have also been linked to ageing and neurodegenerative disorders (Bartzokis *et* al., 2000; Ropele *et al.*, 2011; Ward *et al.*, 2014; Mollet *et al*., 2016). Due to its strong reactivity, excessive iron can lead to the formation of lipid-derived ROS, which is initiated by the Fenton reaction, resulting in a non-classical mode of cell death, termed ferroptosis (Figure 2.2). The fact that iron levels are

significantly decreased in regenerated neuronal tissue, raises the question whether the earthworm can regulate the levels of iron present, when the tissue is at its most vulnerable in order to prevent ROS build up, and cell death by ferroptosis. In fact, a recent study in *E. fetida* has found that ferritin, an intracellular iron storage protein, is differentially expressed between juvenile and adult worms (Thunders *et al.*, 2017), suggesting that iron is regulated according to the developmental stage of the worm. The rCGs have the capacity to restore iron levels until the 10th post-operative week, and as such it can be proposed that brain regeneration in the earthworm is complete (or near completion), when iron levels are reinstated and not when is either anatomically similar to the control or when it exhibits a similar cell density.

The differential expression of zinc and iron highlighted the importance of metal homeostasis during neuronal regeneration in the earthworm. The exposure of earthworms to cadmium revealed that the neuronal tissue is vulnerable to external factors, since the metal was able to accumulate within the tissue (Figure 4.39) and as such it is probable that neuronal regeneration can be influenced by the environmental concentration of metals. A similar conclusion was drawn from a study where cadmium-exposed earthworms were able to regenerate faster, following posterior amputation, compared to their unexposed counterparts (Rorat *et al*., 2017). The presence of cadmium in neuronal tissue will likely result in the induction of neuroprotective genes, including *mt2, cat* and *sod-1*, that could ultimately prime the neuronal tissue to respond more rapidly in the case of CG decerebration. Additional exposure experiments (including cadmium and other metals), coupled with CG decerebration would provide some evidence as to how the CNS of the earthworm can be conditioned to regenerate neuronal systems even more efficiently.

Lastly, even though it is established that ferroptosis is detrimental to neuronal systems, a different mode of cell death, namely apoptosis, can be beneficial or in fact necessary for the development of neuronal tissue (Yamaguchi and Miura, 2015). Here, a TUNEL assay was utilised to characterise apoptosis in control and regenerated CGs in *E. fetida* (Figure 4.41). Low levels of apoptotic cells were identified in control brains, suggesting that the neuronal tissue in earthworms likely undergoes continuous structural changes, through the re-organisation of its neuronal components via programmed cell death. Moreover, the ongoing development of the rCGs beyond the 4wD-5wD mark (period when the rCG is first visible), was further supported by the fact that a higher number of apoptotic cells was identified at the periphery of the rCGs, even at the later stages of regeneration (i.e. 9wD). Further work

needs to be carried out in order to determine whether at 10wD the apoptotic profile of the brains resembles that of the controls.

5.9. Experimental limitations

As in every experimental endeavour, it is important to discuss some of the limitations that are associated with the work carried out. This is especially true in a model that has not been the subject of intense experimental consideration within the field of neurobiology, and as such is hindered by several restrictive factors, such as a poor understanding at the molecular level as well as limited experimental methodologies specifically designed to address the complexities of earthworm research.

The limitations of this work were highlighted throughout, however some which were deemed the most significant are highlighted here. Firstly, even though great care was taken to ensure all dissections were performed concisely at the designated severing points each time, it is possible that some variation observed can be attributed to minor differences in the points where the severing was performed, or even to small individual biological variation that characterises every worm within the population. Moreover, the RNAseq is a process which can harbour false-positives and negatives, particularly in cases where a *de nono* transcriptome must be constructed and demands for a more challenging bioinformatics analysis. The fact that a substantial amount of sequences were not aligned to the scaffold built, suggests that the RNAseq experiment did not provide us with an exhaustive and complete list of all the DEGs that are involved in regeneration, which inevitably signifies that there is more to the process than what this study has uncovered and that additional genes and pathways are likely to play an important role. In addition, it is of great importance, to re-iterate that the annotations assigned to the contigs were based on sequence similarity and as such their identity and function in the earthworm can only be inferred. Also, it is important to highlight that the induction of genes observed throughout the course of regeneration is limited to the transcript level, which does not necessarily correlate with the translation level, hence does not give a conclusive indication on how gene upregulation affects biological activity.

Next, as already highlighted in previous sections, some of the antibodies that were utilised in IHC (for ADAMx and NG2) were not earthworm-specific and this can raise some uncertainty as to the specificity of the signal produced. Even though the IHC results are not

conclusive and can only serve as an indication of the expression and localisation of the proteins the results provided a great platform from which to carry out more targeted experiments in the future.

Lastly, it is vital to acknowledge that even though there has been a considerable amount of work on earthworms across a range of disciplines, there has not been an agreed consensus amongst the scientific community as to the precise storage conditions and maintenance guidelines that experimental methodologies should adhere to. This fact alone can significantly hinder the progress of earthworm research by introducing variables that might not be accounted for, when carrying out comparisons and assessing experimental results across laboratories in different parts of the world.

5.10. Future work

An important aim for this project was to enrich the arsenal of experimental tools that can be employed to provide insights into the workings of the earthworm's CNS. However, as with any experimental endeavour, the results obtained can lead to more questions that demand to be addressed by expanding that arsenal further. Future work that needs to follow this project is highlighted below, which outlines some of the most realistic experiments that can be performed that can add the highest amount of value.

One of the discoveries made in this project demonstrated that the brain continues to develop and regenerate for several weeks following the emergence of the first regenerated structure. The experimental protocol that was devised for RNAseq, involved the study of regenerating tissue (i.e. CC, SOG and VNC) which provided valuable insights into the molecular events that drive the process. However, this approach does not take into consideration the biological processes that take place within the developing brain, which would undoubtedly provide a more comprehensive level of understanding of CG regeneration. To address this, normal CG and rCGs (from 5 weeks onwards) can be subjected to transcriptomic analysis via RNAseq, in order to characterise the differential expression of genes within the tissue. This will provide valuable evidence on how such a complex structure can be formed in such precision, also uncover differences in cell populations in control and rCGs and assess the implications this might have and finally understand how metal homeostasis is regulated in the brain. Moreover, qPCR experiments on the regenerating tissue beyond 5wD will show when the

CC, SOG and VNC cease to contribute towards the regeneration of the brain, by investigating when DEGs return to baseline levels of expression.

Since the earthworm's transcriptome appears to characterised by species-specific genes, of which several can be crucial to regeneration, future projects can give emphasis to identifying and validating the expression of some of these genes that exhibit the strongest differential expression. Subsequently, the next step would be to build RACE libraries through which the full-length sequences can be derived, enabling a wide-ranging *in silico* evaluation of their individual domains and protein structure, that would eventually allow a probable function to be assigned to the proteins.

One of the most interesting aspects of CG regeneration involves the origin of the axons that build up the neuropil and the brain and most importantly how the extending axons are guided to their destination. Several axon guidance molecules have been identified in the transcriptome of the earthworm that can be utilised to study axon growth and neuronal migration. At the time of writing, *in situ* hybridisation probes, complementary to axon guidance sequences, have been designed and will be employed to identify how axons communicate in the worm, as well as uncover the role of the surrounding tissues (e.g. pharynx) in axon guidance.

The present study focused on transcriptomic analysis and the identification of DEGs, and as such little emphasis was given to characterise the regenerative process at the protein level. For instance, several metalloproteases are upregulated during regeneration, which have been linked to ECM remodelling. Even though their function can be reliably inferred through domain characterisation, conclusive evidence on how they regulate neuronal regeneration can be obtained through protein studies. Moreover, since the RNAseq identifies differentially expressed transcripts it gives little information on how this can impact biological phenomena. A way to address the above limitations would be to carry out assays which utilise protein samples, such as Western Blots and zymography assays. Interestingly, a zymography assay would reveal whether the upregulation of metalloproteases observed at the transcript level, also translates to enhanced biological activity by assessing the degree of proteolytic digestion.

Lastly, one of the disadvantages of working with this model, at the time of writing, is the difficulty in genetically manipulating the earthworm, and as such it is challenging to draw conclusions on the importance of some of the genes that have been identified as differentially expressed. In order to understand the complex workings of neuronal system of

earthworms, we first need to dismantle it into its individual components. To do this, primary neuronal cells should be isolated from neuronal tissue and cultured. This would allow the exploitation of a myriad experimental techniques that require cultured cells, in order to appreciate the intrinsic capacity of earthworm neuronal cells to regenerate *in vitro*.

5.11. Conclusions

The earthworm possesses a remarkable capacity for neuronal regeneration, which is poorly understood. This study aimed to provide an experimentally diverse account of different aspects of neuronal regeneration, in order to highlight the utility of earthworms as potential model organisms in developmental neurobiology. Several Regeneration Associated Genes (RAGs) were identified, some of which have never been associated with regeneration before. The annotation of these RAGs enabled the construction of a comprehensive landscape of molecular events that characterise the process, revolving around the re-organisation of the ECM (through the activity of metalloproteases, e.g. ADAMs), regenerative pathways (e.g. reelin and AP-$1^{cFos/JunB}$) and the action of neuroprotective components (e.g. MT2, CAT, SOD1). Furthermore, the upregulation of *gfap* and the downregulation of *ptpσ*, in conjunction with the high expression of *hb*-gam, cspg-*1* and *cspg-4* suggest that the earthworm's CNS is able to regulate neuronal components, some of which have been widely perceived as inhibitory to regeneration, in such a way to form a permissive environment where neuronal growth can thrive. Lastly, the importance of metal homeostasis and the concept of balance has been a theme throughout this project. The differential distribution of zinc and iron, around regenerating and regenerated neuronal tissue respectively, revealed the intricate changes that must take place in order to achieve complete and functional neuronal regeneration. While the earthworm is suggested to express several species-specific transcripts, interestingly, certain pathways and genes seen in other invertebrates, as well as mammals, are also conserved in the regenerative processes in earthworms. This work provides evidence that earthworm's findings within a neurodevelopmental framework, can be utilised to formulate hypothesis in other species beyond its own phylum. The discoveries made here are a testament of how earthworm research can be relevant, not only within the confines of Annelids and invertebrates, but can have a significant impact on the understanding of the workings of neuronal systems in mammals.

The work conducted as part of this project aimed to showcase the breadth of experimental techniques that can be applied towards investigating neuroregenerative processes in the

earthworm. Both molecular and biophysical experimental tools were employed to provide a multidisciplinary characterisation of neuroregeneration, which have demonstrated that the process is driven by a diverse range of biological pathways and events. The large dataset of transcripts associated with the neuronal system of earthworms that have been identified here, have addressed one of the most significant hindrances in earthworm research, which has been, historically, the limited amount of genomic information available. Armed with this knowledge, we have now reached a stage where further, more targeted, studies can be conducted into genes/proteins of interest, that will mark the first step towards characterising their functional significance. Furthermore, my work on XRF, the first of its kind to characterise metal distribution in neuronal tissue in earthworms, aims to establish a platform through which one can track the progression of CG regeneration. This method allows for a more reliable and precise approach of determining when the CG has fully developed, while avoiding the pitfalls associated with relying solely on structural cues to do so.

6. Bibliography

Addison, J. A. & Holmes, S. B. Comparison of forest soil microcosm and acute toxicity studies for determining effects of fenitrothion on earthworms. *Ecotoxicol. Environ. Saf.* **30**, 127–133 (1995).

Agata, K., Saito, Y. & Nakajima, E. Unifying principles of regeneration I: Epimorphosis versus morphallaxis. *Dev. Growth Differ.* **49**, 73–78 (2007).

Albani, J., Demuynck, S., Grumiaux, F. & Leprêtre, A. Fluorescence fingerprints of *Eisenia fetida* and *Eisenia andrei*. *Photochemistry and Photobiology* **78**, 599 (2003).

Alfandari, D. & Taneyhill, L. A. Cut loose and run: The complex role of ADAM proteases during neural crest cell development. *Genesis* **56**, (2018).

Alfandari, D. *et al.* Xenopus ADAM 13 is a metalloprotease required for cranial neural crest-cell migration. *Curr. Biol.* **11**, 918–930 (2001).

Ambron, R. T. & Walters, E. T. Priming events and retrograde injury signals. *Mol. Neurobiol.* **13**, 61–79 (1996).

Anderson, M. A. *et al.* Astrocyte scar formation AIDS central nervous system axon regeneration. *Nature* **532**, 195–200 (2016).

Angeli, J. P. F., Shah, R., Pratt, D. A. & Conrad, M. Ferroptosis Inhibition: mechanisms and opportunities. *Trends Pharmacol. Sci.* **38**, 489–498 (2017).

Araque, A., Parpura, V., Sanzgiri, R. P. & Haydon, P. G. Tripartite synapses: Glia, the unacknowledged partner. *Trends in Neurosciences* **22**, 208–215 (1999).

Arimitsu, N. *et al.* Roles of Reelin/Disabled1 pathway on functional recovery of hemiplegic mice after neural cell transplantation; Reelin promotes migration toward motor cortex and maturation to motoneurons of neural grafts. *Exp. Neurol.* **320**, (2019).

Aros, B., Vigh, B. Regeneration of the neurosecretory system of the cerebral ganglion in the earthworm (*Lumbricus terrestris*), *Acta Biol. Acad. Sci. Hung*. **13**, 323-337 (1962).

Arthur-Farraj, P. J. *et al.* c-Jun reprograms schwann cells of injured nerves to generate a repair cell essential for regeneration. *Neuron* **75**, 633–647 (2012).

Ashraf, A., Clark, M. & So, P.-W. The aging of iron man. *Front. Aging Neurosci.* **10**, 65 (2018).

Assaf, S. Y. & Chung, S. H. Release of endogenous Zn2+ from brain tissue during activity. *Nature* **308**, 734–736 (1984).

Attwell, D. *et al.* Glial and neuronal control of brain blood flow. *Nature* **468**, 232–43 (2010).

Azevedo, F. A. C. *et al.* Equal numbers of neuronal and nonneuronal cells make the human brain an isometrically scaled-up primate brain. *J. Comp. Neurol.* **513**, 532–541 (2009).

Badaracco, M. E., Ortiz, E. H., Soto, E. F., Connor, J. & Pasquini, J. M. Effect of transferrin on hypomyelination induced by iron deficiency. *J. Neurosci. Res.* **86**, 2663–2673 (2008).

Balcioglu, Y. H., Kirlioglu, S. S. & Ozgen, G. Bipolar disorder with marfan syndrome: A case illustration based on possible involvement of TGF-β1 in the common etiopathogenesis: Possible neurobiological underpinnings of co-occurrent bipolar disorder and marfan syndrome. *Psychiatry Clin. Psychopharmacol.* **27**, 403–405 (2017).

Bandtlow, C. E. & Zimmermann, D. R. Proteoglycans in the developing brain: new conceptual insights for old proteins. *Physiol. Rev.* **80**, 1267–90 (2000).

Bandtlow, C., Zachleder, T. & Schwab, M. Oligodendrocytes arrest neurite growth by contact inhibition. *J. Neurosci.* **10**, 3837–3848 (1990).

Barrett, C. P., Guth, L., Donati, E. J. & Krikorian, J. G. Astroglial reaction in the gray matter of lumbar segments after midthoracic transection of the adult rat spinal cord. *Exp. Neurol.* **73**, 365–377 (1981).

Barros, C. S., Franco, S. J. & Müller, U. Extracellular Matrix: Functions in the nervous system. *Cold Spring Harb. Perspect. Biol.* **3**, 1–24 (2011).

Bartzokis, G. *et al.* In vivo evaluation of brain iron in Alzheimer disease using magnetic resonance imaging. *Arch. Gen. Psychiatry* **57**, 47–53 (2000).

Bartzokis, G. *et al.* Myelin breakdown and iron changes in Huntington's disease: Pathogenesis and treatment implications. *Neurochem. Res.* **32**, 1655–1664 (2007).

Bartzokis, G. Schizophrenia: Breakdown in the well-regulated lifelong process of brain development and maturation. *Neuropsychopharmacology* **27**, 672–683 (2002).

Bates, C. A. & Meyer, R. L. The neurite-promoting effect of laminin is mediated by different mechanisms in embryonic and adult regenerating mouse optic axons in vitro. *Dev. Biol.* **181**, 91–101 (1997).

Bélanger, M., Allaman, I. & Magistretti, P. J. Brain energy metabolism: Focus on Astrocyte-neuron metabolic cooperation. *Cell Metab.* **14**, 724–738 (2011).

Bely, A. E. & Nyberg, K. G. Evolution of animal regeneration: re-emergence of a field. *Trends Ecol. Evol.* **25**, 161–170 (2010).

Bely, A. E. Distribution of segment regeneration ability in the Annelida. *Integr. Comp. Biol.* **46**, 508–518 (2006).

Benjamini, Y. & Hochberg, Y. Controlling the false discovery rate: a practical and powerful approach to multiple testing. *J R Statist Soc B.* **57,** 289–300 (1995).

Ben-Ari, Y., Cherubini, E., Corradetti, R. & Gaiarsa, J. L. Giant synaptic potentials in immature rat CA3 hippocampal neurones. *J. Physiol.* **416**, 303–25 (1989).

Ben-Ari, Y., Khazipov, R., Leinekugel, X., Caillard, O. & Gaiarsa, J. L. GABA(A), NMDA and AMPA receptors: A developmentally regulated 'menage a trois'. *Trends Neurosci.* **20**, 523–529 (1997).

Berg, J. M. Zinc fingers and other metal-binding domains. Elements for interactions between macromolecules. *J. Biol. Chem.* **265**, 6513–6 (1990).

Bergers, G. *et al.* Matrix metalloproteinase-9 triggers the angiogenic switch during carcinogenesis. *Nat. Cell Biol.* **2**, 737–744 (2000).

Berry, M. *et al.* Deposition of Scar Tissue in the Central Nervous System. in 31–53 (Springer, Vienna, 1983). doi:10.1007/978-3-7091-4147-2_3

Bezzi, P. *et al.* Prostaglandins stimulate calcium-dependent glutamate release in astrocytes. *Nature* **391**, 281–285 (1998).

Bhambri, A. *et al.* Large scale changes in the transcriptome of *Eisenia fetida* during regeneration. *PLoS One* **13**, e0204234 (2018).

Bignami, A. & Dahl, D. The astroglial response to stabbing. Immunofluorescence studies with antibodies to astrocyte specific protein (GFA) in mammalian and submammalian vertebrates. *Neuropathol. Appl. Neurobiol.* **2**, 99–110 (1976).

Blobel, C. P. ADAMs: key components in EGFR signalling and development. *Nat. Rev. Mol. Cell Biol.* **6**, 32–43 (2005).

Blobel, C. P. *et al.* A potential fusion peptide and an integrin ligand domain in a protein active in sperm-egg fusion. *Nature* **356**, 248–252 (1992).

Bousleiman, J. *et al.* Function of metallothionein-3 in neuronal cells: Do metal ions alter expression levels of MT3? *Int. J. Mol. Sci.* **18**, 1133 (2017).

Bradbury, E. J. *et al.* Chondroitinase ABC promotes functional recovery after spinal cord injury. *Nature* (2002). doi:10.1038/416636a

Bradke, F., Fawcett, J. W. & Spira, M. E. Assembly of a new growth cone after axotomy: The precursor to axon regeneration. *Nat. Rev. Neurosci.* **13**, 183–193 (2012).

Bray, T. M. & Bettger, W. J. The physiological role of zinc as an antioxidant. *Free Radic. Biol. Med.* **8**, 281–291 (1990).

Brenner, M. Role of GFAP in CNS injuries. *Neurosci. Lett.* **565**, 7–13 (2014).

Brini, M., Calì, T., Ottolini, D. & Carafoli, E. Neuronal calcium signaling: Function and dysfunction. *Cell. Mol. Life Sci.* **71**, 2787–2814 (2014).

Bundy, J.G., *et al.* Earthworm species of the genus *Eisenia* can be phenotypically differentiated by metabolic profiling, *FEBS Lett.*, **521**, 115-120 (2002).

Burda, J. E. & Sofroniew, M. V. Reactive gliosis and the multicellular response to CNS damage and disease. *Neuron* **81**, 229–248 (2014).

Bush, T. G. *et al. Leukocyte Infiltration, Neuronal Degeneration, and Neurite Outgrowth after Ablation of Scar-Forming, Reactive Astrocytes in Adult Transgenic Mice provision of metabolic substrates for neurons, and inter-actions with endothelia to create and maintain the b*. *Neuron* **23**, (1999).

Cajal S. Degeneration and regeneration of the nervous system. Oxford, England: Clarendon Press (1928).

Cajal, S. R. y. *Degeneration & regeneration of the nervous system*. Oxford University Press, Humphrey Milford (1928).

Calof, A. L. & Reichardt, L. F. Response of purified chick motoneurons to myotube conditioned medium: Laminin is essential for the substratum-binding, neurite outgrowth-promoting activity. *Neurosci. Lett.* **59**, 183–189 (1985).

Canty, A. J. *et al.* In-vivo single neuron axotomy triggers axon regeneration to restore synaptic density in specific cortical circuits. *Nat. Commun.* **4**, 2038 (2013).

Carbonetto, S. Facilitatory and inhibitory effects of glial cells and extracellular matrix in axonal regeneration. *Curr. Opin. Neurobiol.* **1**, 407–413 (1991).

Cardoso, B. R., Hare, D. J., Bush, A. I. & Roberts, B. R. Glutathione peroxidase 4: A new player in neurodegeneration? *Mol. Psychiatry* **22**, 328–335 (2017).

Carlstedt, T., Dalsgaard, C. J. & Molander, C. Regrowth of lesioned dorsal root nerve fibers into the spinal cord of neonatal rats. *Neurosci. Lett.* **74**, 14–18 (1987).

Case, L. C. & Tessier-Lavigne, M. Regeneration of the adult central nervous system. *Curr. Biol.* **15**, R749–R753 (2005).

Chao, M. V., Rajagopal, R. & Lee, F. S. Neurotrophin signalling in health and disease. *Clin. Sci.* **110**, 167–173 (2006).

Chen, L. Microtubules and axon regeneration in *C. elegans*. *Mol. Cell. Neurosci.* **91**, 160–166 (2018).

Chen, L., Hambright, W. S., Na, R. & Ran, Q. Ablation of the ferroptosis inhibitor glutathione peroxidase 4 in neurons results in rapid motor neuron degeneration and paralysis. *J. Biol. Chem.* **290**, 28097–28106 (2015).

Chernousov, M. A., Yu, W. M., Chen, Z. L., Carey, D. J. & Strickland, S. Regulation of schwann cell function by the extracellular matrix. *Glia* **56**, 1498–1507 (2008).

Cherubini, E., Gaiarsa, J. L. & Ben-Ari, Y. GABA: an excitatory transmitter in early postnatal life. *Trends Neurosci.* **14**, 515–519 (1991).

Chierzi, S., Ratto, G. M., Verma, P. & Fawcett, J. W. The ability of axons to regenerate their growth cones depends on axonal type and age, and is regulated by calcium, cAMP and ERK. *Eur. J. Neurosci.* **21**, 2051–2062 (2005).

Chilton, J. K. Molecular mechanisms of axon guidance. *Dev. Biol.* **292**, 13–24 (2006).

Chintala, S. K., Zhang, X., Austin, J. S. & Fini, M. E. Deficiency in matrix metalloproteinase gelatinase B (MMP-9) protects against retinal ganglion cell death after optic nerve ligation. *J. Biol. Chem.* **277**, 47461–47468 (2002).

Chiquet-Ehrismann, R. & Tucker, R. P. Tenascins and the importance of adhesion modulation. *Cold Spring Harb. Perspect. Biol.* **3**, 1–19 (2011).

Cho, S. J. *et al.* Gene expression profile in the anterior regeneration of the earthworm using expressed sequence tags. *Biosci. Biotechnol. Biochem.* **73**, 29–34 (2009).

Cho, Y. & Cavalli, V. HDAC5 is a novel injury-regulated tubulin deacetylase controlling axon regeneration. *EMBO J.* **31**, 3063–3078 (2012).

Cho, Y., Sloutsky, R., Naegle, K. M. & Cavalli, V. Injury-Induced HDAC5 nuclear export is essential for axon regeneration. *Cell* **155**, 894 (2013).

Cholewa, J. *et al.* Folia histochemica et cytobiologica. *Folia Histochem. Cytobiol.* **44**, 65–71 (2006).

Chung, R. S. *et al.* Neuron-glia communication: metallothionein expression is specifically up-regulated by astrocytes in response to neuronal injury. *J. Neurochem.* **88**, 454–461 (2004).

Chung, R. S. *et al.* Redefining the role of metallothionein within the injured brain: Extracellular metallothioneins play an important role in the astrocyte-neuron response to injury. *J. Biol. Chem.* **283**, 15349–15358 (2008).

Chung, R. S., Vickers, J. C., Chuah, M. I. & West, A. K. Metallothionein-IIA promotes initial neurite elongation and postinjury reactive neurite growth and facilitates healing after focal cortical brain injury. *J. Neurosci.* **23**, 3336–42 (2003).

Chung, R. S., Vickers, J. C., Chuah, M. I. & West, A. K. Metallothionein-IIA promotes initial neurite

elongation and postinjury reactive neurite growth and facilitates healing after focal cortical brain injury. *J. Neurosci.* **23**, 3336–42 (2003).

Chung, W. S., Allen, N. J. & Eroglu, C. Astrocytes control synapse formation, function, and elimination. *Cold Spring Harb. Perspect. Biol.* **7**, (2015).

Clegg, M. S., Hanna, L. A., Niles, B. J., Momma, T. Y. & Keen, C. L. Zinc deficiency-induced cell death. *IUBMB Life* **57**, 661–669 (2005).

Cohen, J. & Johnson, A. R. Differential effects of laminin and merosin on neurite outgrowth by developing retinal ganglion cells. *J. Cell Sci.* **1991**, 1–7 (1991).

Colvin, R. A., Davis, N., Nipper, R. W. & Carter, P. A. Zinc transport in the brain: routes of zinc influx and efflux in neurons. *J. Nutr.* **130**, 1484S-1487S (2000).

Connor, J. R., Menzies, S. L., Martin, S. M. S. & Mufson, E. J. Cellular distribution of transferrin, ferritin, and iron in normal and aged human brains. *J. Neurosci. Res.* **27**, 595–611 (1990).

Connor, J. R., Snyder, B. S., Arosio, P., Loeffler, D. A. & LeWitt, P. A quantitative analysis of isoferritins in select regions of aged, Parkinsonian, and Alzheimer's diseased brains. *J. Neurochem.* **65**, 717–724 (1995).

Connor, J. R., Snyder, B. S., Beard, J. L., Fine, R. E. & Mufson, E. J. Regional distribution of iron and iron-regulatory proteins in the brain in aging and Alzheimer's disease. *J. Neurosci. Res.* **31**, 327–335 (1992).

Corona, C. *et al.* Dietary zinc supplementation of 3xTg-AD mice increases BDNF levels and prevents cognitive deficits as well as mitochondrial dysfunction. *Cell Death Dis.* **1**, e91 (2010).

Corvetti, L., Rossi, F. Degradation of Chondroitin sulfate proteoglycans induces sprouting of intact purkinje axons in the cerebellum of the adult rat. *J. Neurosci.* **25**, 7150–7158 (2005).

Cousins, R. J. Absorption, transport, and hepatic metabolism of copper and zinc: special reference to metallothionein and ceruloplasmin. *Physiol. Rev.* **65**, 238–309 (1985).

Cregg, J. M. *et al.* Functional regeneration beyond the glial scar. *Exp. Neurol.* **253**, 197–207 (2014).

Csoknya, M., Barna, J., Hiripi, L., Hámori, J. & Elekes, K. Reorganization of monoaminergic systems in the earthworm, Eisenia fetida , following brain extirpation. *J. Exp. Zool. Part A Comp. Exp. Biol.* **296A**, 18–29 (2003).

Cua, R. C. *et al.* Overcoming neurite-inhibitory chondroitin sulfate proteoglycans in the astrocyte matrix. *Glia* **61**, 972–984 (2013).

D'Angelo, M., Sarment, D. P., Billings, P. C. & Pacifici, M. Activation of transforming growth factor β in chondrocytes undergoing endochondral ossification. *J. Bone Miner. Res.* **16**, 2339–2347

(2001).

Dallas, S. L., Rosser, J. L., Mundy, G. R. & Bonewald, L. F. Proteolysis of Latent Transforming Growth Factor-β (TGF-β)-binding Protein-1 by Osteoclasts. *J. Biol. Chem.* **277**, 21352–21360 (2002).

David, S. & Aguayo, A. Axonal elongation into peripheral nervous system "bridges" after central nervous system injury in adult rats. *Science* **214**, (1981).

Davies, S. J. A. *et al.* Regeneration of adult axons in white matter tracts of the central nervous system. *Nature* **390**, 680–683 (1997).

Demircan, K. *et al.* ADAMTS1, ADAMTS5, ADAMTS9 and aggrecanase-generated proteoglycan fragments are induced following spinal cord injury in mouse. *Neurosci. Lett.* **544**, 25–30 (2013).

Deng, T. & Karin, M. JunB differs from c-Jun in its DNA-binding and dimerization domains, and respresses c-Jun by formation of inactive heterodimers. *Genes Dev.* **7**, 479–490 (1993).

Dias, D. O. & Göritz, C. Fibrotic scarring following lesions to the central nervous system. *Matrix Biol.* **68**–**69**, 561–570 (2018).

Diaz-Moreno, S. *et al.* The spectroscopy village at Diamond Light Source. *J. Synchrotron Radiat.* **25**, 998–1009 (2018).

Dickendesher, T. L. *et al.* NgR1 and NgR3 are receptors for chondroitin sulfate proteoglycans. *Nat. Neurosci.* **15**, 703–712 (2012).

Dixon, S. J. *et al.* Ferroptosis: An iron-dependent form of nonapoptotic cell death. *Cell* **149**, 1060–1072 (2012).

Do Van, B. *et al.* Ferroptosis, a newly characterized form of cell death in Parkinson's disease that is regulated by PKC. *Neurobiol. Dis.* **94**, 169–178 (2016).

Domínguez, J., Velando, A. & Ferreiro, A. Are *Eisenia fetida* (Savigny, 1826) and *Eisenia andrei* (Oligochaeta, Lumbricidae) different biological species? *Pedobiologia (Jena).* **49**, 81–87 (2005).

Doron-Mandel, E., Fainzilber, M. & Terenzio, M. Growth control mechanisms in neuronal regeneration. *FEBS Lett.* **589**, 1669–1677 (2015).

Dou, C. L. & Levine, J. M. Inhibition of neurite growth by the NG2 chondroitin sulfate proteoglycan. *J. Neurosci.* **14**, 7616–7628 (1994).

Dumin, J. A. *et al.* Pro-collagenase-1 (Matrix Metalloproteinase-1) Binds the α 2β1 Integrin upon Release from Keratinocytes Migrating on Type I Collagen. *J. Biol. Chem.* **276**, 29368–29374 (2001).

Dyczynska, E. *et al.* Proteolytic processing of delta-like 1 by ADAM proteases. *J. Biol. Chem.* **282**, 436–444 (2007).

Edgar, D., Timpl, R. & Thoenen, H. The heparin-binding domain of laminin is responsible for its effects on neurite outgrowth and neuronal survival. *EMBO J.* **3**, 1463–1468 (1984).

Eide, D. J. The SLC39 family of metal ion transporters. *Pflugers Arch. Eur. J. Physiol.* **447**, 796–800 (2004).

Eide, D. J. Zinc transporters and the cellular trafficking of zinc. *Biochim. Biophys. Acta - Mol. Cell Res.* **1763**, 711–722 (2006).

Ertürk, A. *et al.* Three-dimensional imaging of the unsectioned adult spinal cord to assess axon regeneration and glial responses after injury. *Nat. Med.* **18**, 166–171 (2012).

F. Lichtenthaler, S. Alpha-secretase cleavage of the amyloid precursor protein: proteolysis regulated by signaling pathways and protein trafficking. *Curr. Alzheimer Res.* **9**, 165–177 (2012).

Fambrough, D., Pan, D., Rubin, G. M. & Goodman, C. S. The cell surface metalloprotease/disintegrin Kuzbanian is required for axonal extension in Drosophila. *Proc. Natl. Acad. Sci. U. S. A.* **93**, 13233–8 (1996).

Faulkner, J. R. Reactive astrocytes protect tissue and preserve function after spinal cord injury. *J. Neurosci.* **24**, 2143–2155 (2004).

Fazal, S. V. *et al.* Graded elevation of c-Jun in Schwann cells in vivo: Gene dosage determines effects on development, remyelination, tumorigenesis, and hypomyelination. *J. Neurosci.* **37**, 12297–12313 (2017).

Ferguson, T. A. & Muir, D. MMP-2 and MMP-9 increase the neurite-promoting potential of Schwann cell basal laminae and are upregulated in degenerated nerve. *Mol. Cell. Neurosci.* **16**, 157–167 (2000).

Fernandes, K. A., Harder, J. M., Kim, J. & Libby, R. T. JUN regulates early transcriptional responses to axonal injury in retinal ganglion cells. *Exp. Eye Res.* **112**, 106–117 (2013).

Fernández-Klett, F. & Priller, J. The fibrotic scar in neurological disorders. in *Brain Pathology* **24**, 404–413 (2014).

Filous, A. R. *et al.* Entrapment via Synaptic-Like Connections between NG2 Proteoglycan+ Cells and Dystrophic Axons in the Lesion Plays a Role in Regeneration Failure after Spinal Cord Injury. *J. Neurosci.* **34**, 16369–16384 (2014).

Filous, A. R. *et al.* Entrapment via Synaptic-Like Connections between NG2 Proteoglycan+ Cells and Dystrophic Axons in the Lesion Plays a Role in Regeneration Failure after Spinal Cord Injury. *J.*

Neurosci. **34**, 16369–16384 (2014).

Fisher, D. *et al.* Leukocyte common antigen-related phosphatase is a functional receptor for chondroitin sulfate proteoglycan axon growth inhibitors. *J. Neurosci.* **31**, 14051–14066 (2011).

Fitch, M. T. & Silver, J. CNS injury, glial scars, and inflammation: Inhibitory extracellular matrices and regeneration failure. *Experimental Neurology* **209**, 294–301 (2008).

Fitzgerald, M. *et al.* Metallothionein-IIA promotes neurite growth via the megalin receptor. *Exp. Brain Res.* **183**, 171–180 (2007).

Fontana, X. *et al.* C-Jun in Schwann cells promotes axonal regeneration and motoneuron survival via paracrine signaling. *J. Cell Biol.* **198**, 127–141 (2012).

Frederickson, C. J., Koh, J. Y. & Bush, A. I. The neurobiology of zinc in health and disease. *Nat. Rev. Neurosci.* **6**, 449–462 (2005).

Galtrey, C. M. & Fawcett, J. W. The role of chondroitin sulfate proteoglycans in regeneration and plasticity in the central nervous system. *Brain Res. Rev.* **54**, 1–18 (2007).

Gao, X., Wang, Y., Chen, J. & Peng, J. The role of peripheral nerve ECM components in the tissue engineering nerve construction. *Rev. Neurosci.* **24**, 443–453 (2013).

Garcia, A. L., Fetter, R. D. & Goodman, C. S. Genetic analysis of Laminin A in Drosophila: extracellular matrix containing laminin A is required for ocellar axon pathfinding. *Development* **122**, 2611–2621 (1996).

Gardner, R. T. *et al.* Targeting protein tyrosine phosphatase σ after myocardial infarction restores cardiac sympathetic innervation and prevents arrhythmias. *Nat. Commun.* **6**, 6235 (2015).

Garratt, A. N., Britsch, S. & Birchmeier, C. Neuregulin, a factor with many functions in the life of a Schwann cell. *BioEssays* **22**, 987–996 (2000).

Gaub, P. *et al.* HDAC inhibition promotes neuronal outgrowth and counteracts growth cone collapse through CBP/p300 and P/CAF-dependent p53 acetylation. *Cell Death Differ.* **17**, 1392–1408 (2010).

Gaub, P. *et al.* The histone acetyltransferase p300 promotes intrinsic axonal regeneration. *Brain* **134**, 2134–2148 (2011).

Gaultier, A., Cousin, H., Darribère, T. & Alfandari, D. ADAM13 disintegrin and cysteine-rich domains bind to the second heparin-binding domain of fibronectin. *J. Biol. Chem.* **277**, 23336–23344 (2002).

Ge, G. & Greenspan, D. S. BMP1 controls TGFβ1 activation via cleavage of latent TGFβ-binding

protein. *J. Cell Biol.* **175**, 111–120 (2006).

Gerard, J., Borst, G. & Helmchen, F. Calcium influx during an action potential. *Methods Enzymol.* **293**, 352–371 (1998).

Ghosh-Roy, A., Wu, Z., Goncharov, A., Jin, Y. & Chisholm, A. D. Calcium andcyclic AMP promote axonal regeneration in *Caenorhabditis elegans* and require DLK-1 kinase. *J. Neurosci.* **30**, 3175–3183 (2010).

Giancotti, F. G. & Ruoslahti, E. Integrin signaling. *Science (80-.).* **285**, 1028–33 (1999).

Gibbs, P. N., Gore, M. G. & Jordan, P. M. Investigation of the effect of metal ions on the reactivity of thiol groups in human 5-aminolaevulinate dehydratase. *Biochem. J.* **225**, 573–80 (1985).

Gibson, S. *et al.* Calcitonin gene-related peptide immunoreactivity in the spinal cord of man and of eight other species. *J. Neurosci.* **4**, 3101–3111 (1984).

Gilbert, R. J. *et al.* CS-4,6 is differentially upregulated in glial scar and is a potent inhibitor of neurite extension. *Mol. Cell. Neurosci.* **29**, 545–558 (2005).

Giralt, M. *et al.* Metallothionein-1+2 Deficiency increases brain pathology in transgenic mice with astrocyte-targeted expression of interleukin 6. *Neurobiol. Dis.* **9**, 319–338 (2002).

Goldberg, J. L. *et al.* An oligodendrocyte lineage-specific semaphorin, sema5A, inhibits axon growth by retinal ganglion cells. *J. Neurosci.* **24**, 4989–4999 (2004).

González-Billault, C. *et al.* A role of MAP1B in reelin-dependent neuronal migration. *Cereb. Cortex* **15**, 1134–1145 (2005).

Gopi Daisy, N. *et al.* Studies on regeneration of central nervous system and social ability of the earthworm *Eudrilus eugeniae*. *Invertebr. Neurosci.* **16**, 6 (2016).

Göritz, C. *et al.* A pericyte origin of spinal cord scar tissue. *Science.* **333**, 238–242 (2011).

Goto, E., Mukozawa, M., Mori, H. & Hara, M. A rolled sheet of collagen gel with cultured Schwann cells: Model of nerve conduit to enhance neurite growth. *J. Biosci. Bioeng.* **109**, 512–518 (2010).

Gottschall, P. E. & Howell, M. D. ADAMTS expression and function in central nervous system injury and disorders. *Matrix Biol.* **44**–**46**, 70–76 (2015).

Graeber, M. B., Raivich, G. & Kreutzberg, G. W. Increase of transferrin receptors and iron uptake in regenerating motor neurons. *J. Neurosci. Res.* **23**, 342–345 (1989).

GrandPré, T., Nakamura, F., Vartanlan, T. & Strittmatter, S. M. Identification of the Nogo inhibitor of axon regeneration as a Reticulon protein. *Nature* **403**, 439–444 (2000).

Groot, A. J. & Vooijs, M. A. The role of adams in notch signaling. *Adv. Exp. Med. Biol.* **727**, 15–36 (2012).

Guan, C. bing, Xu, H. tai, Jin, M., Yuan, X. bing & Poo, M. ming. Long-Range Ca2+ Signaling from Growth Cone to Soma Mediates Reversal of Neuronal Migration Induced by Slit-2. *Cell* **129**, 385–395 (2007).

Guo, R., Ding, X., Zhong, X., Gao, S., Sun Y. Molecular and ultrastructural insights into the earthworm *Eisenia fetida* of the assessment of ecotoxicity during colistin exposure. *Environ. Sci. Pollut. Res. Int.* **21**, 13405-13411 (2014).

Hajji, K. *et al.* Neuroprotective effects of PACAP against paraquat-induced oxidative stress in the Drosophila central nervous system. *Hum. Mol. Genet.* **28**, 1905–1918 (2019).

Hallgren, B. & Sourander, P. The effect of age on the non-haemin iron in the human brain. *J. Neurochem.* **3**, 41–51 (1958).

Han, Q. *et al.* Linear Ordered collagen scaffolds loaded with collagen-binding brain-derived neurotrophic factor improve the recovery of spinal cord injury in rats. *Tissue Eng. Part A* **15**, 2927–2935 (2009).

Hare, D., Ayton, S., Bush, A. & Lei, P. A delicate balance: Iron metabolism and diseases of the brain. *Front. Aging Neurosci.* **5**, 34 (2013).

Hattori, M., Osterfield, M. & Flanagan, J. G. Regulated cleavage of a contact-mediated axon repellent. *Science (80-.).* **289**, 1360–1365 (2000).

He, Z. & Jin, Y. Intrinsic Control of Axon Regeneration. *Neuron* **90**, 437–451 (2016).

Hebbrecht, G., Maenhaut, W. & Reuck, J. De. Brain trace elements and aging. *Nucl. Instruments Methods Phys. Res. Sect. B Beam Interact. with Mater. Atoms* **150**, 208–213 (1999).

Hehr, C. L., Hocking, J. C. & McFarlane, S. Matrix metalloproteinases are required for retinal ganglion cell axon guidance at select decision points. *Development* **132**, 3371–9 (2005).

Herbert, Z. *et al.* Identification of novel neuropeptides in the ventral nerve cord ganglia and their targets in an annelid worm, *Eisenia fetida*. *J. Comp. Neurol.* **514**, 415–432 (2009).

Herculano-Houzel, S. The glia/neuron ratio: How it varies uniformly across brain structures and species and what that means for brain physiology and evolution. *GLIA* **62**, 1377–1391 (2014).

Herdegen, T. & Leah, J. D. Inducible and constitutive transcription factors in the mammalian nervous system: Control of gene expression by Jun, Fos and Krox, and CREB/ATF proteins. *Brain Research Reviews* **28**, 370–490 (1998).

Hermanns, S., Klapka, N. & Müller, H. W. The collagenous lesion scar - an obstacle for axonal

regeneration in brain and spinal cord injury. *Restor. Neurol. Neurosci.* **19**, 139–148 (2001).

Hidalgo, C. & Núñez, M. T. Calcium, iron and neuronal function. in *IUBMB Life* **59**, 280–285 (John Wiley & Sons, Ltd, 2007).

Hidalgo, C., Carrasco, M. A., Muñoz, P. & Núñez, M. T. a role for reactive oxygen/nitrogen species and iron on neuronal synaptic plasticity. *Antioxid. Redox Signal.* **9**, 245–255 (2006).

Hobson, M. I., Green, C. J. & Terenghi, G. VEGF enhances intraneural angiogenesis and improves nerve regeneration after axotomy. *J. Anat.* **197**, 591–605 (2000).

Homa, J. Earthworm coelomocyte extracellular traps: structural and functional similarities with neutrophil NETs. *Cell Tissue Res.* **371**, 407-414 (2018).

Homa, J. *et al.* Metal-specific effects on metallothionein gene induction and riboflavin content in coelomocytes of *Allolobophora chlorotica*. *Ecotoxicol. Environ. Saf.* **73**, 1937-1943 (2010).

Horigane, S. I. *et al.* Facilitation of axon outgrowth via a Wnt5a-CaMKK-CaMKIα pathway during neuronal polarization. *Mol. Brain* **9**, 8 (2016).

Horigane, S. I., Ozawa, Y., Yamada, H. & Takemoto-Kimura, S. Calcium signalling: a key regulator of neuronal migration. *J. Biochem.* **165**, 401–409 (2019).

Howard, M. J., David, G. & Barrett, J. N. Resealing of transected myelinated mammalian axons in vivo: evidence for involvement of calpain. *Neuroscience* **93**, 807–815 (1999).

Howell, G. A., Welch, M. G. & Frederickson, C. J. Stimulation-induced uptake and release of zinc in hippocampal slices. *Nature* **308**, 736–738 (1984).

Huang, C. C. *et al.* Laminin alpha subunits and their role in C. elegans development. *Development* **130**, 3343–58 (2003).

Huang, L. *et al.* C-Jun gene-modified schwann cells: Upregulating multiple neurotrophic factors and promoting neurite outgrowth. *Tissue Eng. - Part A* **21**, 1409–1421 (2015).

Huang, Y. Z., Pan, E., Xiong, Z. Q. & McNamara, J. O. Zinc-mediated transactivation of TrkB potentiates the hippocampal mossy fiber-CA3 pyramid synapse. *Neuron* **57**, 546–558 (2008).

Hurtado, E. K., Claussen, A. H. & Scott, K. G. Early childhood anemia and mild or moderate mental retardation. *Am. J. Clin. Nutr.* **69**, 115–119 (1999).

Hynes, R. O. Integrins: Bidirectional, Allosteric Signaling Machines. *Cell* **110**, 673–687 (2002).

Iba, K. *et al.* The cysteine-rich domain of human ADAM 12 supports cell adhesion through syndecans and triggers signaling events that lead to β1 integrin-dependent cell spreading. *J. Cell Biol.* **149**, 1143–1155 (2000).

Iba, K., Albrechtsen, R., Gilpin, B. J., Loechel, F. & Wewer, U. M. Cysteine-rich domain of human ADAM 12 (meltrin α) supports tumor cell adhesion. *Am. J. Pathol.* **154**, 1489–1501 (1999).

Inder, T. *et al.* Elevated free radical products in the cerebrospinal fluid of VLBW infants with cerebral white matter injury. *Pediatr. Res.* **52**, 213–218 (2002).

Inman, D. M. & Steward, O. Ascending sensory, but not other long-tract axons, regenerate into the connective tissue matrix that forms at the site of a spinal cord injury in mice. *J. Comp. Neurol.* **462**, 431–449 (2003).

Itoh, A. *et al.* ZPK/DLK, a mitogen-activated protein kinase kinase kinase, is a critical mediator of programmed cell death of motoneurons. *J. Neurosci.* **31**, 7223–7228 (2011).

Itoh, A., Horiuchi, M., Bannerman, P., Pleasure, D. & Itoh, T. Impaired regenerative response of primary sensory neurons in ZPK/DLK gene-trap mice. *Biochem. Biophys. Res. Commun.* **383**, 258–262 (2009).

Iwakura, Y. *et al.* Glutamate-dependent ectodomain shedding of neuregulin-1 type II precursors in rat forebrain neurons. *PLoS One* **12**, e0174780 (2017).

Jarmuł-Pietraszczyk, J. & Jastrzębska, E. Herbicide toxicity to the california earthworms *Eisenia fetida* Sav. and *Dendrobaena veneta* Rosa. *Ecol. Chem. Eng. A* **19**, 1133–1137 (2012).

Jarosz, M., Olbert, M., Wyszogrodzka, G., Młyniec, K. & Librowski, T. Antioxidant and anti-inflammatory effects of zinc. Zinc-dependent NF-κB signaling. *Inflammopharmacology* **25**, 11–24 (2017).

Jin, J. *et al.* Effect of chondroitin sulfate proteoglycans on neuronal cell adhesion, spreading and neurite growth in culture. *Neural Regen. Res.* **13**, 289 (2018).

Jones, L. L., Margolis, R. U. & Tuszynski, M. H. The chondroitin sulfate proteoglycans neurocan, brevican, phosphacan, and versican are differentially regulated following spinal cord injury. *Exp. Neurol.* **182**, 399–411 (2003).

Jones, L. L., Margolis, R. U. & Tuszynski, M. H. The chondroitin sulfate proteoglycans neurocan, brevican, phosphacan, and versican are differentially regulated following spinal cord injury. *Exp. Neurol.* **182**, 399–411 (2003).

Jones, L. L., Sajed, D. & Tuszynski, M. H. Axonal Regeneration through Regions of Chondroitin Sulfate Proteoglycan Deposition after Spinal Cord Injury: A Balance of Permissiveness and Inhibition. *J. Neurosci.* **23**, 9276–9288 (2003).

Jones, L. S. Integrins: Possible functions in the adult CNS. *Trends Neurosci.* **19**, 68–72 (1996).

Jorgenson, L. A., Sun, M., O'Connor, M. & Georgieff, M. K. Fetal iron deficiency disrupts the

maturation of synaptic function and efficacy in area CA1 of the developing rat hippocampus. *Hippocampus* **15**, 1094–1102 (2005).

Jorgenson, L. A., Wobken, J. D. & Georgieff, M. K. Perinatal iron deficiency alters apical dendritic growth in hippocampal CA1 pyramidal neurons. *Dev. Neurosci.* **25**, 412–420 (2003).

Jung, J. H., Park, M. H., Choi, S. Y. & Koh, J. Y. Activation of the Trk signaling pathway by extracellular zinc. Role of metalloproteinases. *J. Biol. Chem.* **280**, 11995–12001 (2005).

Jung, S. *et al.* Macin family of antimicrobial proteins combines antimicrobial and nerve repair activities. *J. Biol. Chem.* **287**, 14246–14258 (2012).

Kalappa, B. I., Anderson, C. T., Goldberg, J. M., Lippard, S. J. & Tzounopoulos, T. AMPA receptor inhibition by synaptically released zinc. *Proc. Natl. Acad. Sci.* **112**, 201512296 (2015).

Kamei, N. *et al.* BDNF, NT-3, and NGF released from transplanted neural progenitor cells promote corticospinal axon growth in organotypic cocultures. *Spine (Phila. Pa. 1976).* **32**, 1272–1278 (2007).

Kantor, D. B. *et al.* Semaphorin 5A is a bifunctional axon guidance cue regulated by heparan and chondroitin sulfate proteoglycans. *Neuron* **44**, 961–975 (2004).

Kelly, E. J., Quaife, C. J., Froelick, G. J. & Palmiter, R. D. Metallothionein I and II protect against zinc deficiency and zinc toxicity in mice. *J. Nutr.* **126**, 1782–1790 (1996).

Kemmerling, U. *et al.* Calcium release by ryanodine receptors mediates hydrogen peroxide-induced activation of ERK and CREB phosphorylation in N2a cells and hippocampal neurons. *Cell Calcium* **41**, 491–502 (2007).

Kerstein, P. C., Nichol IV, R. H. & Gomez, T. M. Mechanochemical regulation of growth cone motility. *Front. Cell. Neurosci.* **9**, 244 (2015).

Kiernan, J. A. Hypotheses concerned with axonal regeneration in the mammalian nervous system. *Biol. Rev.* **54**, 155–197 (1979).

Killilea, D. W., Wong, S. L., Cahaya, H. S., Atamna, H. & Ames, B. N. Iron accumulation during cellular senescence. *Ann. N. Y. Acad. Sci.* **1019**, 365–367 (2004).

Kobayashi, H., Watanabe, E. & Murakami, F. Growth Cones of Dorsal Root Ganglion but Not Retina Collapse and Avoid Oligodendrocytes in Culture. *Dev. Biol.* **168**, 383–394 (1995).

Koch, G. L. E. The endoplasmic reticulum and calcium storage. *BioEssays* **12**, 527–531 (1990).

Kochańczyk, T., Drozd, A. & Krężel, A. Relationship between the architecture of zinc coordination and zinc binding affinity in proteins - Insights into zinc regulation. *Metallomics* **7**, 244–257 (2015).

Køhler, L. B., Berezin, V., Bock, E. & Penkowa, M. The role of metallothionein II in neuronal differentiation and survival. *Brain Res.* **992**, 128–136 (2003).

Komuro, H. & Rakic, P. Selective role of N-type calcium channels in neuronal migration. *Science* **257**, 806–809 (1992).

Koritsánszky, S. & Hartwig, H. G. The regeneration of the monoaminergic system in the cerebral ganglion of the earthworm, Allolobophora caliginosa - A morphological and microspectrofluorimetrical analysis. *Cell Tissue Res.* **151**, 171–186 (1974).

Koziol, B., Markowicz, M., Kruk, J. & Plytycz, B. Riboflavin as a source of autofluorescence in *Eisenia fetida* coelomocytes. *Photochem. Photobiol.* **82**, 570 (2006).

Kragl, M. *et al.* Cells keep a memory of their tissue origin during axolotl limb regeneration. *Nature* **460**, 60–65 (2009).

Kress, G. J., Dineley, K. E. & Reynolds, I. J. The relationship between intracellular free iron and cell injury in cultured neurons, astrocytes, and oligodendrocytes. *J. Neurosci.* **22**, 5848–55 (2002).

Kruszewski, M. Labile iron pool: The main determinant of cellular response to oxidative stress. *Mutat. Res. - Fundam. Mol. Mech. Mutagen.* **531**, 81–92 (2003).

Kudin, A. P., Augustynek, B., Lehmann, A. K., Kovács, R. & Kunz, W. S. The contribution of thioredoxin-2 reductase and glutathione peroxidase to H2O2 detoxification of rat brain mitochondria. *Biochim. Biophys. Acta - Bioenerg.* **1817**, 1901–1906 (2012).

Kumar, H. *et al.* The role of free radicals in the aging brain and Parkinson's disease: Convergence and parallelism. *Int. J. Mol. Sci.* **13**, 10478–10504 (2012).

Laabs, T., Carulli, D., Geller, H. M. & Fawcett, J. W. Chondroitin sulfate proteoglycans in neural development and regeneration. *Curr. Opin. Neurobiol.* **15**, 116–120 (2005).

Lang, B. T. *et al.* Modulation of the proteoglycan receptor PTPs promotes recovery after spinal cord injury. *Nature* **518**, (2015).

Larner, A. J., Johnson, A. & Keynes, R. J. Regeneration in the vertebrate central nervous system: phylogeny, ontogeny, and mechanisms. *Biol. Rev.* **70**, 597–619 (1995).

Larsen, P. H., Wells, J. E., Stallcup, W. B., Opdenakker, G. & Yong, V. W. Matrix Metalloproteinase-9 Facilitates Remyelination in Part by Processing the Inhibitory NG2 Proteoglycan. *J. Neurosci.* **23**, 11127–11135 (2003).

Lazoff, B., Wolf, A. W. & Jimenez, E. Iron-deficiency anemia and infant development: Effects of extended oral iron therapy. *J. Pediatr.* **129**, 382–389 (1996).

Lee, S. R. critical role of zinc as either an antioxidant or a prooxidant in cellular systems. *Oxid. Med. Cell. Longev.* **2018**, (2018).

Lehmann, W. D. & Heinrich, H. C. Impaired phenylalanine-tyrosine conversion in patients with iron-deficiency anemia studied by a L-(2H5)phenylalanine-loading test. *Am. J. Clin. Nutr.* **44**, 468–474 (1986).

Lein, P. J., Higgins, D., Turner, D. C., Flier, L. A. & Terranova, V. P. The NC1 domain of type IV collagen promotes axonal growth in sympathetic neurons through interaction with the α1β1 integrin. *J. Cell Biol.* **113**, 417–428 (1991).

Lepeta, K. *et al.* A normal genetic variation modulates synaptic MMP-9 protein levels and the severity of schizophrenia symptoms. *EMBO Mol. Med.* **9**, 1100–1116 (2017).

Li, J. *et al.* Lentivirus-mediating FGF13 enhances axon regeneration after spinal cord injury by stabilizing microtubule and improving mitochondrial function. *J. Neurotrauma* **35**, 548–559 (2018).

Li, S., Gu, X. & Yi, S. The Regulatory Effects of Transforming Growth Factor-β on Nerve Regeneration. *Cell Transplant.* **26**, 381–394 (2017).

Li, Y. & Raisman, G. Schwann cells induce sprouting in motor and sensory axons in the adult rat spinal cord. *J. Neurosci.* **14**, 4050–4063 (1994).

Li, Y. *et al.* Mobile zinc increases rapidly in the retina after optic nerve injury and regulates ganglion cell survival and optic nerve regeneration. *Proc. Natl. Acad. Sci.* **114**, E209–E218 (2017).

Li, Y. S. *et al.* Cloning and expression of a developmentally regulated protein that induces mitogenic and neurite outgrowth activity. *Science.* **250**, 1690–1694 (1990).

Li, Y., Hough, C. J., Frederickson, C. J. & Sarvey, J. M. Induction of mossy fiber→CA3 long-term potentiation requires translocation of synaptically released Zn 2+. *J. Neurosci.* **21**, 8015–8025 (2001).

Liddell, J. R., Robinson, S. R. & Dringen, R. Endogenous glutathione and catalase protect cultured rat astrocytes from the iron-mediated toxicity of hydrogen peroxide. *Neurosci. Lett.* **364**, 164–167 (2004).

Liebmann, E. New light on regeneration of *Eisenia foetida* (SAV.). *J. Morphol.* **73**, 583–610 (1943).

Liebmann, E. The role of the chloragogue in regeneration of *Eisenia foetida* (Sav.). *J. Morphol.* **70**, 151–187 (1942).

Liesi, P. Laminin-immunoreactive glia distinguish regenerative adult CNS systems from non-regenerative ones. *EMBO J.* **4**, 2505–11 (1985).

Lindholm, D., Heumann, R., Meyer, M. & Thoenen, H. Interleukin-1 regulates synthesis of nerve growth factor in non-neuronal cells of rat sciatic nerve. *Nature* **330**, 658–659 (1987).

Liu, X., Hashimoto-Torii, K., Torii, M., Haydar, T. F. & Rakic, P. The role of ATP signaling in the migration of intermediate neuronal progenitors to the neocortical subventricular zone. *Proc. Natl. Acad. Sci.* **105**, 11802–11807 (2008).

Liuzzi, J. P. & Cousins, R. J. Mammalian zinc transporters. *Annu. Rev. Nutr.* **24**, 151–72 (2004).

Loers, G. *et al.* Identification and characterization of synthetic chondroitin-4-sulfate binding peptides in neuronal functions. *Sci. Rep.* **9**, 1064 (2019).

Löffek, S., Schilling, O. & Franzke, C. W. Biological role of matrix metalloproteinases: A critical balance. *European Respiratory Journal* **38**, 191–208 (2011).

Lorenzetto, E., Panteri, R., Marino, R., Keller, F. & Buffelli, M. Impaired nerve regeneration in reeler mice after peripheral nerve injury. *Eur. J. Neurosci.* **27**, 12–19 (2008).

Lorenzl, S. *et al.* Increased plasma levels of matrix metalloproteinase-9 in patients with Alzheimer's disease. *Neurochem. Int.* **43**, 191–196 (2003).

Love, M., Huber, W. & Anders, S. Moderated estimation of fold change and dispersion for RNA-seq data with DESeq2. *Genome Biol.* **15**, 550 (2014)

Lozoff, B. *et al.* Long-lasting neural and behavioral effects of iron deficiency in infancy. *Nutr. Rev.* **64**, S34-43; discussion S72-91 (2006).

Lozoff, B., Jimenez, E. & Wolf, A. W. Long-Term Developmental Outcome of Infants with Iron Deficiency. *N. Engl. J. Med.* **325**, 687–694 (1991).

Lubics, A., Reglödi, D., Szelier, M. & Lengvári, I. Time-course of the regeneration of the earthworm cerebral ganglion with special reference to serotonergic elements. *Eur. J. Anat.* **6**, 147–152 (2002).

Luizzi, F. J. & Lasek, R. J. Astrocytes block axonal regeneration in mammals by activating the physiological stop pathway. *Science (80-.).* **237**, 642–645 (1987).

Lumsden, A. L. *et al.* Dysregulation of neuronal iron homeostasis as an alternative unifying effect of mutations causing familial alzheimer's disease. *Front. Neurosci.* **12**, 533 (2018).

Lv, L., Han, X., Sun, Y., Wang, X. & Dong, Q. Valproic acid improves locomotion in vivo after SCI and axonal growth of neurons in vitro. *Exp. Neurol.* **233**, 783–790 (2012).

Ma, Z. X., Li, Q. Y., Zhang, Z. Y. & Zheng, Y. F. A Disintegrin and Metalloprotease 10 in neuronal maturation and gliogenesis during cortex development. *Neural Regen. Res.* **8**, 24–30 (2013).

MacDonald, R. S. The role of zinc in growth and cell proliferation. *J. Nutr.* **130**, 1500S-1508S (2000).

Mackenzie, G. G. *et al.* α-Lipoic acid and N-acetyl cysteine prevent zinc deficiency-induced activation of NF-κB and AP-1 transcription factors in human neuroblastoma IMR-32 cells. *Free Radic. Res.* **40**, 75–84 (2006).

Maeda, S., Dean, D. D., Gomez, R., Schwartz, Z. & Boyan, B. D. The first stage of transforming growth factor β1 activation is release of the large latent complex from the extracellular matrix of growth plate chondrocytes by matrix vesicle stromelysin-1 (MMP-3). *Calcif. Tissue Int.* **70**, 54–65 (2002).

Mandolesi, G., Madeddu, F., Bozzi, Y., Maffei, L. & Ratto, G. M. Acute physiological response of mammalian central neurons to axotomy: ionic regulation and electrical activity. *FASEB J.* **18**, 1934–1936 (2004).

Manthorpe, M. *et al.* Laminin promotes neuritic regeneration from cultured peripheral and central neurons. *J. Cell Biol.* **97**, 1882–1890 (1983).

Mao, M. *et al.* The podosomal-adaptor protein SH3PXD2B is essential for normal postnatal development. *Mamm. Genome* **20**, 462–475 (2009).

Maret, W. Oxidative metal release from metallothionein via zinc-thiol/disulfide interchange. *Proc. Natl. Acad. Sci. U. S. A.* **91**, 237–241 (1994).

Maretzky, T. *et al.* ADAM10 mediates E-cadherin shedding and regulates epithelial cell-cell adhesion, migration, and -catenin translocation. *Proc. Natl. Acad. Sci.* **102**, 9182–9187 (2005).

Masand, S. N. *et al.* The effect of glycomimetic functionalized collagen on peripheral nerve repair. *Biomaterials* **33**, 8353–8362 (2012).

Maske, H. A new method for demonstrating A and B cells in the islands of Langerhans. *Klin. Wochenschr.* **33**, 1058 (1955).

Massagué, J. TGFβ signalling in context. *Nat. Rev. Mol. Cell Biol.* **13**, 616–630 (2012).

Massie, H. R., Aiello, V. R. & Williams, T. R. Inhibition of iron absorption prolongs the life span of Drosophila. *Mech. Ageing Dev.* **67**, 227–237 (1993).

Massie, H. R., Aiello, V. R. & Williams, T. R. Iron accumulation during development and ageing of Drosophila. *Mech. Ageing Dev.* **29**, 215–220 (1985).

Matak, P. *et al.* Disrupted iron homeostasis causes dopaminergic neurodegeneration in mice. *Proc. Natl. Acad. Sci.* **113**, 3428–3435 (2016).

Matsui, F. & Oohira, A. Proteoglycans and injury of the central nervous system. *Congenit. Anom. (Kyoto).* **44**, 181–188 (2004).

Maurel, P., Rauch, U., Flad, M., Margolis, R. K. & Margolis, R. U. Phosphacan, a chondroitin sulfate proteoglycan of brain that interacts with neurons and neural cell-adhesion molecules, is an extracellular variant of a receptor-type protein tyrosine phosphatase. *Proc. Natl. Acad. Sci. U. S. A.* **91**, 2512–2516 (1994).

McAllister, A. K., Katz, L. C. & Lo, D. C. Neurotrophins and synaptic plasticity. *Annu. Rev. Neurosci.* **22**, 295–318 (1999).

McCall, K. A., Huang, C. & Fierke, C. A. Function and mechanism of zinc metalloenzymes. *J. Nutr.* **130**, 1437S-1446S (2000).

McCawley, L. J. & Matrisian, L. M. Matrix metalloproteinases: they're not just for matrix anymore! *Curr. Opin. Cell Biol.* **13**, 534–40 (2001).

McEchron, M. D., Cheng, A. Y., Liu, H., Connor, J. R. & Gilmartin, M. R. Perinatal nutritional iron deficiency permanently impairs hippocampus-dependent trace fear conditioning in rats. *Nutr. Neurosci.* **8**, 195–206 (2005).

McKeon, R. J., Höke, A. & Silver, J. Injury-induced proteoglycans inhibit the potential for laminin-mediated axon growth on astrocytic scars. *Exp. Neurol.* **136**, 32–43 (1995).

McKeon, R. J., Jurynec, M. J. & Buck, C. R. The chondroitin sulfate proteoglycans neurocan and phosphacan are expressed by reactive astrocytes in the chronic CNS glial scar. *J. Neurosci.* **19**, 10778–88 (1999).

McKeon, R. J., Schreiber, R. C., Rudge, J. S. & Silver, J. Reduction of neurite outgrowth in a model of glial scarring following CNS injury is correlated with the expression of inhibitory molecules on reactive astrocytes. *J. Neurosci.* **11**, 3398–411 (1991).

McNamara, J. O., Huang, Y. Z. & Leonard, A. S. Molecular signaling mechanisms underlying epileptogenesis. *Sci. STKE* **2006**, re12 (2006).

Menet, V., Prieto, M., Privat, A. & Giménez y Ribotta, M. Axonal plasticity and functional recovery after spinal cord injury in mice deficient in both glial fibrillary acidic protein and vimentin genes. *Proc. Natl. Acad. Sci. U. S. A.* **100**, 8999–9004 (2003).

Merenmies, J. & Rauvala, H. Molecular cloning of the 18-kDa growth-associated protein of developing brain. *J. Biol. Chem.* **265**, 16721–16724 (1990).

Milev, P. *et al.* Differential regulation of expression of hyaluronan-binding proteoglycans in developing brain: Aggrecan, versican, neurocan, and brevican. *Biochem. Biophys. Res. Commun.* **247**, 207–212 (1998).

Miner, J. H. *et al.* Compositional and structural requirements for laminin and basement membranes during mouse embryo implantation and gastrulation. *Development* **131**, 2247–56 (2004).

Mocchegiani, E. *et al.* Zinc, metallothioneins and immunosenescence: Effect of zinc supply as nutrigenomic approach. *Biogerontology* **12**, 455–465 (2011).

Mollet, I. G. *et al.* Low dose iron treatments induce a DNA damage response in human endothelial cells within minutes. *PLoS One* **11**, e0147990 (2016).

Molnar, L. *et al.* Immune system participates in brain regeneration and restoration of reproduction in the earthworm *Dendrobaena veneta*. *Dev. Comp. Immunol.* **52**, 269–279 (2015).

Monnier, P. P., Sierra, A., Schwab, J. M., Henke-Fahle, S. & Mueller, B. K. The Rho/ROCK pathway mediates neurite growth-inhibitory activity associated with the chondroitin sulfate proteoglycans of the CNS glial scar. *Mol. Cell. Neurosci.* **22**, 319–330 (2003).

Moon, M. Y. *et al.* Zinc promotes adipose-derived mesenchymal stem cell proliferation and differentiation towards a neuronal fate. *Stem Cells Int.* **2018**, (2018).

Morgan, T.H. Regeneration. The Macmillan Company, New York: Myohara (1901).

Mott, J. D. & Werb, Z. Regulation of matrix biology by matrix metalloproteinases. *Curr. Opin. Cell Biol.* **16**, 558–564 (2004).

Mu, D. *et al.* The integrin αvβ8 mediates epithelial homeostasis through MT1-MMP-dependent activation of TGF-β1. *J. Cell Biol.* **157**, 493–507 (2002).

Muir, A. M. *et al.* BMP1-like proteinases are essential to the structure and wound healing of skin. *Matrix Biol.* **56**, 114–131 (2016).

Muir, D. Metalloproteinase-Dependent neurite outgrowth within a synthetic extracellular matrix is induced by nerve growth factor. *Exp. Cell Res.* **210**, 243–252 (1994).

Mukhopadhyay, G., Doherty, P., Walsh, F. S., Crocker, P. R. & Filbin, M. T. A novel role for myelin-associated glycoprotein as an inhibitor of axonal regeneration. *Neuron* **13**, 757–767 (1994).

Muñoz, P. *et al.* Effect of iron on the activation of the MAPK/ERK pathway in PC12 neuroblastoma cells. in *Biological Research* **39**, 189–190 (Sociedad de Biología de Chile, 2006).

Myer, D. J., Gurkoff, G. G., Lee, S. M., Hovda, D. A. & Sofroniew, M. V. Essential protective roles of reactive astrocytes in traumatic brain injury. *Brain* **129**, 2761–2772 (2006).

Myers, J. P., Santiago-Medina, M. & Gomez, T. M. Regulation of axonal outgrowth and pathfinding by integrin-ecm interactions. *Dev. Neurobiol.* **71**, 901–923 (2011).

Myohara, M., Niva, C. C. & Lee, J. M. Molecular approach to annelid regeneration: cDNA subtraction cloning reveals various novel genes that are upregulated during the large-scale regeneration of the oligochaete, *Enchytraeus japonensis*. *Dev. Dyn.* **235**, 2051–2070 (2006).

Nakamuta, S. *et al.* Local application of neurotrophins specifies axons through inositol 1,4,5-trisphosphate, calcium, and Ca2+/calmodulin–dependent protein kinases. *Sci. Signal.* **4**, ra76 (2011).

Naus, S. *et al.* Ectodomain shedding of the neural recognition molecule CHL1 by the metalloprotease-disintegrin ADAM8 promotes neurite outgrowth and suppresses neuronal cell death. *J. Biol. Chem.* **279**, 16083–16090 (2004).

Naylor, R. L. *et al.* A discrete domain of the human TrkB receptor defines the binding sites for BDNF and NT-4. *Biochem. Biophys. Res. Commun.* **291**, 501–507 (2002).

Neptune, E. R. *et al.* Dysregulation of TGF-β activation contributes to pathogenesis in Marfan syndrome. *Nat. Genet.* **33**, 407–411 (2003).

Nguyen, M. D., Julien, J. P. & Rivest, S. Innate immunity: The missing link in neuroprotection and neurodegeneration? *Nat. Rev. Neurosci.* **3**, 216–227 (2002).

Nishimura, S. *et al.* Functional synergy between cholecystokinin receptors CCKAR and CCKBR in mammalian brain development. *PLoS One* **10**, e0124295 (2015).

Nishiyama, A., Dahlin, K. J., Prince, J. T., Johnstone, S. R. & Stallcup, W. B. The primary structure of NG2, a novel membrane-spanning proteoglycan. *J. Cell Biol.* **114**, 359–371 (1991).

Nordstrom, L. A., Lochner, J., Yeung, W. & Ciment, G. The metalloproteinase stromelysin-1 (transin) mediates pc12 cell growth cone invasiveness through basal laminae. *Mol. Cell. Neurosci.* **6**, 56–68 (1995).

Novak, U. & Kaye, A. H. Extracellular matrix and the brain: Components and function. *Journal of Clinical Neuroscience* **7**, 280–290 (2000).

Oh, L. Y. *et al.* Matrix metalloproteinase-9/gelatinase B is required for process outgrowth by oligodendrocytes. *J. Neurosci.* **19**, 8464–75 (1999).

Ohtake, Y., Wong, D., Abdul-Muneer, P. M., Selzer, M. E. & Li, S. Two PTP receptors mediate CSPG inhibition by convergent and divergent signaling pathways in neurons. *Sci. Rep.* **6**, 37152 (2016).

Okrzesik, J., Kachamakova-Trojanowska, N., Jozkowicz, A., Morgan, A. J. & Plytycz, B. Reversible inhibition of reproduction during regeneration of cerebral ganglia and celomocytes in the earthworm Dendrobaena veneta. *Invertebr. Surviv. J.* **10**, 151–161 (2013).

Olsen, M. W. B. *et al.* Angiopoietin-4 inhibits angiogenesis and reduces interstitial fluid pressure. *Neoplasia* **8**, 364–372 (2006).

Oohira, A., Matsui, F., Tokita, Y., Yamauchi, S. & Aono, S. Molecular interactions of neural

chondroitin sulfate proteoglycans in the brain development. *Arch. Biochem. Biophys.* **374**, 24–34 (2000).

Ortiz, E. *et al.* Effect of manipulation of iron storage, transport, or availability on myelin composition and brain iron content in three different animal models. *J. Neurosci. Res.* **77**, 681–689 (2004).

Oteiza, P. I., Cuellar, S., Lönnerdal, B., Hurley, L. S. & Keen, C. L. Influence of maternal dietary zinc intake on in vitro tubulin polymerization in fetal rat brain. *Teratology* **41**, 97–104 (1990).

Özpolat, B. D. & Bely, A. E. Developmental and molecular biology of annelid regeneration: a comparative review of recent studies. *Current Opinion in Genetics and Development* **40**, 144–153 (2016).

Paíno, C. L., Fernandez-Valle, C., Bates, M. L. & Bunge, M. B. Regrowth of axons in lesioned adult rat spinal cord: promotion by implants of cultured Schwann cells. *J. Neurocytol.* **23**, 433–452 (1994).

Palazuelos, J., Klingener, M., Raines, E. W., Crawford, H. C. & Aguirre, A. oligodendrocyte regeneration and CNS remyelination require TACE/ADAM17. *J. Neurosci.* **35**, 12241–12247 (2015).

Palmiter, R. D. & Huang, L. Efflux and compartmentalization of zinc by members of the SLC30 family of solute carriers. *Pflugers Arch. Eur. J. Physiol.* **447**, 744–751 (2004).

Palti, H., Meijer, A. & Adler, B. Learning achievement and behavior at school of anemic and non-anemic infants. *Early Hum. Dev.* **10**, 217–223 (1985).

Pan, E. *et al.* Vesicular Zinc Promotes Presynaptic and Inhibits Postsynaptic Long-Term Potentiation of Mossy Fiber-CA3 Synapse. *Neuron* **71**, 1116–1126 (2011).

Park, T. J. & Curran, T. Crk and Crk-like play essential overlapping roles downstream of disabled-1 in the reelin pathway. *J. Neurosci.* **28**, 13551–13562 (2008).

Park, Y. K. & Goda, Y. Integrins in synapse regulation. *Nat. Rev. Neurosci.* **17**, 745–756 (2016).

Parkin, E. & Harris, B. A disintegrin and metalloproteinase (ADAM)-mediated ectodomain shedding of ADAM10. *J. Neurochem.* **108**, 1464–1479 (2009).

Parpura, V. *et al.* Glutamate-mediated astrocyte-neuron signalling. *Nature* **369**, 744–747 (1994).

Pasten, C. *et al.* ApoER2 and Reelin are expressed in regenerating peripheral nerve and regulate Schwann cell migration by activating the Rac1 GEF protein, Tiam1. *Mol. Cell. Neurosci.* **69**, 1–11 (2015).

Paveliev, M. *et al.* HB-GAM (pleiotrophin) reverses inhibition of neural regeneration by the CNS

extracellular matrix. *Sci. Rep.* **6**, (2016).

Penkowa, M. *et al.* Impaired inflammatory response to glial cell death in genetically metallothionein-I- and -II-deficient mice. *Exp. Neurol.* **156**, 149–164 (1999).

Penkowa, M., Carrasco, J., Giralt, M., Moos, T. & Hidalgo, J. CNS wound healing is severely depressed in metallothionein I- and II-deficient mice. *J. Neurosci.* **19**, 2535–45 (1999).

Peron, R., Vatanabe, I. P., Manzine, P. R., Camins, A. & Cominetti, M. R. Alpha-secretase ADAM10 regulation: Insights into Alzheimer's disease treatment. *Pharmaceuticals* **11**, (2018).

Perry, V. H. Contribution of systemic inflammation to chronic neurodegeneration. *Acta Neuropathologica* **120**, 277–286 (2010).

Pfrieger, F. W. & Barres, B. A. New views on synapse-glia interactions. *Curr. Opin. Neurobiol.* **6**, 615–621 (1996).

Pfrieger, F. W. & Barres, B. A. Synaptic efficacy enhanced by glial cells *in vitro*. *Science.* **277**, 1684–1687 (1997).

Pinan-Lucarre, B. *et al.* The core apoptotic executioner proteins CED-3 and CED-4 promote initiation of neuronal regeneration in *Caenorhabditis elegans*. *PLoS Biol.* **10**, e1001331 (2012).

Pizzorusso, T. *et al.* Reactivation of ocular dominance plasticity in the adult visual cortex. *Science.* **298**, 1248–1251 (2002).

Planques, A., Malem, J., Parapar, J., Vervoort, M. & Gazave, E. Morphological, cellular and molecular characterization of posterior regeneration in the marine annelid *Platynereis dumerilii*. *Dev. Biol.* **445**, 189–210 (2019).

Plytycz, B. *et al.* The existence of fertile hybrids of closely related model earthworm species, *Eisenia andrei* and *E. fetida*. *PLoS One*. **13**, e0191711 (2018)

Poo, M. ming. Neurotrophins as synaptic modulators. *Nat. Rev. Neurosci.* **2**, 24–32 (2001).

Popovich, P. G. & Longbrake, E. E. Can the immune system be harnessed to repair the CNS? *Nature Reviews Neuroscience* **9**, 481–493 (2008).

Porter, S., Clarck, I. M., Kevorkian, L. & Edwards, D. R. The ADAMTS metalloproteinases. *Biochem. J.* **386**, 15–27 (2005).

Powell, S. R. Zinc and health: current status and future directions. *J. Nutr* **130**, 1447–1454 (2000).

Prendergast-Miller, M. T. *et al.* Polyester-derived microfibre impacts on the soil-dwelling earthworm *Lumbricus terrestris*. *Environ. Pollut.* **251**, 453–459 (2019).

Prenzel, N. *et al.* EGF receptor transactivation by G-protein-coupled receptors requires

metalloproteinase cleavage of proHB-EGF. *Nature* **402**, 884–888 (1999).

Prockop, D. J. & Kivirikko, K. I. Collagens: Molecular Biology, Diseases, and Potentials for Therapy. *Annu. Rev. Biochem.* **64**, 403–434 (1995).

Purohit, A., Sadanandam, A., Myneni, P. & Singh, R. K. Semaphorin 5A mediated cellular navigation: Connecting nervous system and cancer. *Biochim. Biophys. Acta - Rev. Cancer* **1846**, 485–493 (2014).

Purushothaman, A., Sugaharas, K. & Faissner, A. Chondroitin sulfate 'wobble motifs' modulate maintenance and differentiation of neural stem cells and their progeny. *Journal of Biological Chemistry* **287**, 2935–2942 (2012).

Putney, J. W. & Tomita, T. Phospholipase C signaling and calcium influx. *Adv. Biol. Regul.* **52**, 152–164 (2012).

Qing-Long, M., Qian, Y. & Xiao-Hui, Z. Perineuronal net, CSPG receptor and their regulation of neural plasticity. *Acta Physiol. Sin.* **66**, 387–397 (2014).

Raivich, G. *et al.* The AP-1 transcription factor c-Jun is required for efficient axonal regeneration. *Neuron* **43**, 57–67 (2004).

Raivich, G., Graeber, M. B., Gehrmann, J. & Kreutzberg, G. W. Transferrin receptor expression and iron uptake in the injured and regenerating rat sciatic nerve. *Eur. J. Neurosci.* **3**, 919–927 (1991).

Ramos, P. *et al.* Iron levels in the human brain: A post-mortem study of anatomical region differences and age-related changes. *J. Trace Elem. Med. Biol.* **28**, 13–17 (2014).

Rankin-Gee, E. K. *et al.* Perineuronal net degradation in epilepsy. *Epilepsia* **56**, 1124–1133 (2015).

Rapraeger, A. C. Molecular interactions of syndecans during development. *Semin. Cell Dev. Biol.* **12**, 107–116 (2001).

Rauvala, H. An 18-kd heparin-binding protein of developing brain that is distinct from fibroblast growth factors. *EMBO J.* **8**, 2933–41 (1989).

Rauvala, H., Paveliev, M., Kuja-Panula, J. & Kulesskaya, N. Inhibition and enhancement of neural regeneration by chondroitin sulfate proteoglycans. *Neural Regen. Res.* **12**, 687–691 (2017).

Rehder, V., Jensen, J. R. & Kater, S. B. The initial stages of neural regeneration are dependent upon intracellular calcium levels. *Neuroscience* **51**, 565–574 (1992).

Rhodes, K. E. & Fawcett, J. W. Chondroitin sulphate proteoglycans: Preventing plasticity or protecting the CNS? *J. Anat.* **204**, 33–48 (2004).

Richardson, P. M., McGuinness, U. M. & Aguayo, A. J. Axons from CNS neurones regenerate into PNS grafts. *Nature* **284**, 264–265 (1980).

Rink, S. *et al.* Recovery after spinal cord injury by modulation of the proteoglycan receptor PTPσ. *Exp. Neurol.* **309**, 148–159 (2018).

Rishal, I. & Fainzilber, M. Axon-soma communication in neuronal injury. *Nat. Rev. Neurosci.* **15**, 32–42 (2014).

Rivera, S., Khrestchatisky, M., Kaczmarek, L., Rosenberg, G. A. & Jaworski, D. M. Metzincin proteases and their inhibitors: foes or friends in nervous system physiology? *J. Neurosci.* **30**, 15337–15357 (2010).

Roca-Cusachs, P., Iskratsch, T. & Sheetz, M. P. Finding the weakest link – exploring integrin-mediated mechanical molecular pathways. *J. Cell Sci.* **125**, 3025–3038 (2012).

Rogers, S. L., Letourneau, P. C., Palm, S. L., McCarthy, J. & Furcht, L. T. Neurite extension by peripheral and central nervous system neurons in response to substratum-bound fibronectin and laminin. *Dev. Biol.* **98**, 212–220 (1983).

Rooke, J., Pan, D., Xu, T. & Rubin, G. M. KUZ, a conserved metalloprotease-disintegrin protein with two roles in Drosophila neurogenesis. *Science (80-.).* **273**, 1227–1231 (1996).

Ropele, S. *et al.* MRI assessment of iron deposition in multiple sclerosis. *J. Magn. Reson. Imaging* **34**, 13–21 (2011).

Rorat, A., Vandenbulcke, F., Gałuszka, A., Klimek, B. & Plytycz, B. Protective role of metallothionein during regeneration in Eisenia andrei exposed to cadmium. *Comp. Biochem. Physiol. Part - C Toxicol. Pharmacol.* **203**, 39–50 (2017).

Roy, R., Wewer, U. M., Zurakowski, D., Pories, S. E. & Moses, M. A. ADAM 12 cleaves extracellular matrix proteins and correlates with cancer status and stage. *J. Biol. Chem.* **279**, 51323–51330 (2004).

Rudge, J. & Silver, J. Inhibition of neurite outgrowth on astroglial scars in vitro. *J. Neurosci.* **10**, 3594–3603 (1990).

Ruff, C. A. *et al.* Neuronal c-Jun is required for successful axonal regeneration, but the effects of phosphorylation of its N-terminus are moderate. *J. Neurochem.* **121**, 607–618 (2012).

Ruschel, J. *et al.* Systemic administration of epothilone B promotes axon regeneration after spinal cord injury. *Science (80-.).* **348**, 347–352 (2015).

Russo, M. V. & McGavern, D. B. Immune Surveillance of the CNS following Infection and Injury. *Trends Immunol.* **36**, 637–650 (2015).

Sabin, K. Z., Jiang, P., Gearhart, M. D., Stewart, R. & Echeverri, K. AP-1cFos/JunB/miR-200a regulate the pro-regenerative glial cell response during axolotl spinal cord regeneration. *Commun. Biol.* **2**, 91 (2019).

Samuel, S. *et al.* Autofluorescence in BrdU-positive cells and augmentation of regeneration kinetics by riboflavin. *Stem Cells Dev.* **21**, 2071–2083 (2012).

Santos, C. R. A., Martinho, A., Quintela, T. & Gonçalves, I. Neuroprotective and neuroregenerative properties of metallothioneins. *IUBMB Life* **64**, 126–135 (2012).

Sarig-Nadir, O. & Seliktar, D. The role of matrix metalloproteinases in regulating neuronal and nonneuronal cell invasion into PEGylated fibrinogen hydrogels. *Biomaterials* **31**, 6411–6416 (2010).

Sasaki, M. *et al.* BDNF-hypersecreting human mesenchymal stem cells promote functional recovery, axonal sprouting, and protection of corticospinal neurons after spinal cord injury. *J. Neurosci.* **29**, 14932–14941 (2009).

Sato, M. & Kondoh, M. Recent studies on metallothionein: Protection against toxicity of heavy metals and oxygen free radicals. *Tohoku Journal of Experimental Medicine* **196**, 9–22 (2002).

Sattler, R., Tymianski, M., Feyaz, I., Hafner, M. & Tator, C. H. Voltage-sensitive calcium channels mediate calcium entry into cultured mammalian sympathetic neurons following neurite transection. *Brain Res.* **719**, 239–246 (1996).

Scemes, E., Duval, N. & Meda, P. Reduced expression of P2Y1 receptors in connexin43-null mice alters calcium signaling and migration of neural progenitor cells. *J. Neurosci.* **23**, 11444–52 (2003).

Scharfenberg, F. *et al.* Degradome of soluble ADAM10 and ADAM17 metalloproteases. *Cell. Mol. Life Sci.* 1–20 (2019). doi:10.1007/s00018-019-03184-4

Schéele, S. *et al.* Laminin isoforms in development and disease. *J. Mol. Med.* **85**, 825–836 (2007).

Schikorski, D. *et al.* Microbial challenge promotes the regenerative process of the injured central nervous system of the medicinal leech by inducing the synthesis of antimicrobial peptides in neurons and microglia. *J. Immunol.* **181**, 1083–95 (2008).

Schneggenburger, R., Tempia, F. & Konnerth, A. Glutamate- and AMPA-mediated calcium influx through glutamate receptor channels in medial septal neurons. *Neuropharmacology* **32**, 1221–1228 (1993).

Schousboe, A., Scafidi, S., Bak, L. K., Waagepetersen, H. S. & McKenna, M. C. Glutamate Metabolism in the Brain Focusing on Astrocytes. in *Adv Neurobiol* **11**, 13–30 (2014).

Schreiber, J., Schachner, M., Schumacher, U. & Lorke, D. E. Extracellular matrix alterations, accelerated leukocyte infiltration and enhanced axonal sprouting after spinal cord hemisection in tenascin-C-deficient mice. *Acta Histochem.* **115**, 865–878 (2013).

Schwab, M. E. & Bartholdi, D. Degeneration and regeneration of axons in the lesioned spinal cord. *Physiol. Rev.* **76**, 319–370 (1996).

Seals, D. F. & Courtneidge, S. A. The ADAMs family of metalloproteases: Multidomain proteins with multiple functions. *Genes Dev.* **17**, 7–30 (2003).

Seifert, A. W. & Muneoka, K. The blastema and epimorphic regeneration in mammals. *Dev. Biol.* **433**, 190–199 (2018).

Serrano, F. & Klann, E. Reactive oxygen species and synaptic plasticity in the aging hippocampus. *Ageing Res. Rev.* **3**, 431–443 (2004).

Sfera, A., Bullock, K., Price, A., Inderias, L. & Osorio, C. Ferrosenescence: The iron age of neurodegeneration? *Mech. Ageing Dev.* **174**, 63–75 (2018).

Shen, J. *et al.* Iron metabolism regulates p53 signaling through direct Heme-p53 interaction and modulation of p53 localization, stability, and function. *Cell Rep.* **7**, 180–193 (2014).

Shen, Y. *et al.* PTPσ Is a Receptor for Chondroitin Sulfate Proteoglycan, an Inhibitor of Neural Regeneration. *Science.* **326**, 592–596 (2009).

Sherman, L. S. & Back, S. A. A 'GAG' reflex prevents repair of the damaged CNS. *Trends in Neurosciences* **31**, 44–52 (2008).

Shin, J. E. *et al.* Dual leucine zipper kinase is required for retrograde injury signaling and axonal regeneration. *Neuron* **74**, 1015–1022 (2012).

Shubayev, V. I. & Myers, R. R. Matrix metalloproteinase-9 promotes nerve growth factor-induced neurite elongation but not new sprout formation in vitro. *J. Neurosci. Res.* **77**, 229–239 (2004).

Shukla, A., Agarwal, K. N., Chansuria, J. P. N. & Taneja, V. Effect of latent iron deficiency on 5-hydroxytryptamine metabolism in rat brain. *J. Neurochem.* **52**, 730–735 (1989).

Sian-Hülsmann, J., Mandel, S., Youdim, M. B. H. & Riederer, P. The relevance of iron in the pathogenesis of Parkinson's disease. *J. Neurochem.* **118**, 939–957 (2011).

Siebert, J. R., Conta Steencken, A. & Osterhout, D. J. Chondroitin sulfate proteoglycans in the nervous system: inhibitors to repair. *Biomed Res. Int.* **2014**, (2014).

Siesjö, B. K. Basic mechanisms of traumatic brain damage. *Ann. Emerg. Med.* **22**, 959–969 (1993).

Silva, N. A., Sousa, N., Reis, R. L. & Salgado, A. J. From basics to clinical: A comprehensive review on spinal cord injury. *Progress in Neurobiology* **114**, 25–57 (2014).

Silver, J. The glial scar is more than just astrocytes. *Exp. Neurol.* **286**, 147–149 (2016).

Silver, J., Schwab, M. E. & Popovich, P. G. Central nervous system regenerative failure: Role of oligodendrocytes, astrocytes, and microglia. *Cold Spring Harb. Perspect. Biol.* **7**, (2015).

Simakov, O. *et al.* Insights into bilaterian evolution from three spiralian genomes. *Nature* **493**, 526–531 (2013).

Sivasankaran, R. *et al.* PKC mediates inhibitory effects of myelin and chondroitin sulfate proteoglycans on axonal regeneration. *Nat. Neurosci.* **7**, 261–268 (2004).

Smart, T. G., Xie, X. & Krishek, B. J. Modulation of inhibitory and excitatory amino acid receptor ion channels by zinc. *Progress in Neurobiology* **42**, 393–441 (1994).

Smith-Thomas, L. C. *et al.* Increased axon regeneration in astrocytes grown in the presence of proteoglycan synthesis inhibitors. *J Cell Sci* **108**, 1307–1315 (1995).

Snow, D. M., Brown, E. M. & Letourneau, P. C. Growth cone behavior in the presence of soluble chondroitin sulfate proteoglycan (CSPG), compared to behavior on CSPG bound to laminin or fibronectin. *Int. J. Dev. Neurosci.* **14**, 331–349 (1996).

Sofroniew, M. V. Molecular dissection of reactive astrogliosis and glial scar formation. *Trends in Neurosciences* **32**, 638–647 (2009).

Solt, Z. & Molnar, L. Investigation of the development of a ventral nerve cord ganglion in *Eisenia fetid*a: a histological and histochemical study. *Neurobiology* **9**, 59–60 (2001).

Somogyi, I. *et al.* Pituitary adenylate cyclase-activating polypeptide-like compounds could modulate the activity of coelomocytes in the earthworm. *Ann. N. Y. Acad. Sci.* **1163**, 521–523 (2009).

Song, I. & Dityatev, A. Crosstalk between glia, extracellular matrix and neurons. *Brain Research Bulletin* **136**, 101–108 (2018).

Song, Y. *et al.* The mechanosensitive ion channel piezo inhibits axon regeneration. *Neuron* **102**, 373-389.e6 (2019).

Stenersen, J., Brekke, E. & Engelstad, F. Earthworms for toxicity testing; species differences in response towards cholinesterase inhibiting insecticides. *Soil Biol. Biochem.* **24**, 1761–1764 (1992).

Stephan, A. H., Barres, B. A. & Stevens, B. The complement system: an unexpected role in synaptic pruning during development and disease. *Annu. Rev. Neurosci.* **35**, 369–89 (2012).

Stephens, K. E. *et al.* RNA-seq of spinal cord from nerve-injured rats after spinal cord stimulation. *Mol. Pain* **14**, (2018).

Sternlicht, M. D. & Werb, Z. How matrix metalloproteinases regulate cell behavior. *Annu. Rev. Cell Dev. Biol.* **17**, 463–516 (2001).

Stevens, B. *et al.* The classical complement cascade mediates cns synapse elimination. *Cell* **131**, 1164–1178 (2007).

Stichel, C. C. *et al.* Inhibition of collagen IV deposition promotes regeneration of injured CNS axons. *Eur. J. Neurosci.* **11**, 632–646 (1999).

Stirling, D. P. & Stys, P. K. Mechanisms of axonal injury: internodal nanocomplexes and calcium deregulation. *Trends Mol. Med.* **16**, 160–170 (2010).

Stürzenbaum, S. R., Winters, C., Galay, M., Morgan, A. J. & Kille, P. Metal ion trafficking in earthworms. Identification of a cadmium-specific metallothionein. *J. Biol. Chem.* **276**, 34013–34018 (2001).

Sun, Y. *et al.* Chondroitin sulfate proteoglycans inhibit the migration and differentiation of oligodendrocyte precursor cells and its counteractive interaction with laminin. *Int. J. Mol. Med.* **40**, 1657–1668 (2017).

Swindell, W. R. Metallothionein and the biology of aging. *Ageing Res. Rev.* **10**, 132–45 (2011).

Szklarczyk, D. *et al.* STRING v11: Protein-protein association networks with increased coverage, supporting functional discovery in genome-wide experimental datasets. *Nucleic Acids Res.* **47,** D607-D613 (2019)

Takacs, V. *et al.* Exposure of Eisenia andrei (Oligochaeta; Lumbricidea) to cadmium polluted soil inhibits earthworm maturation and reproduction but not restoration of experimentally depleted coelomocytes or regeneration of amputated segments. *Folia Biol. (Praha).* **64**, 275–284 (2016).

Takada, Y., Ye, X. & Simon, S. The integrins. *Genome Biol.* **8**, 215 (2007).

Tang, B. L. & Hong, W. ADAMTS: A novel family of proteases with an ADAM protease domain and thrombospondin 1 repeats. *FEBS Lett.* **445**, 223–225 (1999).

Tang, X., Davies, J. E. & Davies, S. J. A. Changes in distribution, cell associations, and protein expression levels of NG2, neurocan, phosphacan, brevican, versican v2, and tenascin-C during acute to chronic maturation of spinal cord scar tissue. *J. Neurosci. Res.* **71**, 427–444 (2003).

Tasiemski, A. & Salzet, M. Neuro-immune lessons from an annelid: The medicinal leech. *Dev. Comp.*

Immunol. **66**, 33–42 (2017).

Tauchi, R. *et al.* The endogenous proteoglycan-degrading enzyme ADAMTS-4 promotes functional recovery after spinal cord injury. *J. Neuroinflammation* **9**, 545 (2012).

Tedeschi, A. & Bradke, F. Spatial and temporal arrangement of neuronal intrinsic and extrinsic mechanisms controlling axon regeneration. *Curr. Opin. Neurobiol.* **42**, 118–127 (2017).

Theis, V. & Theiss, C. VEGF – a stimulus for neuronal development and regeneration in the CNS and PNS. *Curr. Protein Pept. Sci.* **19**, 589–597 (2018).

Thomsen, M. S., Routhe, L. J. & Moos, T. The vascular basement membrane in the healthy and pathological brain. *J. Cereb. Blood Flow Metab.* **37**, 3300–3317 (2017).

Timpl, R. & Dziadek, M. Structure, development, and molecular pathology of basement membranes. *Int. Rev. Exp. Pathol.* **29**, 1–112 (1986).

Todorich, B., Pasquini, J. M., Garcia, C. I., Paez, P. M. & Connor, J. R. Oligodendrocytes and myelination: The role of iron. *Glia* **57**, 467–478 (2009).

Tom, V. J., Steinmetz, M. P., Miller, J. H., Doller, C. M. & Silver, J. Studies on the development and behavior of the dystrophic growth cone, the hallmark of regeneration failure, in an in vitro model of the glial scar and after spinal cord injury. *J. Neurosci.* **24**, 6531–9 (2004).

Tousseyn, T. *et al.* ADAM10, the rate-limiting protease of regulated intramembrane proteolysis of notch and other proteins, is processed by ADAMS-9, ADAMS-15, and the γ-secretase. *J. Biol. Chem.* **284**, 11738–11747 (2009).

Trakhtenberg, E. F. *et al.* Zinc chelation and Klf9 knockdown cooperatively promote axon regeneration after optic nerve injury. *Exp. Neurol.* **300**, 22–29 (2018).

Trendelenburg, G. *et al.* Serial analysis of gene expression identifies metallothionein-II as major neuroprotective gene in mouse focal cerebral ischemia. *J. Neurosci.* **22**, 5879–88 (2002).

Truong-Tran, A. Q., Carter, J., Ruffin, R. E. & Zalewski, P. D. The role of zinc in caspase activation and apoptotic cell death. *BioMetals* **14**, 315–330 (2001).

Unger, E. L. *et al.* Early iron deficiency alters sensorimotor development and brain monoamines in rats. *J. Nutr.* **137**, 118–124 (2007).

Vadon-Le Goff, S., Hulmes, D. J. S. & Moali, C. BMP-1/tolloid-like proteinases synchronize matrix assembly with growth factor activation to promote morphogenesis and tissue remodeling. *Matrix Biol.* **44**–**46**, 14–23 (2015).

Vallee, B. L. The function of metallothionein. *Neurochem. Int.* **27**, 23–33 (1995).

Vanňhara, P. & Šmarda, J. Jun: The master regulator in healthy and cancer cells. *J. Appl. Biomed.* **4**, 163–170 (2006).

Vaudry, D. *et al.* PACAP protects cerebellar granule neurons against oxidative stress-induced apoptosis. *Eur. J. Neurosci.* **15**, 1451–1460 (2002).

Vergnano, A. M. *et al.* Zinc dynamics and action at excitatory synapses. *Neuron* **82**, 1101–1114 (2014).

Verkhratsky, A., Orkand, R. K. & Kettenmann, H. Glial calcium: homeostasis and signaling function. *Physiol. Rev.* **78**, 99–141 (1998).

Verstraeten, S. V., Zago, M. P., Mackenzie, G. G., Keen, C. L. & Oteiza, P. I. Influence of zinc deficiency on cell-membrane fluidity in Jurkat, 3T3 and IMR-32 cells. *Biochem. J.* **378**, 579–587 (2004).

Vitulo, N., Dalla Valle, L., Skobo, T., Valle, G. & Alibardi, L. Transcriptome analysis of the regenerating tail vs. the scarring limb in lizard reveals pathways leading to successful vs. unsuccessful organ regeneration in amniotes. *Dev. Dyn.* **246**, 116–134 (2017).

Vogt, K., Mellor, J., Tong, G. & Nicoll, R. The actions of synaptically released zinc at hippocampal mossy fiber synapses. *Neuron* **26**, 187–196 (2000).

von Reyn, C. R. *et al.* Calpain mediates proteolysis of the voltage-gated sodium channel -subunit. *J. Neurosci.* **29**, 10350–10356 (2009).

Wagner, K. R., Sharp, F. R., Ardizzone, T. D., Lu, A. & Clark, J. F. Heme and Iron Metabolism: Role in Cerebral Hemorrhage. *J. Cereb. Blood Flow Metab.* **23**, 629–652 (2003).

Wakatsuki, S., Yumoto, N., Komatsu, K., Araki, T. & Sehara-Fujisawa, A. Roles of meltrin-β/ADAM19 in progression of schwann cell differentiation and myelination during sciatic nerve regeneration. *J. Biol. Chem.* **284**, 2957–2966 (2009).

Waller, R. *et al.* Metallothionein-I/II expression associates with the astrocyte DNA damage response and not Alzheimer-type pathology in the aging brain. *Glia* **66**, 2316–2323 (2018).

Wang, H. *et al.* Chondroitin-4-sulfation negatively regulates axonal guidance and growth. *J. Cell Sci.* **121**, 3083–3091 (2008).

Wang, K. C. *et al.* Oligodendrocyte-myelin glycoprotein is a Nogo receptor ligand that inhibits neurite outgrowth. *Nature* **417**, 941–944 (2002).

Ward, R. J., Zucca, F. A., Duyn, J. H., Crichton, R. R. & Zecca, L. The role of iron in brain ageing and neurodegenerative disorders. *Lancet Neurol.* **13**, 1045–60 (2014).

Watkins, T. A. *et al.* DLK initiates a transcriptional program that couples apoptotic and regenerative responses to axonal injury. *Proc. Natl. Acad. Sci.* **110**, 4039–4044 (2013).

Webber, C. A., Hocking, J. C., Yong, V. W., Stange, C. L. & McFarlane, S. Metalloproteases and guidance of retinal axons in the developing visual system. *J. Neurosci.* **22**, 8091–8100 (2002).

Wee Yong, V., Forsyth, P. A., Bell, R., Krekoski, C. A. & Edwards, D. R. Matrix metalloproteinases and diseases of the CNS. *Trends Neurosci.* **21**, 75–80 (2002).

Weidhase, M., Helm, C. & Bleidorn, C. Morphological investigations of posttraumatic regeneration in *Timarete cf. punctata* (Annelida: Cirratulidae). *Zool. Lett.* **1**, 20 (2015).

Welsbie, D. S. *et al.* Functional genomic screening identifies dual leucine zipper kinase as a key mediator of retinal ganglion cell death. *Proc. Natl. Acad. Sci.* **110**, 4045–4050 (2013).

Wen, T. H., Binder, D. K., Ethell, I. M. & Razak, K. A. The perineuronal 'safety' net? perineuronal net abnormalities in neurological disorders. *Front. Mol. Neurosci.* **11**, 270 (2018).

White, J. M. ADAMs: Modulators of cell-cell and cell-matrix interactions. *Curr. Opin. Cell Biol.* **15**, 598–606 (2003).

Wilhelm, M., Koza, A., Engelmann, P., Németh, P. & Csoknya, M. Evidence for the presence of thyroid-stimulating hormone, thyroglobulin and their receptors in *Eisenia fetida*: A multilevel hormonal interface between the nervous system and the peripheral tissues. *Cell Tissue Res.* **324**, 535–546 (2006).

Wolf, J. A., Stys, P. K., Lusardi, T., Meaney, D. & Smith, D. H. Traumatic axonal injury induces calcium influx modulated by tetrodotoxin-sensitive sodium channels. *J. Neurosci.* **21**, 1923–30 (2001).

Xiong, X. *et al.* Protein turnover of the Wallenda/DLK kinase regulates a retrograde response to axonal injury. *J. Cell Biol.* **191**, 211–223 (2010).

Xu, Z., Maroney, A. C., Dobrzanski, P., Kukekov, N. V & Greene, L. A. The MLK family mediates c-jun n-terminal kinase activation in neuronal apoptosis. *Mol. Cell. Biol.* **21**, 4713–4724 (2001).

Yamada, J., Nadanaka, S., Kitagawa, H., Takeuchi, K. & Jinno, S. Increased Synthesis of Chondroitin Sulfate Proteoglycan Promotes Adult Hippocampal Neurogenesis in Response to Enriched Environment. *J. Neurosci.* **38**, 8496–8513 (2018).

Yamaguchi, Y. & Miura, M. Programmed cell death in neurodevelopment. *Dev. Cell* **32**, 478–490 (2015).

Yamamori, H. *et al.* Plasma levels of mature brain-derived neurotrophic factor (BDNF) and matrix metalloproteinase-9 (MMP-9) in treatment-resistant schizophrenia treated with clozapine. *Neurosci. Lett.* **556**, 37–41 (2013).

Yan, Y., Shirakabe, K. & Werb, Z. The metalloprotease Kuzbanian (ADAM10) mediates the

transactivation of EGF receptor by G protein-coupled receptors. *J. Cell Biol.* **158**, 221–226 (2002).

Yang, H. Y., Lieska, N., Shao, D., Kriho, V. & Pappas, G. D. Proteins of the intermediate filament cytoskeleton as markers for astrocytes and human astrocytomas. *Mol. Chem. Neuropathol.* **21**, 155–176 (1994).

Yang, W. S. & Stockwell, B. R. Ferroptosis: Death by lipid peroxidation. *Trends Cell Biol.* **26**, 165–176 (2016).

Yang, Z. & Wang, K. K. W. Glial fibrillary acidic protein: From intermediate filament assembly and gliosis to neurobiomarker. *Trends in Neurosciences* **38**, 364–374 (2015).

Yao, M. *et al.* Targeting proteoglycan receptor PTPσ restores sensory function after spinal cord dorsal root injury by activation of Erks/CREB signaling pathway. *Neuropharmacology* **144**, 208–218 (2019).

Ye, D., Shi, Y., Xu, Y. & Huang, J. PACAP Attenuates Optic Nerve Crush-Induced Retinal Ganglion Cell Apoptosis Via Activation of the CREB-Bcl-2 Pathway. *J. Mol. Neurosci.* **68**, 475–484 (2019).

Yehuda, S., Youdim, M. E. H. & Mostofsky, D. I. Brain iron-deficiency causes reduced learning capacity in rats. *Pharmacol. Biochem. Behav.* **25**, 141–144 (1986).

Ying, W., Han, S.-K., Miller, J. W. & Swanson, R. A. Acidosis Potentiates Oxidative Neuronal Death by Multiple Mechanisms. *J. Neurochem.* **73**, 1549–1556 (2002).

Yokoyama, M., Koh, J. & Choi, D. W. Brief exposure to zinc is toxic to cortical neurons. *Neurosci. Lett.* **71**, 351–355 (1986).

Yokozeki, T. *et al.* Meltrin β (ADAM19) mediates ectodomain shedding of Neuregulin β1 in the Golgi apparatus: Fluorescence correlation spectroscopic observation of the dynamics of ectodomain shedding in living cells. *Genes to Cells* **12**, 329–343 (2007).

Yong, V. W. Metalloproteinases: Mediators of Pathology and Regeneration in the CNS. *Nat. Rev. Neurosci.* **6**, 931–944 (2005).

Yu, Q. & Stamenkovic, I. Cell surface-localized matrix metalloproteinase-9 proteolytically activates TGF-beta and promotes tumor invasion and angiogenesis. *Genes Dev.* **14**, 163–76 (2000).

Yu, S. *et al.* Angiogenic microspheres promote neural regeneration and motor function recovery after spinal cord injury in rats. *Sci. Rep.* **6**, (2016).

Yurchenco, P. D. & Schittny, J. C. Molecular architecture of basement membranes. *FASEB J.* **4**, 1577–1590 (2018).

Zattara, E. E. & Bely, A. E. Evolution of a novel developmental trajectory: Fission is distinct from

regeneration in the annelid *Pristina leidyi*. *Evol. Dev.* **13**, 80–95 (2011).

Zattara, E. E. *et al.* Long-term time-lapse live imaging reveals extensive cell migration during annelid regeneration. *BMC Dev. Biol.* **16**, 6 (2016).

Zecca, L. *et al.* The role of iron and copper molecules in the neuronal vulnerability of locus coeruleus and substantia nigra during aging. *Proc. Natl. Acad. Sci.* **101**, 9843–9848 (2004).

Zecca, L., Zucca, F. A., Albertini, A., Rizzio, E. & Fariello, R. G. A proposed dual role of neuromelanin in the pathogenesis of Parkinson's disease. *Neurology* **67**, S8-11 (2006).

Zhao, T. *et al.* PHBV/PLA/Col-based nanofibrous scaffolds promote recovery of locomotor function by decreasing reactive astrogliosis in a hemisection spinal cord injury rat model. *J. Biomed. Nanotechnol.* **14**, 1921–1933 (2018).

Zheng, P., Shao, Q., Diao, X., Li, Z. & Han, Q. Expression of stem cell pluripotency factors during regeneration in the earthworm *Eisenia foetida. Gene* **575**, 58–65 (2016).

Zhong, J. *et al.* Chondroitin sulfate proteoglycan represses neural stem/progenitor cells migration via PTPσ/α-actinin4 signaling pathway. *J. Cell. Biochem.* **120**, 11008–11021 (2019).

Zhu, S. *et al.* Chondromodulin-1 in health, osteoarthritis, cancer, and heart disease. *Cell. Mol. Life Sci.* [Epub ahead of print] (2019). doi:10.1007/s00018-019-03225-y

Zhu, Y. Y., Machleder, E. M., Chenchik, A., Li, R. & Siebert, P. D. Reverse transcriptase template switching: A SMART™ approach for full-length cDNA library construction. *BioTechniques* **30**, 892–897 (2001).

Ziv, N. E. & Spira, M. E. Axotomy induces a transient and localized elevation of the free intracellular calcium concentration to the millimolar range. *J. Neurophysiol.* **74**, 2625–2637 (1995).

Ziv, N. E. & Spira, M. E. Spatiotemporal distribution of Ca2+ following axotomy and throughout the recovery process of cultured aplysia neurons. *Eur. J. Neurosci.* **5**, 657–668 (1993).

Zündorf, G. & Reiser, G. Calcium dysregulation and homeostasis of neural calcium in the molecular mechanisms of neurodegenerative diseases provide multiple targets for neuroprotection. *Antioxid. Redox Signal.* **14**, 1275–88 (2011).

Zuo, J., Ferguson, T. A., Hernandez, Y. J., Stetler-Stevenson, W. G. & Muir, D. Neuronal matrix metalloproteinase-2 degrades and inactivates a neurite-inhibiting chondroitin sulfate proteoglycan. *J. Neurosci.* **18**, 5203–11 (1998).

7. Appendix

Table 7.1 List of primers

Assigned Gene ID	Contig	Sense/ Antisense	Length (nts)	Sequence (5' to 3')	Amplicon size (nts)
gapdh	N/A	sense	20	ATGGTCCAAGCAACAAGGAC	126
gapdh	N/A	antisense	20	TTCCAGTCAGTTTGCCATTG	
coII	N/A	sense	19	CAAGATGCCGCATCTTCTG	497
coII	N/A	antisense	20	ACGGCATCTACTTTTACGCC	
mt2	N/A	sense	21	TGAAAAGTGAGTGCTTGCCG	186
mt2	N/A	antisense	21	CGTATTTCAATGCCTCGGCTC	
T7P	N/A	sense	20	TAATACGACTCACTATAGGG	N/A
SP6	N/A	antisense	19	CATTTAGGTGACACTATAG	
adam8	274492	sense	20	AAGTCTGGAACATGGGCAAC	224
adam8	274492	antisense	20	ATACACGTCCCCAACAAAGG	
adam10	88163	sense	20	GGCTCGCCTGACAAACTTAC	159
adam10	88163	antisense	20	TTGCTGCTTGGAGTGTGAAC	
adam12	36723	sense	20	GAAGCCTCCGACTTGAACAG	157
adam12	36723	antisense	20	TCGGCACCTACTACGGAAAC	
adam19	167825	sense	20	ATGGTTGGTAAGCGGAACTG	150
adam19	167825	antisense	20	GGCCACAGGATCAAGATGAG	
adam28	169508	sense	20	CGTCATGCTCGATTCAACAG	180
adam28	169508	antisense	20	AACAGGCGCTGTTACATTCC	
adamts2	50247	sense	20	GTTTCTCGGGAGACTGTTGC	160
adamts2	50247	antisense	20	GAGCACGTAGAACAGCATCG	
cat	24496	sense	20	TGCAGGACTTTGTCTTCAGG	138
cat	24496	antisense	20	TCGCTTTGCAGTACTTGGTG	
sod1	40309	sense	20	GCTTCAAGGTTTGGTTCGAC	113
sod1	40309	antisense	20	ACAGCGAACGAGGTTTTCAC	
junb	326	sense	20	TTGCGAAAGATGGAACTGTG	134
junb	326	antisense	20	GGTAATGCTCACCCACAACC	
cckar	35513	sense	20	GTCTCGGCAACTACCTTCGG	163
cckar	35513	antisense	20	CGAACGATACGCTTCTTCGC	
sema5a	65221	sense	20	GTTTCCGATACACCCACGAC	129
sema5a	65221	antisense	20	GATGGTCATTGGTCAACGTG	
gfap	32756	sense	20	ACGAGACGTTGCTTCATGTG	160
gfap	32756	antisense	20	ATCTCGCTCTTCCACAGCTC	
bmp1	40070	sense	20	CTTTCGGAGCCGTAATGTTC	105
bmp1	40070	antisense	20	TCAATGCTTCACCGACAGAG	
ptpσ	96408	sense	20	CAGATCCGTGCCTACACCAG	154
ptpσ	96408	antisense	20	AGGATGGAGGATCCCAGGTC	
lect1	11879	sense	20	TCCAGTAACGCATCCAACCC	126
lect1	11879	antisense	20	CCAAAGACAAAGCGCGAGAC	

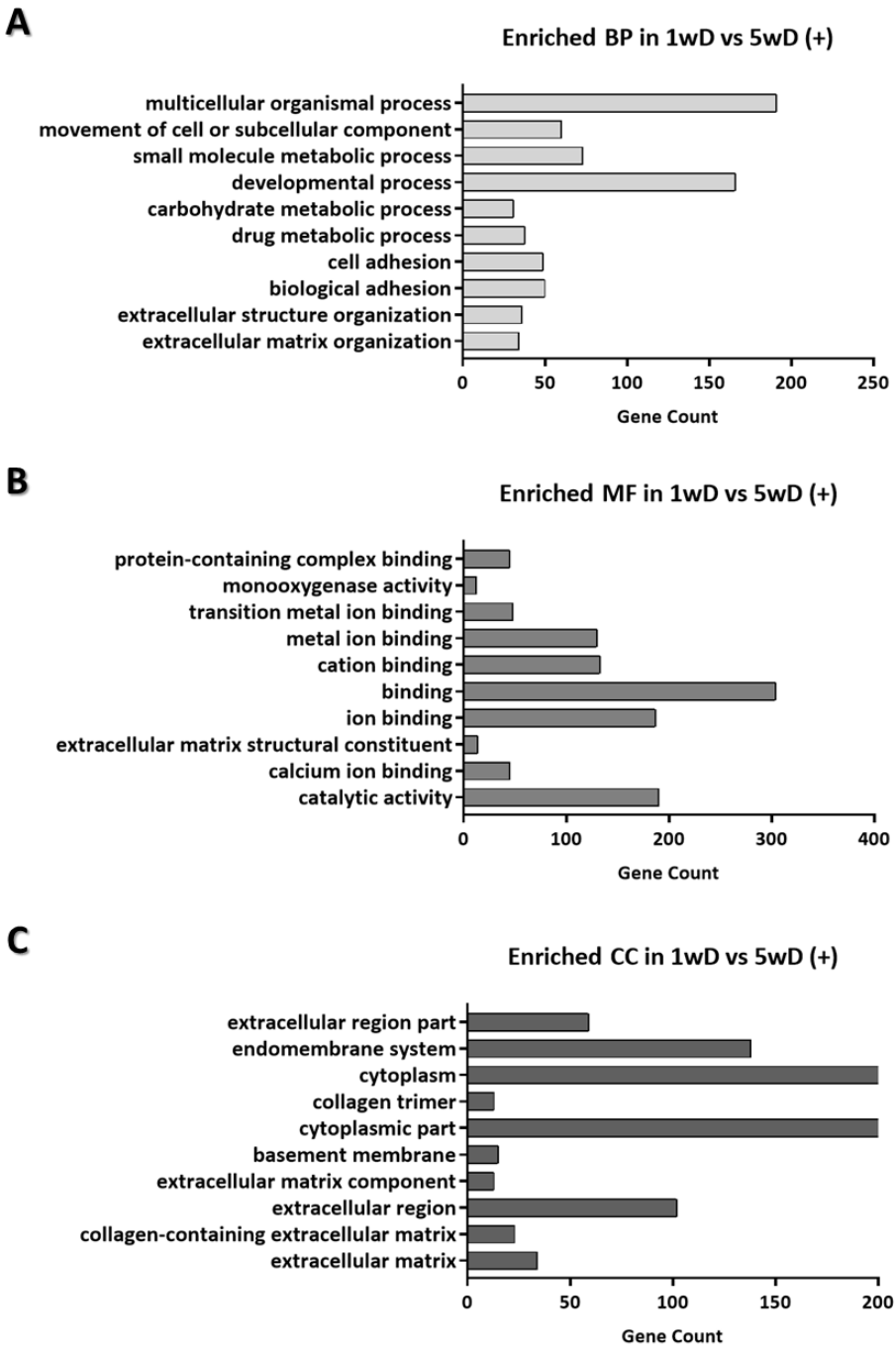

Figure 7.1 Histogram representing the gene ontology classification and functional enrichment of upregulated (+) genes in 1wD vs 5wD obtained in STRING. A. The 10 most significantly enriched (false discovery rate <0.05) Biological Processes (BPs) confirmed that at the latter stages (5wD) of regeneration a higher ECM re-organisation is taking place compared to earlier stages of regeneration (1wD). **B.** The 10 most significantly enriched (false discovery rate <0.05) Molecular Functions (MF) revealed that there is a more pronounced metal binding activity at 5wD compared to 1wD. **C**. The 10 most significantly enriched (false discovery rate <0.05) Cellular Components (CC) suggest that there are more upregulated genes which are positioned on the cell membrane and have an interaction with ECM components

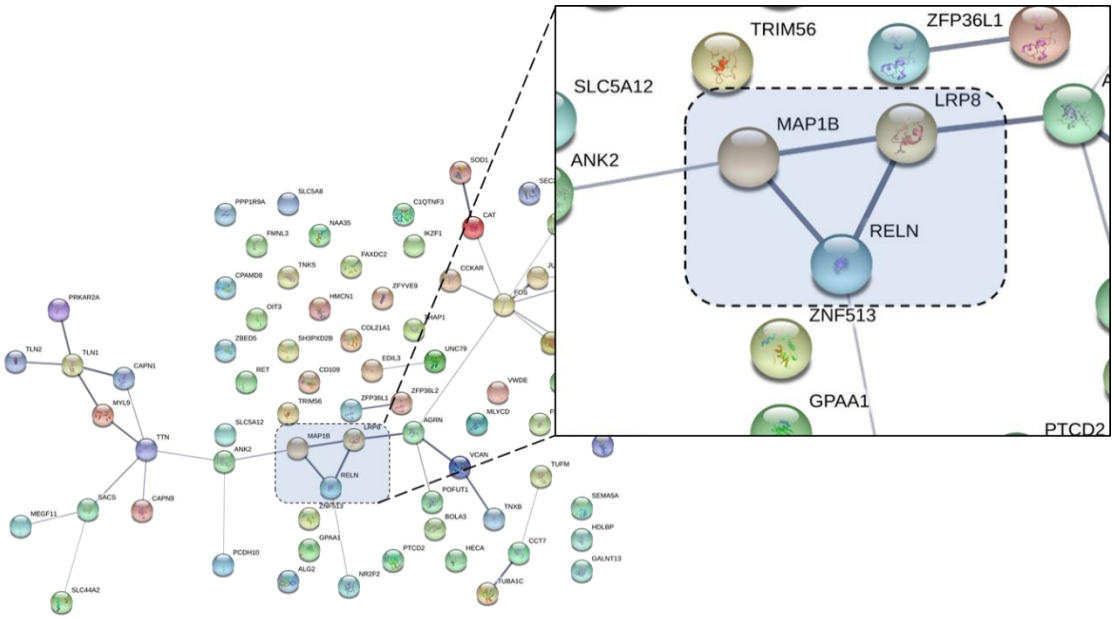

Figure 7.2 Interaction network showing the connections between upregulated genes in sham vs 1wD in STRING, which take part in the reelin-mediated signalling pathway. The interaction between two members of the reelin-mediated signalling pathway (RELN and LRP8) with MPA1B is highlighted, which provides strong evidence that there is a functional link amongst the three protein. The thickness of the lines (edges) which connect the nodes, denotes the degree of confidence in the interactions observed.

ADAM19 (contig_167825) domain characterisation in *Eisenia fetida*

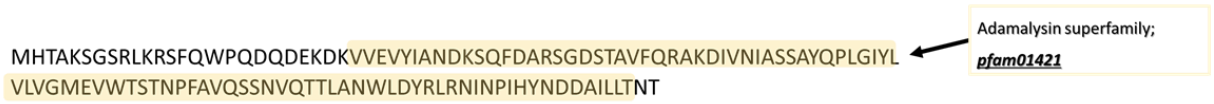

ADAM8 (contig_274492) domain characterisation in *Eisenia fetida*

ADAM28 (contig_169508) domain characterisation in *Eisenia fetida*

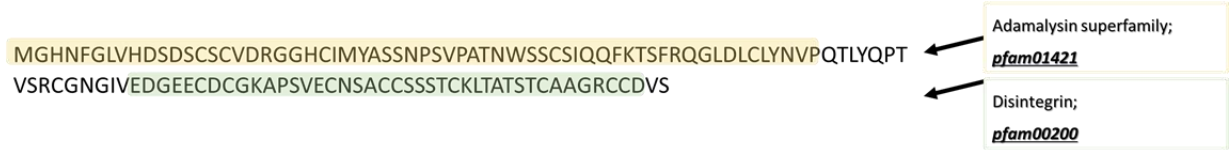

ADAM12 (contig_36723) domain characterisation in *Eisenia fetida*

Figure 7.3 Partial protein sequences and domains of ADAMs, which are upregulated during CG regeneration. The domains identified, appear to be evolutionary conserved and as such the function of ADAMs in the earthworm can be reliably inferred based on work on other species

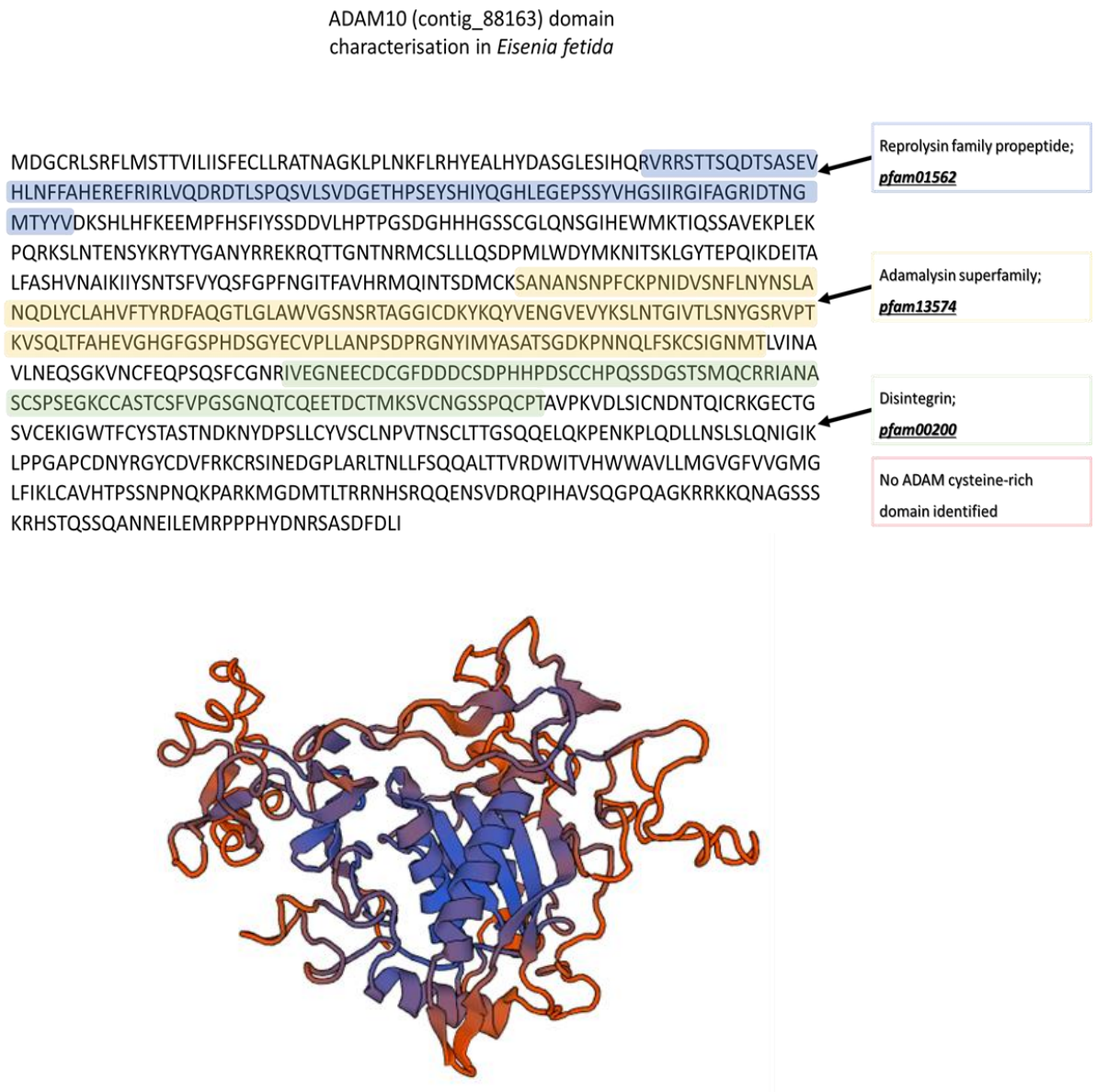

Figure 7.4 Full protein sequence and domains of ADAM10. The domains identified, appear to be evolutionary conserved and as such the function of ADAM10 in the earthworm can be reliably inferred based on work on other species. An *in silico* tertiary structure prediction is also presented which can be used to assess structural similarities with mammalian counterparts and assign a function to the protein more reliably. The modelling was performed on Swiss Model and a QMEAN cutoff of 4 was set, in order to increase the confidence in the modelling.